Utilisation of VOC in Diesel Engines

Ignition and combustion of VOC released by crude oil tankers

by
Øyvin Melhus

Thesis submitted in partial fulfilment
of the requirements for the degree

Doktor Ingeniør

Department of Marine Engineering
Norwegian University of Science and Technology

Acknowledgements

This study was initiated in 1997 as cooperation between the Division of Marine Engineering at the Norwegian University of Science and Technology and Statoil R&D in Trondheim. This thesis is part of the requirements for the degree *Doktor Ingeniør* at the Department of Marine Engineering at The Norwegian University of Science and Technology (NTNU).

I want to thank Professor Terje Almås for giving me the opportunity to accomplish this work. He was one of the main initiators of the concept to utilise VOC as fuel in shuttle tankers. Assistant Professor Tore Hansen has given advice and support concerning the computer acquisition and control system of the test installation (DyFo). Mechanical engineer Ola Dalsbø has given invaluable practical help to make the DyFo test rig function properly. Oddvar Paulsen in the workshop at MTS has given me a helping hand whenever I needed assistance of mechanical character. Sven Føllesdal in the electronic workshop at MTS has also given me assistance frequently. Thank also to the graduate students Bjarte Lund and Marianne Haug for cooperation in some of the test work.

Financial support of the work has been given by Statoil R&D for 2,5 years. In addition, the contact person at Statoil, Ola Ruch, has given valuable support to the design and problem-solving concerning the complicated hydraulic system of the DyFo.

An additional and considerable part of the financial support has been equipment and production of parts in the Statoil R&D workshop. Whenever needed for the experiments on the DyFo, Stig Jørgensen and Einar Lund have assisted in producing parts and making equipment available.

The Division of Marine Engineering and the Faculty of Marine Technology at MTS have financially supported the final part of the study involving writing of this thesis.

Finally I will thank my wife Hanne Marte and the rest of my family for their patience and support throughout my work and for inspiration and motivation to carry on the work in times of despair.

Trondheim, March 2002

Øyvin Melhus

Abstract

The emission of VOC (Volatile Organic Compound) has been identified as a significant source of hydrocarbon pollution. It is many sources of VOC emission. A major one in Norway is caused by the offshore oil industry. In the Norwegian part of the North Sea, the contribution from shuttle tankers loading crude oil at the oil fields is about 215000 tons a year (1997). This emission represents both an energy loss and an environmental problem.

Gas tankers have used boil-off gas from the cargo tanks as fuel for some time. However, for the current VOC project a new fuel injection concept is designed for tankers to take advantage of the energy present in the VOC evaporated from crude oil. The VOC is mixed with inert gas in these tankers, and thus the utilisation of this gas represents new challenges. The VOC project uses the concept of «Condensate Diesel Process» with pilot ignition.

An experimental study of ignition and combustion of VOC Fuels reported here was initiated by the time it was decided to start a pilot project converting propulsion engines in shuttle tankers to use VOC Fuel. It is an experimental study carried out at the Marine Technology Centre (MTS). The objective was to study ignition and combustion of the chosen process in comparison with an ordinary diesel process.

The experimental results have been discussed and are compared with theoretical considerations of injection, ignition and combustion.

For experiments on combustion, a rapid compression machine "DyFo", which was developed during the years from 1992 to 1997, was redesigned to use VOC Fuel. The DyFo test rig was initially designed to study ignition and early combustion of spark ignited homogeneous gas/air charges. To study the ignition and early combustion of VOC Fuel injected at high pressure and ignited by pilot diesel fuel, a redesign was necessary. An important feature of the DyFo, is the visualisation of the combustion.

The advantage of the DyFo test rig, compared to an engine, is its simplicity and controllability. All test parameters and variables are better controlled and this makes comparable tests easier to perform. In an engine the visualisation would suffer from combustion deposits disturbing the view through the quartz glasses, making the images more difficult to interpret. The simplicity is on the other side a drawback. Correct thermal conditions inside the cylinder is hard to obtain as the piston only is moved one half stroke (from BDC to TDC) for each test. External heating of the test rig is necessary, and this makes it difficult to obtain correct thermal conditions for other than low load conditions.

An injector of a new, common rail type design is developed for injection of the VOC Fuel. The design, based on a conventional, redesigned diesel fuel nozzle involved a lot of practical problems. Leakages of gas into the combustion chamber have led to some accidents resulting in too high cylinder pressures. However, broken quartz glasses have been the most serious result of the malfunctions.

The main purpose of this investigation has been to study the combustion of alkanes present in the VOC evaporated from crude oil. The primary objective was to verify whether or not the concept of the «Condensate Diesel Process» with pilot ignition can be used to utilise these hydrocarbons as fuel in Diesel engines. VOC Fuels of different composition have been tested.

The experiments carried out have not revealed any problems concerning combustion when using pilot ignited VOC Fuel. Both ignition and combustion seem to follow the traditional diesel scheme. The composition of the VOC Fuel seems not to affect the ignition delay. A study of varying the value of different parameters has not unveiled any surprises regarding the ignition or early combustion.

Separate tests with pure VOC Fuel components, however, show great differences in the ignition delay (both regarding mean value and variance) for different components. The component being most unwillingly and most unstable to ignite is propane. If, for some reason, the pilot ignition should fail, a VOC Fuel with mainly n-butane and higher alkanes will probably give no great operating problems, at least not at medium to high engine load.

These conclusions are mainly based on the analysis of the dynamic signals from the pressure sensor giving the cylinder pressure curves. Where found appropriate, Schlieren images have been included in the discussion. However, the use of Schlieren images has been found to be less valuable for the Diesel process than for the Otto process. The reason for this is mainly that the radiation of visible light from the diffusion combustion of diesel oil and VOC Fuel (i.e. propane, iso-butane and n-butane) are quite different. First, this radiation disturbs the Schlieren image and second, the radiation from the combustion of diesel oil is far more intense than that of the VOC Fuel.

The light VOC fraction of the vent gas – methane and ethane – is not utilised in the concept of «Condensate Diesel Process». This fraction represents about 15 % of the total energy in the VOC release when loading crude oil at the Statfjord field. At other fields as Gullfaks, this fraction can represent up to 50% or more of the total energy. After the VOC Fuel is produced, a residual VOC consisting of methane, ethane, some propane and inert gas is lost.

A useful and simple way of utilising even this fraction is to mix it with the charge air at low pressure and feed the mixture into the cylinder where a pilot fuel spray ignites the charge. The method is found to have potential of being a suitable way, at least theoretically, to utilise the light VOC fraction. Some practical difficulties, however, may restrict the use of this fraction to medium and high engine loads. At lower loads the ignition delay increases due to the dilution with great quantities of inert gas.

Another option to utilise the light VOC fraction is by capturing the gas in hydrates. No real study of this concept has been carried out, but an initial survey of possible solutions is described. A final conclusion of the potential of this concept cannot be drawn until more detailed work has been carried out. However, simply using the light VOC fraction extracted by melting the hydrate will be the most likely way.

As a main conclusion it can be stated that the use of VOC Fuel in a «Condensate Diesel Process» is a feasible way of utilising energy otherwise lost. Venting the VOC to the atmosphere when loading crude oil into shuttle tankers represents both an energy loss and an environmental problem. By reducing both, the idea of using VOC as an engine fuel seems to be a good one.

Contents Page

Nomenclature

Abbreviations and chemical symbols

AROHR - Accumulated Heat Release (J/s) (page 4, 24)
BDC - Bottom Dead Centre. Lowest position of piston in the cylinder (page 48)
BMEP - Brake Mean Effective Pressure (bar) (page 19)
CAP - Charge Air Pressure (bar) (page 55)
CAT - Charge Air Temperature (ºC or K) (page 55)
CCD - Charge Coupled Device (page 37)
CL - Collimating Lens (page 37)
CH_4 - methane (page 5)
C_2H_6 - ethane (page 7)
C_3H_8 - propane (page 7)
iC_4H_{10} - iso-butane (page 7)
nC_4H_{10} - normal-butane (page 7)
iC_5H_{12} - iso-pentane (page 7)
nC_5H_{12} - normal-pentane (page 7)
CO_2 - carbon dioxide (page 7)
DL - Dispersing Lens (page 37)
DI - Direct Injected (Diesel Engine) (page 24)
DWT - Dead Weight Tonnage (page 6)
FL1, FL2 - Focusing Lens no. 1, no. 2 (page 37)
HC - HydroCarbon (page 82)
HFO - Heavy Fuel Oil (page 2)
IG - Inert Gas (page 82)
IMO - UN's International Maritime Organization (page 1)
LHV - Lower Heating Value (MJ/kg) (page 7, 84)
LNG - Liquid Natural Gas (page 1)
LPG - Liquid Product Gas (=propane) (page 1)
NG - Natural Gas (page 2)
N_2 - nitrogen (page 7)
NMVOC - non-methane volatile organic compound (page 5)
NO_X - oxides of nitrogen (page 5)
NTNU - Norwegian University of Science and Technology (page 3)
O_2 - oxygen (page 7)
PFM - Pilot Fuel Mass (mg) (page 55)
PM - particulate matter (page 2)
RIT - Relative Injection Timing (page 55)
ROHR - Rate of Heat Release (J/s) (page 4, 24)
STD - Standard Deviation (page 57)
TDC - Top Dead Centre. Highest position of piston in the cylinder (page 48)
VFM - VOC Fuel Mass (mg) (page 55)
VLCC - Very Large Crude Carrier (page 6)
Å - ångstrom (10^{-10} m) (page 90)

Roman letters and expressions

A - Arrhenius pre-exponential constant (page 18, 20)
A, n - constants dependent on the fuel (page 20)
Alfa - ratio of VOC in the vent-gas mixture of VOC and inert gas (page 6)
A_n - nozzle minimum area (m^2) (page 16)

A_w - surface area of the combustion chamber (m^2) (page 17)
$A\ exp(-E_a/RT)$ - Arrhenius expression for the reaction rate coefficient (page 18)
B - constant (page 19)
c - overall concentration (-) (page 18)
c - speed of light (km/s) (page 36)
c^* - speed of light in vacuum (km/s) (page 36)
c_p - specific heat at constant pressure (kJ/kg K) (page 26)
c_v - specific heat at constant volume (kJ/kg K) (page 17)
C_D - drag coefficient of nozzles (-) (page 16)
d_n - nozzle hole diameter (m) (page 13)
$dm_f/dt = \dot{m}_f$ - mass fuel delivery rate (mg/s) (page 11, 24)
dT/dt - temperature change pr. unit time (page 17)
E_a - activation energy (page 18)
E_A - apparent activation energy for the fuel autoignition process (kJ/kmole) (page 20)
F - reactants (page 27)
f_{FL1} - focal length of the Focusing Lens no. 1 (mm) (page 37)
DH_R - heat of reaction (J/kg) (page 18)
h_f - the sensible enthalpy of the injected fuel (J/kg) (page 24)
h_w - heat transfer coefficient to the wall (W/m^2K) (page 17)
k_i - rate of reaction for reaction no. *i* (page 27)
m - mass inside the cylinder (kg) (page 24)
n - overall reaction order (=2 for most hydrocarbon-air reactions) (page 18)
n - refractive index (-) (page 35)
n_0 - refractive index at 0 ºC and 760 mmHg (-) (page 35)
$\partial n/\partial x$, $\partial n/\partial y$ - gradients in refractive index (-) (page 35)
dp/dt - change of chamber pressure pr. unit time (bar/s) (page 26)
Dp - pressure drop across the nozzle (Pa) (page 16)
p - combustion chamber pressure (bar) (page 20)
p_i - injection pressure (bar) (page 14)
P - products (page 27)
$\dot{q}_R$ - rate of energy released by the chemical reactions (J/ms) (page 17)
$\dot{q}_L$ - rate of thermal energy loss (J/ms) (page 17)
Q - heat transfer to the gas within the cylinder (J) (page 24)
dQ_{ch}/dt - rate of chemical heat release (J/s) (page 24)
dQ_{ht}/dt - rate of thermal heat loss to the combustion chamber walls (J/s) (page 24)
dQ_n/dt - rate of net heat release (J/s) (page 24)
Q_R - energy content of fuel (J) (page 25)
R - radicals (page 27)
R - the universal gas constant (kJ/kmole K) (page 18, 20)
RR - reaction rate (kg/m^3s) (page 18)
S - spray tip penetration (mm) (page 11)
S/V - surface to volume ratio of the combustion chamber (-) (page 19)
T_g - gas temperature inside the combustion chamber (K)
T_w - wall temperature (K) (page 17)
T - reactant mixture temperature (K) (page 18)
T - chamber temperature (K) (page 20)
Dt - open period of the nozzle (s) (page 16)
t - time after the start of injection (ms)
$U=mu$ - the sensible internal energy of the cylinder charge (J/kg) (page 24)
V - combustion chamber volume (m^3) (page 18)
dV/dt - change of chamber volume pr. unit time (m^3/s) (page 26)

Greek letters

a	- multiplication factor for radicals (page 28)
a	- angle of incident/deflected light (page 36)
? = c_p/c_v	- index of isentropic (adiabatic) expansion or compression (page 26)
e	- deflection (page 37)
e	- compression ratio (page 103)
?	- fuel spray angle (degrees) (page 11)
?	- excess air ratio (-) (page 3)
?	- wavelength (nm) (page 35)
?	- density (kg/m^3)
r_f	- fuel density upstream the nozzle (kg/m^3) (page 16)
r_g	- gas density inside the combustion chamber (kg/m^3) (page 13)
r_l	- liquid fuel density inside the combustion chamber (kg/m^3) (page 13)
s	- standard deviation (SD) (page 25)
t, t_{id}	- ignition delay (milliseconds) (page 20)

Subscripts

ch	- chemical value
f	- value present for fuel
g	- value present for gas
VOC	- value present for VOC Fuel
th	- thermal value
pilot	- value present for pilot fuel
op	- value present by operation
cal	- value present by calibration

1 Introduction

1.1 Background

The history of air pollution dates back to the time of the industrial revolution. The burning of coal for use in domestic heating and factories resulted in harmful fumes in densely populated areas. As the economy of the western world continued to expand, the problems of air pollution increased, reaching a climax in the early 1970s due in large part to the voluminous emissions produced by the use of the internal combustion engine (1)[1].

In the 1970s smog problems started a process making the air quality better in California. A US federal air pollution control law (the Clean Air Act of 1970) initiated the process of reducing the exhaust emission from automobiles. Concerning the emissions from gasoline fuelled automobiles, the final solution so far was found when introducing the three-way catalyst. The establishment of automotive emission standards in the 1980s demanding this solution excluded the use of leaded gasoline and served as a primary driving force for the development of the air pollution control work (1).

Since then the environmental awareness has steadily grown and other sources of harmful emissions - mainly situated on-shore - have gained focus. Better knowledge of the pollution problem has also emphasised on new harmful components.

During the last 10 years air pollution from ships has been explored. Exhaust emissions from ship engines have been brought to focus by the UN International Maritime Organisation (IMO).

One of more aspects concerning ships that have gained an increased interest recently, is the loss of gaseous hydrocarbons (VOC, cf. section 2.1) when handling crude oil and in particular when loading crude oil shuttle tankers at the oil fields. During all kinds of handling of crude oil the light components evaporate, whatever the oil is loaded into the tanks or splashed around in the tanks during the voyage to the oil terminals. It is expected that IMO will propose restrictions to the emission of VOC from the cargo tanks in the near future.

When the light components of the crude oil evaporate, the pressure inside the tanks increases. To keep the pressure at a safe level, normally below 1,14 bar, the gas is vented to the atmosphere. This gas, the so-called *vent gas*, is VOC mixed with inert gas (cf. section 2.1) in order to reduce the risk of explosions.

All crude oil tankers are subject to this phenomenon. In the North Sea the problem has been taken seriously by the oil companies, one of them being Statoil. In co-operation with the diesel engine manufacturer MAN B&W a number of oil companies decided to go along with a pilot project, the "VOC Fuel project", converting propulsion engines to use VOC (2, 3). The first conversion, a full-scale test, is made on "Navion Viking" (4, 5) transporting crude oil from North Sea oil fields to Mongstad and Amsterdam. This conversion is based on the experience MAN B&W has with gas injection in medium speed diesel engines (6) and the use of natural gas ignited by pilot fuel injection in a large 2-stroke slow speed engine in Ciba, Japan (51).

To use gas in diesel engines is an old idea. Actually, Rudolf Diesel planned to run his engine on gaseous fuel more than 100 years ago. Tankers carrying gas (LNG and LPG) have in many years used the inevitable boil-off from the cargo tanks as a supplementary fuel in the boilers for steam

[1] Numbers in brackets refer to the references in "Bibliography".

turbines. The use of gaseous fuels in diesel engines has been a research activity at the Marine Technology Centre (MTS) in more than 20 years (45, 46). The use of the VOC from the vent gas, however, gives a lot of new challenges and requires special solutions for successful engine operation.

A number of research programmes are carried out (1, 7, 8), and several methods have been tested to solve the problems caused by VOC emission from a lot of different sources and industries. Re-absorbing the VOC gas is a common solution in most of these programmes, and even Statoil has developed a system to handle the VOC emission by this method (9). However, no references are found, indicating that the method Statoil and MAN B&W (9, 10) has chosen to solve the problem with emission of VOC has been proposed by others. This method, using VOC from the *vent gas* in large diesel engines is new, and will when successfully implemented reduce both VOC emission and fuel consumption.

1.2 Motivation and objectives

The VOC in the vent gas consists of a mixture of hydrocarbons with different physical properties and are well suited as engine fuel. "Light" components (methane and ethane) and "heavy" components (propane, butanes and pentanes) are all parts of the VOC blend.

The light fraction (methane and ethane) with methane being the main component in natural gas (NG) has been used as fuel in internal combustion engines for a long time. One way of using NG is mix gas and air and charge the mixture to the engine through the air intake and ignite the charge with a diesel fuel spray (pilot spray). A more common concept is ignition by a spark plug.

The heavy components ("VOC Fuel") have never been adopted as a commercial fuel for diesel engines.

From an environmental point of view, the use of any gaseous fuel as a replacement of diesel fuel and especially heavy fuel oil (HFO) is a positive contribution to the offshore pollution situation. The contribution of gaseous pollution from ships is considerable, but no legislation has been applied to reduce exhaust pollution offshore until lately. IMO introduced the first emission legislation controlling NO_X emission in January 2000. Emission of particulate matter (PM) is not yet included, but legislation is expected soon. As to PM emission the introduction of gas will give significant reductions.

The idea of using VOC released from shuttle tankers as replacement for diesel fuel or HFO on board ships has 3 objectives:

a) – it is a way of saving fuel
b) – it is a contribution for reducing exhaust pollution
c) – it is a very effective way of reducing VOC emission to the atmosphere

There are two basic methods to use the vent gas to be considered:

i) – condensation of the heavy fraction and injection as a liquid fuel
ii) – feeding the vent gas in the charge air system with pilot fuel ignition

If the first method is chosen, a residual gas fraction will remain after condensation. This fraction contains inert gas and mainly methane in addition to ethane. The energy content of the residual gas fraction is considerable and should be utilised too (cf. section 6.1 and 6.3).

In order to learn more about the ignition and combustion of the hydrocarbons present in the VOC Fuel, the work presented here was initiated in co-operation between the Department of Marine Engineering, NTNU and Statoil R&D, Trondheim.

To simplify the test work in the laboratory, a combustion test rig – a rapid compression machine called "DyFo" – was prepared to simulate the diesel engine process.

1.3 Scope of work

Several studies are published about the diesel engine performance with NG. The main component in NG is methane. The "heavy" components present in the VOC are, however, not normally present in the gas used for Diesel engines. The engine performance when using those components as fuel is not fully explored yet.

Ignition and combustion in diesel engines is very complicated. The work presented in this thesis is limited to give a contribution to the following two questions:

1. Is it likely that use of VOC Fuel causes any significant differences in ignition and combustion performance in a diesel engine compared to diesel fuel?

2. Do the VOC components influence the performance?

The presentation of the work reports different tests carried out with VOC. The main part of the work covering high-pressure injection of VOC Fuel ignited by a pilot fuel spray, is a study of ignition and early combustion of different heavy components present in the VOC:

- pure propane
- pure iso-butane
- pure n-butane
- a mixture of propane, iso-butane and n-butane

The effects of varying some engine parameters are reported as a main part of the work reported in this study.

The utilisation of the "residual VOC" and ignition and combustion properties of a homogenous charge of air and "residual VOC" is a minor part of the study. The tests are performed with variation of excess air ratio (λ) as the only parameter.

Intentionally, the use of light VOC components captured in hydrates was to be intensively studied too, but of different reasons, this has ended up as an additional, minor part of the work.

Video pictures of injection, ignition and early combustion are an important part of the work. In the test rig used it is possible to take pictures in 2 directions, but mainly one direction is used for analysis. In this presentation, a few numbers of pictures are shown together with the analysis. More pictures are found in the Appendices.

1.4 Framework of the thesis

The thesis consists of three main sections. The first section gives a description of the VOC emission in the North Sea and introduces the fundamental processes in combustion of fuel in a diesel engine (or a test rig like the DyFo) (chapter 2 & 3). Section two describes the methods of investigation (chapter 4 & 5), and section three contains results, discussion and conclusions (chapter 6 – 9).

Chapter 2 describes the origin of VOC and what it is. In some more detail the release and composition of VOC from the shuttle tanker loading process in the oil fields is outlined.

Chapter 3 describes the relevant basics of the Diesel process. Fuel injection, ignition and combustion including the chemistry of hydrocarbon fuels in the diesel process in theory and linked to the experience from the DyFo test rig are covered.

Chapter 4 gives a description of the imaging theory by the Schlieren technique and shows some examples of phenomena captured by this imaging method.

Chapter 5 describes the DyFo test rig, necessary developments and changes made for the experiments. The experimental test matrix is described.

Chapter 6 presents the results from the first part of the work (the main part) covering high-pressure injection of VOC Fuel ignited by a pilot fuel spray. Plots of dynamic signals (cylinder pressure and injector needle lifts), computed values of Rate of Heat Release (ROHR) & accumulated heat release (AROHR) in addition to images (video frames) of the injection, ignition and early combustion constitute the presentation.

Chapter 7 presents the test results and shows selected video pictures from the second part of the work - the additional work carried out with homogenous combustion of "residual VOC".

Chapter 8 describes the idea of using hydrates, the possibility to trap VOC inside and what will be the result of burning VOC released from hydrates. Some test results with methane injected into the DyFo are presented.

Chapter 9 discusses the results and contains the conclusions of the work. Recommendations for further work are also given.

2 VOC as an engine fuel.

2.1 Basic characteristics of VOC

Volatile Organic Compound (VOC) is the common name of chemical species – especially hydrocarbons - that are easily evaporated. Just like crude oil, a lot of other chemicals contain light, volatile components that evaporate when handled. In addition, VOC is formed by combustion.

VOC is undesired mainly because it forms ground level ozone by reacting with oxides of nitrogen (NO_X) in the presence of sunlight. Ozone is detrimental to plants and harmful to eyes and lungs of humans and animals. The emission of VOCs is divided in two main parts – non-methane VOC (NMVOC) and methane (CH_4). The reason for this division is that methane is much less reactive than other VOC components.

The emission figures from different sectors are somewhat uncertain and different statistics exist. Table 2.1 shows the latest calculated distribution of NMVOC and CH_4 according to Statistics Norway (Statistisk Sentralbyrå, SSB) (11).

Table 2.1 Official statistics of the 1995 VOC emissions in Norway (11).

	NMVOC (Tonnes)	CH_4 (Tonnes)	Total (Tonnes)
Oil industry	**221 606**	**28 563**	**250 169**
- Crude oil	215 110	15 095	230 205
- Natural gas	6 484	12 468	18 952
- Petrol coke	12	992	1 004
- LPG	0	8	8
Heating	**13 706**	**14 643**	**28 349**
- Gas	1 426	177	1 603
- Paraffin	725	62	787
- Oil	281	63	344
- Wood etc.	11 274	14 341	25 615
Coastal transport	**3 028**	**421**	**3 449**
- Marine fuels	2 651	365	3 016
- Special distillate	257	31	288
- HFO	120	25	145
Road traffic	**91 672**	**1 803**	**93 475**
- Auto petrol	85 402	1 637	87 039
- Auto diesel	6 270	166	6 436
Agriculture	**-**	**96 545**	**96 545**
- Manure	-	16 363	16 363
- Animals	-	80 182	80 182
Waste disposal (refuse)	**340**	**322 137**	**322 477**
Solvents	**44 656**	**-**	**44 656**
Coal, coal coke	**1 839**	**5 267**	**7 106**
Nutrients	**774**	**-**	**774**
Total	**377 615**	**469 370**	**856 985**

The emissions from the different sources are calculated in an emission model by SSB (12). If new emission factors or data are found, the emissions for previous years are recalculated. For

this reason, the values in the emission tables of VOCs in Norway can vary according to the date of publication. The emission values for 1995 shown in Table 2.1 are published in 2000.

The statistics used by Statoil (9) in the feasibility study report for the conversion of "Navion Viking" is based on different data and contain values listed in Table 2.2 below.

Table 2.2 Emission of non-methane VOC (NMVOC) in Norway, 1995 (9).

	NMVOC emission (Tonnes)	NMVOC emission (%)
Oil industry (crude oil loading off-shore)	200 000	58
Road traffic	76 000	22
Solvents	33 000	10
Other domestic industry	24 000	7
Heating	11 000	3
Total	344 000	100

The methane content in the VOC release by crude oil loading offshore is assumed to be 2 - 19 wt% on the different oil fields. The content of methane at Statfjord (2,1 wt%) and Gullfaks A (18,9 wt%) makes the basis for these limits (cf. Figure 2.1). An estimate of the methane emission based on the mean value gives about 23 000 tonnes of methane. This amount is 50 % more than given by official statistics (cf. Table 2.1), but is probably more correct and is used in the further calculations.

Why do oil tankers emit VOC? The reason is as follows: The oil vapour (VOC) released in the crude oil cargo tanks is left in the tanks together with air after unloading the crude oil. The oil vapour makes an explosive mixture with the air in the empty cargo tanks if no precautions are taken. To prevent the oil vapour/air mixture to explode, the tanks are topped up – and the VOC mixed - with inert gas consisting of cleaned exhaust gas from the main engine of the tanker or produced in separate inert gas generators. The inert gas normally contain about 83 % N_2, 5 % O_2 (must be less than 8 %!) and 12 % CO_2. In the 1970s - when the cargo capacity of new crude oil tankers increased to about 500000 DWT and before the filling of tanks with inert gas was mandatory - this phenomenon led to many severe accidents and several VLCCs[2] were lost on the seven seas.

2.2 Characteristics of VOC from North Sea oil fields.

When starting the loading process of crude oil, the cargo tanks nowadays are filled with inert gas. This has been done during the previous unloading. During loading, the gas phase composition above the crude oil changes from pure inert gas to a mixture of inert gas and an amount of increasing light hydrocarbon components, typically as shown in Figure 2.1 (right Figure). The fraction of hydrocarbons in the vent gas mixture is denoted Alfa. The VOC mixture from the crude oil tanks consists of many different components. Figure 2.1 (left Figure) shows typical compositions from two actual oil fields in the North Sea.

Table 2.3 shows some typical properties of the components in the vent gas at different times during loading a typical shuttle tanker. For the Statfjord field, Alfa is 0,2 at the start of the loading process and 0,7 at the end of the loading process (3).

[2] VLCC = Very Large Crude Carrier

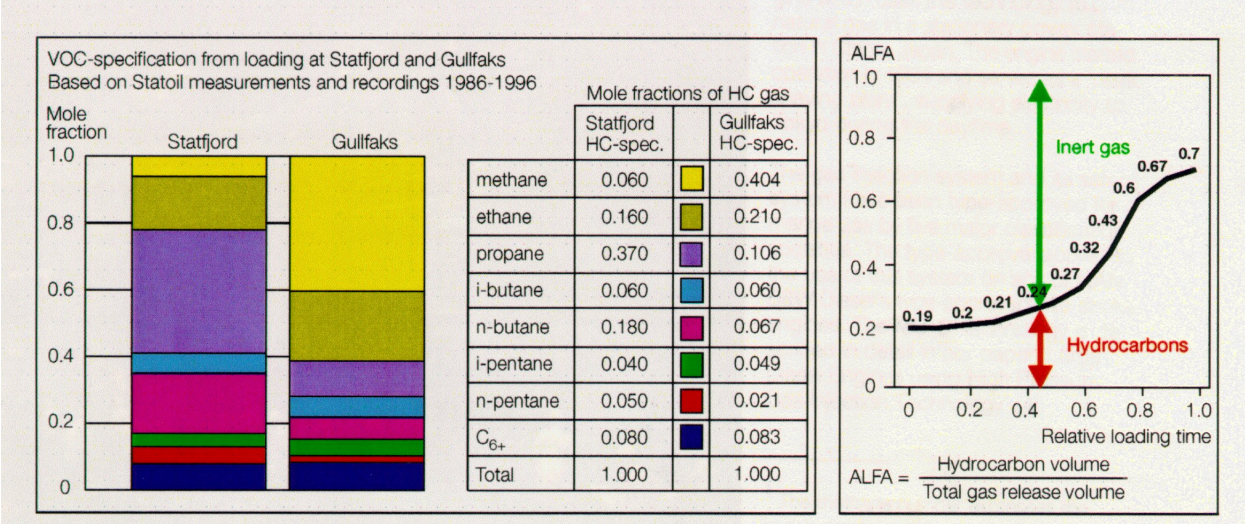

Figure 2.1 Composition of VOC and vent gas from two oil fields in the North Sea (2).

Table 2.3. Typical raw vent gas properties at different loading times (Statfjord oil field) (13).

Raw VOC - Statfjord				Alfa = 0,2			Alfa = 0,7		
	LHV	**Density (273 K, 1 atm)**		**Mole fraction**	**Volume**	**"Power"**	**Mole fraction**	**Volume**	**"Power"**
	(MJ/Sm^3)	**(kg/kmol)**	**(kg/Sm^3)**	**(-)**	**(Sm^3/s)**	**(MJ/s)**	**(-)**	**(Sm^3/s)**	**(MJ/s)**
CH_4	35,833	16,04	0,716	0,020	0,080	2,87	0,056	0,224	8,022
C_2H_6	64,438	30,07	1,342	0,036	0,144	9,27	0,126	0,504	32,46
C_3H_8	92,919	44,10	1,969	0,072	0,288	26,74	0,252	1,007	93,60
iC_4H_{10}	121,667	58,12	2,595	0,014	0,056	6,80	0,049	0,196	23,83
nC_4H_{10}	123,611	58,12	2,595	0,032	0,128	15,81	0,112	0,448	55,34
iC_5H_{12}	125,000	72,15	3,221	0,010	0,040	5,00	0,035	0,140	17,49
nC_5H_{12}	130,000	72,15	3,221	0,008	0,032	4,16	0,028	0,112	14,55
Higher alkanes	140,000	86,18	3,847	0,012	0,048	6,72	0,042	0,168	23,51
N_2	0	28,01	1,251	0,676	2,702	0	0,255	1,019	0
CO_2	0	44,01	1,965	0,080	0,320	0	0,030	0,120	0
O_2	0	32,00	1,429	0,040	0,160	0	0,015	0,060	0
Sum	-	-	-	1,000	4,000	77,37	1,000	4,000	268,80

In order to reduce the emission of harmful hydrocarbons to the atmosphere, Statoil has as Step 1 in the "VOC Fuel project" modified one of their shuttle tankers to use "condensed VOC" (3). The idea is to liquefy the part of the VOC that easily (and economically!) can be condensed, i.e. components with 3 or more carbon atoms (propane, butane, pentane and hexane), for convenience called "VOC Fuel". Different methods have been discussed by the oil industry to prevent the uncondensed, light VOC fraction (methane and ethane) from escaping to the atmosphere. It is a very costly process to separate this fraction from the inert gas by condensation, as the boiling temperature for methane and ethane is –161,5 and –88,6 ^oC respectively. In the above-mentioned project, methane and ethane will therefore not be utilised as fuel until better technology is developed.

On board "Navion Viking" the heavy hydrocarbon components present in the VOC are condensed and separated from the light ones and stored in a separate tank as VOC Fuel. They are all gaseous at temperatures higher than - 42 °C, cf. Table 2.4 (14, 15). For best efficiency of the condensation process the VOC is compressed and cooled. For all components to remain liquid when used for combustion, the VOC Fuel has to be stored at an elevated pressure.

Table 2.4 Some physical properties of the VOC components (15).

Property		Methane	Ethane	Propane	n-Butane	iso-Butane	iso-Pentane	Neo-pentane	n-Pentane
		CH_4	C_2H_6	C_3H_8	n-C_4H_{10}	i-C_4H_{10}	i-C_5H_{12}	C_5H_{12}	n-C_5H_{12}
Density	(kg/kmole)	16,043	30,07	44,096	58,123	58,123	72,15	72,15	72,15
Density (#STP)	(kg/Nm^3)	0,7158	1,3416	1,9674	2,5932	2,5932	3,2190	3,2190	3,2190
Critical Temperature	(K)	190,58	305,42	369,82	425,18	408,14	460,43	433,76	469,65
Critical Pressure	(MPa)	4,604	4,880	4,249	3,797	3,848	3,361	3,199	3,369
Melting Point	(K)	90,87	90,35	85,44	134,86	113,54	113,25	256,58	143,42
Normal Boiling Point	(K)	111,66	184,56	231,11	272,65	261,43	300,99	282,85	309,22
Std. Net Heat of Combustion	(MJ/kmole)	-802,3	-1428,8	-2043,1	-2657,5	-2649,0	-3240,3	-3250,4	-3250,4
Refractive index at 298 K	(-)	1,0004	1,0047	1,2881	1,3292	1,3292	1,3509	1,3390	1,3547
Flammability Limit, Upper	(vol%)	15	12,5	9,5	8,5	8,5	7,6	7,5	7,8
Flammability Limit, Lower	(vol%)	5	3	2,1	1,8	1,8	1,4	1,4	1,4
Autoignition Temp.	(K)	873	788,15	723,15	678,15	678,15	693,15	723,15	533,15

2.3 Benefits of using VOC as replacement for HFO.

When using VOC Fuel onboard shuttle tankers, several benefits for the environment are obtained. First of all the emission of VOC is reduced. Second, exhaust pollution is reduced as burning VOC instead of HFO produces less CO_2 and NO_X, sulphur and particulates.

The total release of VOC is, as shown in section 2.1, assumed to be 223000 tons per year. In the example below the CO_2 emission by releasing the VOC and burning HFO is compared to the amount of the CO_2 emission when substituting the HFO with VOC.

The VOC consists of approximately 23000 tons methane and 200000 tons of NMVOC, cf. section 2.1. The greenhouse effect of methane is 21 times larger than the effect of CO_2. Contrary to methane, the NMVOC is today treated as oxidising to CO_2 in the atmosphere - a practice considered very conservative by Norwegian authorities (48). Burning one ton of HFO gives approximately 3,2 tons of CO_2 whereas one ton of NMVOC corresponds to approximately 3,0 tons of CO_2.

Table 2.5 sums up the two cases described above if all VOC otherwise released is burned. The VOC Fuel is ignited by pilot injection of HFO which amount 10% of the total energy input to the engine. The cases represent the worst and the best environmental conditions. In the first stage, the light VOC fraction (methane and ethane) will not be utilised, reducing the benefit for the environment compared with the results tabulated in Table 2.5.

Table 2.5 Release of CO_2 equivalents in case of releasing and burning VOC.

	Equivalent CO_2 emission (tons) to the atmosphere		
	CASE #1 – releasing VOC		CASE #2 – burning VOC
	Unburnt release	Burnt release	Burnt release
Methane	483 000	-	63 250
Non-methane	600 000	-	600 000
HFO	-	713 000	71 300
Total	1 796 000		734 550

The total saving for the environment is more than 1 million equivalent tons of CO_2 when burning all VOC compared to releasing it to the atmosphere.

When using VOC as a fuel no extra solutions reducing the exhaust pollution to the minimum possible should be necessary. The main purpose is to reduce the release of the VOC. Besides the exhaust pollution from an engine run on VOC is most certainly, in any case, far lower than if the same engine is using liquid fuel, which in the case of shuttle tankers means heavy fuel oil.

The environmental aspects of the alternative of releasing or burning the VOC emitted from the shuttle tankers in the North Sea are not discussed any further in this work. Even if it is very interesting and was a strong motivating factor in initiating the project converting the "Navion Viking", it is not a part of the study reported in this thesis.

2.4 Utilising VOC emitted at the oil fields

The ideal solution of the "VOC problem" would be to use all the components evaporated from the crude oil for combustion. This would be theoretically possible but in practice, the light and the heavy fractions have to be handled by different systems.

The VOC evaporated during handling can be used in a diesel engine in various ways. In the following, different ways of using gas in diesel engines are listed with names of the specific processes:

1. «Standard Otto Process»: VOC mixed with air at low pressure to a homogeneous charge and fed into the cylinders for compression and combustion as a gas and ignited by a spark plug in an Otto process.

2. «Direct Injection Otto Process»: VOC injected at high pressure as a compressed gas into the cylinders near TDC and ignited by a spark plug as in an Otto process.

3. «Dual Fuel Diesel Process»: VOC mixed with air at low pressure to a homogeneous charge and fed into the cylinders for compression and combustion as a gas and ignited by pilot injected diesel fuel in a Diesel process.

4. «Gas Diesel Process»: VOC injected at high pressure as a compressed gas into the cylinders near TDC and ignited by pilot injected diesel fuel in a Diesel process.

5. «Condensate Diesel Process»: VOC condensed to liquid phase, pressurised and injected at high pressure as liquid fuel and ignited by pilot injected fuel – diesel or HFO - in a Diesel process.

6. by a combination of method 3 and 5.

3 Fundamentals of the Diesel process.

In the study reported in this thesis the attention is focused on the "heavy", condensed fraction of the VOC – the VOC Fuel - and the combustion tests have been performed using the «Condensate Diesel Process» (cf. section 2.4). The residual VOC has also been given some attention. In Chapter 7 use of this energy resource is discussed. Chapter 8 gives a brief introduction to another concept for using the residual VOC.

In the following sections, a review of the sequence of events of the Diesel combustion process is given. Fuel injection, fuel ignition and combustion in diesel engines are presented. The details of the three events vary, according to the relevance to the experimental work referred to.

3.1 Fuel injection

The fuel is injected into the cylinder through an injection nozzle to ensure atomisation and good mixing with air. Today control of the injection characteristics is easy to obtain by means of electronics. In production diesel engines a cylinder pressure of 50 – 100 bars and an injection pressure of 200 – 2000 bars are normal depending on the type and size and operating load of the engine. The forces thus acting upon the fuel will atomise it into small droplets to enable rapid evaporation. It is important that the droplets still have enough momentum to traverse the cylinder to mix it as effectively as possible with the charge air. Studies of fuel spray behaviour normally cover the following factors (cf. Figure 3.1):

- the fuel spray angle q
- spray tip penetration S
- mass fuel delivery rate dm_f/dt

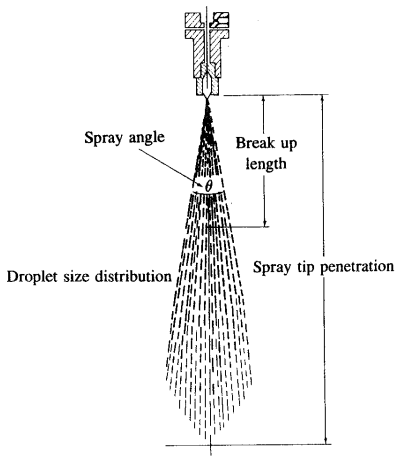

Figure 3.1 Definition of parameters in the fuel spray (17).

Spray tip penetration S and mass fuel delivery rate dm_f/dt are vital factors for the performance of engines – and of particular interest in the DyFo test rig in this study. Evaluating engine performance when using different fuel types must take into account the difference in these two parameters. Gaseous fuels and marine diesel fuels have very different densities and viscosities. Engines designed to use both fuel types are equipped with separate injection systems to account for these differences.

Figure 3.2 shows examples of injection of VOC Fuel (i.e. propane) into air. In the DyFo test rig special attention was given to the design of injection systems for both pilot fuel and VOC Fuel. The systems and nozzles are described in more detail in section 5.1. The spray angle q can be found from these pictures.

Figures 3.3 and 3.4 show artificial coloured Schlieren images of a diesel spray in compressed air made in the DyFo. The images are originally greyscale pictures. Artificial colours are added from a so-called Look-Up-Table (LUT) in the software where each level in the greyscale corresponds to a unique colour. Different LUTs are available in the image-processing program, NIH Image (52). A LUT called FIRE1 giving colours resembling the normal visual impression of a flame is used. Figures 3.3 - 3.5 show FIRE1 coloured images of diesel and propane

injections without combustion in the DyFo. The timing of the images is set relative to the start-of-injection signal to the fuel injectors.

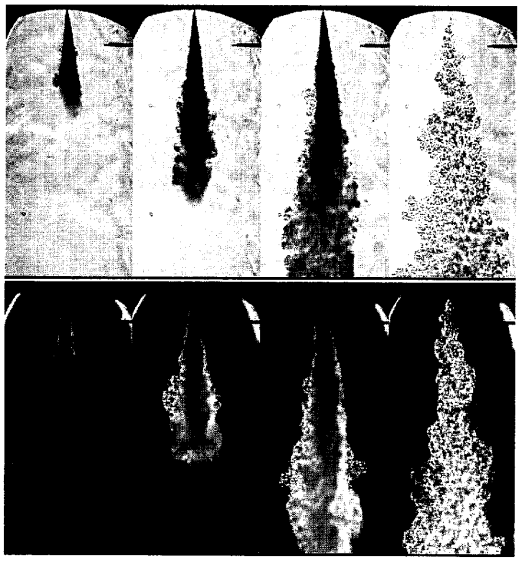

Figure 3.2 Shadowgraph (top) and Schlieren (bottom) images of liquid propane injected into air (16).

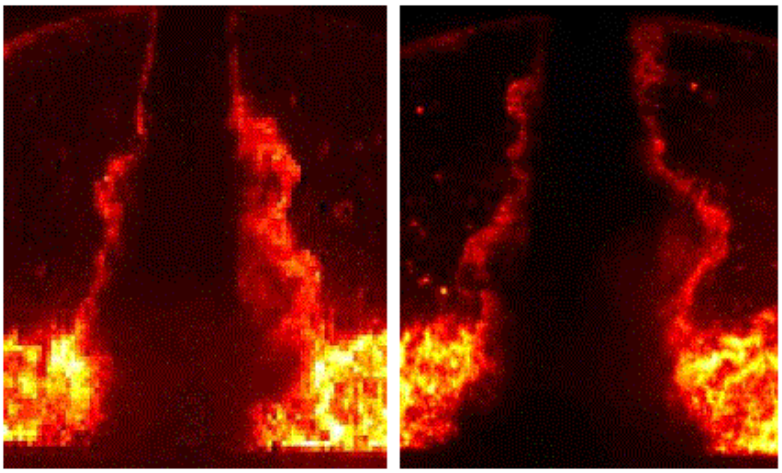

Figure 3.3 Images of consecutive injections of pilot diesel fuel in the DyFo taken prior to ignition at the same timing.

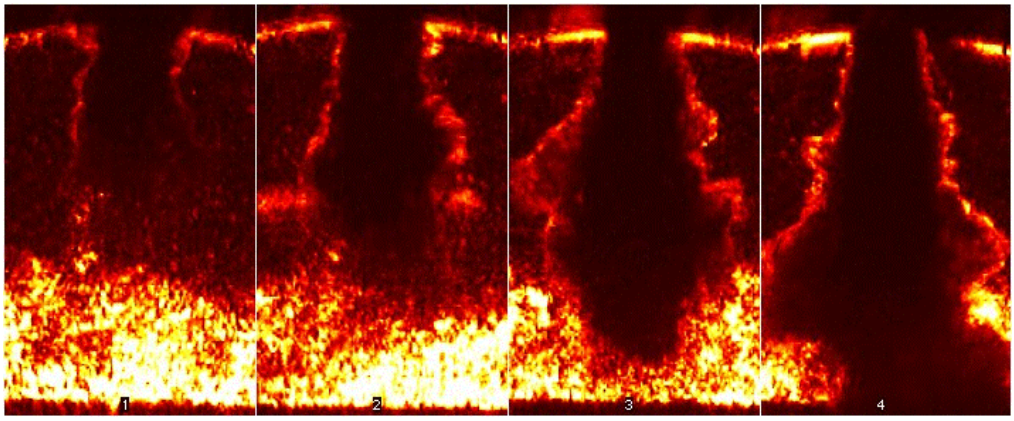

1,5 ms 1,6 ms 1,7 ms 1,8 ms

Figure 3.4 Images of consecutive injections of pilot diesel fuel in the DyFo taken prior to ignition at different timing.

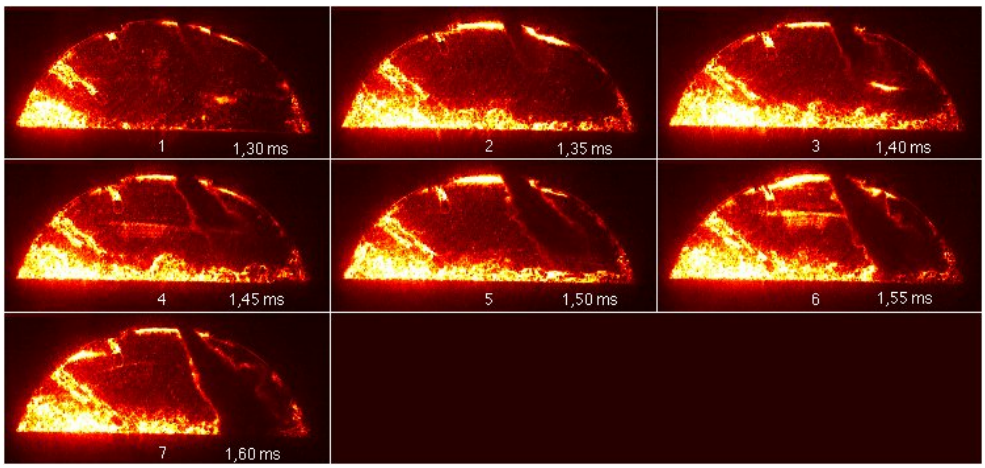

Figure 3.5 Images of consecutive injections of liquid propane in the DyFo taken prior to ignition at different timing.

3.1.1 Fuel spray penetration and atomisation related to DyFo experiments.

The distance a spray travels across the combustion chamber depends on the nozzle geometry and the fuel and charge air densities and pressures. In addition in a real engine, the turbulence in the combustion chamber is of vital importance. In a diesel engine it is desirable to mix the fuel with the charge air before it reaches cool surfaces (cylinder wall and/or piston top). Still it is essential that the spray does not split up too early since this will reduce the volume of air available for fuel mixing. The distance S (in mm) the fuel spray tip travels can be modelled by many techniques of different complexity. One method is to create an empirical correlation equation based on regression analysis of measured data expressed by equation 3.1.1[3] (17) and equation 3.1.2 (18, 19):

$$S = 3.07\left(\frac{\Delta p}{r_g}\right)^{1/4}(td_n)^{1/2}\left(\frac{294}{T_g}\right)^{1/4} \qquad (3.1.1)$$

$$S = 2{,}95\left(\frac{\Delta p}{r_g}\right)^{1/4}(td_n)^{1/2} \qquad (3.1.2)$$

Dp - pressure drop across the nozzle (Pascal)
r_g - gas density inside the combustion chamber (kg/m^3)
t - time after the start of injection (ms)
d_n - nozzle hole diameter (m)
T_g - gas temperature inside the combustion chamber (K)

For gas temperatures above 345 K equation 3.1.2 will give higher values than equation 3.1.1 [2,95 > 3,07(294/T_g)^{¼}]. The calculated gas temperature in the experiments is about 650 K. Measured values of spray penetration correlate best with the lowest values calculated and therefore equation 3.1.1 is used.

In the first part of injection, when the spray is concentrated and the penetration is shorter than the "break up length" in Figure 3.1, the travel is according to equation 3.1.3 (17):

$$S = 0.39(2\Delta p / r_l)^{0,5} \cdot t \qquad (3.1.3)$$

[3] Valid for nozzles with $2 \le L_n/d_n \le 4$ and cylinder pressure < 100 atm. (17).
L_n – length of nozzle hole

To obtain a good combustion of the VOC Fuel, it is favourable that the travel and penetration of the spray tip is of the same length as for diesel fuel. In a test rig the spray behaviour should resemble the "real life" obtained in a diesel engine.

In the DyFo, the spray tip travel of both the VOC Fuel and the pilot diesel fuel is undisturbed for less than 1 ms or a distance of about 25 mm. By this time/distance the pilot fuel spray reaches the piston top and the VOC Fuel spray reaches the piston top and/or the cylinder wall. The ignition delay of the pilot fuel is longer and the fuel is bouncing back into the combustion chamber. With the present, fixed geometry of the test rig, few things can change this undesired situation. Two possibilities were however checked out prior to the start of the experiments:

1) reducing the stroke to extend the free travel path of the fuel sprays
2) use a pilot fuel with an ignition delay shorter than the "free travel" time

The first measure implies that the compression ratio and thus the end compression temperature are reduced causing an increased ignition delay. The second measure was impossible to fulfil, as the ignition delays obtained in the DyFo, even with high-quality fuels, never was less than 1 ms.

For the evaluation of test results, it is of importance to find any differences in the performance of the DyFo test rig compared to real production engines prior to and during the ignition and combustion. The DyFo fuel injection process as described above, is not typical for production engines. However, this type of injection actually exists in diesel engines too, especially in small engines at part load. The injection pressure is then reduced due to the dynamics of the injection system resulting in bigger fuel droplets. This increases the ignition delay and may very well lead to fuel droplets hitting cool surfaces as in the DyFo.

Verification of correspondence between the measured spray penetration of pilot diesel fuel from the images in Figure 3.4 and the calculated spray penetration using the correlation formulas 3.1.1 and 3.1.3 is shown in Figure 3.6. For VOC fuel injection, verification of correspondence between reality and theory based on measured spray penetration (cf. Figure 3.5) and calculated spray penetration using the formulas 3.1.1 and 3.1.3 is shown in Figure 3.7.

The conditions applying to the tests are shown in Table 3.1 below. Cylinder pressures are shown in detail in Appendix 4. A pressure interval is indicated for VOC Fuel because different RIT means that the VOC Fuel is injected by different piston positions and thus different cylinder pressures.

Table 3.1 Conditions applying to the DyFo experiments verifying correspondence between theory and practice.

	Test (test series)*	Pilot diesel fuel	VOC Fuel
Cylinder pressure, p_g (bar) by the start of injection	112113 (1121)	57	59 (54–66)
	121113 (1211)	44	45 (42-49)
	122123 (12212)	60	60 (60-66)
	122113 (12211)	57	59 (55-67)
	121213 (1212)	44	45 (43-47)
Injection pressure, p_i (bar)		400	400
Nozzle hole diameter, d_n (mm)		0,35	0,55
Gas density, r_g *(kg/m^3)*		$p_g/(R_gT_g)$ **)	$p_g/(R_gT_g)$ **)
Injection delay registered (ms)		1,30 ± 0,05	1,20 ± 0,05

* *Explanation of test numbering cf. section 5.1.6.*

**) *By using $r_g = p_g/(R_gT_g)$ (gas constant R_g = 287 J/(kg K)), the temperature is cancelled in equation 3.1.1.*

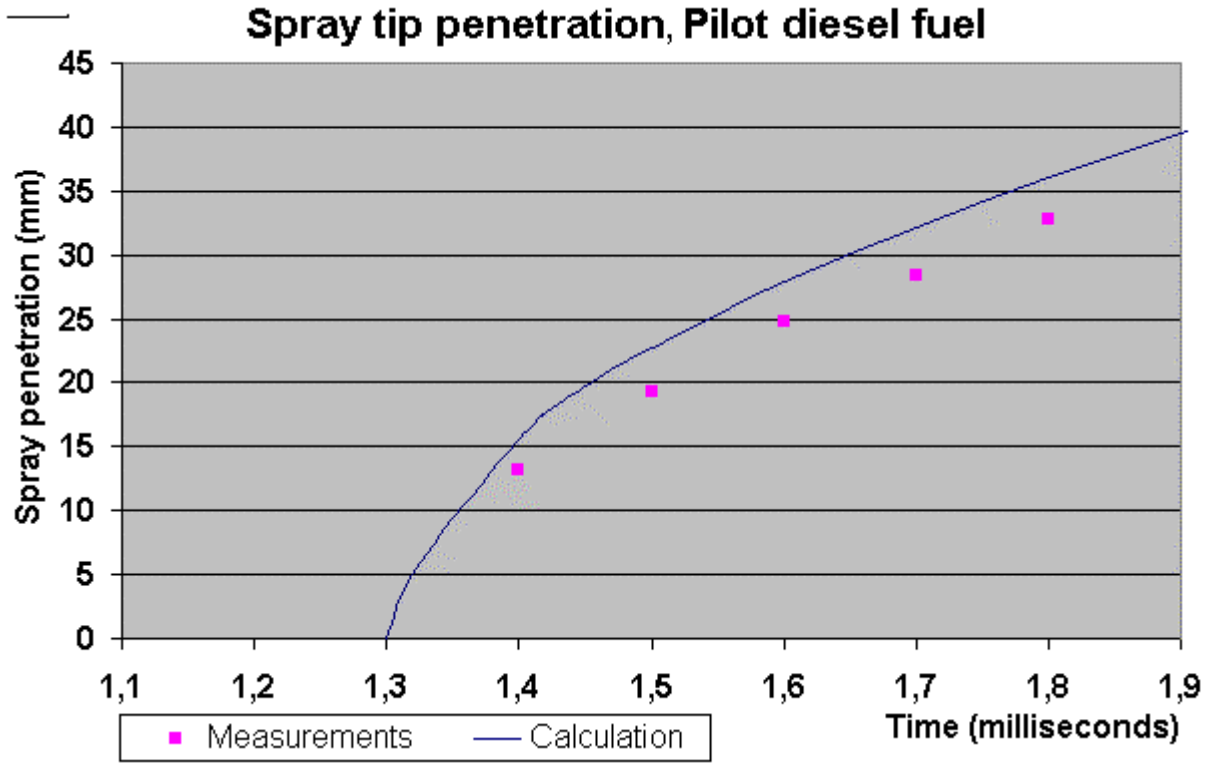

Figure 3.6 *Measured and calculated spray penetration of pilot diesel fuel in the DyFo. Time is relative to signal for start of injection.*

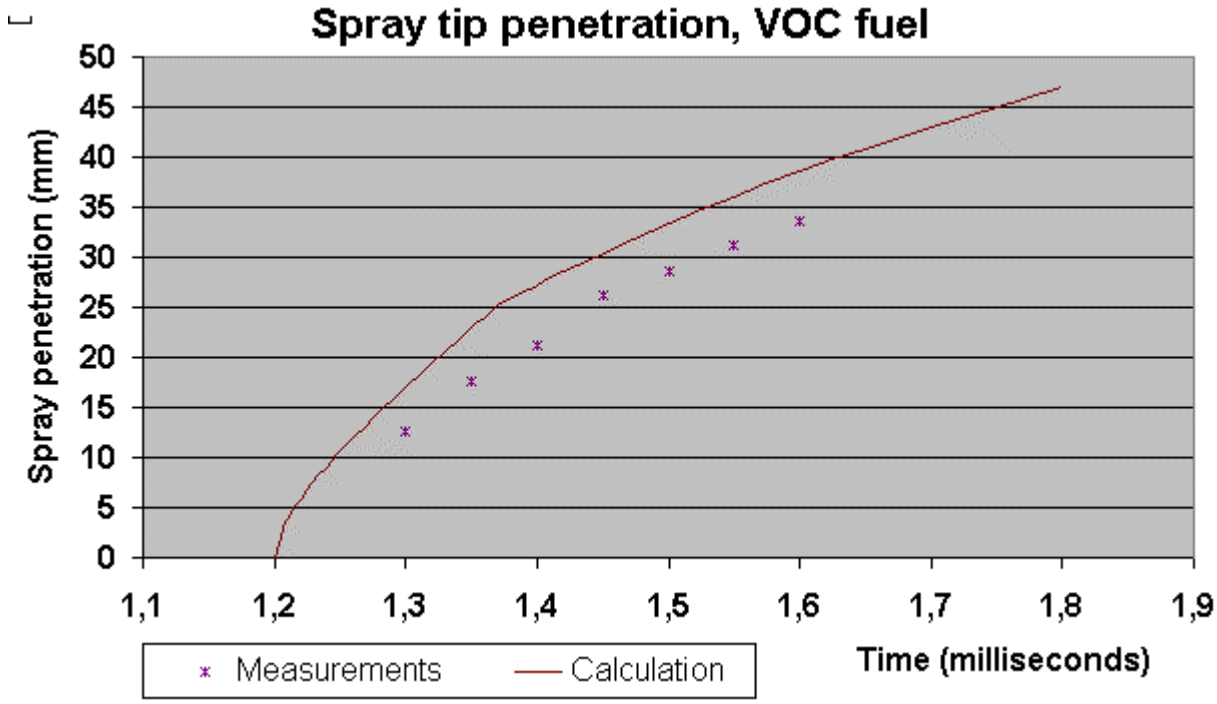

Figure 3.7 *Measured and calculated spray penetration of VOC fuel in the DyFo. Time is relative to signal for start of injection.*

As indicated by Figure 3.6 and 3.7 the fuel spray behaviour of both pilot diesel fuel and VOC Fuel seems to be in good agreement with classical theory.

Measurements always contain some uncertainties that affect the agreement between theoretical expressions and measurements. The accuracy of time measurements is ±0,05 ms (cf. section 5.1.3 "Pilot diesel fuel injection timing"). A time lag of 0,05 ms less for the measurements than indicated in Figures 3.6 and 3.7 will make the agreement with the theory nearly perfect!

3.1.2 Fuel mass delivery

When injecting fuel into a single shot test rig it is a problem to measure the fuel mass delivered through the nozzle. Since the operation is discontinuous, it is not possible to measure the fuel mass delivered as a mass flow with standard equipment. It is necessary to find the amount of fuel delivered by every single injection, and the calibration of the nozzle has to be carried out outside the combustion chamber. This means a change of the operational conditions for injection compared to inside the test rig.

To correct the real fuel mass delivery, a model for injected mass flow (dm_f/dt) through a nozzle is used. Equation 3.1.4 is a common model for this mass flow (17) and equation 3.1.5.applies to the injected mass m_f .

$$\dot{m}_f = dm_f / dt = C_D A_n \left(2 r_f \Delta p\right)^{0,5} \qquad (3.1.4)$$

$$m_f = C_D A_n \left(2 r_f \Delta p\right)^{0,5} \cdot \Delta t \qquad (3.1.5)$$

C_D – discharge coefficient (-)
A_n - nozzle minimum area (m^2)
r_f - fuel density upstream the nozzle (kg/m^3)
Dp - pressure drop across the nozzle (Pa)
Dt - open period of the nozzle (s)

Assuming that C_D is constant for a pressure drop variation across the nozzle in the region of 300 – 400 bars and that the open period of the nozzle is kept constant, the change in fuel mass injected can be calculated by using equation 3.1.5 to create the expression shown below:

$$\frac{m_{f,op}}{m_{f,cal}} = \frac{C_D A_n \sqrt{2 r_{f,op} \Delta p_{op}}}{C_D A_n \sqrt{2 r_{f,cal} \Delta p_{calp}}} \cdot \frac{\Delta t_{op}}{\Delta t_{cal}} = \frac{\sqrt{r_{f,op} \Delta p_{op}}}{\sqrt{r_{f,cal} \Delta p_{cal}}} = \sqrt{\frac{r_{f,op}}{r_{f,cal}}} \sqrt{\frac{\Delta p_{op}}{\Delta p_{cal}}}$$

$$m_{f,op} = m_{f,cal} \sqrt{\frac{r_{f,op}}{r_{f,cal}}} \sqrt{\frac{\Delta p_{op}}{\Delta p_{cal}}} = m_{f,cal} \cdot r - factor \cdot \Delta p - factor$$

Subscript *op* denotes values present by operation and *cal* denotes values by calibration.

Both injection systems at the DyFo are operated at a pressure of 400 bars. The injection of pilot fuel and VOC Fuel are made at nearly the same time and thus at equal conditions in the cylinder (cf. Table 3.1). In addition both systems are subject to the same variation in the fuel temperature, which will affect the fuel density and thus the fuel mass delivery.

How these two facts affect the fuel mass delivery in the experiments is shown in Section 5.1.5.

3.2 Fuel ignition

In internal combustion engines, the ignition is important for the engine performance. If it were purely a chemical phenomenon, section 3.3.3 - combustion chemistry of hydrocarbons - would cover the process. In addition to the chemical reactions, however, thermal considerations are of vital importance for ignition of the fuel (20). In the literature two main principles of ignition are described, *forced ignition* and *spontaneous ignition*. Forced ignition is performed by an external energy source like a spark, hot surface, pilot flame, shock wave etc. (18). Spontaneous ignition is defined as follows: "*when a reactive mixture is formed, raised to a definite temperature and pressure, and then left alone, it may burst into flame after a certain time"*. At the moment of spontaneous ignition, there is normally a rapid temperature rise, light radiation and rapid chemical reactions (21).

According to the definitions above, the pilot fuel in the DyFo ignites by spontaneous ignition, while the VOC Fuel is ignited by forced ignition.

The temperature necessary for spontaneous ignition to occur is defined as the self-ignition temperature of the fuel. In diesel engines the fuel ignites when this self-ignition temperature level is reached. The time it takes for the fuel-air mixture to reach this temperature is an important property of the fuel. Measured from the instant of the start of fuel injection, the induction time until ignition occurs is called the *ignition delay* (cf. section 3.2.3).

3.2.1 Classical thermal ignition theory

One general definition of ignition is *the process of transition from a non-reactive state to a reactive state leading to a thermo-chemical runaway followed by a self-sustained combustion process* (21). In the reaction chamber two main processes governing the ignition takes place:

1. Heat is generated by chemical reactions, $\dot{q}_R$
2. Heat is transported away from the reaction to the chamber walls, $\dot{q}_L$

In other words, the process is to a great extent governed by thermal conditions present in the combustion chamber and is often referred to as a *thermal spontaneous ignition*. Mathematically the ignition process can be described by the equation of overall energy conservation for a control volume *V*:

$$\dot{q}_R - \dot{q}_L = rc_V V \frac{dT}{dt} \qquad (3.2.1)$$

The right hand side of Eq. 3.2.1 expresses the energy accumulated in the control volume *V* and the temperature change *dT* pr. unit time *dt*. The condition for ignition is present when the rate of thermal energy release $\dot{q}_R$ by the chemical reactions becomes greater than the thermal energy loss $\dot{q}_L$. The heat loss can be expressed by the linear function expressed by Eq. 3.2.2 below:

$$\dot{q}_L = h_w A_w (T - T_w) \qquad (3.2.2)$$

- h_w: heat transfer coefficient to the wall (W/m^2K)
- A_w: surface area of the combustion chamber (m^2)
- T_w: wall temperature (K)

The expression for $\dot{q}_R$ is non-linear and is shown in Eq. 3.2.3:

$$\dot{q}_R = DH_R\, V\, RR = DH_R\, V\, c^n\, A\, exp(-E_a/RT) \qquad (3.2.3)$$

- DH_R: heat of reaction (J/kg)
- V: combustion chamber volume (m^3)
- RR: reaction rate (kg/m^3s) where c is the overall concentration, n the overall reaction order (=2 for most hydrocarbon-air reactions), $A\, exp(-E_a/RT)$ is the Arrhenius expression for the reaction rate coefficient. (A - Arrhenius pre-exponential constant, E_a - activation energy, R - universal gas constant, T - reactant mixture temperature).

$\dot{q}_R$ and $\dot{q}_L$ can be plotted versus the bulk temperature T of the reactant mixture as shown in Figure 3.8. Depending of the combustion chamber wall temperature, there are three different cases possible (21). In Figure 3.8 $T_{w1}>T_{w2}>T_{w3}$.

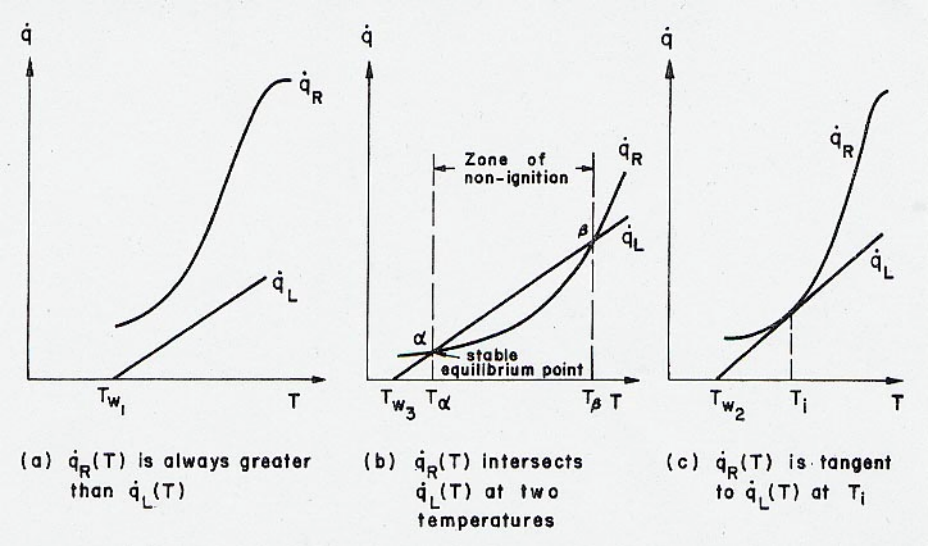

Figure 3.8 Three cases of relationship between the rate of heat release and heat loss (21).

In case a) the chemical process will always lead to a thermal runaway giving a combustion (or explosion) since $\dot{q}_R$ is greater than $\dot{q}_L$ for all temperatures T.

In case b) $\dot{q}_R$ intersects $\dot{q}_L$ at two temperatures T_a and T_b. At T_a the chemical reactions will generate heat ($\dot{q}_R$) in equilibrium with the heat loss ($\dot{q}_L$) and to give a thermal runaway the temperature of the reactants must be raised to T_b by some other means than the self-heating of the process.

In case c) $\dot{q}_R$ is tangent to $\dot{q}_L$ at a temperature T_i. This implies that the reactant mixture will self-heat to T_i and then a thermal runaway will occur. The temperature T_i is the ignition temperature.

From case c) the ignition temperature can be found since the tangent point is defined by:

$$\dot{q}_R = \dot{q}_L \text{ and } d\dot{q}_R/dT = d\dot{q}_L/dT \qquad (3.2.4)$$

These conditions give the following expression for the ignition temperature (20, 21):

$$T_i = T_w + (RT_w^2/E_a) \qquad (3.2.5)$$

It can also be shown (20, 21) that the correlation between pressure and initial temperature T_w takes the form of the so-called *Semenov expression* shown in Eq. 3.2.6:

$$\ln (p/T_w^2) = E_a/2RT_w + B \qquad (3.2.6)$$

The constant *B* includes a term of the surface to volume *(S/V)* ratio of the combustion chamber in addition to other physical and chemical properties of the reaction system. The *Semenov expression* is graphically illustrated in Figure 3.9.

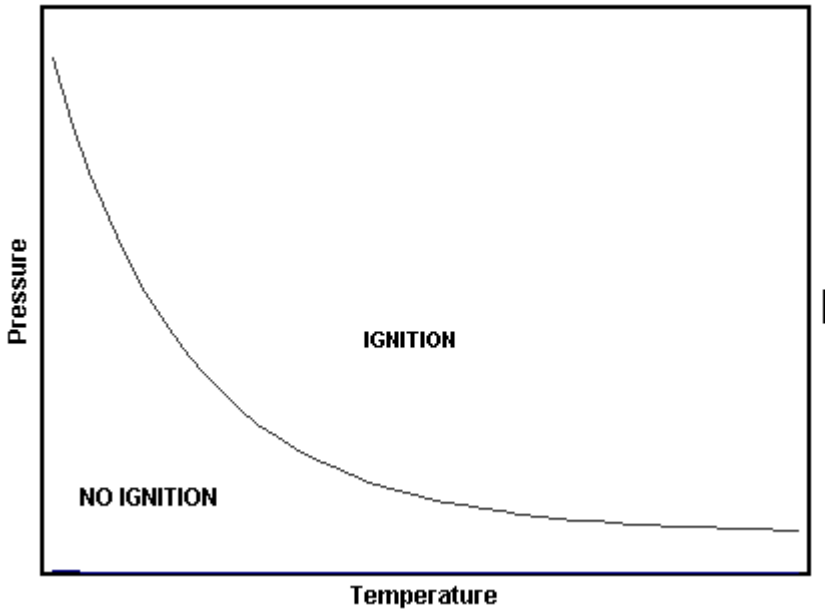

Figure 3.9 Critical conditions of ignition according to the Semenov expression (19).

3.2.2 Methods for ignition of VOC Fuel

Spark ignition

In gas engines for transport and power generation the most common method for ignition is by a spark plug. In this case the gas is premixed with air and introduced into the inlet system at low pressure. The charge is compressed as in ordinary gasoline engines and must have sufficient anti-knocking performance and ignition properties as ordinary gasoline engines. To obtain this, the charge has to be lean enough to withstand knock but still rich enough to ignite.

In medium sized four stroke engines it is possible with best available technology to run at $\lambda = 1.6$ and BMEP approximately 20 bars. The method is less suitable for large bore engines. In such engines the combustion is difficult to control by homogeneous charge and spark ignition.

Ignition by injection of pilot fuel ("Pilot ignition")

This concept can be used in two different types of engine processes.

1) Replacing the spark ignition system of a homogeneous charge engine with a diesel pilot injection system makes the ignition more stable especially at leaner mixtures since more ignition energy can be introduced. The demand for closed loop lambda control is basically as for a spark ignition engine. To be able to optimise the combustion for low emissions, the pilot system is normally injecting <10 % of the total fuel energy - in some engines <1 % (micro injection).

Referring to the nomenclature introduced in section 2.4, these engines are working according to the «Dual Fuel Diesel Process»

2) Engines with pilot ignition and high-pressure gas injection represent a new concept for gas engines. The gas is injected at high pressure directly into the combustion chamber. According to the nomenclature introduced in section 2.4, the engine process is the «Gas Diesel Process». One of the advantages with this process is that the engine is working only with air during the compression. In modern engines the injection is electronically controlled. Ignition is stabilised by means of an integrated gas and diesel pilot injector or by two separate injectors; one for gas and one for pilot diesel fuel. Engines of this type in service are using compressed natural gas or methane. The fuel must be of stable quality and concentrated. Gas blended with inert gas could theoretically be used, but that would mean larger gas nozzles and increased compressor-work to compress the gas/inert-gas blend to be injected.

The MAN B&W Engine converted for use of VOC Fuel for the shuttle tanker “Navion Viking” is of the «Condensate Diesel Process» type since the gas is condensated. The VOC Fuel used mainly consist of propane and butanes, but the composition will vary and has also been measured to consist of approximately 30% of both butanes, pentanes and higher alkanes with only ~10% propane (10). Due to the condensation process all inert gas is removed. The engine developed for “Navion Viking” is equipped with a standard HFO injection system with two injectors also used for the 8% pilot fuel injection in addition to an injection system for the VOC Fuel – also with two injectors. An advanced injection control system allows for instantaneous changeover from gas to diesel and vice versa. Engines with high-pressure gas injection may have as much as 3 different injector systems. The engines on "Navion Viking" operate on HFO in periods when gas is not available and at engine loads <30% (10).

3.2.3 Ignition delay

When the fuel is injected into the pressurised, hot charge air, it is – as described above - not ignited immediately. The period between the start of injection and ignition - the ignition delay - is fuel type dependent and is of great importance for a diesel engine. Methane and short, straight chain alkanes have long ignition delays (cf. section 3.3.3 Combustion chemistry). Fuels of this type do not selfignite readily at temperatures present in the cylinder at all engine loads. To ensure stable ignition assistance is needed especially at low engine loads.

Ignition delays (in milliseconds) can be calculated and represented (17, 21) by the Arrhenius expression shown in Eq. 3.2.7:

$$t_{id} = Ap^{-n} \exp\left(\frac{E_A}{R} \cdot \frac{1}{T}\right) \qquad (3.2.7)$$

t_{id}	-	ignition delay (milliseconds)
E_A	-	apparent activation energy for the fuel autoignition process (kJ/kmole)
R	-	the universal gas constant (kJ/kmole K)
A, n	-	constants dependent on the fuel
T	-	chamber temperature (K)
p	-	chamber pressure (bar)

T, p and t_{id} can normally be measured in combustion rigs such as constant-volume bombs, steady-flow reactors and rapid compression machines. E_A are tabulated values for different fuels and A and n can be found by multiple regression analysis of measured data.

Ignition delays can normally be graphically represented as shown in Figure 3.10 below.

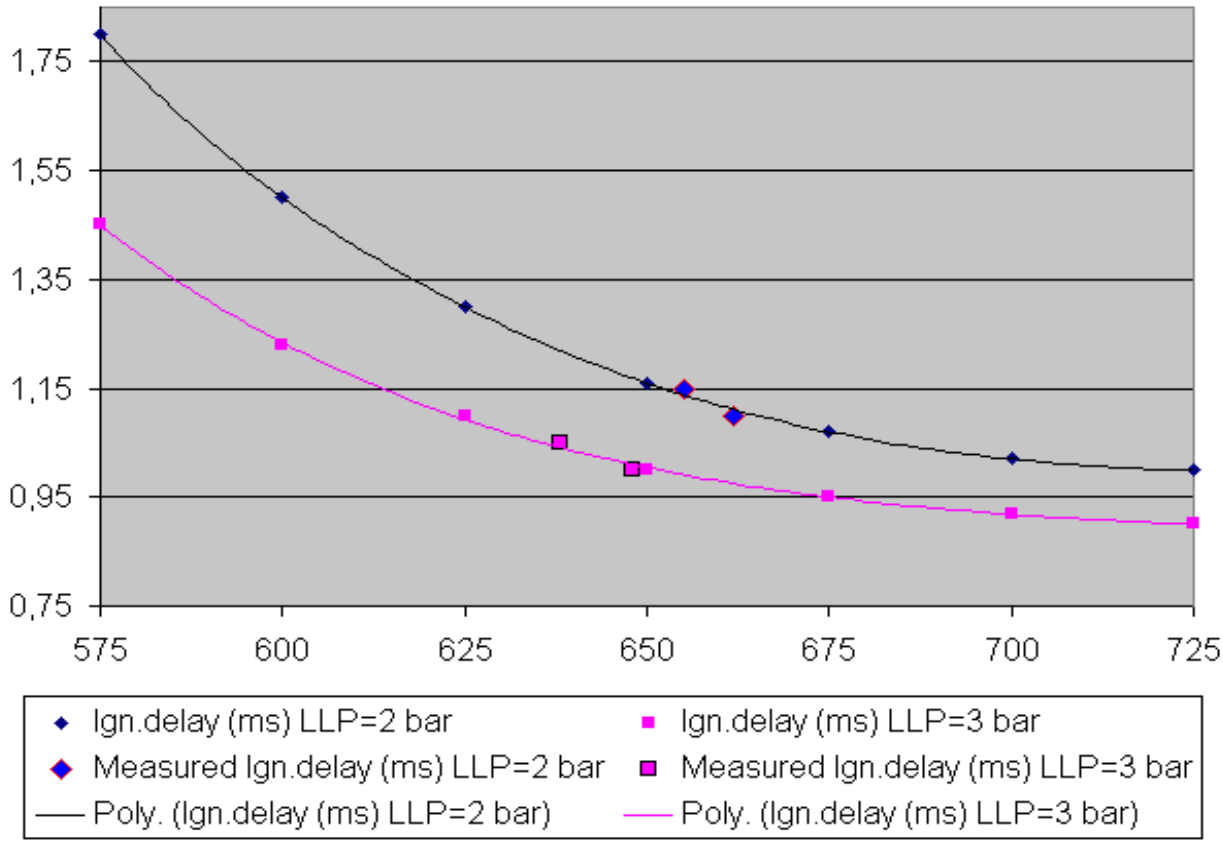

Figure 3.10 Ignition delay shown as function of pressure and temperature.

In this thesis, the objective was to perform tests with variation of many parameters. The test matrix was therefore designed with only two levels of each parameter. During the tests, pressure and temperature were kept as constant as possible. In case of the regression model for ignition delay, only two points of each correlation curve exist, and no polynomial curve can be constructed based on the measured data. As an example from the tests four data points are included in Figure 3.10.

In rapid compression machines and engines, the combustion chamber temperature is not easy to measure correctly. The sensors available for such measurements do not respond quickly enough to give reliable values or they are not suited for installation in combustion chambers. A computed temperature derived by using the ideal gas law and the measured cylinder pressure is used instead (22, 23) as correct pressure can be measured without any problems. In the DyFo test rig the cylinder pressure is measured with a piezoelectric sensor (Kistler 6053). Appendix 1 gives an example of the temperature calculation, and Figure 3.12 shows how cylinder pressure and temperature correspond by this type of calculations.

In classical combustion theory (21), the ignition delay is divided into a chemical part (τ_{ch}) and a thermal part (τ_{th}). Considering an adiabatic system, the heat of reaction will self-heat the system until the temperature of the mixture moves the system into the explosive reaction regime. This type of event is called a two-stage ignition, including the chemical and thermal ignition delays. Normally $\tau_{ch} >> \tau_{th}$ and in practice no distinction of the two periods is made.

When the ignition of a low-cetane fuel is assisted, the ignition delay may be divided in two periods in different ways. In a previous work at the Department of Marine Engineering concerning 'hot surface assisted compression ignition in a direct injection natural gas engine'

(19), the ignition delay was divided in a penetration delay (τ_{ph}) – the time for the spray to reach the hot surface - and a chemical delay (τ_{ch}).

Since the concept of «Condensate Diesel Process» includes diesel pilot fuel assisted ignition of the VOC Fuel, it could be appropriate to divide the ignition delay in separate parts for each fuel. From the dynamic signals of the cylinder pressure transducer, it is possible to find a marked change in the pressure gradient at two places. The places represent the ignition of the two fuels. However, the early combustion of the VOC Fuel seems to be progressive (cf. Figure 3.11), and the ignition delay of this fuel cannot be defined exactly. When the pilot fuel ignites, the chemical reactions have had long time to prepare for ignition of the VOC Fuel. The sudden temperature rise following the ignition of the pilot fuel comes quickly and is so intense that the VOC Fuel is forced to ignite. $\tau_{VOC} - \tau_{pilot} << \tau_{pilot}$, and therefore no distinction of ignition delays are made.

3.2.4 Ignition of two fuels injected in the combustion chamber.

When injecting two fuels with different ignition properties as pilot diesel fuel and VOC Fuel in the DyFo, the two fuels will not be in the same state prior to ignition. The fuel with the shortest ignition delay will raise the temperature when it ignites and thus shorten the ignition delay of the other, i.e. it serves as an igniter for the other fuel. As an example from the test work Figure 3.11 below shows the cylinder pressure when injecting a) VOC Fuel (propane) + pilot fuel, b) VOC Fuel (propane) only and c) Pilot fuel only. The injection timing is the same for all fuels.

As shown in Figure 3.11 pure propane ignites much later when injected as a single fuel than it does when diesel is pilot injected simultaneously. Pilot diesel fuel will, on the other hand, ignite a little bit later when injected together with VOC Fuel. The ignition delay increases mainly due to the reduced access to air when more fuel is injected. Reduced charge air temperature due to the evaporation of the fuel is another significant factor. In the DyFo test rig, this factor is more important than in a diesel engine because of the “single shot” process this test rig is operated by. Normally more fuel increases the thermal load in the engine and thus the temperature as heat is accumulated in the structure surrounding the combustion chamber. By “single shot” operation there is no heat accumulation, and thus the temperature will be lower in the DyFo.

The dynamic nature of the VOC Fuel combustion is visualised in Figure 3.11. The VOC Fuel starts to burn slowly when the pilot fuel ignites and the cylinder pressure curve follows the "Pilot diesel" curve. When the pilot fuel no longer raises the pressure, the VOC Fuel combustion generates a steeper pressure gradient indicating an increased reaction rate.

As described later in section 3.3.3, a very important process ahead of ignition and combustion is the production of radicals. This process is temperature and pressure dependent. Hydrocarbons with many C-atoms need lower temperature to ignite (20); this is further explained later.

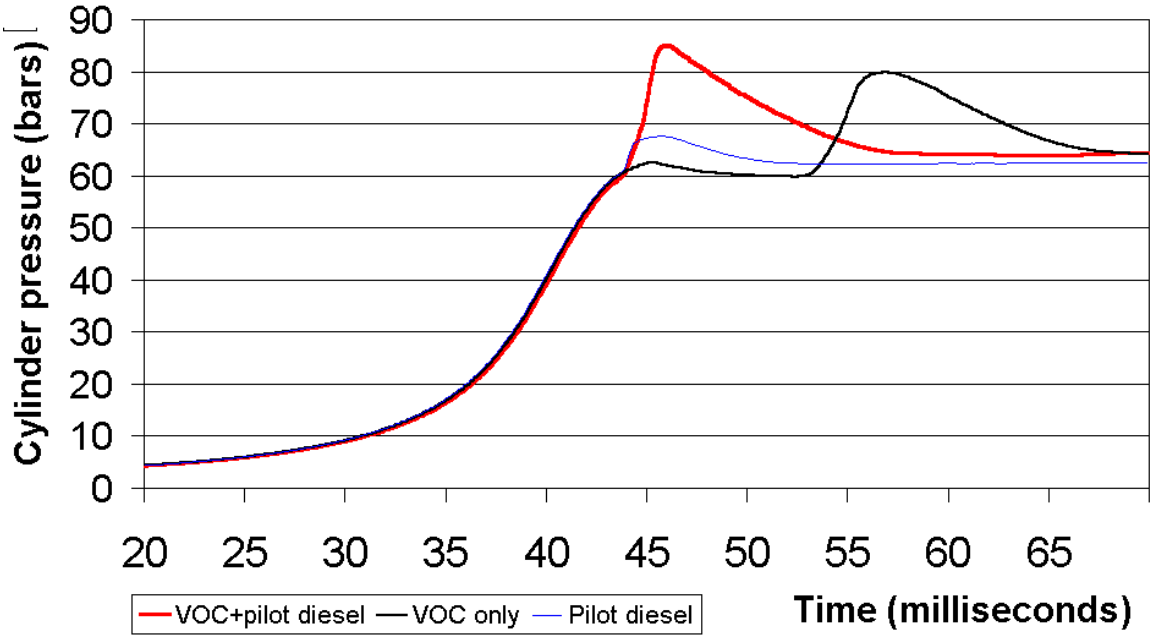

Figure 3.11 Ignition delay of pilot fuel ignited VOC Fuel, VOC Fuel only and pilot fuel only in the DyFo.

The ignition delays in the DyFo tests are measured as the time from the needle lift ≥ 10% of its maximum value and till the pressure gradient increases 3 times or more; i.e. $(dp/dt)_i \geq 3(dp/dt)_{i-1}$ as indicated in Figure 3.12 (needle lift = 10% of max at 41,3 ms, $(dp/dt)_i \geq 3(dp/dt)_{i-1}$ at 42,5 ms).

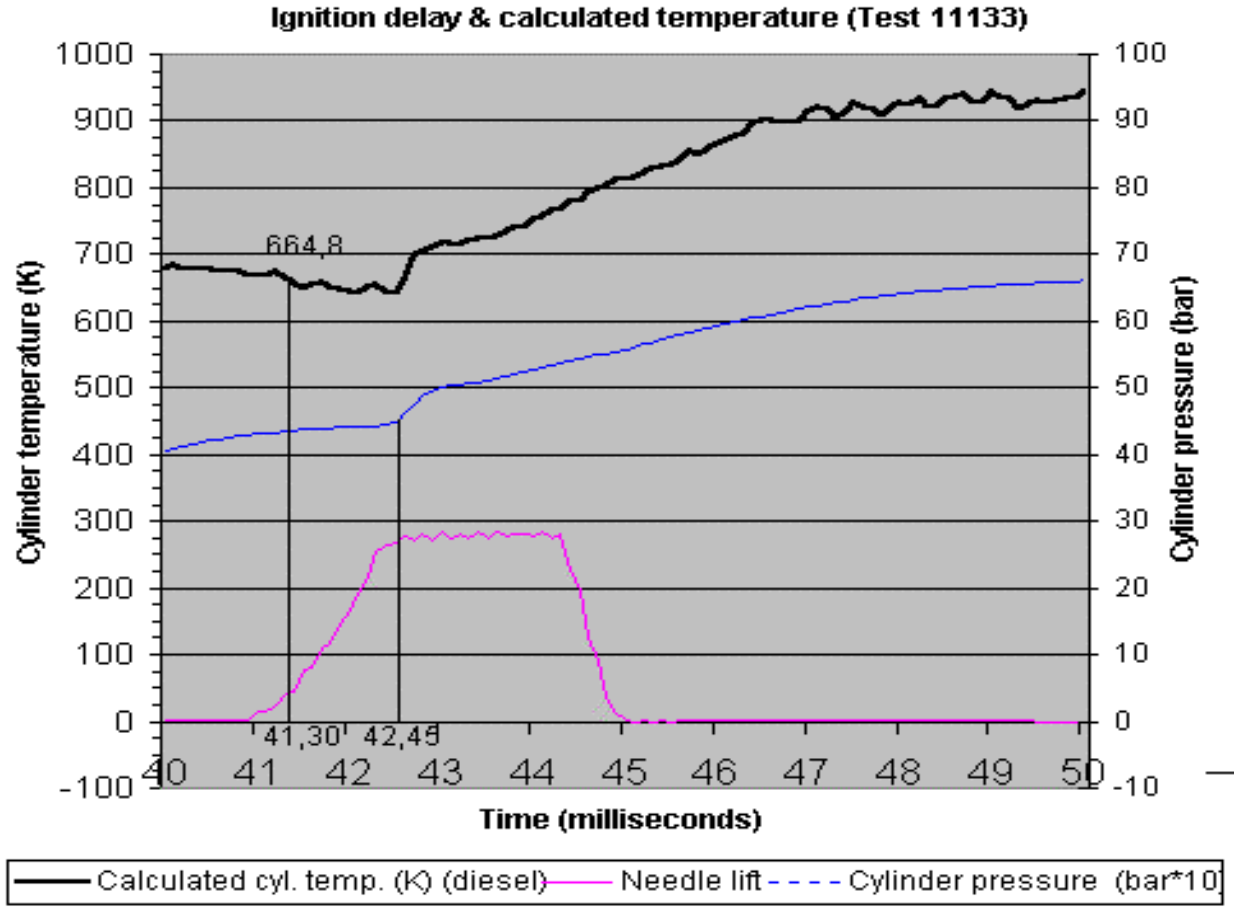

Figure 3.12 Measurement of ignition delay in the DyFo tests.

3.3 Combustion in the Diesel process

When injecting a liquid fuel directly into the combustion chamber the following events will occur before the controlled combustion starts:

- opening of injector, needle lifts to allow the pressurised fuel to be injected
- atomisation of the liquid fuel into small droplets as it enters the cylinder
- vaporisation of droplets and mixing with air in the cylinder
- spontaneous ignition in regions where the fuel-air mixture has obtained an air/fuel ratio within the combustible limits after a short delay period

Whether the fuel is diesel or propane, butane or any other liquefied VOC component or mix, these periods will occur as long as the fuel injection pressure is high or at least above the critical pressure for fuels normally being gaseous at standard conditions (1 bar, 273 K).

3.3.1 Phenomenological model of combustion

Analysis of engine cylinder pressure data and studies of photographs of DI diesel engine combustion have led to an accepted model describing the combustion process in engines following the diesel process. The concept of Rate of Heat Release (ROHR = dQ/dt) is essential in the model, and is defined as the rate at which the chemical energy bound in the fuel is released in the combustion process.

When applying the first law of thermodynamics on an open system with uniform distribution of both pressure and temperature, the following equation results:

$$\frac{dQ}{dt} - p\frac{dV}{dt} + \dot{m}_f h_f = \frac{dU}{dt} \qquad (3.3.1)$$

By making the approximation that the temperature in the cylinder is uniformly distributed at each instant of time during the combustion, two common methods are used to obtain combustion information from the pressure data using this equation.

a. Rate of Heat Release analysis.

U and h_f are taken to be the sensible internal energy of the cylinder charge and the sensible enthalpy of the injected fuel.

b. Fuel mass burning rate analysis.

U=mu where *m* is the mass inside the cylinder and the mass flow $\dot{m}_f = dm/dt$

Q is the heat transfer to the gas within the cylinder.

In the following the Rate of Heat Release (ROHR) analysis will be described since this method is used in the evaluation of experimental data. For this analysis the cylinder pressure and the piston motion signals are processed in the computer using a software program system called LabVIEW (53).

3.3.2 Rate of heat release analysis

With the assumptions mentioned above, the enthalpy expressed as $\dot{m}_f h_f$ in Eq. 3.3.1 will be eliminated ($h_f \approx 0$). Taking into account the heat loss to the combustion chamber walls with a rate dQ_{ht}/dt, there remains a net heat release dQ_n/dt being the difference between the chemical heat release dQ_{ch}/dt and the heat loss dQ_{ht}/dt. Eq. 3.3.1 becomes:

$$\frac{dQ_n}{dt} = \frac{dQ_{ch}}{dt} - \frac{dQ_{ht}}{dt} = p\frac{dV}{dt} + \frac{dU}{dt} \qquad (3.3.2)$$

Figure 3.13 (17) shows how the heat release accumulates and to what magnitude the heat losses amount (~25% from the figure).

The heat loss dQ_{ht}/dt in the experiments is divided in two parts for convenience. The first part equals the heat loss to the walls due to the heat flux generated from the heated charge air compressed by the piston movement. The second part equals the heat loss to the walls due to the heat flux generated by combustion.

In each of the different experimental test series (cf. section 4.2.5 and chapter 5) the first of these two heat loss parts is established by running the test rig without fuel injection. The "heat release" curve thus generated is subtracted from the curve generated with fuel injection. Figure 3.14 shows a plot of processed data in the LabVIEW program for ROHR analysis where the "net heat release" curve appears.

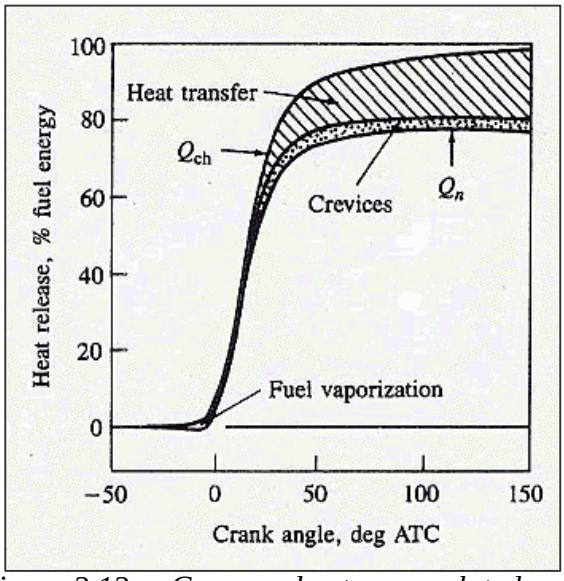

Figure 3.13 Gross and net accumulated heat release (17).

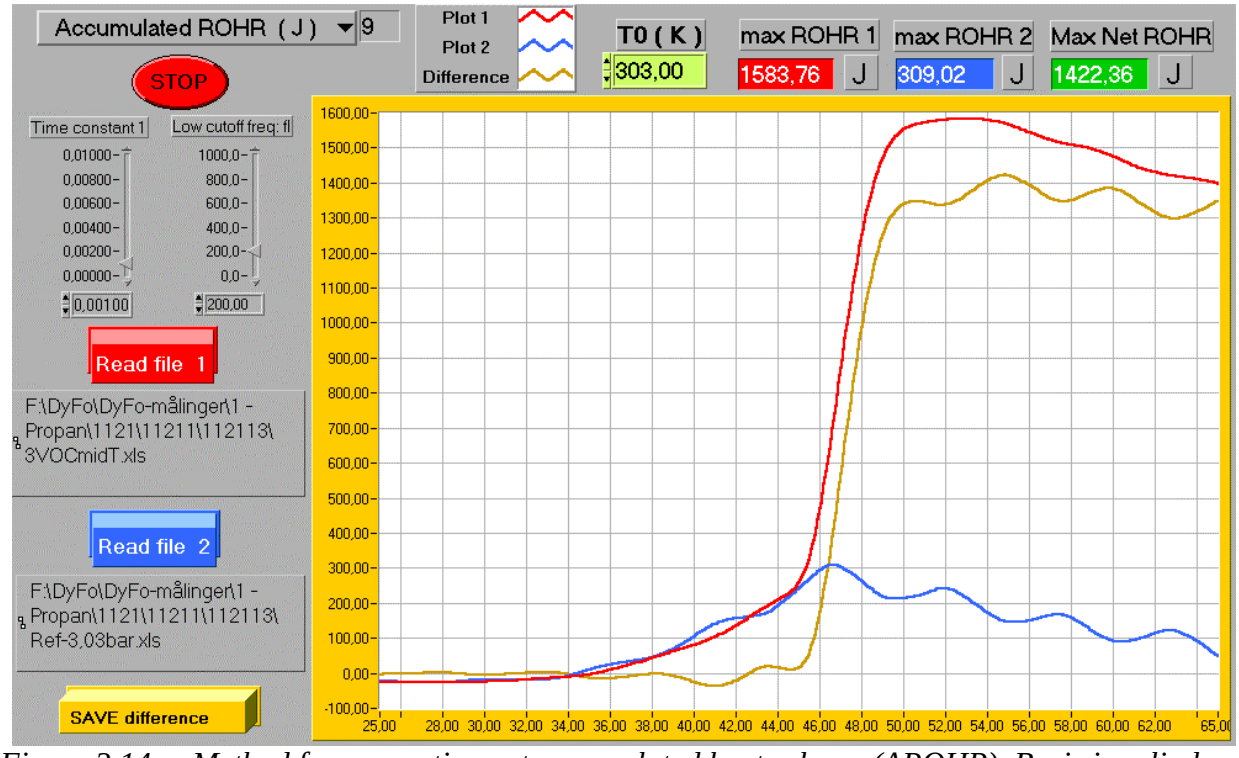

Figure 3.14 Method for generating net accumulated heat release (AROHR). Basis is cylinder pressure curves from tests with and without fuel injection and combustion.

The oscillation of the cylinder pressure curve from the test without injection is due to mechanical vibrations set up in the DyFo test rig by the piston motion. If the oscillation is ignored, it is seen that the accumulated heat release in Figure 3.14 is of the same nature as in Figure 3.13.

The second part - heat loss due to radiation from the flames in the combustion - is neglected in the ROHR analysis of the experiments because of various reasons:

a. Conditions are assumed to be the same for all tests in a series.
b. No satisfactory model of heat loss was found in agreement with the special geometry of the combustion chamber of the DyFo.
c. Comparison of tests can be compared to cycle-by-cycle variations in an engine. Other researchers then neglect the heat loss to the walls (19).

Since the gross accumulated heat release should equal the energy injected by the fuel, a measure of this second part of the heat loss can be found. However, the problems to measure the fuel mass injected by each "single shot" correctly, makes such a calculation less accurate. Mean values for fuel injected gives for the test shown in Figure 3.14 a value $Q_R = m_f h_f$ *(pilot+VOC)*= 26,2 mg* 42,5 MJ/kg + 21,9 mg*47,19 MJ/kg = 2148,60 J. Calculated accumulated net heat release is 1422,31 J. The two heat loss parts then account to 33,8 %. This is 8,8%-points more than indicated by Figure 3.13. The standard deviation s of the measured fuel masses injected is 7 % for both fuels and if the actual fuel masses were $1s$ less than the mean values, the total heat loss would account for ~27 % of the injected energy. It is very likely that this has been the situation during the experiments.

We assume that the cylinder charge can be treated as an ideal gas and that the ideal gas law ($pV=mRT$) is applicable. Then we get

$$\frac{dQ_n}{dt} = p\frac{dV}{dt} + mc_v\frac{dT}{dt} \qquad (3.3.3)$$

Logarithmic derivation of the ideal gas law (with constant value of m (cylinder charge) and R (universal gas constant)) gives us:

$$\frac{dp}{p} + \frac{dV}{V} = \frac{dT}{T} \qquad (3.3.4)$$

This equation and the ideal gas law can be used to eliminate T in Eq. 3.3.3:

$$\frac{dQ_n}{dt} = p\frac{dV}{dt} + mc_v\frac{T}{dt}\left(\frac{dp}{p} + \frac{dV}{V}\right) = p\frac{dV}{dt} + mc_v\frac{\frac{pV}{mR}}{dt}\left(\frac{dp}{p} + \frac{dV}{V}\right)$$

$$\frac{dQ_n}{dt} = p\frac{dV}{dt} + \frac{c_v}{R}\frac{pV}{dt}\left(\frac{dp}{p} + \frac{dV}{V}\right) = p\frac{dV}{dt} + \frac{c_v}{R}\left(V\frac{dp}{dt} + p\frac{dV}{dt}\right)$$

By inserting $R = c_p - c_v$ and reorganising the terms, the final equation for ROHR becomes:

$$\frac{dQ_n}{dt} = \frac{1}{g-1}\left(g\frac{pdV}{dt} + \frac{Vdp}{dt}\right) \qquad (3.3.5)$$

This equation is used in a LabVIEW program calculating ROHR in the experiments carried out in the dynamic combustion rig DyFo. By test analysis *p, V, dV/dt* and *dp/dt* can be read out of the collected data from the DyFo.

Unfortunately, the signal of the piston position that gives input to the expression for the cylinder volume V is rather uneven; the derivative dV/dt gives a very flickering curve. The reason for this is that two MOOG servo valves regulate the piston movement. By the end of the piston stroke, the MOOG valves control the oil flow attempting to make a smooth retardation of the piston. The dynamic nature of the control loop generates a movement not very smooth. Figure 3.15

shows the unsteady nature of the registered piston position signal and how the first time derivative (=piston speed) of the signal looks like.

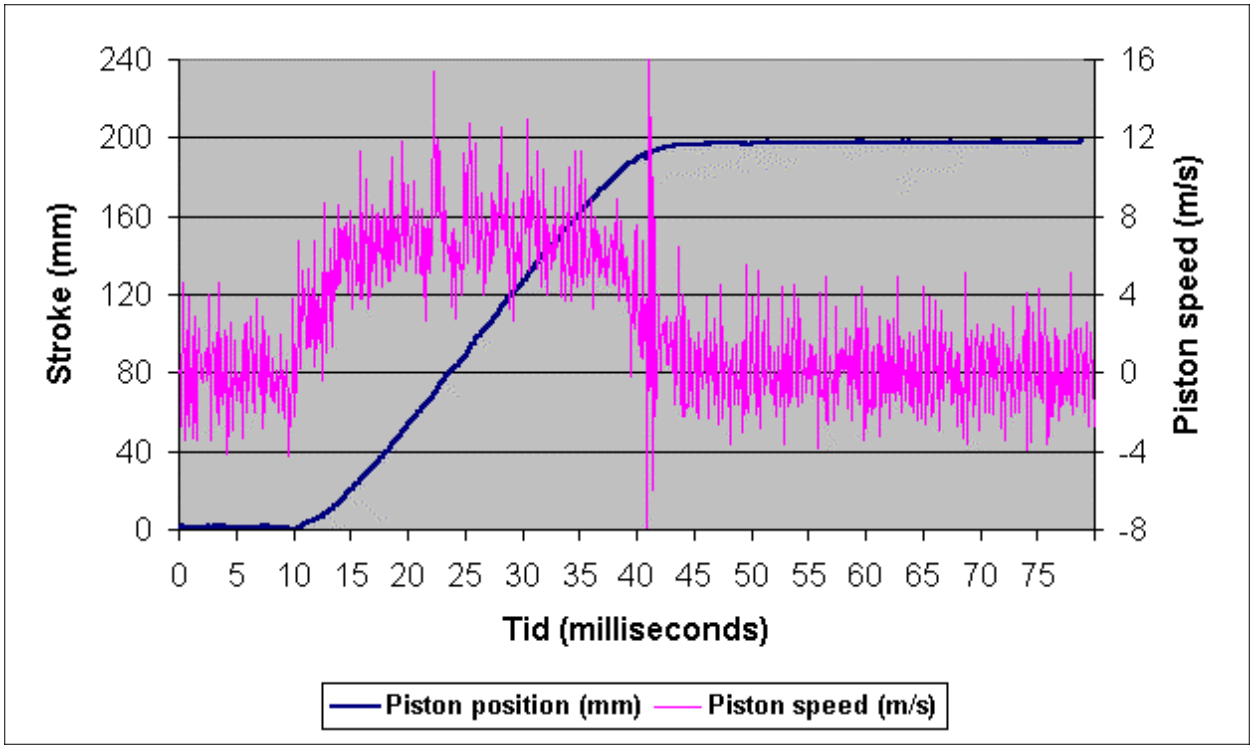

Figure 3.15 Registered piston position signal and first time derivative (=piston speed).

An unsteady signal like this does not make ROHR calculations generate smooth curves!

3.3.3 Combustion chemistry of hydrocarbons

Combustion of propane as model for the VOC Fuel is the main part of the experiments. The overall chemical reaction for propane is:

$$C_3H_8 + 5\lambda\,(O_2+3{,}76N_2) \Rightarrow 3\,CO_2 + 4\,H_2O + 5(\lambda-1)\,O_2 + 18{,}80\lambda N_2 \qquad \{1\}$$

Ahead of this reaction, a series of other reactions will occur depending of the temperature and pressure in the reaction chamber. Generally, the chemical reactions can be divided in a high temperature part (above some 1100 K) and a low temperature part (below about 900 K). In diesel engine combustion, the low temperature part is of vital importance for ignition (24), as the process temperature after the end of the charge air compression normally lies below this limit.

General steps in combustion

Generally any combustion (oxidation) includes the following steps (20) with the specific reaction rate constants k_i, i = 1, 2,…..n shown in the equations {2} – {6}:

1. Initiating steps: Initial production of radicals (R) from a pool of reactants (F) {2}
2. Chain branching steps: Reaction leading to more radicals (R) and new reactants (F') {3}
3. Chain propagating steps: Reaction leading to both products (P) and new radicals (R) {4}
4. Chain terminating steps: Reaction leading to products (P' & P") only {5} & {6}

$$F \xrightarrow{k_1} R \qquad \{2\}$$

$$R + F \xrightarrow{k_2} aR + F' \qquad \{3\}$$

$$R + F \xrightarrow{k_3} P + R \qquad \{4\}$$

$$R + F \xrightarrow{k_4} P' \qquad \{5\}$$

$$R \xrightarrow{k_5} P'' \qquad \{6\}$$

In the above equations, R represents all types of radicals that are so called chain carriers; i.e. molecules that make the reaction go on. F and F' are different reactant molecules and P, P' and P'' are different products, P being the main product. The size of α, the multiplication factor for radicals, is of vital importance for the reaction rate, but will be left no further discussion here.

Fuel structure and atomic bonds (20, 25).

Before any further description of combustion reactions, some details of the composition of hydrocarbon fuels suited for diesel engines must be explained.

Hydrocarbons of higher order (alkanes, alkenes, alkynes and arenes) consist of C and H atoms in different configurations, the main groups being CH_3, CH_2 and CH. The fuel molecules are combinations of these groups in straight or branched chains or ring structures (cycloalkanes, cycloalkenes and -alkynes). Propane is a straight chain molecule [CH_3-CH_2-CH_3], iso-butane is a branched chain molecule 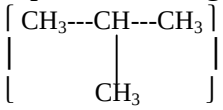 and cyclopropane 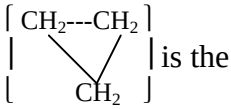 is the smallest ring structured alkane.

The connections between the atoms are called bonds. Each C atom makes connections to 4 other atoms and the strength of the bond in each connection represents an energy level dependent of the bond structure. Bonds between the C atoms (CC bonds) can be single, double and triple; the bond strength increases in the same order. In alkanes only single bonds are present, in alkenes one or more double bonds exist and alkynes have at least one triple bond. Arenes (often called *aromatics*) are based on the ring-structured benzene containing three single bonds and three double bonds. HC's containing other than single CC bonds are often called *unsaturated* (because new CH bonds can be built by adding more H atoms (hydrogenation)). Table 3.2 shows a list of some CC bond strengths (20). Leaving groups are shown in *Italic style* in the tables below.

Table 3.2 Strength of some CC bonds in hydrocarbons.

Hydrocarbon		Bond strength
Name	Structure	(kcal/mole)
Ethane	CH_3-*CH_3*	90,4
Ethene	CH_2=*CH_2*	~152
Propane	CH_3-CH_2-*CH_3*	85,8
Propene	CH_2=CH-*CH_3*	100,6
n-Butane	CH_3-CH_2-CH_2-*CH_3*	86,5
1-Butene	CH_2=CH-CH_2-*CH_3*	74,4
iso-Butane	$(CH_3)_2$-CH-*CH_3*	85,7
n-pentane	CH_3-CH_2-CH_2-CH_2-*CH_3*	81

As shown in Table 3.2 the CC bond strength decreases when the molecule length increases. As a matter of fact this is even the case with the CH bonds, cf. Table 3.3 (20).

Table 3.3 Strength of some CH bonds in hydrocarbons.

Hydrocarbon		Type of CH bond broken	Bond strength (kcal/mole)
Name	Structure		
Methane	CH_3-*H*	Primary	105,1
Ethane	CH_3-CH_2-*H*	Primary	98,2
Ethene	CH_2=CH-*H*	Secondary	110
Propane	CH_3-CH_2-CH_2-*H*	Primary	97,9
Propane	CH_2=CH-*H*-CH_3	Secondary	95,1
iso-Butane	$(CH_3)_2$-CH-CH_2-*H*	Primary	~98
n-Butane	CH_3-CH_2-CH-*H*-CH_3	Secondary	95,5
iso-Butane	$(CH_3)_3$-C-*H*	Tertiary	93,2
Benzene	C_6H_5-*H*	Tertiary	~112
Methyl-Benzene	C_6H_6-CH_2-*H*	Primary	~ 85
Acetylene	HC≡C-*H*	Tertiary	~125

The bonds between C and H atoms (CH bonds) are of 3 different types:

1. Primary CH bonds. The C atom is attached to one other C atom (CH_3 groups).
2. Secondary CH bonds. The C atom is attached to two other C atoms (CH_2 groups).
3. Tertiary CH bonds. The C atom is attached to three other C atoms (CH groups).

In a hydrocarbon molecule the relative strength of CH bonds is decreasing from primary to secondary to tertiary. The absolute strength of CH bonds depend on the length of the molecule and what types of CC bonds is present (cf. Table 3.3). The radicals attacking the fuel molecules choose which site to attack according to the bond strength; each radical have their own "selective scale". The selectivity of the most important radicals for abstraction of H atoms from CH bonds is shown in Table 3.4 (the higher the value is the higher the priority for selection is).

Table 3.4 Selectivity of H atom abstraction in CH bonds for radicals.

Radical	Tertiary CH	Secondary CH	Primary CH
H	13	4	1
O	10	5	1
OH	4	3	1
HO_2	10	3	1

Normally, both fuels for otto (SI) engines and diesel (CI) engines are blends of different types of hydrocarbons (alkanes, alkenes, alkynes and arenes). In diesel fuels, it is desirable that the fuel ignites easily. This means that the preferred components have as weak bonds as possible and as many bonds as possible that the radicals prefer to attack.

This makes straight chain alkanes a preferred type of hydrocarbon for diesel engines, since only single CC bonds are present and the number of primary CH bonds is the lowest possible. Long chains are easier to break than short ones (more CC bonds and weaker ones) and diesel fuel molecules are for this reason long. However, as diesel fuels are blends, components with both double CC bonds and tertiary CH bonds normally will be present. For this reason diesel engine combustion calculation often are performed with a model of the fuel as $C_{16}H_{30}$ - a molecule with 2 double and 13 single CC bonds and 6 primary, 20 secondary and 4 tertiary CH bonds. For the components in the VOC Fuel, the molecules are relatively short, straight chain alkanes (propane – C_3H_8, butane – C_4H_{10}, pentane – C_5H_{12} and hexane – C_6H_{14}).

Low temperature reactions

The temperature in a diesel engine does not exceed 900 K at the end of compression and by the time the fuel is injected at all loads. In the combustion test rig DyFo this temperature is never reached.

At temperatures below 900 K the initiation of the chain reaction is:

$$RH + O_2 \leftrightarrows R\bullet + HO_2\bullet \qquad \{7\}$$

In diesel engines prior to ignition, this reaction is dominating over the fuel decomposition (cf. *High and medium temperature reactions*). This reaction is only of importance to initiate the build-up of radicals. First started, other reactions start to attack the fuel and abstract H-atoms. A pool of H•-, O•- and OH•-radicals is established, OH• as the most important one (partly because of its low selectivity, cf. Table 3.4). The OH• radical is very reactive, while the $HO_2\bullet$ radical is not at temperatures below 850 K. The main reaction of the fuel attack is:

$$RH + OH\bullet \leftrightarrows R\bullet + H_2O \qquad \{8\}$$

Until the temperature exceeds 1000 K and fuel decomposition "takes off", the alkyl radical R• produced is oxidised in an important reaction:

$$R\bullet + O_2 \leftrightarrows RO_2\bullet \qquad \{9\}$$

The radical $RO_2\bullet$ (peroxy radical) is an important radical in the further low temperature reaction scheme. This radical has three main reaction routes; a) the reverse of reaction {9}, b) external H-abstraction (small reaction rate):

$$RO_2\bullet + RH \leftrightarrows ROOH\bullet + R\bullet \qquad \{10\}$$

and c) the most important, the so-called internal H-abstraction (also called isomerisation):

$$RO_2\bullet \leftrightarrows QOOH\bullet \qquad \{11\}$$

Here Q is an alkene structure. The reaction rate of reaction {11} depends on the type of CH bond to be broken for the H atom release and the number of atoms between the OO•-site and this H atom. The OO• radical site has to approach the H-atom physically; to make this possible the number of atoms between the two sites must at least be 5 (the H atom + the two O atoms included). Because of the tetrahedral structure of the bonds in hydrocarbon molecules, this is most likely to occur in molecules with 5 or more C atoms. In such long molecules the sites where internal H-abstraction can occur are many more than in short molecules like propane. In addition the H-abstraction reaction rate is lowest for primary CH bonds and fastest for tertiary, secondary CH bonds lying in between. In other words, short alkanes and branched alkane isomers are not very likely to have this reaction since the CH bonds mainly are primary. In Figure 3.16 the structures of *n*-heptane (7 C-atoms) and propane (3 C-atoms) are shown to explain why it is like this.

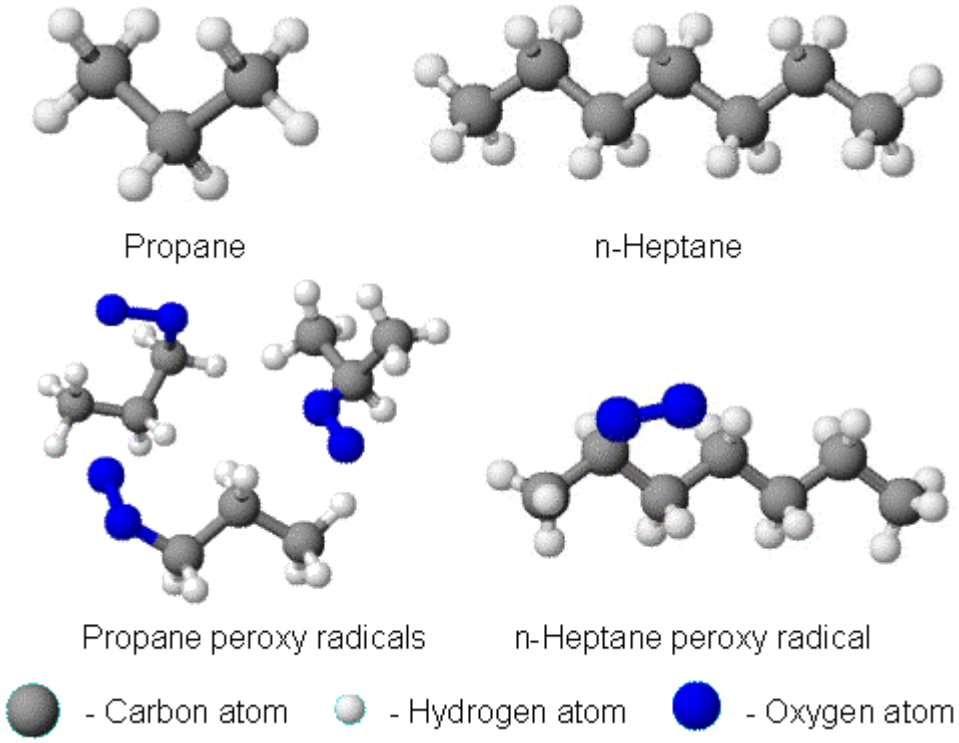

Figure 3.16 Structure of some alkanes and their peroxy radicals.

The isomerisation is the most important reaction in the ignition of diesel fuels. It is also used to explain why iso-octane, a branched alkane (2,2,4-trimethylpentane) with 8 C atoms, di- and tri-substituted with methyl and having 15 primary, 2 secondary and 1 tertiary CH bonds, has a high octane number.

Following the isomerisation, chain branching is obtained during the following reactions:

$$ROOH \leftrightarrows RO\cdot + OH\cdot \qquad \{12\}$$

$$QOOH\cdot \leftrightarrows QO\cdot + OH\cdot \qquad \{13\}$$

The production of $OH\cdot$ radicals is very important for a fast combustion necessary in an internal combustion engine like a reciprocating diesel engine. The further oxidation of the intermediate products formed in the low temperature reaction regime to give H-abstraction, is supposed to occur by $OH\cdot$ (and to some extent $HO_2\cdot$) attack.

These low temperature reactions fulfil what we normally call the ignition of the fuel, and as can be seen from the equations, the ignition delay for different hydrocarbons can be explained.

High and medium temperature reactions

High and medium temperature reactions will not start until the low temperature reactions have initiated the combustion (ignited the fuel) and raised the temperature.

In the high temperature part of the combustion ($T \geq 1100$ K) the most important reaction is a decomposition of the fuel molecules to smaller and smaller alkyl radicals and alkenes. Figure 3.17 shows that this part ends with oxidating CH_3 (methyl radical) and C_2H_5 (ethyl radical) (24).

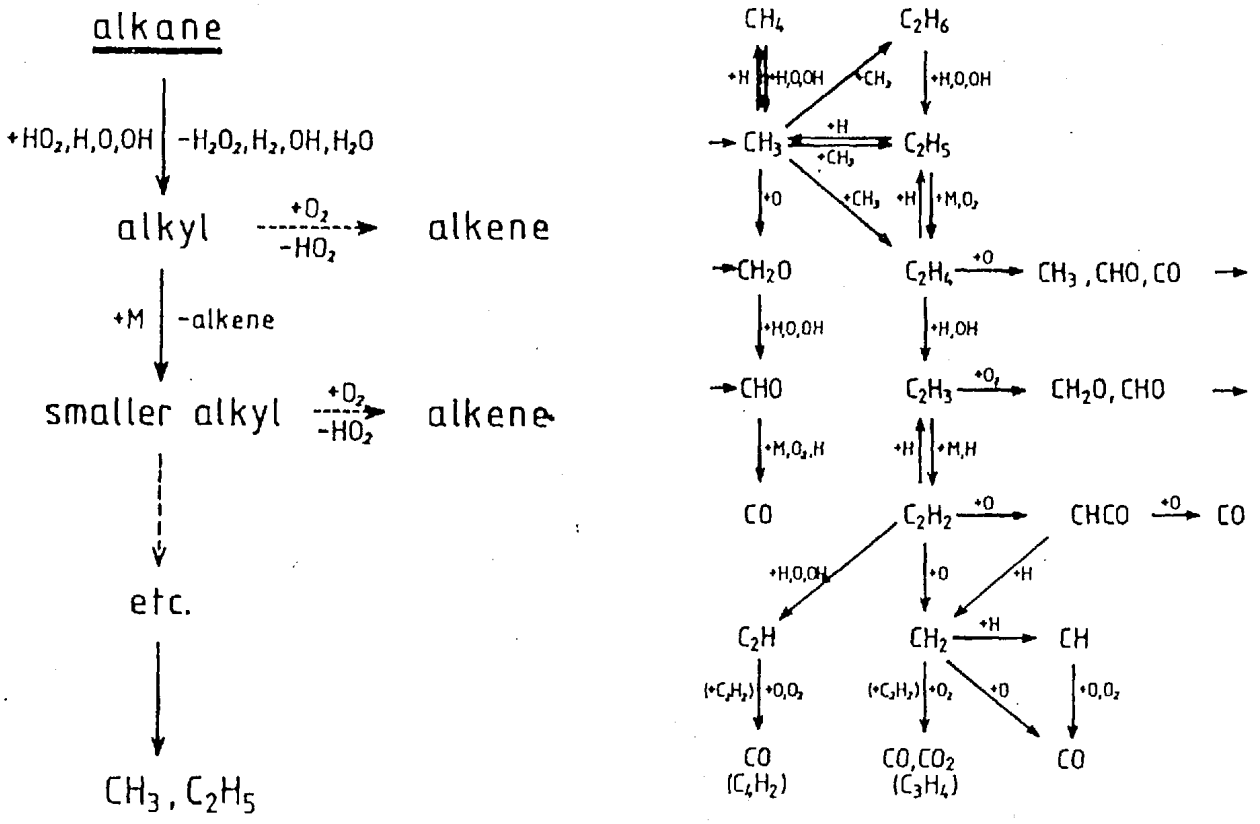

Figure 3.17 High temperature decomposition of higher alkanes (24).

The end oxidation of these radicals will produce hydrogen and carbon monoxide, and this is why classical combustion theory (e.g. 20) always introduces the reader to the chemical reactions of H_2, CO and methane before mentioning higher order hydrocarbons. Some combustion researchers state that lean and nearly stoechiometric hydrocarbon combustion can be regarded as H_2 - CO - O_2 combustion fed by the hydrocarbon fuel.

At high temperature the main chain branching mechanism according to this scheme is:

$$H\cdot + O_2 \leftrightarrows OH\cdot + O\cdot \qquad \{14\}$$

At temperatures between 1100 K and 900 K two additional reactions give chain branching:

$$HO_2\cdot + RH \leftrightarrows H_2O_2 + R\cdot \qquad \{15\}$$

$$H_2O_2 + M \leftrightarrows OH\cdot + OH\cdot + M \qquad \{16\}$$

RH represents the fuel (F), R· is a fuel radical, H·, OH·, O· and HO_2· are ordinary radicals (often generalised by X·) and M is a third body species not participating in the reaction.

From the above-mentioned H_2- and CO-combustion, the radical pool (X·) now prepare for the final attack on the decomposed fuel molecules.

Overall reactions

In hydrocarbon combustion it is always three distinct but coupled zones:

1) After the ignition, primary fuel disappears with a minimum of heat release and hydrogen and alkenes (or other unsaturated HC's) are produced. A small amount of the hydrogen is simultaneously oxidised to water (high temperature reactions).

2) The unsaturated components are oxidised to CO and H. At the same time, the present, and formed H is oxidised to water (H_2 and CO combustion).

3) At last the CO amounts formed are oxidised to CO_2 and most of the heat release from the overall reaction is obtained (CO combustion).

In the first zone the radical pool builds up to initiate the combustion reaction. When ignited, the fuel is decomposed by internal bond breaking, and the weakest bond is the CC bond.

Summary

The VOC Fuel for use in the shuttle tanker diesel engines and in the experiments in the DyFo consists of mainly short alkane molecules. As already mentioned the VOC Fuel needs assistance to ignite, and this is done by pilot injection of diesel fuel. With this fuel, long straight alkanes are injected and the production of $OH\cdot$ radicals is speeded up.

Without the pilot diesel injection, the ignition delay will increase (as shown in Figure 3.11) due to the slower production of $OH\cdot$ radicals.

To conclude, the ignition in diesel processes (compression ignition) is faster in long, straight alkanes than in short and branched chains because of:

1. Larger number of secondary CH bonds (giving easier H abstraction than from primary CH bonds) than in branched molecules.

2. Less resistance for $RO_2\cdot$ isomerisation resulting in faster $OH\cdot$ radical production at low temperature.

4 Imaging of diesel combustion. The Schlieren technique.

4.1 Principle of measurement and optical set-up.

A lot of phenomena are normally not visible to the human eye or in ordinary photographs; flowing air around aeroplanes or from a heated surface, mixing of fluids and combustion products from flames. By the use of the Schlieren technique these phenomena can be visualised.

The principle of measurement used in the Schlieren technique is the **refraction of light** due to gradients ($\partial n/\partial x$, $\partial n/\partial y$) in the refractive index (n) of the medium along the light path. The Schlieren technique is one of several methods based on this principle. The country of origin to the method (and the name) is Germany where it was introduced to detect inhomogeneous regions in optical glass often in the form of streaks (= *schlieren* in German).

When it comes to combustion, the medium to be studied in the test section (the DyFo combustion chamber) will vary in composition and density during the working process it undergoes. During compression, the density will change mainly because of the increase in pressure. During injection and evaporation of fuel, the density will change mainly because of change of medium composition and component concentrations. During ignition and combustion of fuel, the density changes mainly because of the temperature rise. This variation will result in a change in the refractive index of the medium.

Refractive index and dependence of temperature

The refractive index will vary across the test section to be studied due to the presence of different substances or because the density of the substances vary or the temperature and pressure is non-uniform (26). In fields of interest consisting of gaseous substances, the refractive index n is related with sufficient accuracy to the density r by equation 4.1:

$$n - 1 = (n_0 - 1)(r/r_0) \qquad (4.1)$$

where n_0 and r_0 are the values at 0 °C and 760 mmHg. The equation of state ($r = m/V = p/RT$ assuming the actual gases to be perfect) gives a simple connection between refractive index, pressure and temperature. Table 4.1 shows the refractive indices for some actual gases and vapours.

Table 4.1 Refractive indices for some gases and vapours (at 0 °C, 760 mmHg) and for light of l = 589,3 nm (sodium D line).

Gas or vapour	n_0	Gas or vapour	n_0
Helium	1,000035	CO	1,000450
Hydrogen	1,000138	Methanol	1,000550
Water vapour	1,000257	Acetylene (etyn)	1,000606
Oxygen	1,000272	Ethylen (eten)	1,000720
Argon	1,000284	Chlorine	1,000768
Air	1,000292	Ethane	1,000770
Nitrogen	1,000297	Ethanol	1,000874
CO_2	1,000334	Propane	1,001081
Methane	1,000442	Butane	1,001390

Light of different wavelengths has different refractive indices (cf. the spectrum produced by refraction of visible, white light in a prism). For best experimental results monochromatic light has to be used.

The speed of light c through different substances and the refractive index n are connected through equation 4.2:

$$c = c^*/n \qquad (4.2)$$

where c^* is the velocity in vacuum. This relationship indicates that when the light meets a section of the test field with a gradient in the refractive index, the light will be deflected due to the reduced speed of light as the refractive index increases. The magnitude of this deflection is found by equation 4.3 (Snell's law):

$$n_1 \sin a_1 = n_2 \sin a_2 \qquad (4.3)$$

a_1 and a_2 are the angles of the incident and the deflected light beam relative to the axis of incidence respectively; n_1 and n_2 are the refractive indices in the two fields.

From the above equations we can conclude that for perfect gases (where $r = m/V = p/RT$):

1. the refractive index increases with increasing pressure and decreasing temperature.
2. an incident light beam is deflected to the axis of incidence when travelling into an area of higher density (= higher pressure or lower temperature).

In the DyFo experiments it is mainly the temperature that differs throughout the test section after the fuel is injected and atomised/evaporated. When the fuel ignites, the temperature increases rapidly and the density in the ignition “spots” will decrease. Consequently the light will be spread, as shown in Figure 4.1.

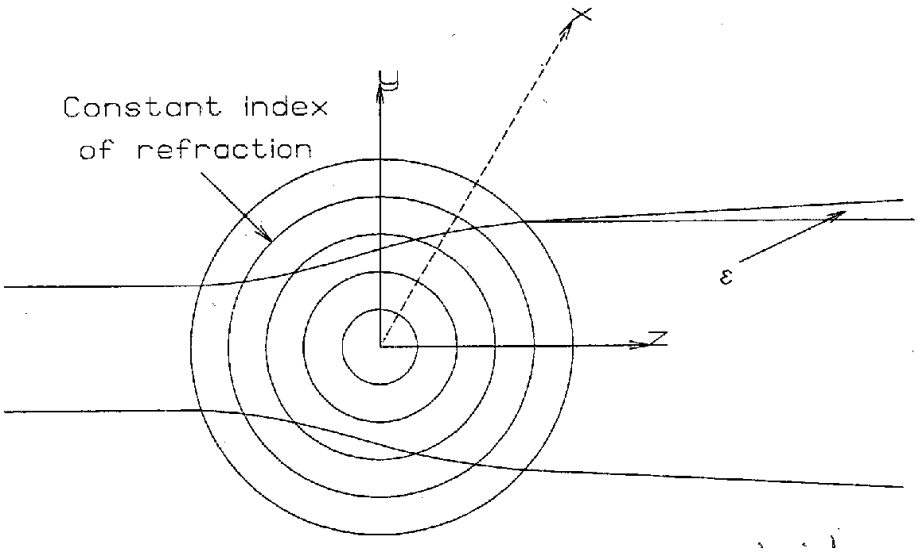

Figure 4.1 Deflection of light passing through a hot spot of ignited fuel-air mixture (16).

When a light beam (travelling in direction z) pass through an area with gradients in the refractive index (in the x- and/or y-direction) it will be deflected an angle *e*. This deflection can be registered in different ways depending of the optical set-up (26 - 28). In the Schlieren system this deflection of the light path can be described mathematically in the 3-D case by the 2nd derivative:

$$\frac{\partial^2 x}{\partial z^2} = \frac{1}{n}\frac{\partial n}{\partial x} \quad , \quad \frac{\partial^2 y}{\partial z^2} = \frac{1}{n}\frac{\partial n}{\partial y} \qquad (4.4, 4.5)$$

The deflection (ε_X and ε_Y) caused by any change in refractive index is the 1st derivative of the light path equation:

$$e'_X = \frac{\partial x}{\partial z} = \int_z \frac{1}{n}\frac{\partial n}{\partial x} dz \quad , \quad e'_Y = \frac{\partial y}{\partial z} = \int_z \frac{1}{n}\frac{\partial n}{\partial y} dz \qquad (4.6, 4.7)$$

When the optical disturbance occurs inside the test section (as in the DyFo), the deflection of the light beam when leaving the test section will follow the Snell's law (4.3), *n sine' = n_0 sine*, *n* and n_0 being the refractive index inside the DyFo and in the surrounding air, respectively. The final deflection *e* will then be:

$$e_X = \frac{\partial x}{\partial z} = \frac{1}{n_0}\int_z \frac{\partial n}{\partial x} dz \quad , \quad e_Y = \frac{\partial y}{\partial z} = \frac{1}{n_0}\int_z \frac{\partial n}{\partial y} dz \qquad (4.8, 4.9)$$

4.2 Optical set-up and working principle of a Schlieren system

The optical set-up of the Schlieren system used with the DyFo test rig is shown in Figure 4.2 and consists of (in systematic order):

- A light source (Ne/He-laser, monochromatic light with wavelength λ=632,8 nm)
- A dispersing lens spreading the laser light beam
- A collimating lens making the light beam parallel through the test section
- A focusing lens
- A cut-off aperture placed in the focus of the aforementioned focusing lens
- A second focusing lens
- A screen, film camera, video camera or other image presenting item

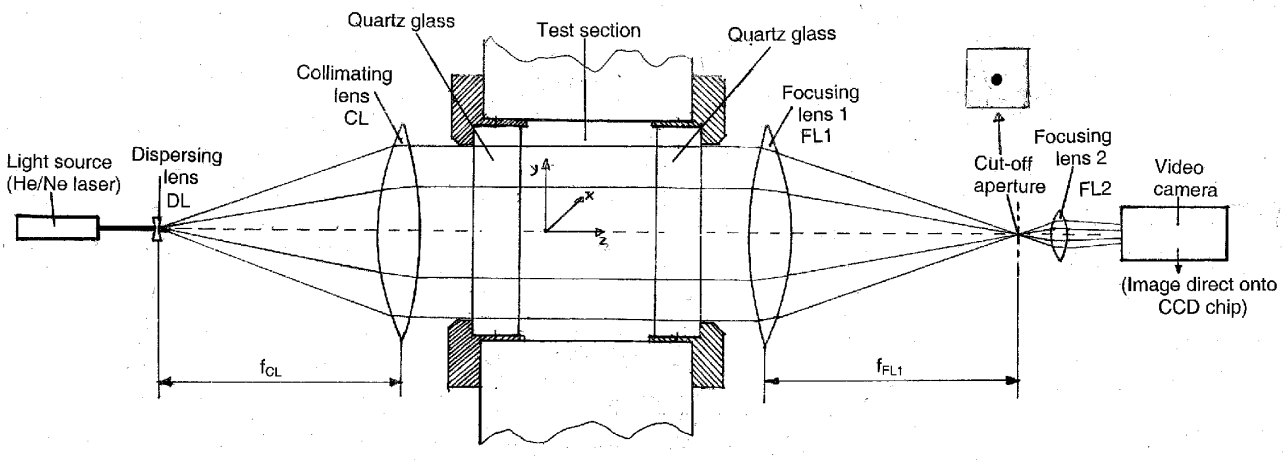

Figure 4.2 Optical set-up of the Schlieren system.

The system is working in the following manner (26):

The laser light is dispersed in a lens (DL) and thus creates a monochromatic light source at DL. The lens DL is placed in the focus of the collimating lens (CL) giving a parallel light beam through the test section. The focusing lens (FL2) behind the test section creates an image of the light source in its focal plane (cf. Figure 4.3). The focusing lens FL2 behind this plane makes an image of the phenomenon to be studied in the test section on the CCD chip in the video camera.

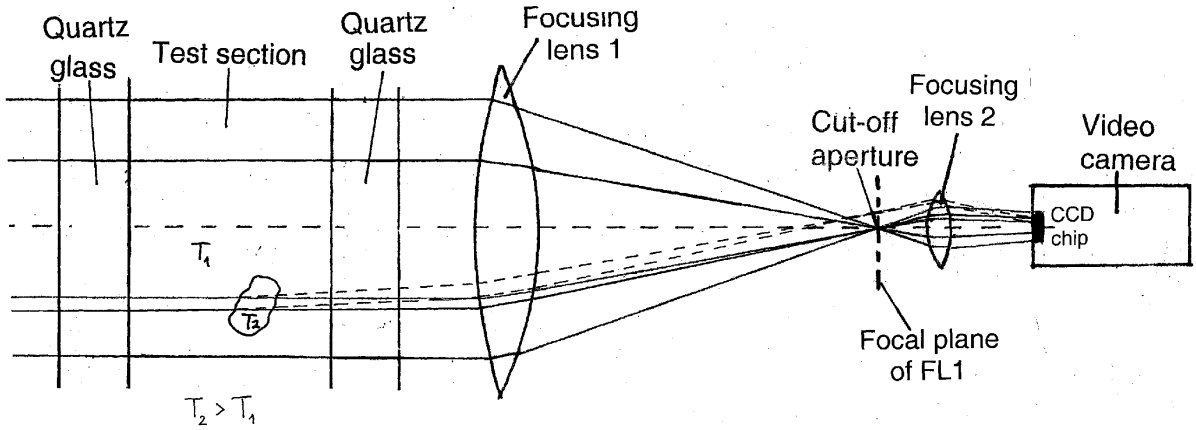

Figure 4.3 *Details of how the Schlieren system register changes in refractive index. Undisturbed light is shown solid-drawn, disturbed light dotted.*

Since the light is parallel through the test section, light from each point in the *xy* plane (cf. Figure 4.2) can be regarded as giving individual images of the light source (emerging from DL) in the focal plane of the lens FL1. If no gradients in the refractive index exist (or the gradient is uniform), all these images will coincide. With gradients in the test section (e.g. in a small area as shown in Figure 4.3) light rays from these areas will get an angular deflection e and the corresponding images in the focal plane of FL1 will be displaced by $f_{FL1}{}^{x}e$ (with good enough accuracy). Irrespective the direction of the deflection, all light from a point in the phenomenon studied in the test section will be brought to a focus at the CCD chip.

The image is hence not displaced by the deflection of parts of the light travelling through the test section. The major idea of the Schlieren method is to catch these deflected light rays in that focus, but not the undisturbed ones. By putting a cut-off aperture in the focal point of lens FL1, the undisturbed light is masked away, and only light deflected outside it reaches the CCD chip (as shown in Figure 4.3).

The light intensity (or illumination) I of the image captured at the CCD chip will vary with the deflection in areas of differing refractive index. In combustion both pressure and temperature increase, but the dominating factor for refractive index gradients is the temperature. In practice this means that increasing light intensity means increased temperature in the corresponding area of the test section.

The explanation of the change in intensity I with the use of a cut-off aperture and deflection of light is given in the literature (26–29).

In the DyFo Schlieren system the light intensity with the cut-off aperture in place according to the theory should be reduced to zero. However, imperfections in the lenses and the optical alignment of the set-up will give some light transmission to the CCD chip even if the aperture in use completely covers the direct image. The light intensity from the He/Ne-laser governs the "strength" of this direct image. For obtaining the best results, the He/Ne-laser light intensity must be adjusted; this is done by a pair of polarization filters (one in front of the laser and one in front of the camera).

In addition the video camera has a set of adjustments that can be operated remotely. The most important is the GAIN. By adjusting this setting, the camera will change its sensitivity for light. In the pre-electronic age, such an adjustment had to be done with the Schlieren set-up alone.

Both changing the camera GAIN and the light intensity from the He/Ne-laser can adjust the sensitivity and working range.

Figure 4.4 shows how the DyFo Schlieren system works with the chosen cut-off aperture and varying the sensitivity of the camera (reduced step-by-step from upper left to lower right). The result is like changing the light intensity from the laser. In addition the size of the aperture affects the sensitivity of the Schlieren system. The image shows the visible area of the DyFo combustion chamber through the two quartz glasses. The two dominating streaks in the images are made from oily exhaust outside one of the glasses leaking out of the combustion chamber during periods of high pressure (due to compression and combustion). The cut-off aperture fully covers the direct image in the focal point of the 1st focusing lens. Because of the oily exhaust streaks, the light deflects and gives an image even when the camera GAIN has reduced the sensitivity to the minimum level.

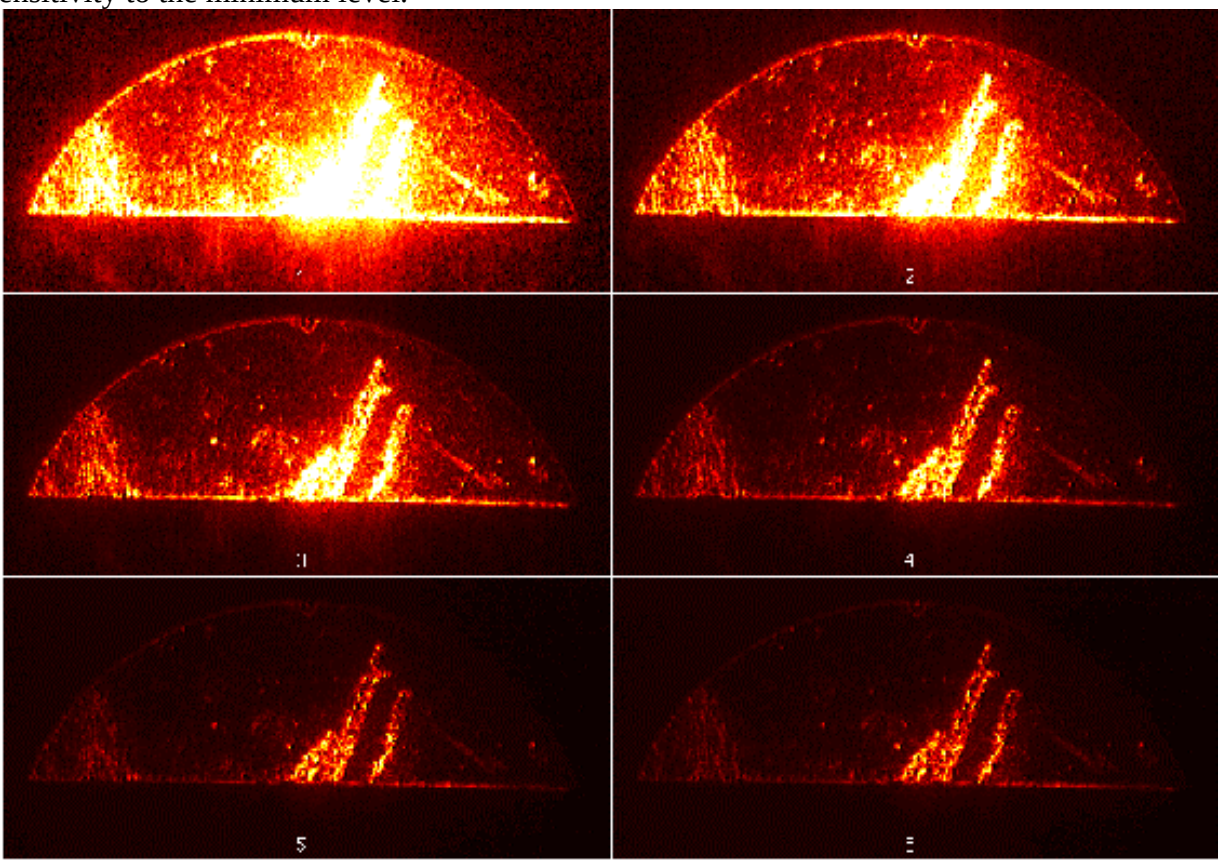

Figure 4.4 Light intensity of a DyFo-image with varying video camera GAIN.

4.3 Schlieren images of diesel combustion.

Practical difficulties

When using the Schlieren technique for imaging diesel ignition and combustion, the main difficulty is the same as in all Schlieren set-ups: accurate alignment of the optical components and absolutely no movement of them during the test period.

When working with diesel combustion, the quartz glasses must be cleaned with short intervals because of exhaust fouling. The fastening of the glasses is part of the alignment of the system, which has to be done with the compact laser beam. Then the dispersing lens in front of the laser has to be removed. This implies practical problems.

Light transmission

In the diesel spray, the mass distribution makes the light transmission very restricted. In the core, the spray is liquid and no light is transmitted. Only in the outer periphery, where the fuel droplets are mixed with air, the density is low enough to transmit some of the light. In the DyFo the normal view of the situation by injection of pilot diesel fuel spray is like the image shown in Figure 4.5 (the visible section through the quartz glasses is the enlightened ½-circle).

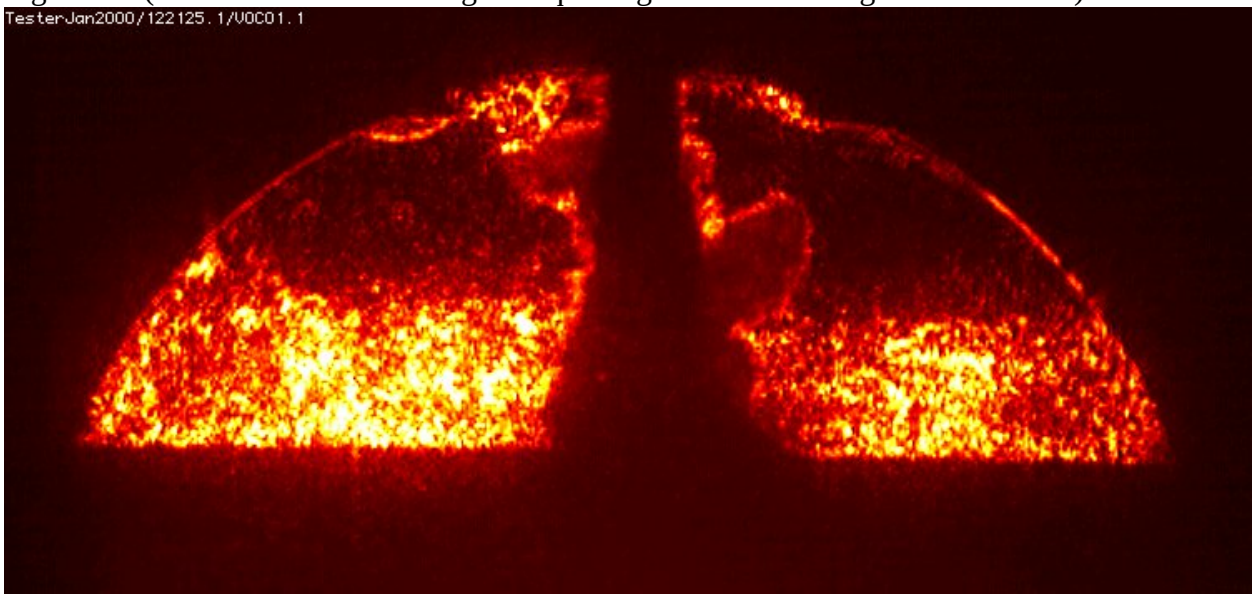

Figure 4.5 Schlieren image of pilot fuel injected in the DyFo filled with air.

The upper dark part of the image shows quiet air. The lower border is the top of the piston. Ahead of this border on each side of the fuel spray, light intensified by deflection in the turbulent layer on top of the piston is shown.

Density gradients will arise when different components don't mix homogeneously in the combustion chamber. Figure 4.6 shows a Schlieren image obtained when propane in great quantities by accident leaked into the combustion chamber in the DyFo prior to injection and resulted in a far too high combustion pressure (160 bar - the construction limit is 120 bar). Consequence: the quartz glasses were broken!

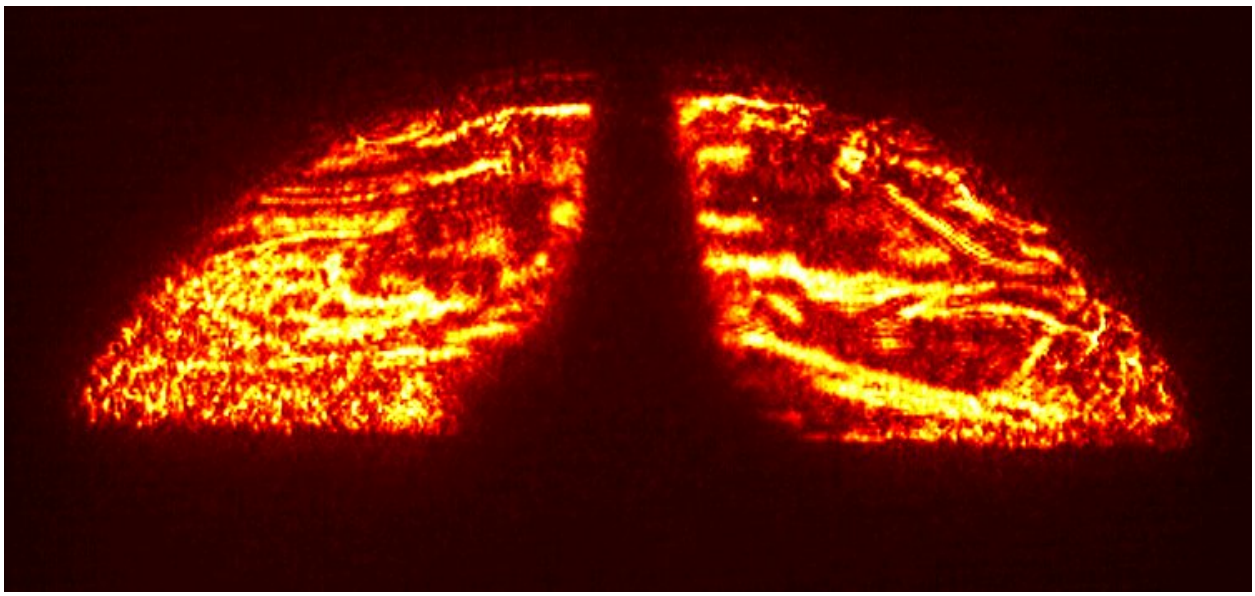

Figure 4.6 Schlieren image of pilot fuel injected in the DyFo filled with air & propane.

Light emitted from flames

When the fuel ignites, light produced in the flame will be emitted in all directions. This light will consist of many wavelengths (polychromatic, “white light”) in contrast to the mono-chromatic laser light (wavelength λ=632,8 nm) sent through the combustion chamber. The Schlieren image created by the laser light will then be disturbed. To interpret such images, experience is needed. In Figure 4.7 two images taken of the same combustion (however from 2 different injections) are shown, the upper with a band pass filter (transmitting only light with λ=633±5 nm) and the lower without any filter.

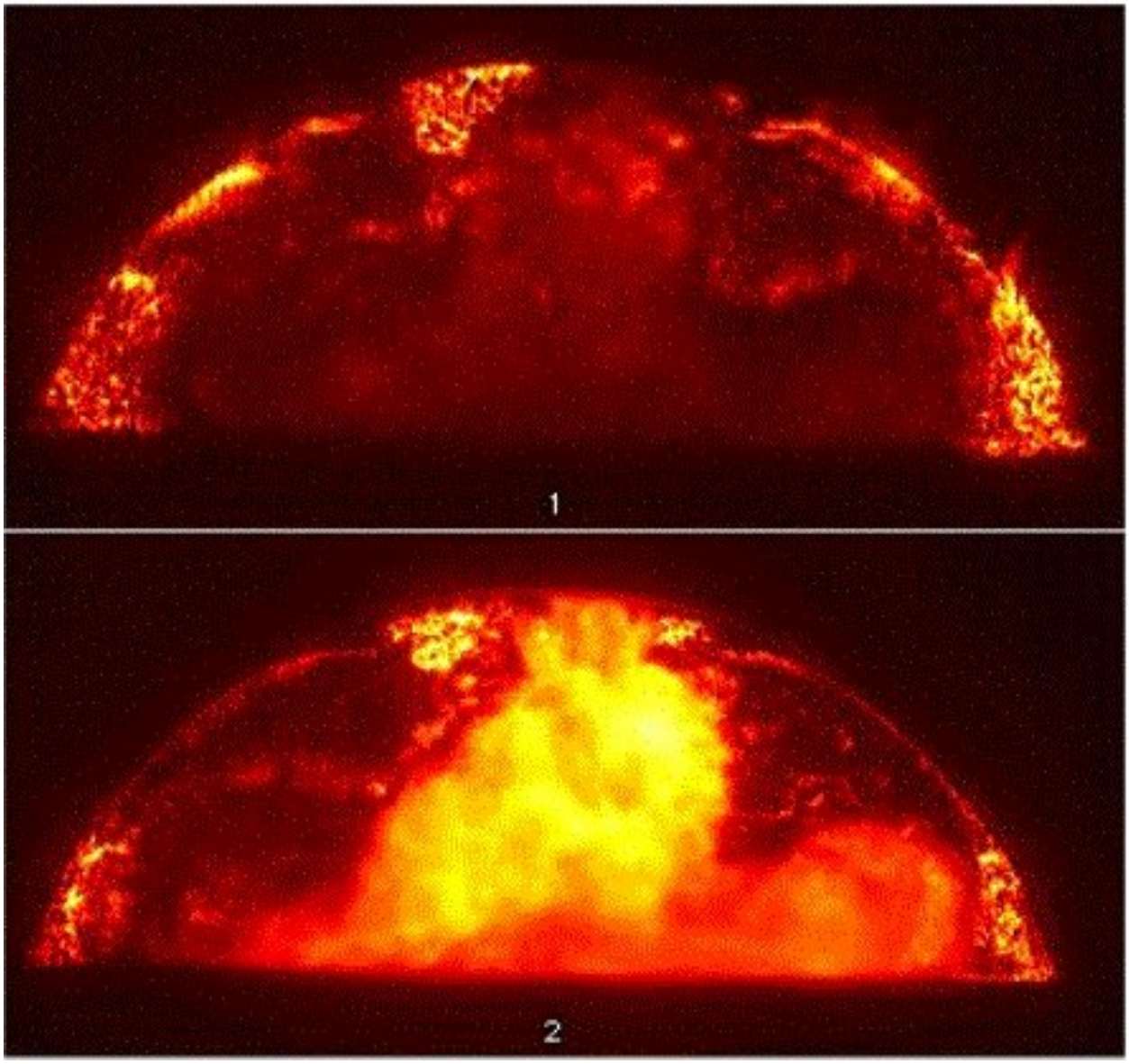

Figure 4.7 Images of early combustion in diesel pilot fuel recorded with (upper) and without (lower) a band pass filter in front of the CCD on the video camera.

However, when studying the early phases of the combustion including the moment of ignition, it is very convenient to register the emitted light from the first flames. This light gives distinct information of when and where the ignition occurs contrary to the refraction of laser light due to temperature gradients - Figure 4.7 being an excellent example.

Experience from low speed piston tests

When starting the study before redesigning the test rig, the piston speed was very low and ignition delays correspondingly long. The end compression temperature was low and according to section 3.3.3 the low temperature reactions were slow compared to after the redesign of the rig (cf. section 5.1). To get used to operate the test rig, preliminary tests were carried out. In addition to the main target - to be acquainted with the DyFo – some interesting results were found as well.

As can be seen from Figures 4.8 and 4.9, the pilot fuel spray reaches the piston top before ignition occurs. This makes it more difficult to see what happens immediately before ignition occurs, as the fuel concentration increases in the lower part of the cylinder. This is where the ignition normally starts. By studying ignition and combustion, this is not a desired situation, but it is not unusual in diesel engines. However, the combustion chamber geometry, the fuel spray velocity and the ignition delay (due to combustion chemistry) restrict the possibilities to change this fact by studies in the DyFo (cf. section 3.1.1).

In the preliminary tests the observed ignition delays of standard reference diesel fuel were very long (8 – 10 milliseconds). This implies that the temperature at the end of compression was low, the reason thought to be the low piston speed. Unfortunately, this conclusion has not been verified. As the tests were preliminary, no dynamic signals were recorded and the actual temperature at the end of compression is not calculated.

Some interesting images were recorded during this first period - Figure 4.8 showing "ignition nuclei" after diesel fuel injection in residual VOC/charge air mixture according to the «Dual Fuel Diesel Process».

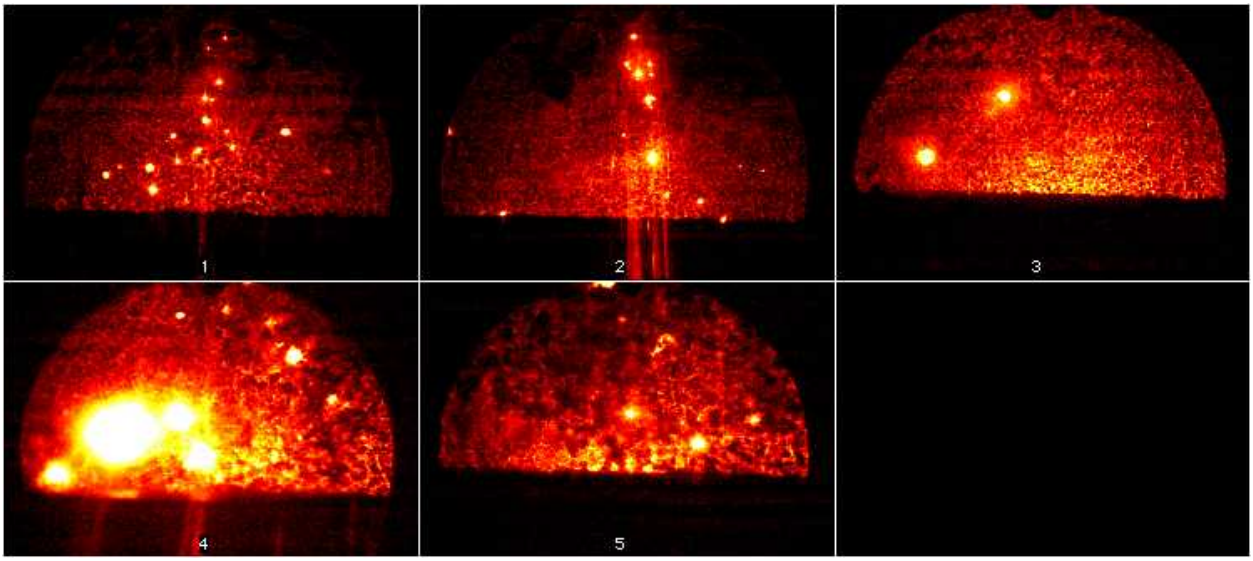

Figure 4.8 "Slow speed" combustion of diesel fuel and residual VOC. Images taken 15, 18, 30, 50 and 60 ms after start of fuel injection.

Figure 4.9 shows the same "ignition nuclei" when VOC Fuel and pilot diesel fuel were injected simultaneously into the charge air according to the «Condensate Diesel Process» in the DyFo test rig operating with low speed piston movement.

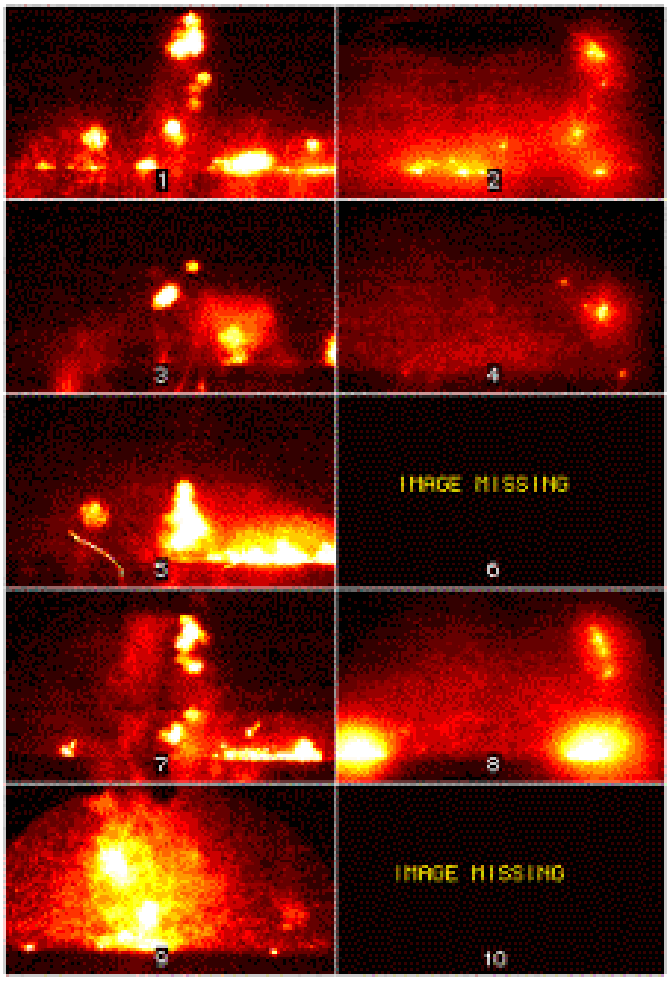

Figure 4.9 *"Slow speed" combustion of VOC Fuel and pilot diesel fuel. The images taken in two directions 10, 11.5, 12, 12.5 and 13 ms after start of injection.*

Although the picture quality is not good and the contour of the combustion chamber is diffuse, the images show that the fuel ignites at many places simultaneously both high and low in the combustion chamber. This is not in good agreement with classical combustion theory for the diesel process.

However, when the ignition delay is long, the fuel-air mixing process duration will also be long. The correct air-fuel ratio therefore can be prepared in a large part of the combustion chamber. A long ignition delay also implies that the low temperature reactions are dominating on the time scale and that the radical pool generation (cf. section 3.3.3) is slow. The diesel fuel "normally" ignited at the spray tip therefore is given more time to mix with the charge air. Thus the premixed part of the combustion is increased, as well as the condition in a large part of the combustion chamber is prepared for ignition of the fuel.

It is not registered any "ignition nuclei" when studying the combustion following high-speed piston movement. When the end compression temperature is lower than in normal diesel operation, all chemical reactions are retarded, and what was observed as "ignition nuclei" by the aforementioned "slow speed" combustions probably is a common step in all combustions, but not possible to observe when the process is speeded up.

5 Experimental setup

5.1 Experimental hardware (test rig)

The test rig for the experiments performed for this thesis is a rapid compression machine named "DyFo" (abbreviated from the Norwegian words for "dynamic combustion rig" – Dynamisk Forbrenningsrigg). The rig consists of (numbers in brackets refer to positions in Figure 5.1):

a) Hydraulic working cylinder, combustion chamber with optical access and valves for inlet/outlet of charge air/exhaust (1a-1d/4a-4b)
b) Fuel injection systems for pilot diesel and VOC Fuel (not shown)
c) Hydraulic system (300 bars) (2a-2F)
d) Computer system to control the injection and sample dynamic signals and images from the injection, ignition and combustion (3a-3e)
e) Visualisation system with lasers, lenses, video cameras and computers (5a-5j)

A principal drawing of the system is shown in Figure 5.1 (30).

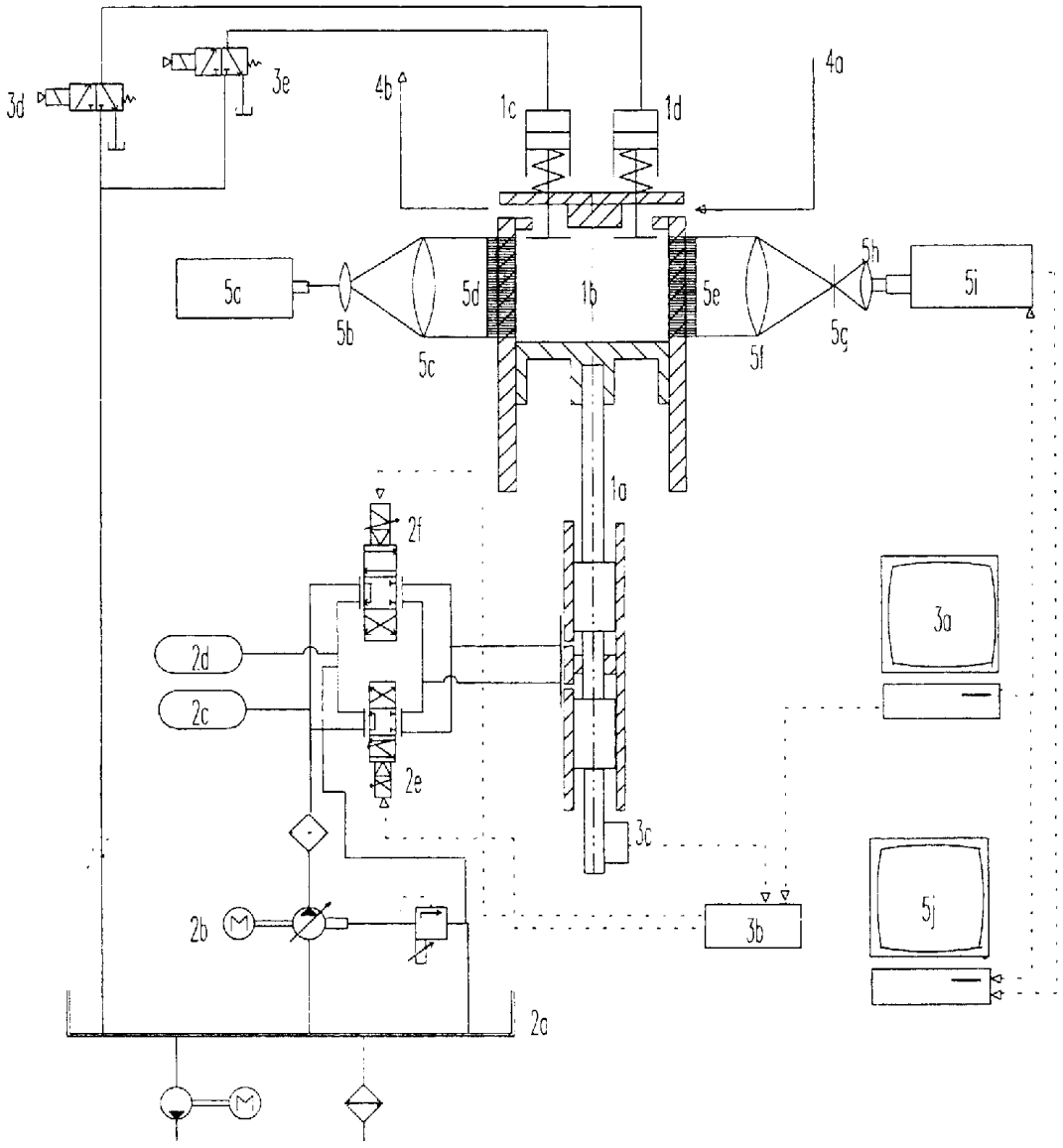

Figure 5.1 Schematic drawing of the DyFo and its sub-systems (30).

By diesel combustion, as shown in section 3.2.2 and discussed in section 3.3.3, the temperature at the end of compression is of great importance for ignition. The original DyFo test rig design, made for Otto process combustion, resulted in a temperature too low for normal diesel engine operation. A redesign of the DyFo (described in Appendix 2) was therefore made to increase this temperature in order to reduce the ignition delay.

Before the change of the hydraulic system, when the obtainable mean piston speed was about 1 m/s, it was believed that increasing this speed would reduce the heat and mass losses in such a way that the ignition delay would be drastically reduced. The result (with a mean piston speed of about 7 m/s) was according to this philosophy - the ignition delay for the reference diesel oil was reduced to approximately 1 millisecond.

To check if low piston speed in the new configuration would give the same result as before the redesign of the DyFo, tests with different piston speeds were conducted. The piston reference motions used were 25, 10 and 5 Hz inverse ½ cosine waveform giving a real piston mean speed of about 7, 4 and 2 m/s. The resulting motion and cylinder pressures are shown in Figure 5.2 and 5.3.

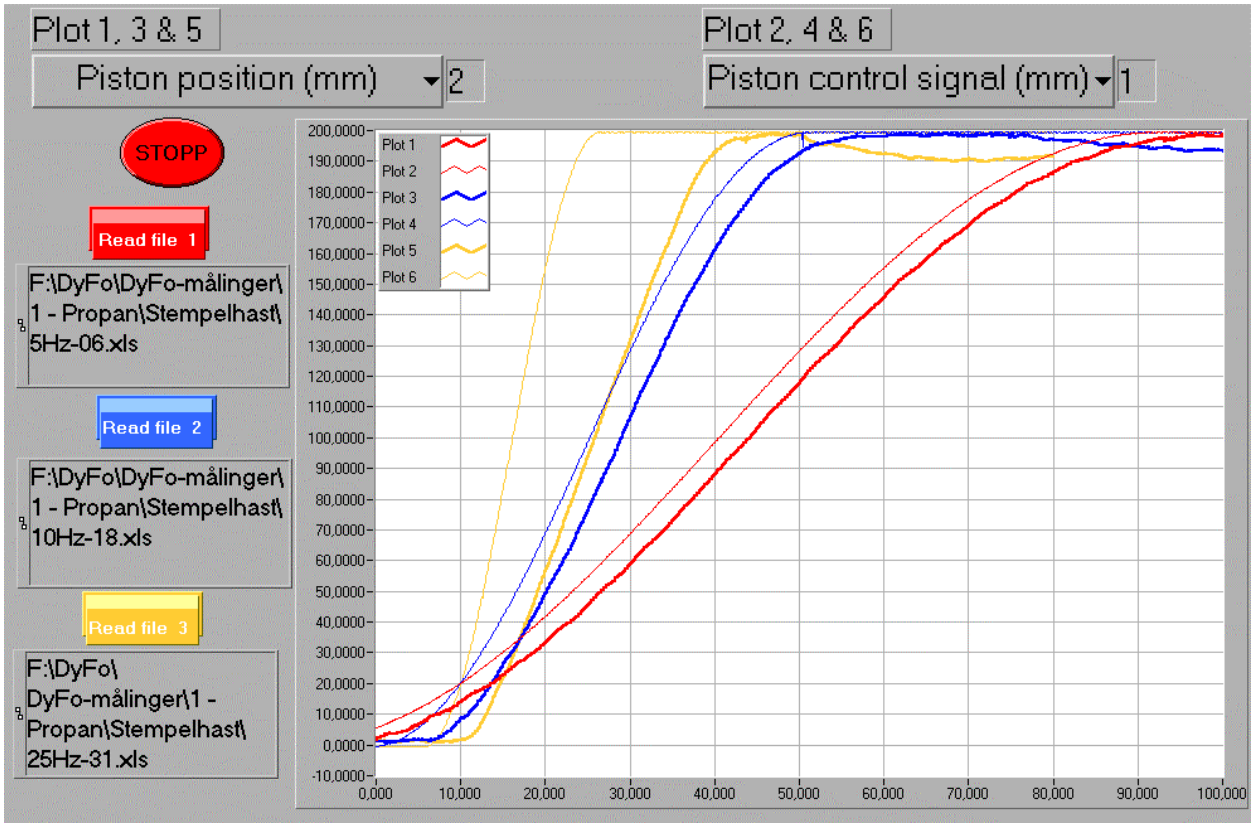

Figure 5.2 Plots of piston movement – reference and real values for 25, 10 and 5 Hz inverse ½ cosine waveform reference signals

As shown in Figure 5.3 the different piston speeds only give very small variations in the cylinder pressure obtained. By studying Figure 5.4 it can in addition be observed that the ignition delay for pilot diesel fuel do not differ very much either. This must mean that the leakage of both heat and charge air mass have been reduced by the redesign process.

In Figure 5.4 both the VOC Fuel mass and the pilot fuel injection timing relatively to the piston position varies, but none of these variations affects the findings above.

Unfortunately no tests with similar conditions have been saved from the initial DyFo design to make a comparison possible. However, the goal - reduced ignition delay - was reached.

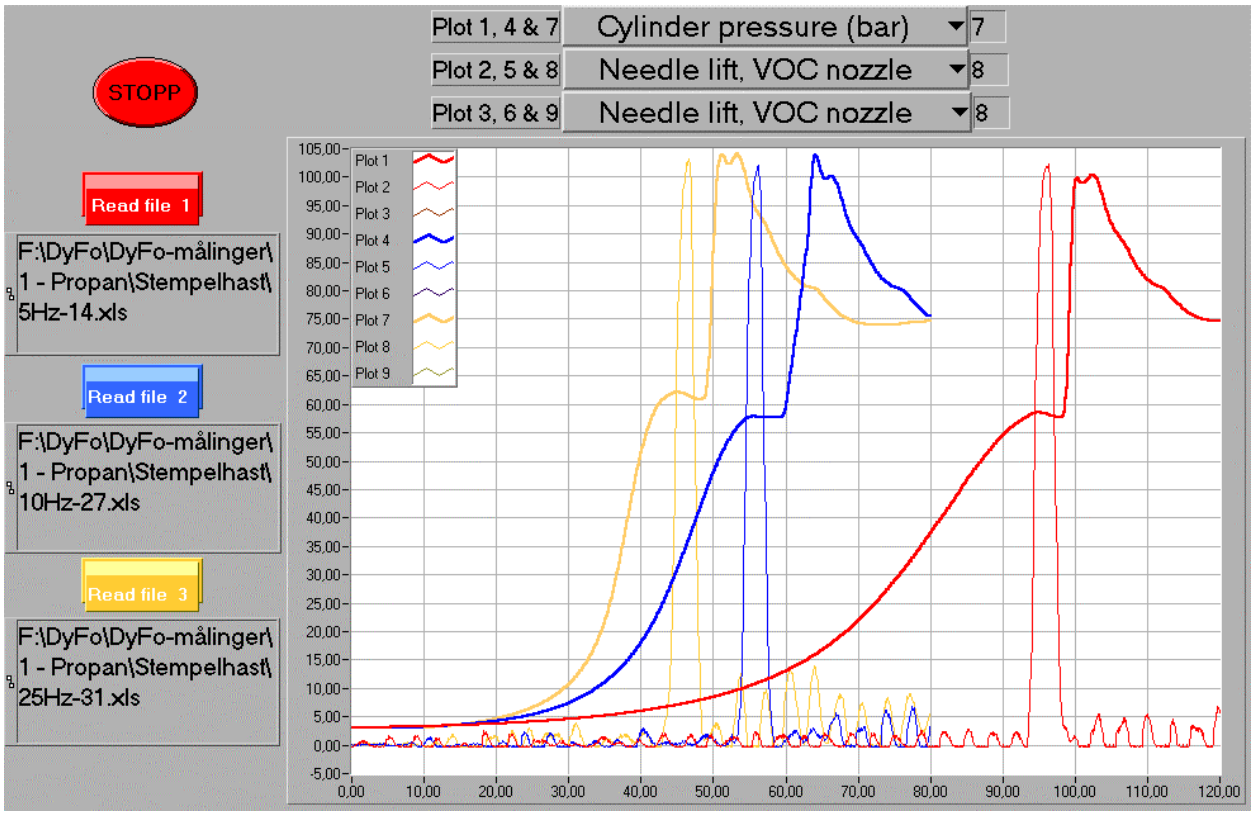

Figure 5.3 *Combustion of VOC Fuel only. Plots of cylinder pressure and VOC Fuel nozzle needle lift for 25, 10 and 5 Hz inverse ½ cosine waveform reference signals.*

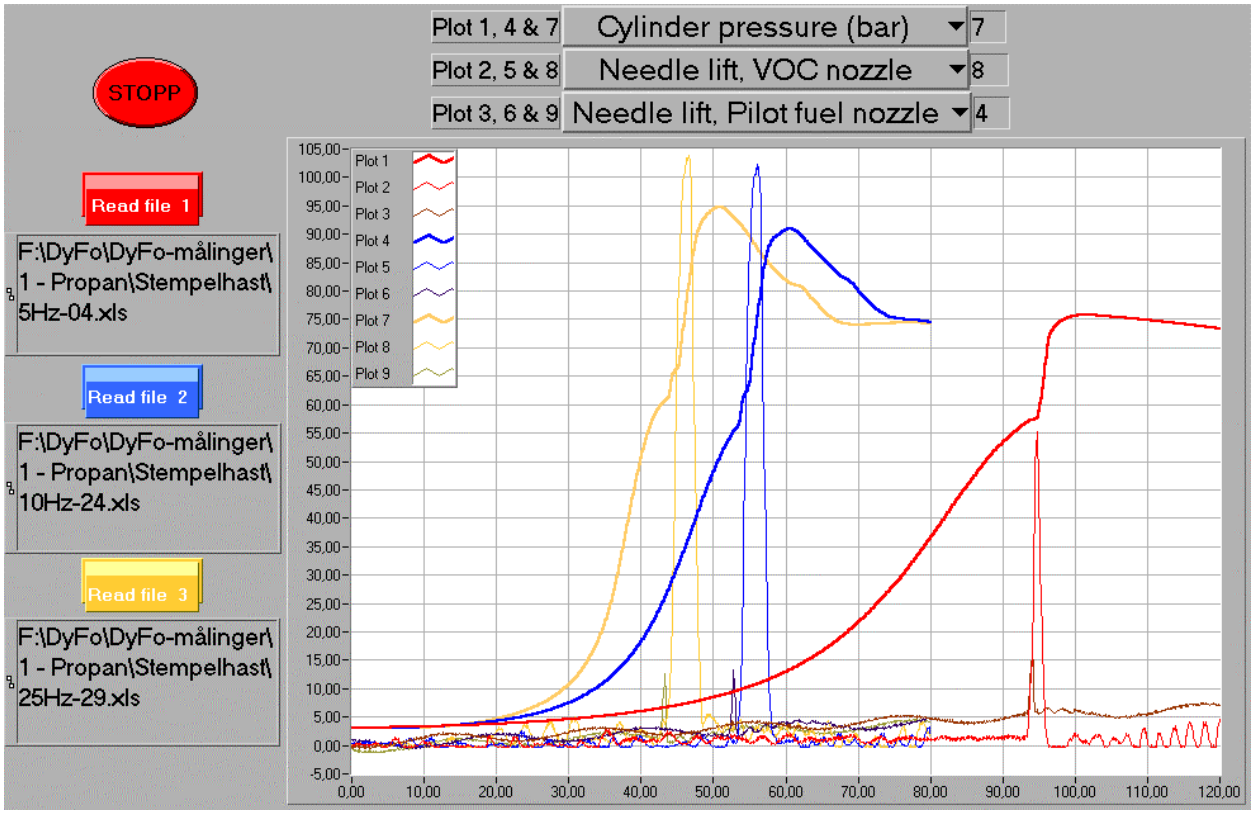

Figure 5.4 *Combustion of VOC Fuel + pilot diesel. Plots of cylinder pressure, VOC Fuel nozzle and pilot nozzle needle lift values for 25, 10 and 5 Hz inverse ½ cosine waveform reference signals.*

5.1.1 Hydraulic working cylinder, combustion chamber and charge air system

A working cylinder driven by hydraulic oil at ≤ 350 bars activates the piston in the DyFo. The working cylinder is redesigned to be able to handle the forces the required high piston speed gives. It has been manufactured in the workshop at Statoil R&D centre in Trondheim.

The DyFo combustion chamber (1b in Figure 5.1) is shown in detail in Appendix 2. The special shape is a result of the need for optical access in two directions and a high compression ratio. During the tests reported in this thesis the following details for the combustion chamber applies:

	Diesel process	Otto process
Stroke (max - min):	200 - 0 mm	200 - 0 mm
Bore:	80,5 mm	80,5 mm
Swept volume (max - min):	1017,92 cm^3	1017,92 cm^3
Volume at BDC:	1117,92 cm^3	1163,34 cm^3
Volume at TDC:	100 cm^3	145,42 cm^3
Compression ratio (max):	11,1792 : 1	8 : 1
Charge air pressure:	2,5 – 3,0 bar	2,0 – 3,0 bar
Compression pressure:	45 – 70 bar	35 – 55 bar
Normal hydraulic oil pressure:	300 bar	300 bar

Charge air is fed to the combustion chamber from a gas cylinder with pressurised air. On its way it is heated in a water-to-air heat exchanger as described above.

5.1.2 Fuel injection systems for pilot fuel and VOC Fuel

The test rig is designed for experiments with most kind of fuels - both liquid and gaseous (30). In the tests reported in this thesis, two fuels have been injected in liquid phase through two separate fuel injection systems.

The pilot fuel is injected through an electronic operated common rail system (31). Computer control of this system enables accurate timing and duration of the injection, and the repeatability is documented by cylinder pressure and ROHR plots of several injections over a long period.

The VOC Fuel is injected through an electronically controlled and hydraulic actuated injector. The VOC Fuel fuel system is developed during the work with this thesis and consists of:

- hydraulic oil tubing
- a rapid electronically operated control valve (DIGIvalve)
- an air driven high pressure liquid fluid pump (Haskel pump)

A standard Bosch diesel injector (KBL 70 S177/4 230) is modified to allow for common rail operation. Hydraulic oil at 300 bars opens the VOC Fuel nozzle by lifting the needle valve as long as the control valve (32) is set to lead the oil into the injector. The duration of this opening period is controlled by the computer system. The nozzle is closed by two springs at the end of the control signal for opening and the hydraulic oil is released.

During the tests reported in this thesis the following details for the injectors applies:

	Pilot fuel injector	VOC Fuel injector
Nozzle type	Bosch DSLA 0PV3378543 / 670	Bosch DLLA 28 S589
Nozzle hole diameter (mm)	0,35	0,55
Needle lift (mm)	0,10	0,15
Injection pressure (bar)	400	400

A sectional drawing of the VOC Fuel injector is shown in Figure 5.5.

The system for feeding VOC Fuel to the injector is schematically shown in Figure 5.6.

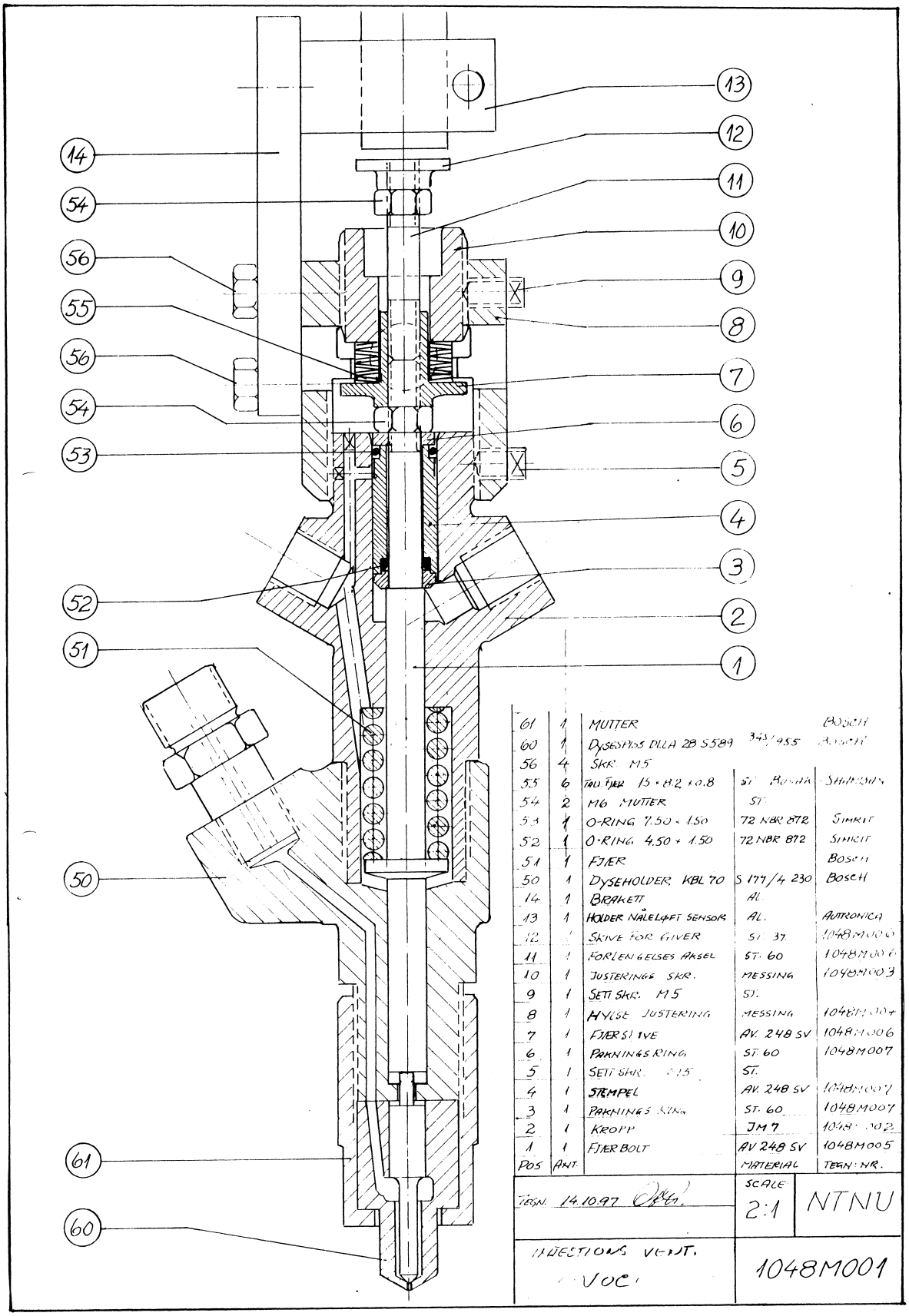

Figure 5.5 Sectional drawing of the VOC Fuel single hole injector.

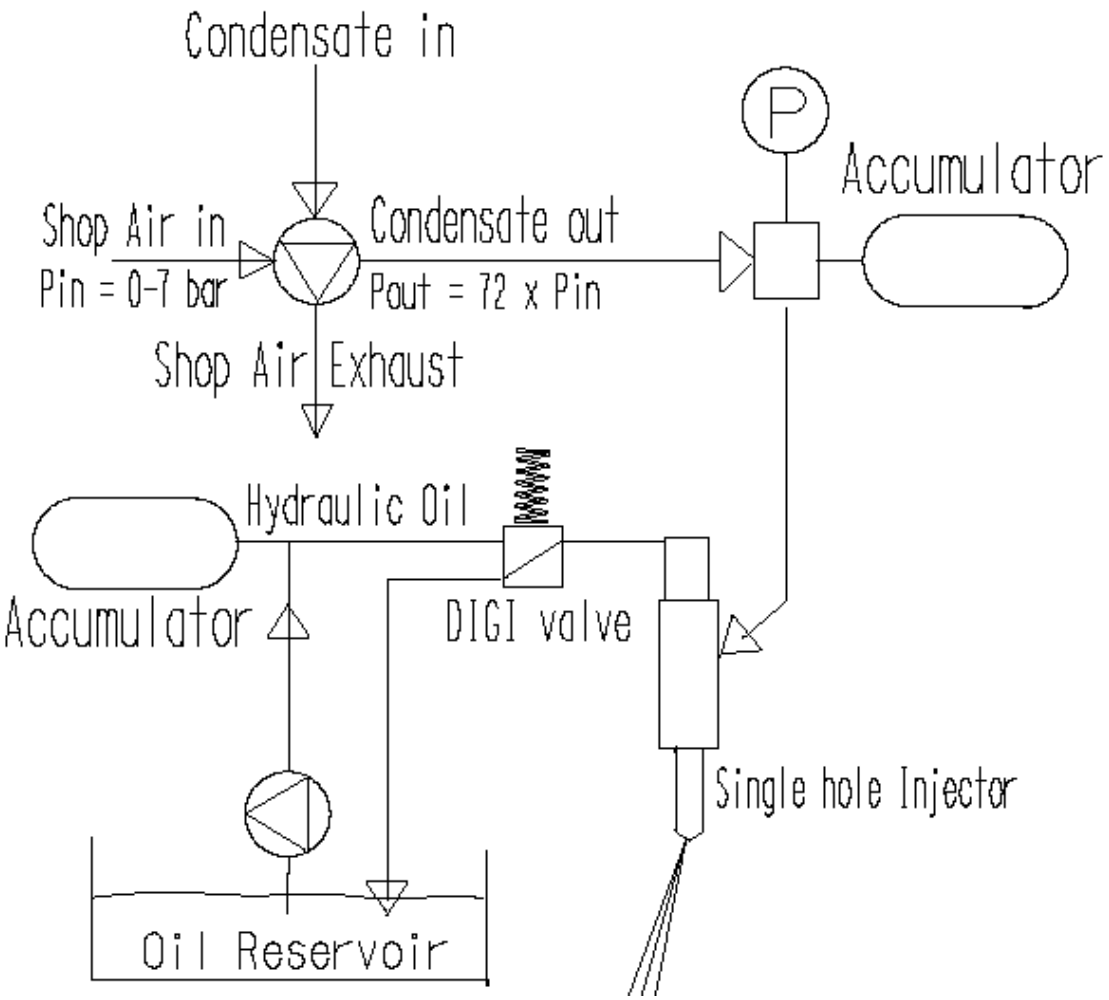

Figure 5.6 System for feeding VOC Fuel (condensate) to the injector.

5.1.3 Hydraulic system

The main features of the hydraulic system are described in (30). For the experiments reported in this thesis no major changes were made to this system. To obtain the required high piston speed the two MOOG servo valves were operated in parallel. The only addition that was made to the system was to connect the hydraulically operated electronic control valve (DIGIvalve) for operating the VOC Fuel injector. This additional injector and hydraulic system, however, caused a lot of trouble and slowed down the progress in the experiments for many months.

5.1.4 Visualisation system

The visualisation system is described in detail in a previous publications (30, 54, 55). A description of the principle of the system is given in Chapter.4. It has only been made minor changes and adjustments to the system for the work reported here. The main components are:

- 2 light sources (He/Ne lasers)
- 4 quarts glasses in stainless steel holders for optical access
- 2 sets of optical lenses to direct the light correctly through the cylinder
- 2 aperture stops

5.2 Experimental test matrix

The practical execution of the work to support Statoil to solve the environmental problem of the huge VOC releases in connection with loading crude oil in the North Sea led to a threefold set of actual experiments:

1. The major part of the work has been to perform *diffusion combustion of VOC Fuel* injected at high pressure and ignited by a pilot diesel spray.

2. A minor part of the work has been tests with *homogeneous combustion of residual VOC/air charge* fed at low pressure and ignited by a pilot diesel spray.

3. As a third part, the intention was to perform tests with *combustion of light VOC fractions trapped in hydrates*. This part has been reduced to a short survey of possibilities of using this method and a few combustion tests with pilot diesel ignition of methane in the DyFo.

5.2.1 Diffusion combustion of VOC Fuel injected at high pressure

The main part of this study consists of experiments with the condensed fraction of VOC (VOC Fuel) injected at high pressure and ignited with a pilot fuel spray. In an attempt to find characteristically ignition and combustion properties of the different fractions in the VOC Fuel, the experiments have mainly dealt with single VOC components. Studies of the following fuels are performed:

- Propane
- iso-Butane
- n-Butane
- a blend of Propane/iso-Butane/n-Butane
  (to simulate the condensed VOC fraction at the Statfjord field)

To conduct these experiments, different test variables and parameters were chosen to constitute an initial test plan. Details of the test plan are shown in Appendix 3. During the progress of the work, however, several changes to this plan had to be made. In Chapter 6 this work is reported.

5.2.2 Homogeneous combustion of residual VOC/air charge

A minor part of the work has been a study of homogeneous combustion of a mixture of the non-condensed fractions of VOC (mainly methane and ethane + the inert gas fraction) and air at different values of Alfa (cf. Chapter 1 and 2). This work is reported in Chapter 7.

5.2.3 Combustion of light VOC fractions trapped in hydrates

This part is limited to some theoretical aspects and simple tests with methane injected at high pressure and ignited by pilot diesel fuel in the DyFo. In the plans of Statoil, the "VOC Hydrate" part ranges at the bottom of priorities. Chapter 8 includes the work done in this part.

5.2.4 Experimental details for diffusion combustion of VOC Fuel.

In the main work (diffusion combustion of VOC Fuel), the following set of parameters has been used to study the ignition and early combustion of VOC in the dynamic combustion rig (DyFo).

a. Injection timing.

The effect of different injection timings for VOC Fuel and diesel pilot fuel were studied by varying the following test parameters:

- start of injection of pilot fuel relative to the piston position
- start of injection of VOC relative to start of injection of pilot fuel

b. Air-fuel ratio (l).

The ignition delay in the DyFo has proved to be dependent of the total excess air ratio, and the following test parameters were varied:

- amount of pilot fuel (low & high)
- amount of VOC Fuel (low & high)

These variations give 4 values of the ratio pilot/VOC fuel amount (low-low, low-high, high-low and high-high).

c. Operational parameters.

The ignition delay is dependent of the compression temperature in the cylinder, and the compression temperature depends on a set of parameters controlling the operation of the test rig. However, in the experiments the only parameters tested were:

- charge air temperature (low & high)
- charge air pressure (low & high)

Other test parameters and adjustments have been varied prior to the experiments to find the best test design regarding the ignition delay for diesel fuel - by increasing the cooling water temperature from 80 to 120 °C, the ignition delay was considerably reduced. Tests with only diesel fuel are the basis in the study and exist as a reference to all the tests in this study.

d. Spray direction of VOC Fuel

It is possible to direct the VOC Fuel spray in different angles relative to the diesel pilot spray. The VOC Fuel injector is mounted at an angle of 35 ° relative to the vertical and inline visualisation direction no. 1. The nozzle hole makes an angle of 28 ° relative to the vertical direction of the injector. Depending of the mounting of the VOC Fuel injector in the cylinder head, the following settings of the VOC Fuel spray direction are obtainable:

a) Along the roof of the combustion chamber (35 ° + 28 ° = 63 ° relative to the direction of the pilot fuel spray) in the direction of laser beam no. 1 and through the diesel pilot spray.

b) Down from the roof of the combustion chamber (35 ° - 28 ° = 7 ° relative to the direction of the pilot fuel spray) in the direction of laser beam no. 1, not in contact with the pilot fuel spray until reaching the piston top (i.e. 180 ° turned according to alt. a)).

These two directions represent the limits. By turning the VOC Fuel nozzle holder between these two directions, the VOC Fuel spray will be removed from the diesel pilot spray and the contact between the two sprays will thereby be altered. The third setting will be:

c) The VOC Fuel nozzle holder turned 90 ° relative to the directions in a) and b). The VOC Fuel spray will be injected with an inclination of 35 ° to the pilot fuel spray direction and 28 ° inclined to the direction of laser beam no. 1.

For practical reasons concerning the connection of the fuel pipe to the injector and the orientation of the nozzle in the injector, the settings a) and b) were used initially. However, the VOC Fuel spray direction by these settings was found to be unfavourable as the VOC Fuel spray was directed through the diesel spray (setting a) or reached the piston top too soon (setting b). The ignition delay was found to be negatively affected by these facts and as a consequence, all tests reported here were conducted with the VOC Fuel injected at an angle of 90 ° (setting c).

5.2.5 Test matrix of experiments

A test matrix of possible experiments was set up (shown in Appendix 3). The experiments involve images of the injection/ignition/combustion. Interpolation between images is very complicated, and for this reason no statistical test planning were made. Only a part of the more than 80 different experiments have been carried out - one major reason being a lot of time consuming practical problems occurring during the performance of the experiments. However, all the parameters mentioned in section 5.2.4 have been varied at least once during the test work.

The set of selected tests that have been performed according to the concept of the «Condensate Diesel Process» is shown in Figure 5.7 below. In addition to these tests, some tests with only VOC Fuel have been carried out. This extension to the test matrix was made as a result of a discussion with the manufacturer - MAN B&W – of the engine on board "Navion Viking"(49).

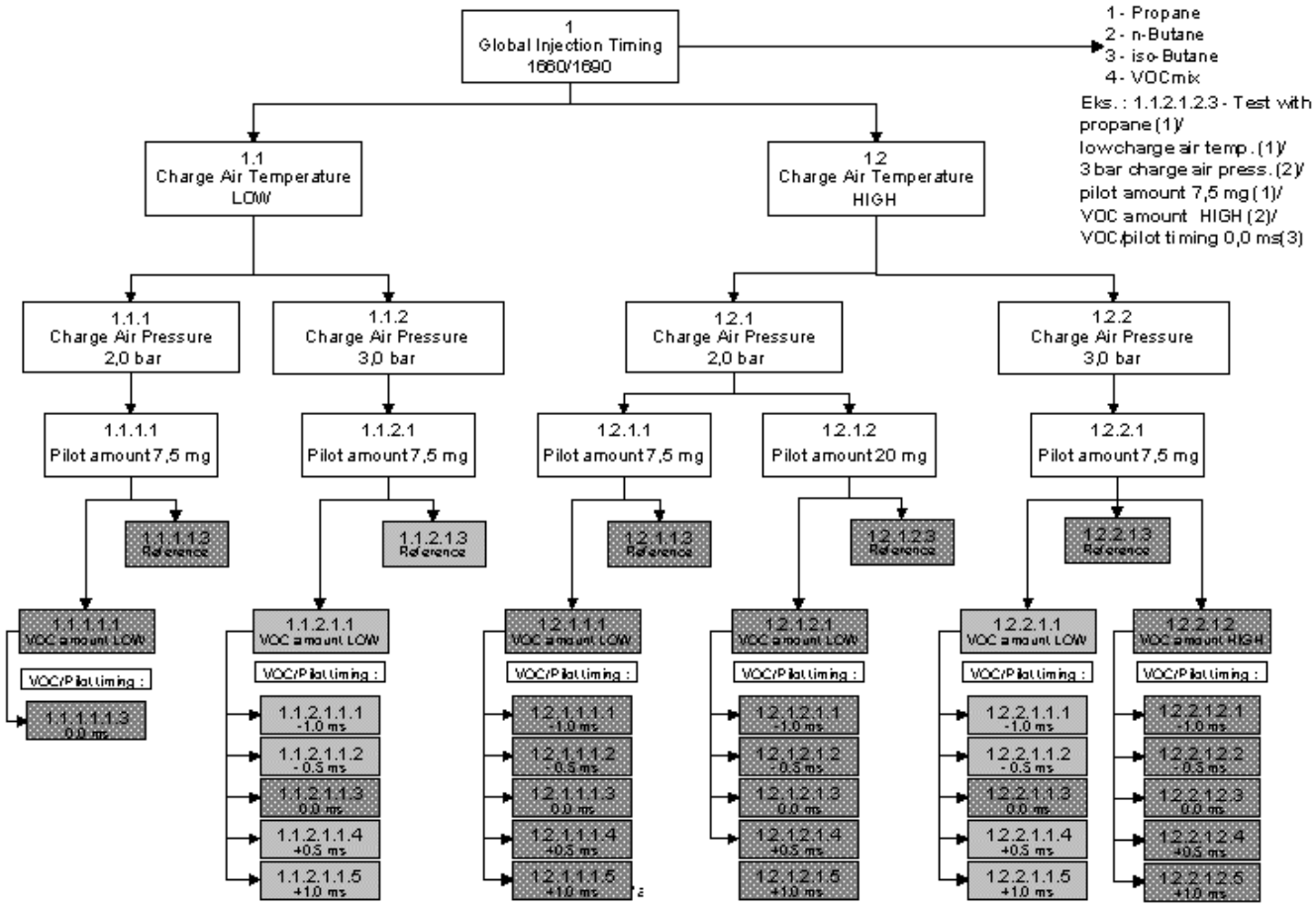

Figure 5.7 Matrix of performed experiments with VOC Fuel

The two different shadings of the boxes in the test set indicate that the tests have been performed under slightly different conditions. The tests in the boxes with the lightest shade were performed before it was found out that the piston was loose on the piston rod. The piston movement has therefore been somewhat different, a fact confirmed by studying the dynamic signals (mainly the piston position and cylinder pressure signals).

6 Diffusion combustion of VOC Fuel

6.1 Test conditions and variables.

The main part of the experimental work is the study of ignition and early combustion of the VOC Fuel. Hydrocarbons present in the VOC Fuel have significantly longer ignition delays than diesel fuel. When injected in a diesel engine, some measures must be taken to improve the ignition. Long ignition delay will give operational problems especially at low loads. In order to avoid these problems, pilot injection of diesel fuel has been used to stabilise the ignition.

To carry out this part of the work, the «Condensate Diesel Process» concept (cf. section 2.4) had to be applied to the DyFo test rig. In brief, this included the development of a "VOC Fuel injector" and positioning and adjustment of the fuel injectors. Important parameters like injection timing and injection pressure for the fuels had to be optimised. For both injection systems a pressure of 400 bars was chosen as the best option based on tests with different injection pressures (200 – 600 bars). The "VOC Fuel injector" manufactured in the workshop at MTS was not fully developed before the tests started. Because of this some changes had to be done during the experiments.

6.1.1 VOC Fuel for the experiments

As shown in Chapter 2 (Figure 2.1) the content of hydrocarbons ranges from methane to hexane. The components available as condensates in the study are those with 3 or more carbon atoms (2) (cf. Table 2.2).

The HC-specification of the VOC released at the Statfjord oil field (Figure 2.1 and Table 2.1) is used as model for the experimental fuels. For the main part of the experiments the VOC fuels used have been delivered as single fuel components by HydroGas. The investigation was started with propane. The tests with this fuel were fairly comprehensive. The experience with the propane tests was used to select the type and number of tests needed with other fuels. The other fuels selected were n-butane, iso-butane and a blend containing 60% propane, 10% iso-butane and 30% n-butane.

All the components of the VOC Fuels are liquid at moderate pressures at room temperature. At 25 ºC propane is liquid at approximately 8 bars, n- and iso-butane at approx. 4 bars and the VOC blend at approx. 6 bars. The VOC Fuel was pressurised by an air driven piston pump with a maximum compression ratio of 71:1 to ensure a constant injection pressure of 400 bars. The outlet pressure in this pump was dependent on both the inlet pressure and the driving air pressure (shop air) (cf. Figure 4.6). To boost propane at 8 bars to 400 bars is straight forward, but the other VOC Fuel types with lower condensation pressure were pre-boosted to 10 bars by helium to ensure the correct injection pressure.

6.1.2 Test parameters and variables.

The parameters varied in the experiments, as mentioned in Chapter 4, are:

- Relative Injection Timing - VOC Fuel relative to pilot fuel (RIT)
- Composition of VOC Fuel
- Pilot Fuel Mass (PFM)
- VOC Fuel Mass (VFM)
- Charge Air Pressure Level (CAP)
- Charge Air Temperature level (CAT)

The four last parameters all affect the total air/fuel ratio (or excess air ratio λ) – cf. section 5.1.6.

Injecting fuel into the DyFo combustion chamber should be carried out in such a way that the process resembles a real diesel engine process as closely as possible. This means among other factors that the injection timing giving the shortest ignition delay in the DyFo had to be found.

Eight dynamic signals are registered every 0,1 millisecond during each test run. More signals should preferably have been sampled, but the amount is restricted by the capacity of the A/D converter by the sample frequency of 10 kHz. The signals are both test parameters set by the operator and test variables used for evaluation of the tests:

1. Piston position control signal (test parameter)
2. Real piston position signal (test variable)
3. Cylinder pressure signal (test variable)
4. Needle lift signal, pilot fuel nozzle (test variable)
5. Needle lift signal, VOC Fuel nozzle (test variable)
6. Charge air pressure signal (test variable)
7. Video camera trigging signal (test parameter)
8. DIGIvalve control signal (test parameter)

Signal 2 - 6 are registered with separate sensors (cf. Appendix 2) while the 3 others are measured from the control signal directly. In addition a control signal is given to start the pilot fuel injection, but this signal is not registered.

The DyFo test rig process has one simplification compared to a real engine process as the piston is left in the upper position (TDC) after compression. The shape of the piston position control signal is an inverse ½ cosine curve. As the piston is not forced to move by a crank arm, but controlled by a hydraulic oil flow, it was found to be most convenient to stop the piston at TDC. The hydraulic oil flow is delayed relative to the piston position control signal. If the piston position control signal were to move the piston back to BDC, this delay would cause the piston not to reach TDC by approx. 2 mm meaning that the compression temperature would be lower.

6.1.3 Pilot diesel fuel injection timing

Injection of the VOC Fuel is adjusted relative to the pilot fuel injection timing. The pilot fuel injection timing is stored in the control program as a value between 0 and 4000. The number of measurements taken by the data acquisition system is also 4000, but the measurement array is delayed relative to the control array. In this way there is no direct dependency between the set point of injection timing and the time scale or piston position. On the other side, the starting instant remains constant, which ensures equal conditions for the tests even if some of the test parameters are changed. The trigging of images is always set relative to the control signal for pilot fuel injection.

The measurements start at a predefined set point before the piston starts its movement. This set point is 10 milliseconds before the time where the control value for the piston movement exceeds 20 mm. In the registered data files, the trigger marks are converted to a timescale in milliseconds starting at 0 at this set point. In the result plots shown in this chapter, however, normally only a part of the total registered datasets are shown, giving timescales of various start point and length.

The increment between measurements is 0,1 ms giving a total duration of measurements of 0,4 seconds. The maximum duration of the control array, however, is 0,2 seconds. The only reason for this is that with the increment reduced to 0,05 ms it is possible to take twice as many images in the same time interval.

To obtain the shortest ignition delay of the fuel, the injection starts near the end of the piston stroke. Because the timing position depends on the response of the control and measurement system, the best choice was found by "trial and error". In order to find the injection timing giving the shortest ignition delay, experiments were carried out varying the injection timing in the range from 1600 to 1700 (of the 4000 points). The shortest ignition delay was obtained at 1690 with the charge air pressure at 3,0 bars and at 1660 with charge air pressure at 2,0 bars. These two values were used throughout the tests giving an ignition delay between 1,0 and 1,5 ms.

6.1.4 Actual fuel mass delivery

In Section 3.1.2 the effect of test conditions on fuel mass delivery was illustrated. Both temperature and pressure drop across the nozzle influence the fuel mass delivery. When calibrating the fuel injectors by ~ 20 °C and 1 bar outside the nozzle, both density and pressure drop differ from the operational conditions, ~ 120 °C and 45 - 64 bars outside the nozzle. The fuel density varies with the temperature. Table 6.1 below shows the density correction factors applied. More details of calculating correction factors are given in Appendix 3.

Table 6.1 Density correction factors for the pilot fuel and VOC Fuel.

	Diesel	VOC Fuel (Propane)
ρ_f (kg/m^3) 20 °C	815,0	555,6
$\rho_{f,op}$ (kg/m^3) 120 °C	746,3	481,0
$\rho_{f,cal}$ (kg/m^3) 20 °C	815,0	578,3*)
Density factor $\sqrt{\rho_{f,op}/\rho_{f,cal}}$	0,957	0,912

**) Calibration of VOC Fuel delivery was made with VOC blend (cf. Appendix 3)*

The cylinder pressure at the time of injection varies with the piston position and the charge air pressure. Table 6.2 shows pressure drop correction factors for the most used test conditions. Appendix 4 gives more details. Applying these factors gives the fuel masses shown in Table 6.3.

Table 6.2 Correction factors due to pressure drop for the fuels used in the tests.

		Diesel	VOC
VOC/pilot relative injection timing (RIT)		-	0,0 ms
Δp, operation (bar)	CAP 2 bar	355	352,5
	CAP 3 bar	340	336
Δp, calibration (bar)		399	399
Δp factor $\sqrt{\Delta p_{op}/\Delta p_{cal}}$ (CAP 2 bar)		0,943	0,940
Δp factor $\sqrt{\Delta p_{op}/\Delta p_{cal}}$ (CAP 3 bar)		0,923	0,918

Table 6.3 Corrected fuel conditions in the test series.

Fuel mass level		LOW		HIGH	
		Mean	STD	Mean	STD
* Calibrated pilot fuel mass (mg)		7,60	0,62	21,70	0,12
Actual pilot fuel mass (mg)	2 bar	6,86	0,56	19,58	0,11
	3 bar	6,71	0,55	19,17	0,11
* Calibrated VOC Fuel mass (mg)		26,20	1,83	78,50	4,84
Actual VOC Fuel mass (Propane) (mg)	2 bar	22,47	1,58	67,33	4,20
	3 bar	21,93	1,54	65,71	4,10

6.1.5 Selection of test series

For the «Condensate Diesel Process» tests, the following parameter set was chosen (test series number indication refers to the matrix shown in section 5.2.5):

- Composition of the VOC Fuel (Test series **0**xxxxx – **4**xxxxx)
  Charge Air Temperature (CAT) LOW vs. HIGH (Test series x**1**xxxx vs. x**2**xxxx)
- Charge Air Pressure (CAP) LOW vs. HIGH (Test series xx**1**xxx vs. xx**2**xxx)
- Pilot Fuel Mass (PFM) LOW vs. HIGH (Test series xxx**1**xx vs. xxx**2**xx)
- VOC Fuel Mass (VFM) LOW vs. HIGH (Test series xxxx**1x** vs. xxxx**2x**)
- Relative Injection Timing (RIT) (Test series xxxxx**1** – xxxxx**5**)

Composition of VOC Fuel: 0 = propane, 1 = iso-butane, 3 = n-butane and 4 = VOC blend.

If the digit indicating PFM or VFM is 0, it means that no fuel of this type was injected.

Relative injection timing (RIT) was altered in steps of 0,5 ms. The VOC Fuel is injected 1,0 ms before the pilot fuel by RIT setting no. 1, 0,5 ms before by setting no. 2, at the same time (0,00 ms) by setting no. 3, 0,5 ms after by setting no. 4 and 1,0 ms after by RIT setting no. 5. To make the test work as time efficient as possible to perform (of a total of 80), only one check of each of the 4 first comparisons were made. Table 6.4 shows the test series, each one consisting of up to 152 single tests, which are used in the subsequent evaluation. Details of the selection of tests are given in Appendix 3.

Table 6.4 Selected test series from the matrix of test series in section 5.2.

	Test series	**VOC Fuel**	**CAT**	**CAP**	**PFM**	**VFM**	**RIT**
1	1**1**1113	Propane	Low	Low	Low	Low	0,00 ms
2	1**1**211*1*	- " -	- " -	High	- " -	- " -	- 1,00 ms
3	1**1**211*2*						- 0,50 ms
4	1**1**211*3*						0,00 ms
5	1**1**211*4*						+ 0,50 ms
6	1**1**211*5*						+ 1,00 ms
7	121**1***1*	- " -	High	Low	- " -	- " -	- 1,00 ms
8	121**1***2*						- 0,50 ms
9	121**1***3*						0,00 ms
10	121**1***4*						+ 0,50 ms
11	121**1***5*						+ 1,00 ms
12	1**2**211*1*	- " -	High	High	Low	- " -	- 1,00 ms
13	1**2**211*2*						- 0,50 ms
14	1**2**211*3*						0,00 ms
15	1**2**211*4*						+ 0,50 ms
16	1**2**211*5*						+ 1,00 ms
17	121**2***1*	- " -	High	Low	High	- " -	- 1,00 ms
18	121**2***2*						- 0,50 ms
19	121**2***3*						0,00 ms
20	121**2***4*						+ 0,50 ms
21	121**2***5*						+ 1,00 ms
22	1221**2**3	- " -	- " -	High	Low	High	0,00 ms
23	212113	Iso-butane	Low	- " -	- " -	Low	- " -
24	312113	n-butane					- " -
25	412113	VOC blend	- " -	- " -	- " -	- " -	- " -
26	012015	Diesel	Low	- " -	none	Low	+ 1,00 ms
27	112015	Propane	- " -	- " -	none	- " -	+ 1,00 ms
28	212015	Iso-butane	- " -	- " -	none	- " -	+ 1,00 ms
29	312015	n-butane	- " -	- " -	none	- " -	+ 1,00 ms
30	412015	VOC blend	- " -	- " -	none	- " -	+ 1,00 ms

The total number of test series made for the evaluation of the «Condensate Diesel Process» is 28. 3 of the test series shown above were repeated. The 5 last test series listed in Table 6.4 are tests carried out without pilot diesel fuel ignition to study the "ignition quality" of different VOC Fuel components.

Results are recapitulated in the subpart 6.2. Results with more detailed plots from a limited selection of the tests representing the different test conditions presented in Table 6.4 are given in the Appendices 5 – 10.

6.1.6 Air-fuel ratio.

The excess air ratio λ highly influences the combustion. To study this effect, the amount of both pilot diesel fuel and VOC Fuel was altered in two levels – low and high.

While the amount of fuel mainly affects λ only, the charge air condition– i.e. charge air pressure and temperature – will affect both λ and the thermal conditions governing ignition and combustion. This fact has been discussed in section 3.3.3.

Mean values of injected fuel masses – both nominal and corrected - are listed in Table 6.3. Nominal λ's are in the range of 1,6 – 5,1 and corrected λ's are in the range of 3,0 – 8,7. More details are found in Appendix 3.

As explained in section 3.1.2, the calibrated values of fuel mass delivery are found under conditions different from the test conditions (pressure/temperature), and corrections must be done. The charge air condition is registered immediately before it enters the DyFo cylinder, as is the normal procedure in any engine. The recorded pressure and temperature of the charge air is thus not what it is inside the cylinder. However, actual values measured inside the cylinder of the DyFo test rig are not available, and computation of any adjustments is not relevant. Besides, experience from the test work is that the pressure is easily maintained constant, while the temperature varies during the execution of a test series. The thermal influence is less controllable than the pressure. The charge air pressure could be adjusted both up and down by the regulator at the gas bottle if changes occurred during the execution of a test series. The temperature, however, was controlled by a water-to-air heat exchanger. Increasing the temperature was always possible and in practice occurring during the execution of a test series due to heat accumulation in the test cell and in the test equipment. Reducing the temperature, however, is not possible in practice. The water temperature in the heat exchanger cannot be reduced by any other means than natural convection and conduction.

As shown, the air-fuel ratio varies significantly when only one parameter is changed at a time. This fact is impossible to change – if tests with different values of only one specified parameter at a time are to be performed, the variation in air-fuel ratio must be accepted.

6.2 Test results.

6.2.1 Tests with diesel fuel

In the redesigned DyFo test rig, diesel fuel is normally injected as pilot fuel through the pilot fuel nozzle with a nozzle hole diameter of 0,35 mm and VOC Fuel is normally injected through the VOC Fuel nozzle with a nozzle hole diameter 0,55 mm. The fuel mass flow rates through the two nozzles are quite different, and the cylinder pressure curve is therefore very different when injecting the same fuel through each of the nozzles. To demonstrate this difference, and to study the

behaviour of ignition and combustion following injection through the two nozzles, some tests with different diesel fuel amounts were carried out. Figure 6.1 shows curves from three different test cases:

1) Diesel fuel injection (pilot fuel injector, injection duration 1,5 ms) – the two lower curves
2) Diesel fuel injection (pilot fuel injector, duration 3 & 3,5 ms) - the two middle curves
3) Diesel fuel injection (VOC Fuel injector, injection duration 4 ms) - the upper curve

Case 1): The actual diesel fuel mass corresponding to an injection duration of 1,5 ms through the pilot fuel injector is 6,9 mg. This is the pilot fuel mass used in most of the «Condensate Diesel Process» tests (cf. Table 6.4).

Case 2): Injection durations of 3 and 3,5 ms through the pilot fuel injector correspond to actual fuel masses of 33 to 36 mg. These fuel masses are used only in these tests.

Case 3): The actual diesel fuel mass corresponding to an injection duration of 4 ms through the VOC Fuel injector is 48 mg. This case shows the difference between the cylinder pressures development by combustion of the same fuel by different injection rates.

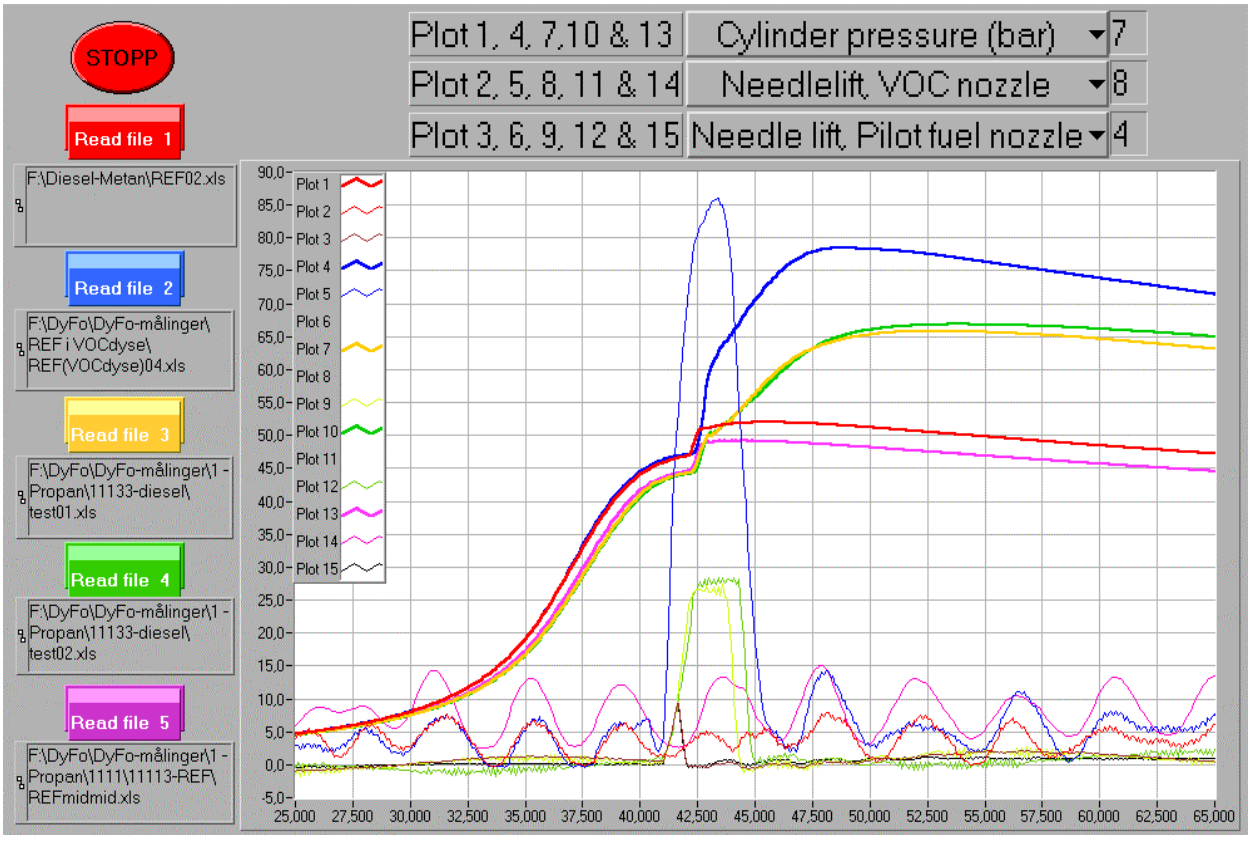

Figure 6.1 Combustion of diesel oil in the DyFo injected through the pilot fuel injector (red, yellow, green & pink curves) and the VOC Fuel injector (blue curve).

Figure 6.1 shows that the ignition delay and the pressure gradient in the initial combustion phase is of the same magnitude regardless which of the nozzles the fuel is injected through and that the total pressure rise in this phase is controlled by the fuel mass delivery rate. Also the observed ignition delay is about the same whether the diesel fuel is injected through the pilot fuel injector or the VOC Fuel injector.

The injection nozzles are mounted on different locations in the cylinder head, cf. section 5.1 and Appendix 3. These tests were made to confirm that the location and orientation of the injector would not influence the registered ignition delay.

The differences in compression pressure shown in Figure 6.1 are due to variable gas leakage through the quartz windows in the cylinder. During the test work this leakage increased with the time. As mentioned before (section 4.2), some tests gave pressure peaks higher than the quartz windows could stand, and new ones had to be fitted. In each window the quartz glass is glued in a stainless steel holder, and the leakage is due to porous joint seam.

When studying the Rate of Heat Release (ROHR) in Figure 6.2, it is found that the difference in compression pressure makes no significant difference to the ROHR curves. The curves for 7,6 mg of pilot diesel fuel show nearly identical ROHR. It is also found that the ROHR curves are very similar for the two nozzles for the first 0,5 – 1,0 ms (red, blue and pink curves). The difference of the ROHR curve when injecting 33 - 36 mg (yellow and green curves) compared to 6,9 mg of diesel is due to stochastic variations.

Oscillations of the ROHR curves calculated from the pressure and piston position recordings in the DyFo are another typical feature already discussed in section 3.3.2 (cf. Figure 3.15). These oscillations make ROHR curves from single tests not very smooth as shown in Figure 6.2. If calculating ROHR and accumulated heat release for mean values of registered data, the oscillations will equalize and a relatively smooth curve will result as shown later in this chapter.

Work on the test rig to reduce mechanical vibrations reduced the oscillations, but it was not possible to get rid of them. In fact it was evident when performing the tests on the DyFo rig that the entire construction was vibrating. The main problem is maybe that the DyFo Rig is not isolated from the base by shock absorbing dampers. It was not possible to solve this problem during the time available for experiments.

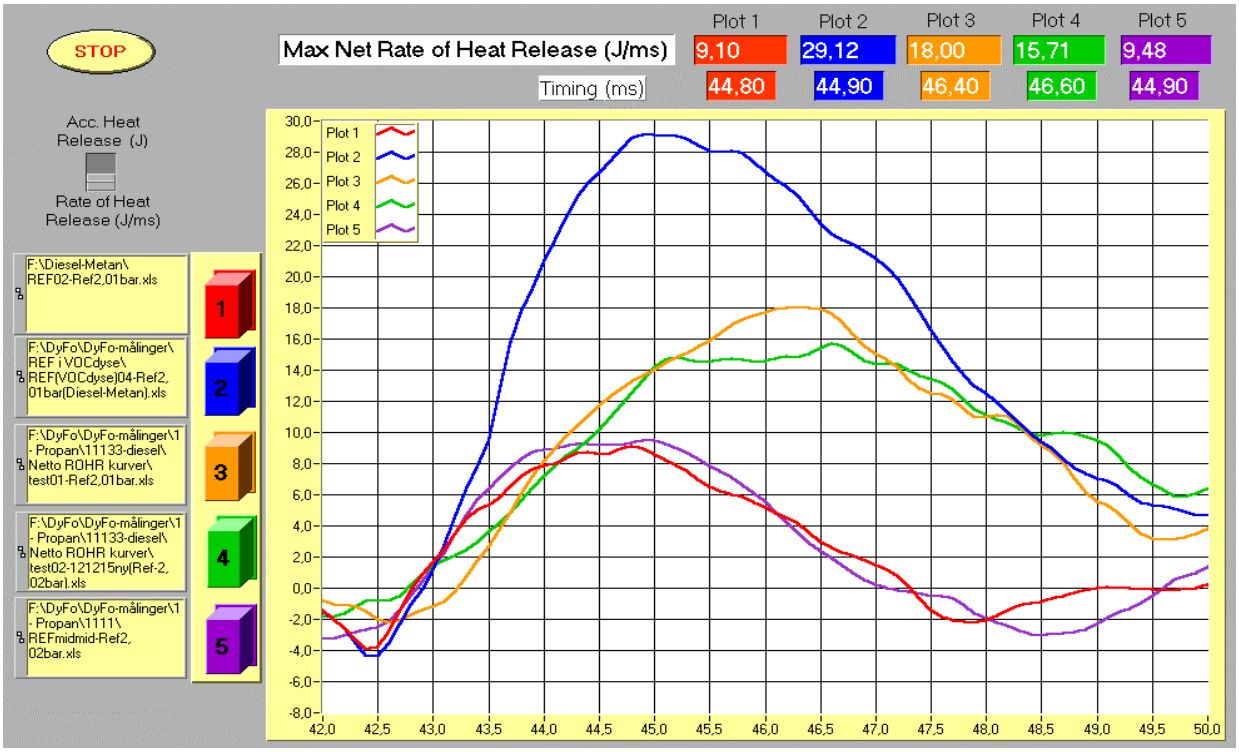

Figure 6.2 *Rate of Heat Release for diesel fuel injected through the pilot fuel and the VOC Fuel nozzles. Red & pink curve: 6,9 mg, pilot fuel nozzle, blue curve: 48 mg, VOC Fuel nozzle, yellow & green curve: 33 - 36 mg, pilot fuel nozzle.*

In the period from 42,5 to 45 ms, ignition and most of the premixed combustion takes place. Figure 6.2 show that diesel fuel injected at different rates and in nozzles of different geometry have very similar ROHR in the first 0,75 ms of this period (42,5 – 43,25 ms).

The accumulated heat release curves in Figure 6.3 give little additional information. It is shown that 30 - 40 % of the total heat release is made within this first period (42,5 – 45 ms).

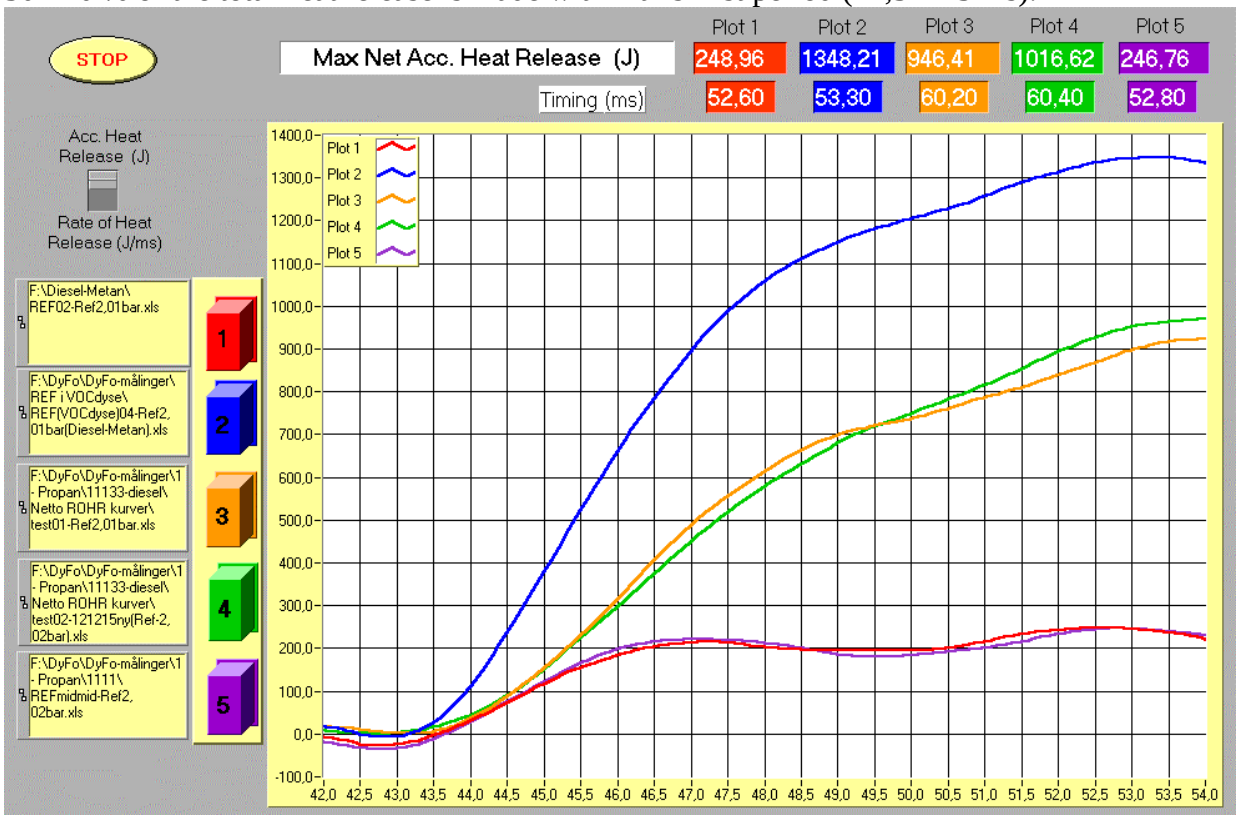

Figure 6.3 *Accumulated heat release for diesel fuel injected through the pilot fuel and the VOC Fuel nozzles. Red & pink curve: 6,9 mg, pilot fuel nozzle, blue curve: 48 mg, VOC Fuel nozzle, yellow & green curve: 33 & 36 mg, pilot fuel nozzle.*

These test results show that the duration of the different phases of combustion seems not to be significantly affected by the injection nozzle geometry or location in the cylinder. A slight difference in ignition delay is observed in the tests with low fuel mass compared to the tests with high fuel mass. This difference is due to increased cooling of the charge when the fuel evaporates inside the cylinder.

6.2.2 Tests with pure VOC Fuel components

The VOC Fuel components will burn without problems if the temperature at the instant of injection is high enough. This will be the case in a marine diesel engine at high load (49), but not at low load. The test conditions in the DyFo test rig best of all simulates low engine load, and tests were made to study ignition and combustion of different VOC Fuel components without pilot fuel ignition at these conditions.

Injection of pure VOC Fuel components will give cylinder pressure curves, ignition delays and accumulated heat release as shown in Figures 6.4 - 6.6. In the tests the charge air was at 30 °C, 3 bar, no pilot fuel, VOC Fuel mass = HIGH (67,5 mg) and RIT = + 1,0 ms. The tests were carried out at different times and thus small differences in test conditions may apply. However, small deviations in the test conditions as pressure level, injected fuel mass etc. is of less importance as the main target is to study differences in ignition delay for the VOC Fuel components.

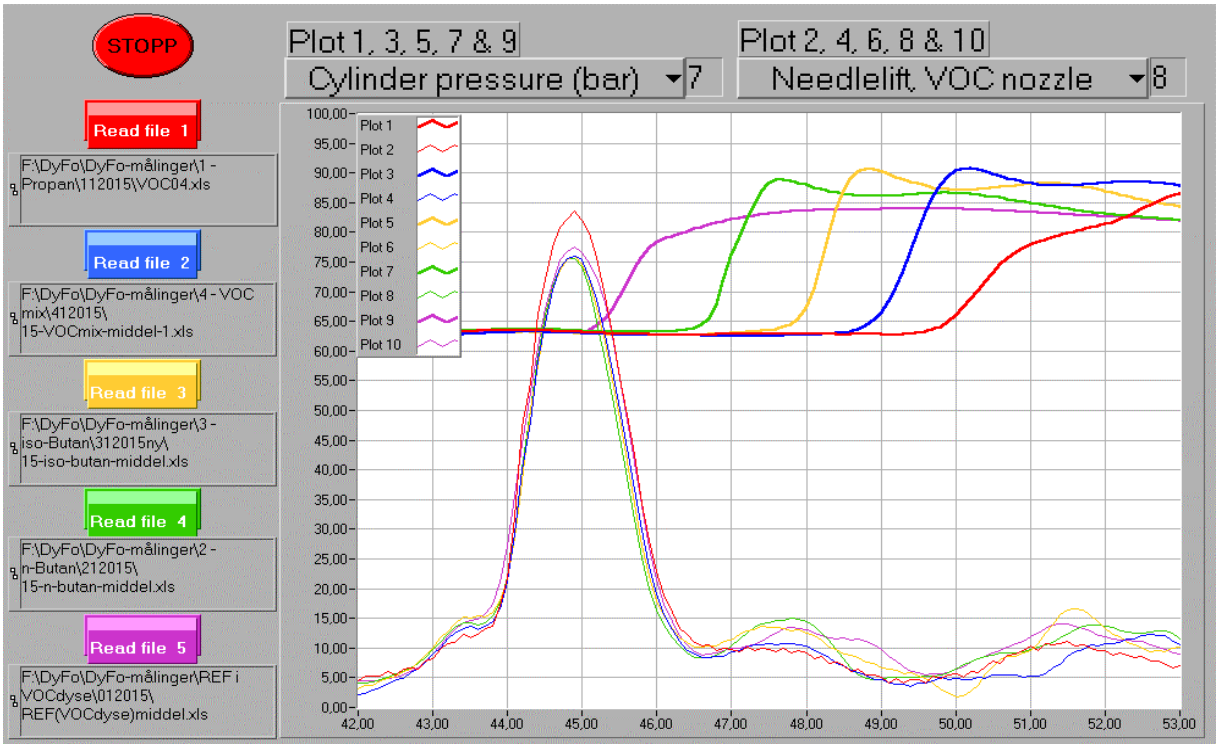

Figure 6.4 Cylinder pressure and needle lift by combustion of pure VOC Fuel components (red curve: Propane, blue curve: VOC mixture, yellow curve: iso-butane, green curve: n-butane) in the DyFo compared to diesel fuel (pink curve). VOC Fuel nozzle.

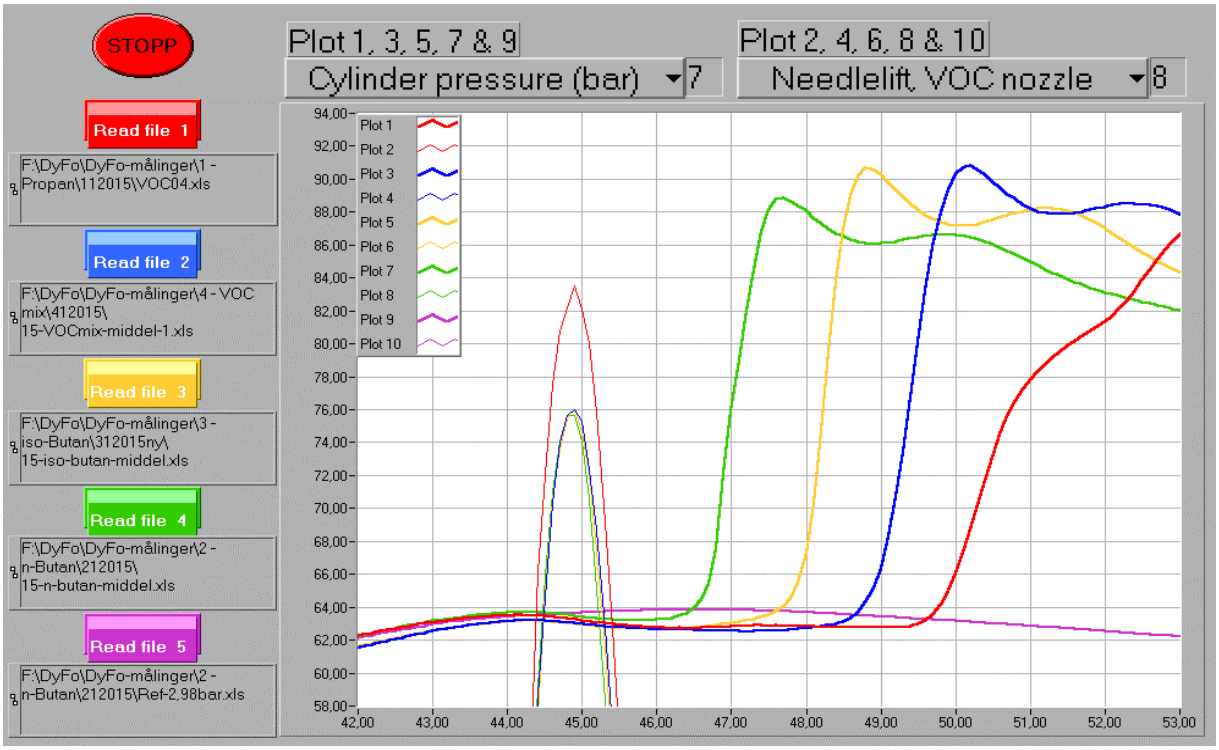

Figure 6.5 Close-up view of cylinder pressure by combustion of pure VOC Fuel components (red curve: propane, blue curve: VOC mixture, yellow curve: iso-butane, green curve: n-butane) in the DyFo compared to fuel-free compression (pink curve).

From the cylinder pressure curves in Figures 6.4 it is observed that the different VOC Fuel components have ignition delays decreasing with the length of the fuel molecule (cf. section 3.3.3). From Figure 6.5 it is observed that the cylinder pressure falls shortly after the fuel is injected as the fuel evaporates. For diesel combustion (pink curves - plot 9 & 10 - in Figure 6.4) this phenomenon

is not observed due to the shorter ignition delay. By studying Figure 6.5, it is also seen that the cylinder pressure slowly recovers during the ignition delay period. This implies that the low temperature reactions slowly proceed increasing the temperature in the cylinder and building up the radical pool necessary for the "thermal run-away" (cf. section 3.3.3) that defines the moment of ignition.

Figure 6.6 shows the accumulated net heat release from the combustion of the pure VOC Fuel components in the DyFo compared to diesel fuel (all fuels injected through the VOC Fuel nozzle). The accumulation of released energy curves have nearly the same gradient for all fuel types, propane and diesel showing a slight reduced gradient compared to the others. Most dominating is the fall-off in gradient for diesel at about 50 ms. This fall-off implies the start of the diffusion controlled combustion, and the gaseous fuel types show less tendency to this type of combustion with the actual fuel mass injected. Combustion of high-pressure injected gaseous fuel is thus shown to be faster than combustion of diesel fuel once it is ignited.

Propane shows a combustion rate (accumulated heat release gradient) more like diesel fuel in these experiments, but lacks the fall-off implying the start of diffusion combustion. This result must, however, be evaluated considering the very unstable ignition delay for propane, as shown in Figure 6.7.

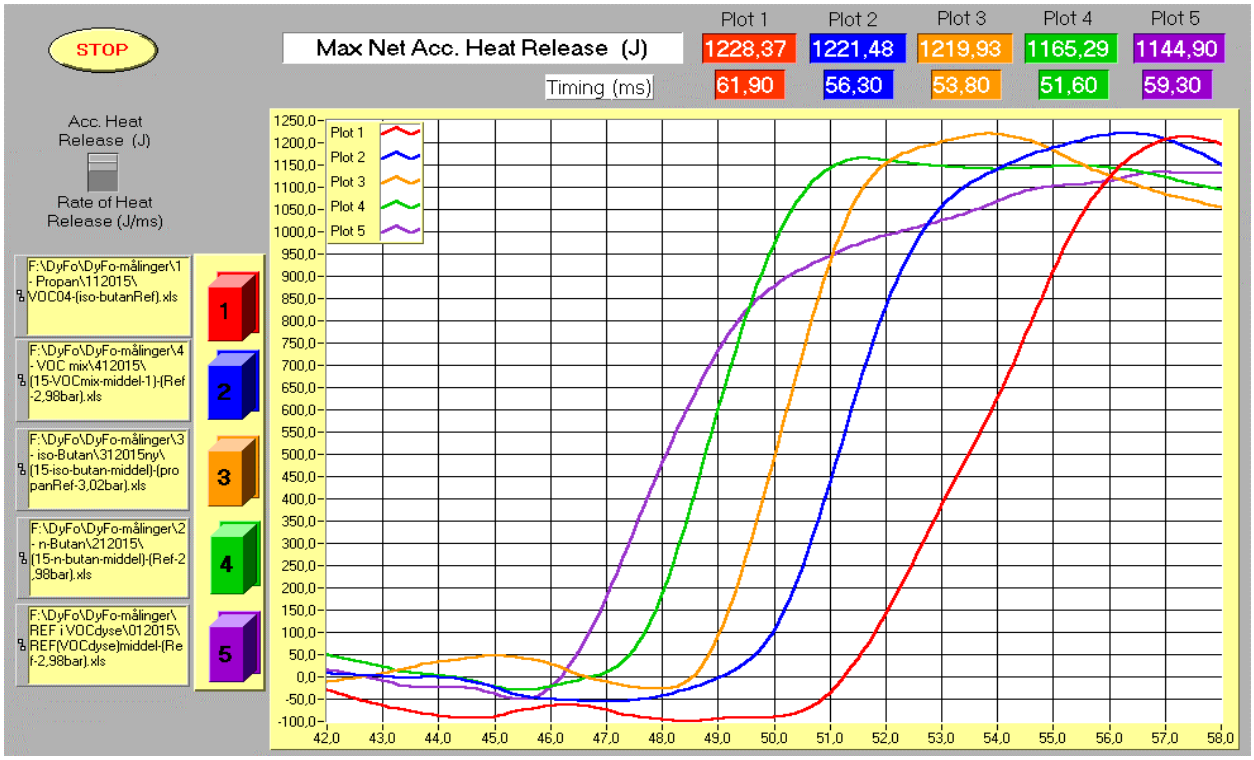

Figure 6.6 *Accumulated heat release by combustion of pure VOC Fuel components (red curve: Propane, blue curve: VOC mixture, yellow curve: iso-butane, green curve: n-butane) in the DyFo compared to diesel fuel (pink curve). VOC Fuel nozzle.*

The curves for accumulated heat release drops below zero as a consequence of the cooling effect when the liquid VOC Fuels evaporates when entering the cylinder. The curves are of slightly different shapes due to the effect of subtracting the compression curve from the curves with combustion (cf. section 3.3.2). The shape of the registered curves varies quite much from test to test, especially before ignition. For this reason the resulting "net" heat release curves fluctuates around zero, instead of being maintained at zero until the fuel evaporation should have drawn heat out of the charge followed by a rapid heat release when the fuel ignites.

Figures 6.7 - 6.9 show details of how the stability of the combustion of three tested VOC Fuel components - propane, iso-butane and n-butane - varied. The tests were run with charge air at 70 °C

and 3 bar, no pilot fuel, VOC Fuel mass = HIGH and RIT = + 1,00 ms. The red cylinder pressure curve in all three figures shows the pressure obtained by pilot ignition of the VOC Fuel. As is seen from Figure 6.7, this curve completely coincides with the pressure curve for injection of only pilot diesel fuel. As the injection of VOC Fuel is set extremely late (+1,00 ms), the initial pressure rise is due only to combustion of pilot injected diesel fuel.

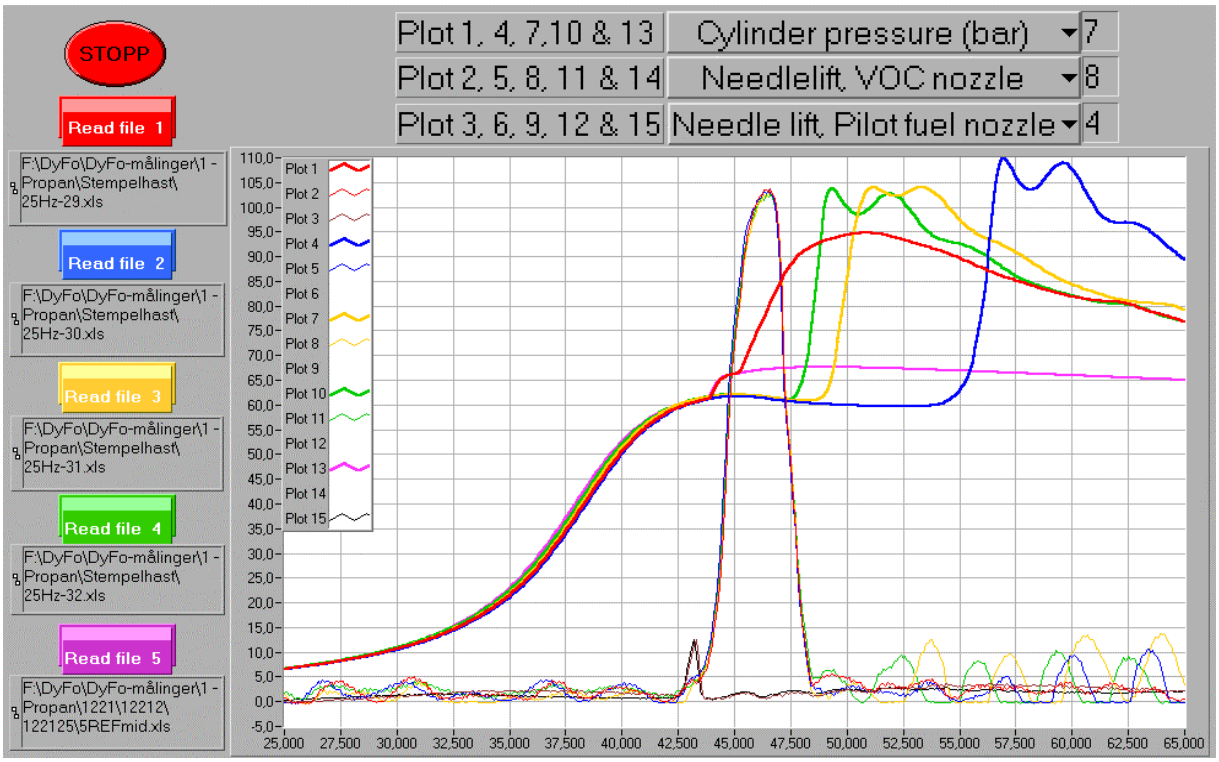

Figure 6.7 *Combustion of pure VOC Fuel (propane- blue, yellow & green curves) compared with pilot fuel combustion (pink curve) and pilot ignited VOC Fuel (red curve).*

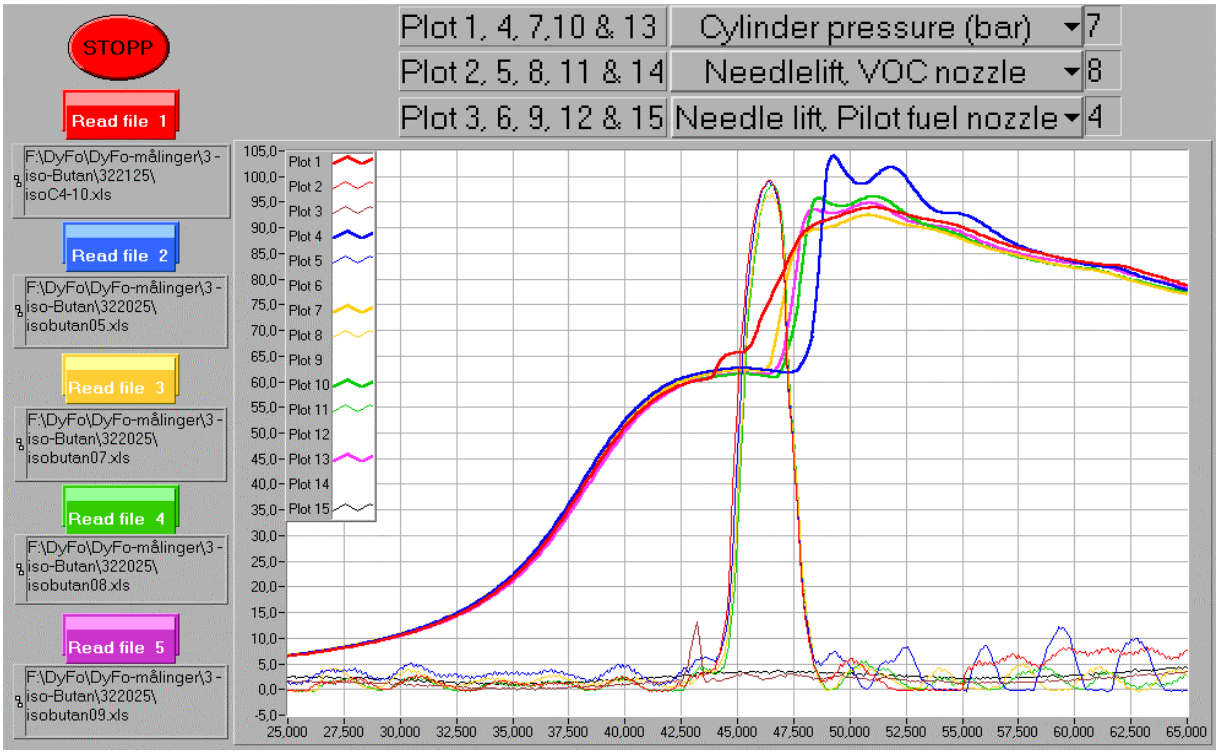

Figure 6.8 *Combustion of pure VOC Fuel (iso-butane - blue, yellow, green & pink curves) compared with pilot ignited VOC Fuel (red curve).*

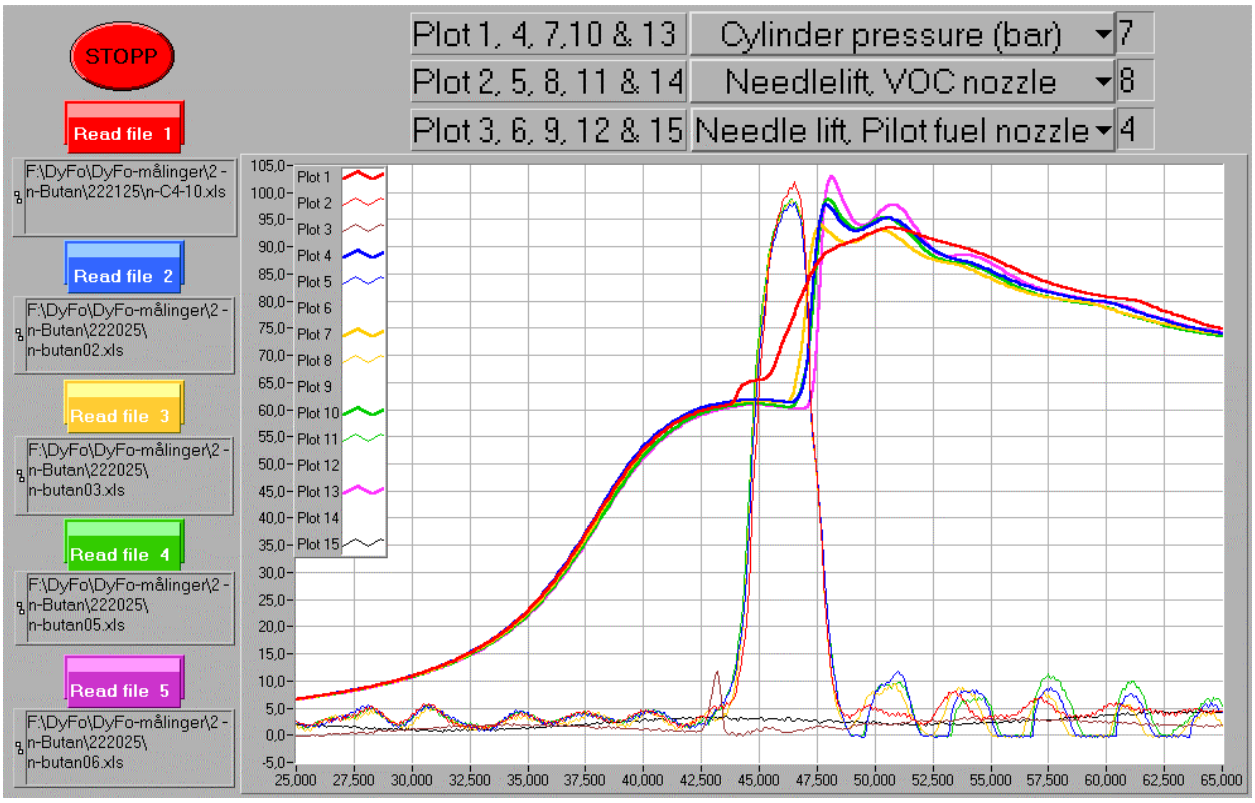

Figure 6.9 Combustion of pure VOC Fuel (n-butane - blue, yellow, green & pink curves) compared with pilot ignited VOC Fuel (red curve).

From Figures 6.7 – 6.9 it is obvious that injecting only VOC Fuel will give engine operational problems since the ignition delay varies so much. Propane is the most problematic component giving the longest delays and most unsteady ignition. Iso-butane is more willingly to ignite, while n-butane is the best of the three pure components tested. Compared to pilot fuel ignited VOC Fuel according to the «Condensate Diesel Process» concept, all three components will give far too long ignition delays for problem-free engine operation.

6.2.3 Tests with VOC Fuel components ignited by pilot fuel

To answer the key question, whether ignition and early combustion of VOC Fuel by the «Condensate Diesel Process» concept will give any significant differences of the ignition and combustion compared to normal diesel fuel operation (cf. section 1.3), the test matrix described in section 5.2 was prepared. In the following section the results of the test parameter variations are presented and discussed.

Effect of relative injection timing (VOC Fuel relative to pilot fuel).

To study the correlation between ignition delay and relative injection timing (RIT), this parameter has been varied from 1,0 millisecond ahead of pilot fuel injection to 1,0 millisecond behind in 5 equal steps.

Figure 6.10 shows the results from tests performed with the charge air at 3,0 bars and about 70 °C and a corrected overall $\lambda = 2{,}96$.

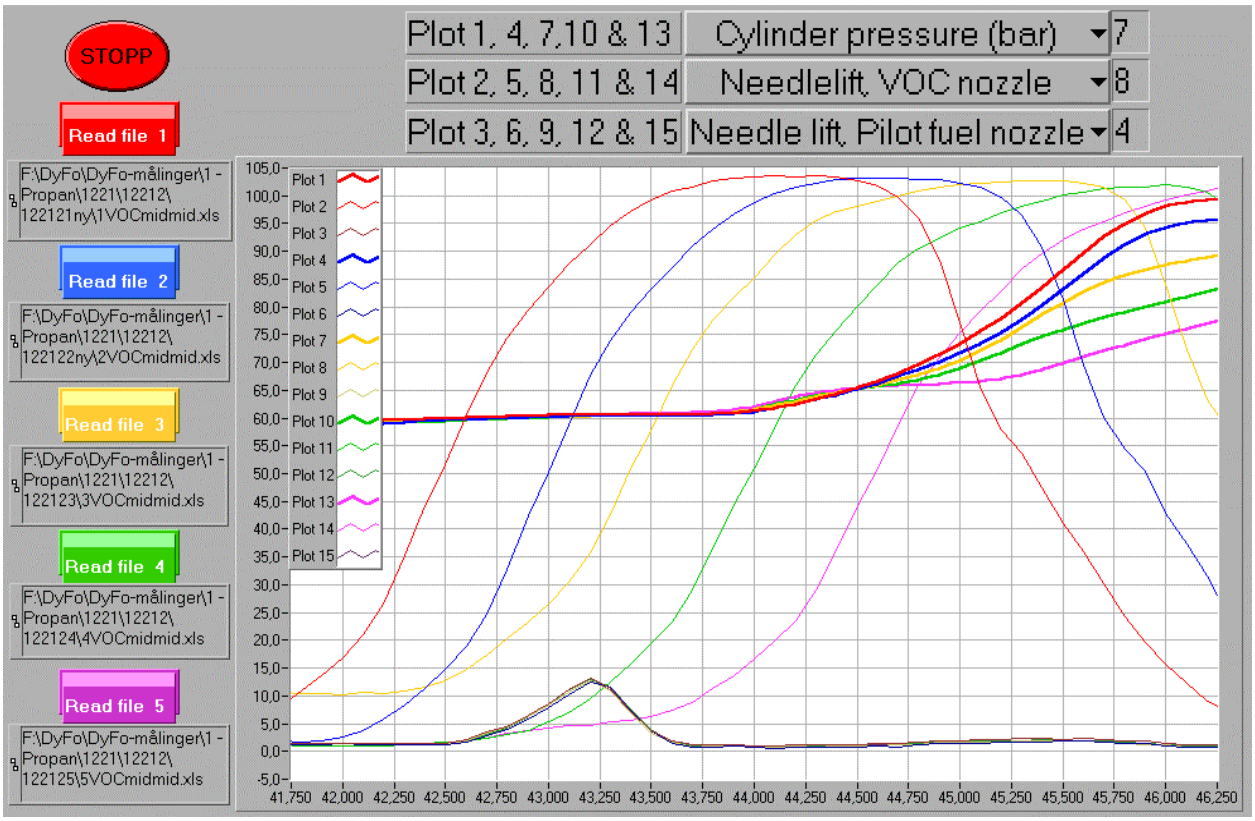

Figure 6.10 *Effect of relative injection timing (RIT). Details of the pilot fuel and the VOC Fuel nozzle needle lifts and the cylinder pressure at the instant of ignition ± 2 ms. Signal for pilot injection given at 41,75 ms. Red curve: RIT=-1,00 ms, blue curve: RIT=-0,50 ms, yellow curve: RIT=0,00 ms, green curve: RIT=+0,50 ms & pink curve: RIT=+1,00 ms.*

From the plots it is seen that early injection of VOC Fuel slightly increases the ignition delay (=gives a later pressure rise) of the pilot fuel compared to late injection. It is also obvious that even if the VOC Fuel is injected into the cylinder when the pilot diesel has ignited, there will be a distinct delay before it ignites (cf. the pink cylinder pressure curve - "5VOCmidmid").

From Figure 6.10 the data shown in Table 6.5 for ignition delays of pilot fuel and VOC Fuel are found.

Table 6.5 Correlation between ignition delays for pilot fuel, VOC Fuel and relative injection timing (RIT).

Relative Injection Timing (RIT)	Ignition delay, pilot fuel	Ignition delay, VOC Fuel
- 1,00 ms	1,35 ms	2,70 ms
- 0,50 ms	1,35 ms	2,15 ms
0,00 ms	1,30 ms	1,70 ms
+ 0,50 ms	1,25 ms	1,50 ms
+ 1,00 ms	1,20 ms	1,25 ms

From these findings a logic conclusion is that the best relative injection timing tested is + 1,00 ms (late injection of VOC Fuel). However, this is not the conclusion when studying the complete cylinder pressure curves, shown in Figure 6.11.

In an engine high efficiency requires that the combustion takes place as fast as possible after TDC. A compromise has however to be made to limit the combustion noise resulting from a steep pressure gradient. In the DyFo test rig the position of the piston is related to the time-scale. From

6.11 it is seen that the TDC position is ~43,5 ms (where the pressure curve has been horizontal). The preferred pressure curve reaches its maximum value as soon as possible after TDC - this is obtained with the relative injection timing at –1,00 ms (early VOC Fuel injection)!

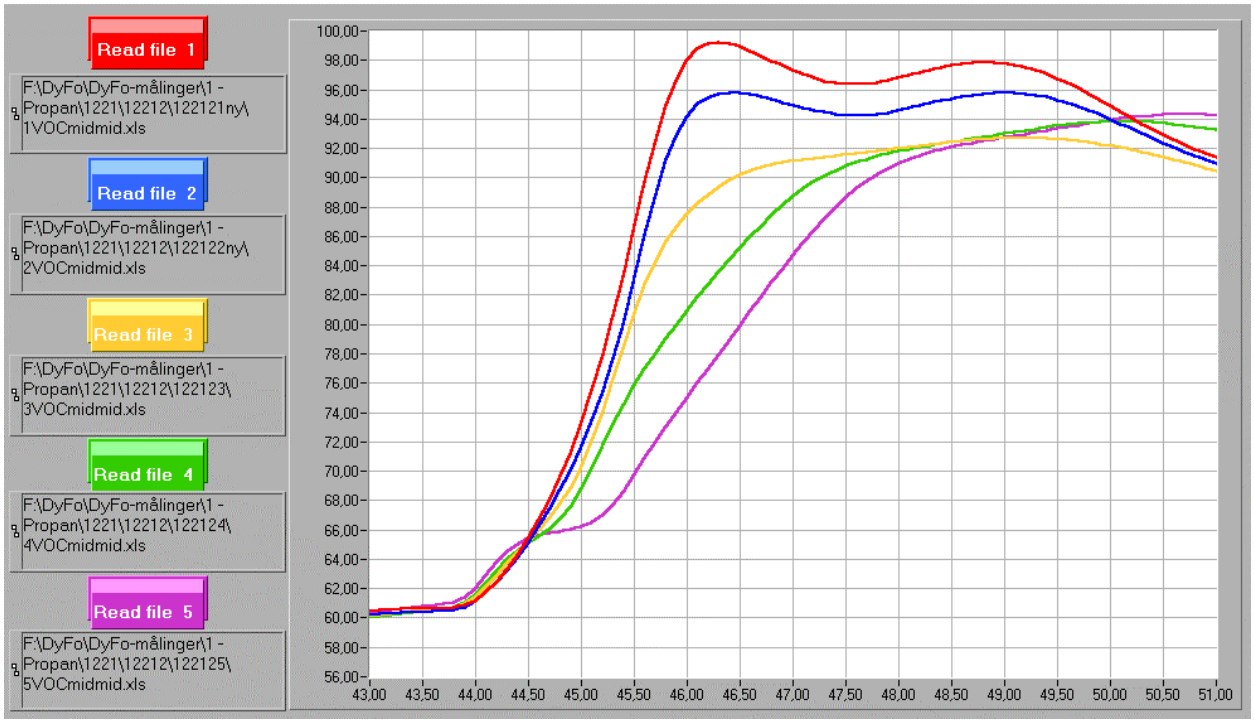

Figure 6.11 Cylinder pressure curves when varying the Relative Injection Timing in the DyFo. Red curve: RIT=-1,00 ms, blue curve: RIT=-0,50 ms, yellow curve: RIT=0,00 ms, green curve: RIT=+0,50 ms & pink curve: RIT=+1,00 ms.

When studying the Schlieren images of the ignition and early combustion resulting from the different relative VOC/pilot injection timings (RIT), the conclusion is less distinct. The images show that the earliest ignition occurs when RIT = 0,00 ms, i.e. when both fuels are injected at the same time. Earlier as well as later injection of the VOC Fuel seems to “disturb” the diesel pilot flame. By early injection, it seems that the ignition delay period of the VOC Fuel is totally covered by the ignition delay period of the diesel pilot fuel. Figure 6.12 shows Schlieren images of injection, ignition and very early combustion in tests with the charge air at 2,0 bars and about 70 °C and with a corrected overall λ = 5,03.

The registered time referred to as "Camera trigging" in these Schlieren images is the total elapsed time from the signal for start of injection is given by the computer control program. The injection system has an “injection delay” of 1,2 – 1,3 ms (cf. Figures 3.6 & 3.7). The shortest ignition delay obtained thus was 1,3 ms (= 2,50 – 1,2 ms) with RIT = 0,00 ms. In the images there is observed lighter areas much earlier than 2,50 ms. These areas, however, are light due to a density gradient caused by the turbulence in the charge air as a result of the rapid piston movement and not due to temperature gradient resulting from combustion (cf. Chapter 4 on Schlieren imaging of diesel combustion).

When the injection timing is varied, the energy release varies as shown in Figure 6.13 (ROHR) and Figure 6.14 (accumulated heat release). The results origins from tests with the charge air at 3,0 bars and about 70 °C and with a corrected overall λ = 2,96.

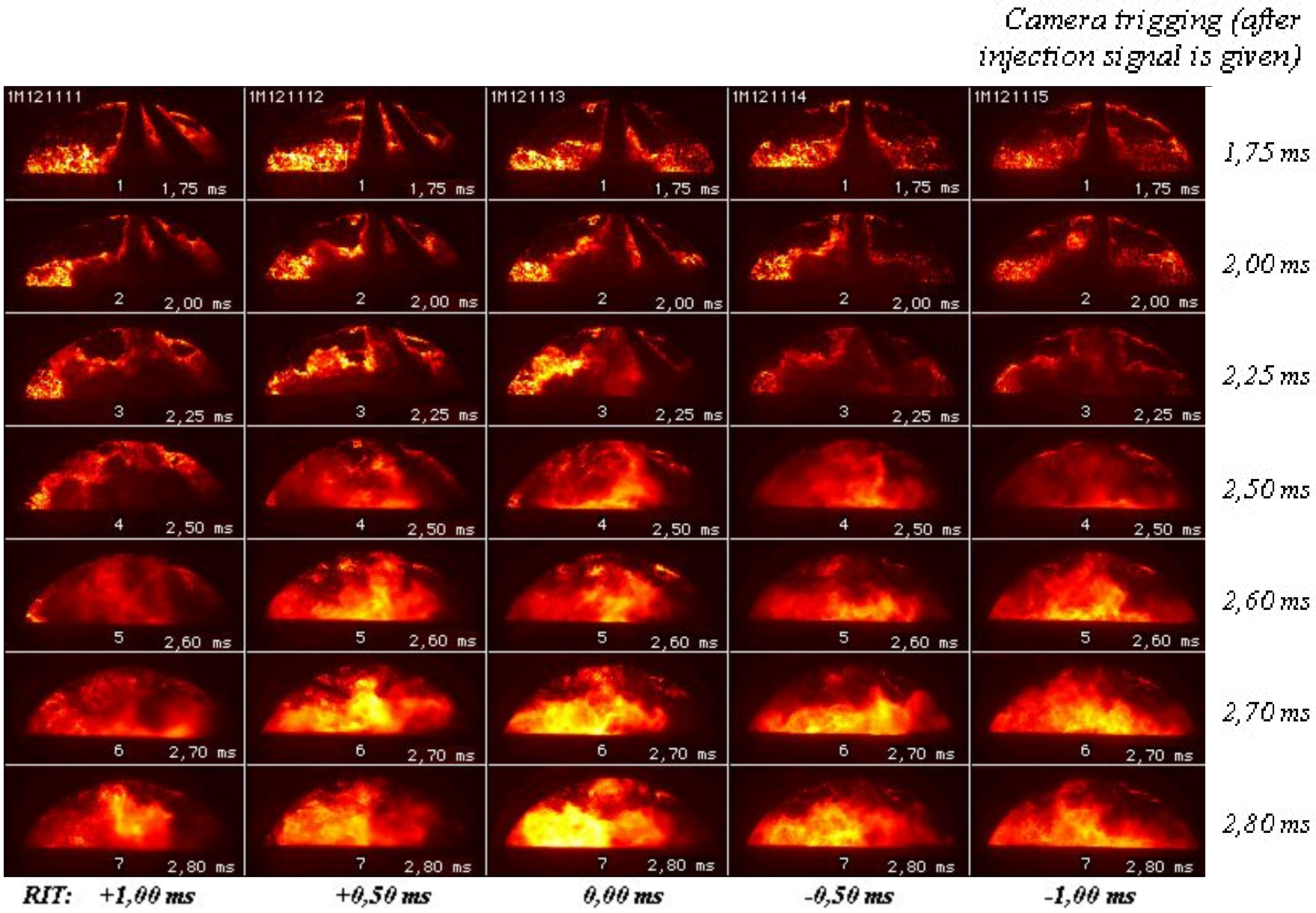

Figure 6.12 *Effect of relative injection timing, RIT. Images from tests with the charge air at 2,0 bars, about 70 °C and with a corrected overall λ = 5,03.*

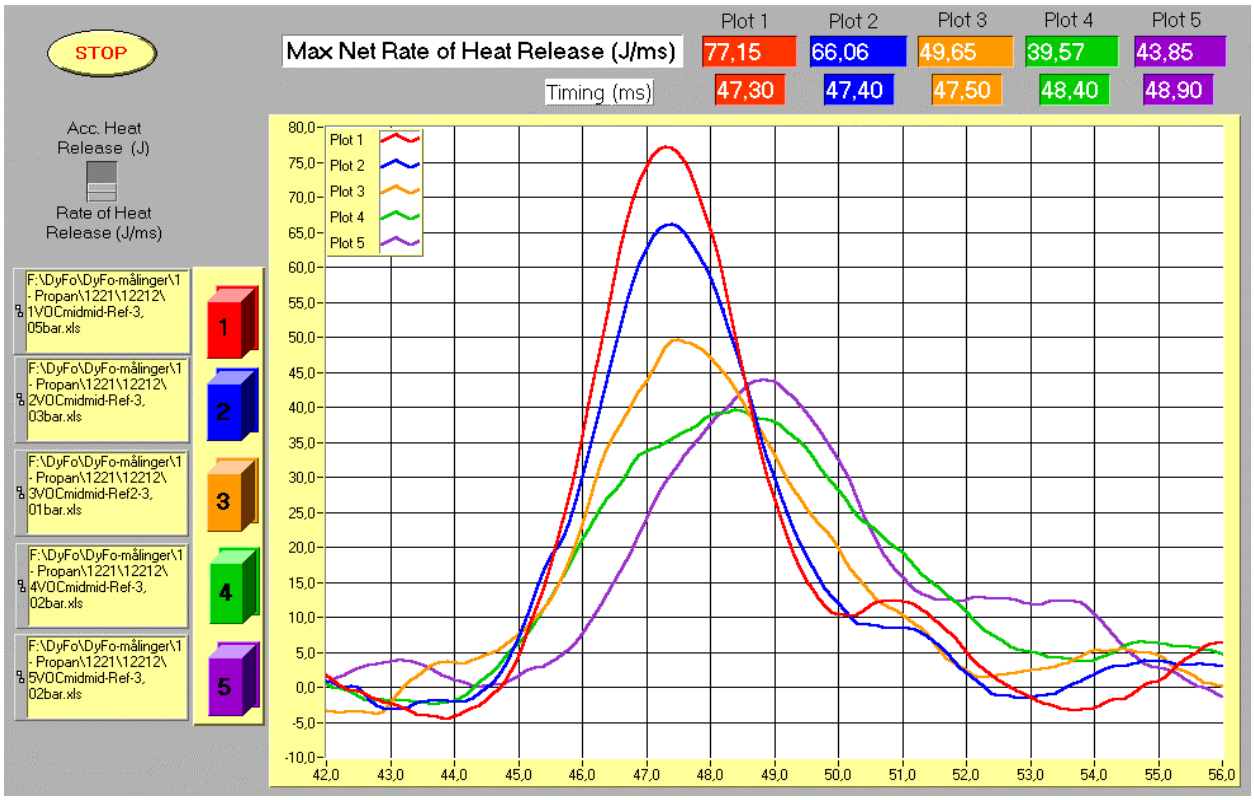

Figure 6.13 *Effect of relative injection timing. ROHR plots from tests with the charge air at 2,0 bars, about 70 °C and with a corrected overall l = 2,96. Red curve: RIT=-1,00 ms, blue curve: RIT=-0,50 ms, yellow curve: RIT=0,00 ms, green curve: RIT=+0,50 ms & pink curve: RIT=+1,00 ms.*

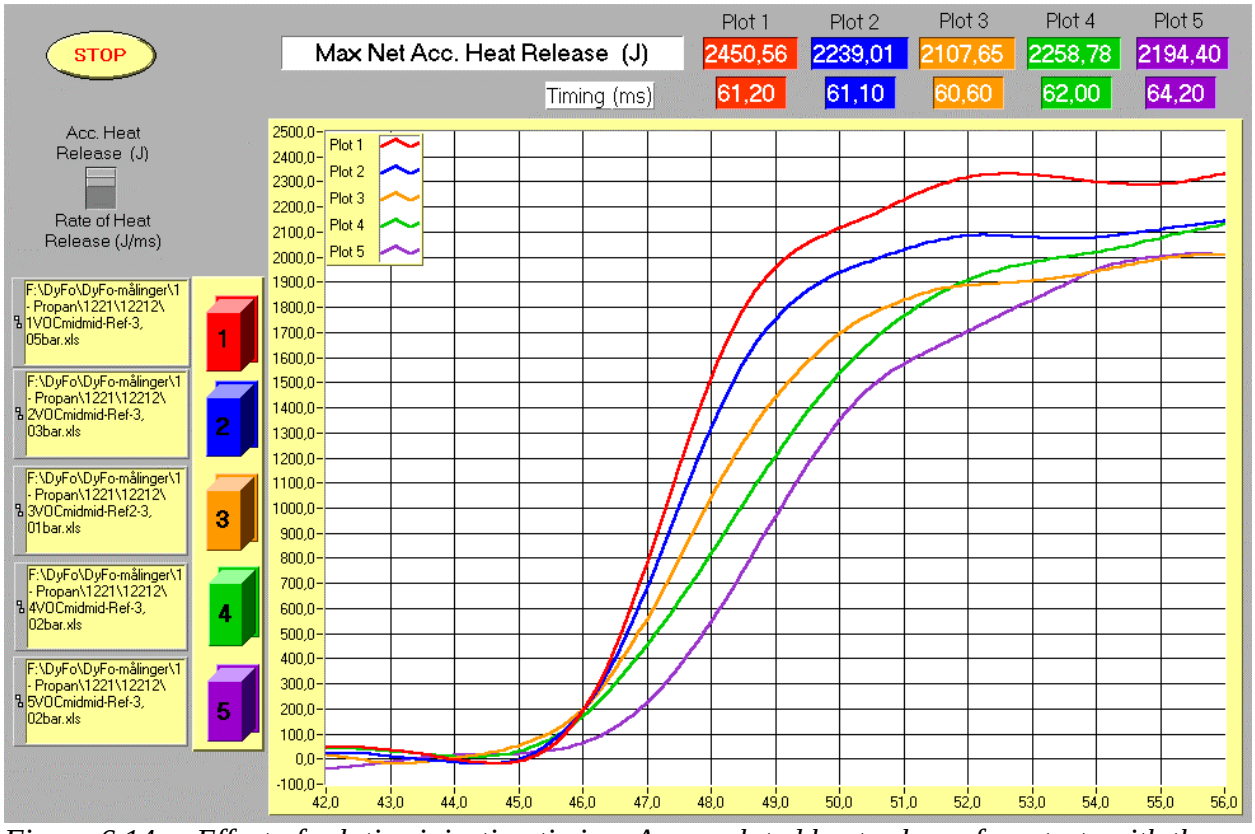

Figure 6.14 *Effect of relative injection timing. Accumulated heat release from tests with the charge air at 2,0 bars, about 70 °C and with a corrected overall l = 2,96. Red curve: RIT=-1,00 ms, blue curve: RIT=-0,50 ms, yellow curve: RIT=0,00 ms, green curve: RIT=+0,50 ms & pink curve: RIT=+1,00 ms.*

From the Schlieren images in Figure 6.12 and the plots of rate of heat release and accumulated heat release in Figures 6.13 and 6.14 it seems that the ignition delay is shortest with RIT=0,00 ms (simultaneous injection of pilot fuel and VOC Fuel).

By test bed runs of the diesel engine converted for use of VOC Fuel at MAN B&W in Copenhagen, the same experience was actually made (49). It is thus concluded that this is the best compromise.

When studying the images of the early combustion phase in more detail, very small variations in the temperature distribution from the combustion is found regardless the RIT of the VOC Fuel. This is because the images only show the very first part of the combustion in the DyFo, and actually no VOC Fuel (=propane in Figure 6.14) has started to burn. The Schlieren effect observed is only due to the combustion of the pilot fuel, as the VOC Fuels not start burning until after 2,70 ms (cf. Table 6.5).

Appendix 5 gives more examples of the effect of varying the RIT.

Effect of VOC Fuel mass injected

In an engine the fuel mass injected is varied for changing the power output. When injecting more fuel, the temperature increases and in an engine heat is accumulated. The DyFo test rig is a "single shot" combustion machine and the time between combustions is so long that no heat accumulates. This must be kept in mind when studying the effect of VOC Fuel mass injected on ignition and combustion in the DyFo. The result is shown in Figure 6.15 and 6.16 below.

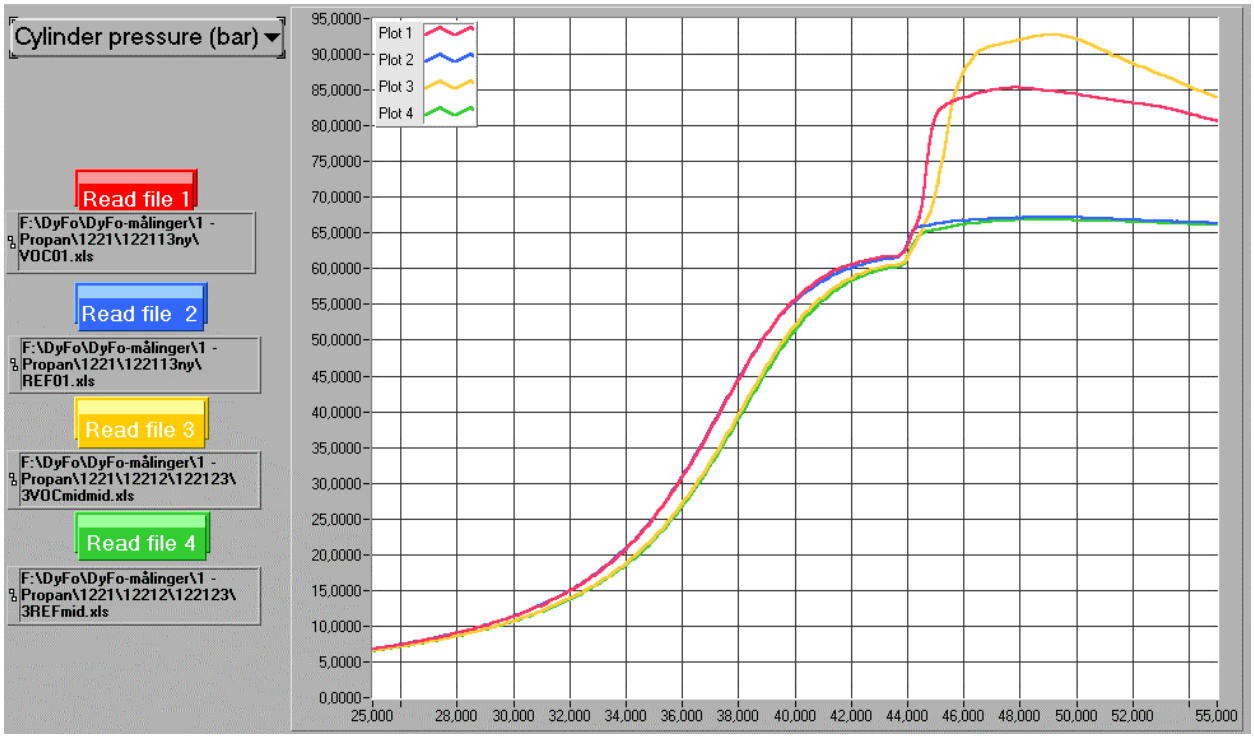

Figure 6.15 Combustion of LOW (red curve) and HIGH (yellow curve) VOC Fuel mass - cylinder pressure. Reference curves (blue & green) with only pilot diesel fuel for comparison. The compression pressure curves differ slightly as a result of minor changes in the "in-cylinder" conditions.

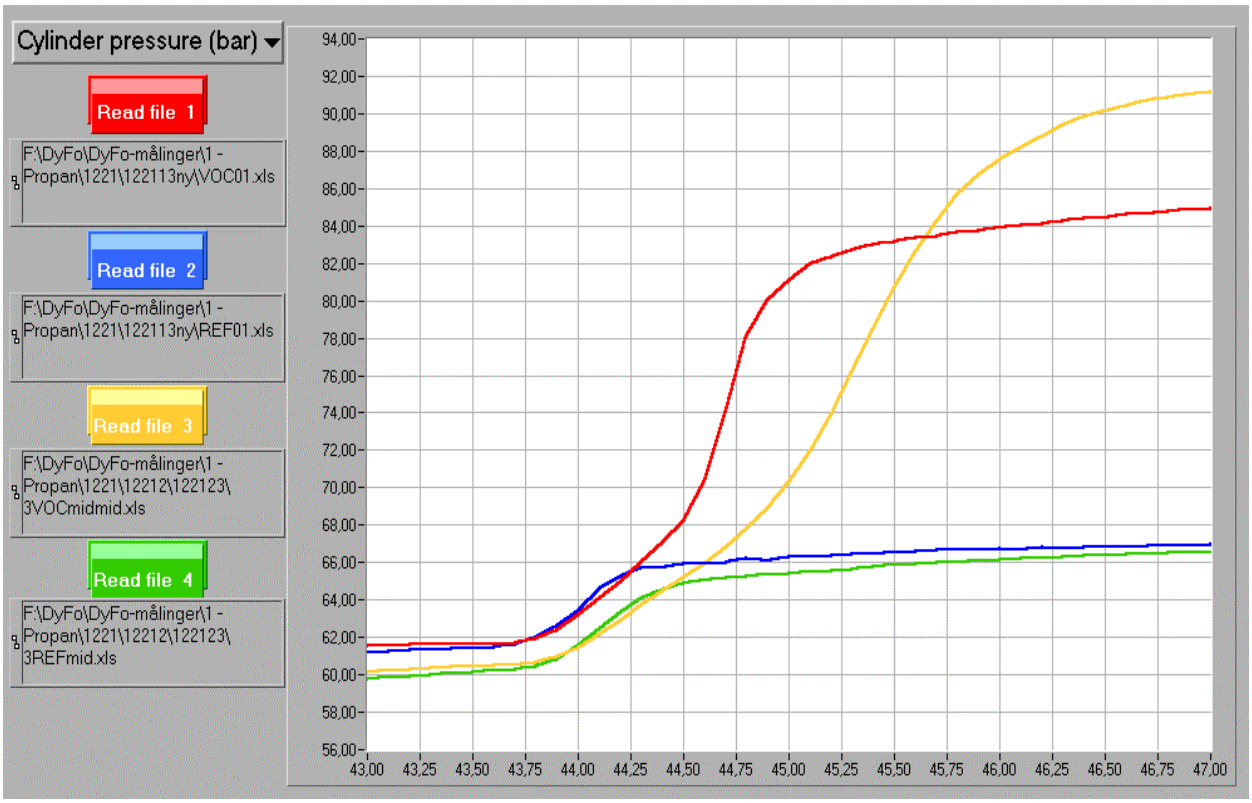

Figure 6.16 *Combustion of LOW (red curve) and HIGH (yellow curve) VOC Fuel mass - close-up of cylinder pressure. Reference curves (blue & green) with only pilot diesel fuel for comparison.*

From Figures 6.15 and 6.16 it is found that the VOC Fuel mass injected influences the ignition and early combustion less than the other parameters studied. The ignition delay increases a little (0,1 – 0,2 ms) with increased VOC Fuel mass. The pressure gradient is seen to be greater with LOW VOC Fuel mass injected, but the difference is little and should not be of any problem to a diesel engine running according to the «Condensate Diesel Process».

The excess air ratio λ varies with the VOC Fuel mass injected. For the LOW VOC Fuel mass (test series 12211) λ= 7,55, for the HIGH VOC Fuel mass λ= 2,96. This is most probably a main reason why the pressure gradient with LOW VOC Fuel mass is steeper than with HIGH VOC Fuel mass. This result thus implies that the combustion speed (= chemical reaction rate) increases when the excess air ratio λ increases.

Effect of pilot diesel fuel mass injected

To study the effect of varying the amount of pilot diesel fuel on the ignition and early combustion of the VOC Fuel, this parameter has been set to 7,6 mg (LOW nominal value) and 21,7 mg (HIGH nominal value). The actual test series (1212 and 1211) both have charge air pressure 2,0 bars and charge air temperature about 70 °C. The tests with HIGH amount of pilot diesel fuel have a nominal overall excess air/fuel ratio λ = 3,61. The tests with LOW amount of pilot diesel fuel have λ = 5,03. A close-up view of the cylinder pressure curve and both the needle lift curves with RIT = +0,5 ms is shown in Figure 6.17.

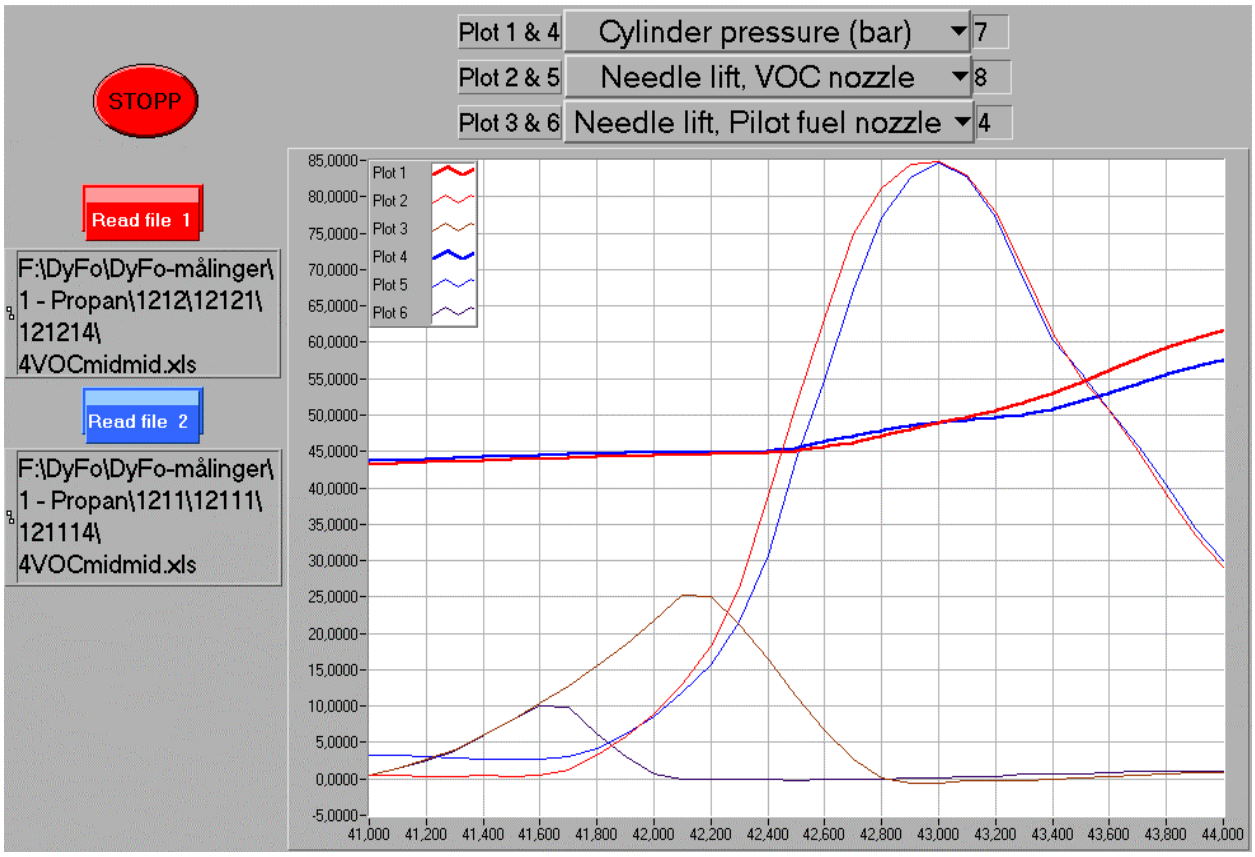

Figure 6.17 *Effect of pilot diesel fuel amount. Close-up view of cylinder pressure (red curve: High, blue curve: Low) and needle lift (brown curve: High, blue curve: Low) around the instant of ignition (42,50 ± 1,50 ms).*

From Figure 6.17 it is seen that more pilot diesel fuel (test 121214) seems to reduce the ignition delay of the VOC Fuel (propane). This finding may be explained by the fact that more ignition energy is present in the pilot diesel fuel spray giving a higher energy state in the charge prior to the ignition of the VOC Fuel. In other words – the temperature rise is faster, probably due to a greater production rate of radicals.

From the Schlieren images in Figure 6.18 it is observed that the light indicating the start of combustion of pilot diesel fuel appears later (about 0,1 ms) when the HIGH amount of pilot fuel mass is injected compared to the LOW amount. This implies that the ignition delay increases with increasing the pilot fuel mass injected. This observation is in accordance with the interpretation of the cylinder pressure curve shown in Figure 6.17.

The pilot fuel mass injected influences the ignition delay in the DyFo test rig when burning VOC Fuel ignited with pilot injected diesel fuel. The influence is however a specific effect in the DyFo. As mentioned, this test rig is a "single shot" combustion machine without heat accumulation and increasing temperature level as the injected fuel mass is increased. The tests show a small effect on the ignition delay. In a diesel engine the effect will probably not be of significant size to give any problems by combustion of VOC Fuel.

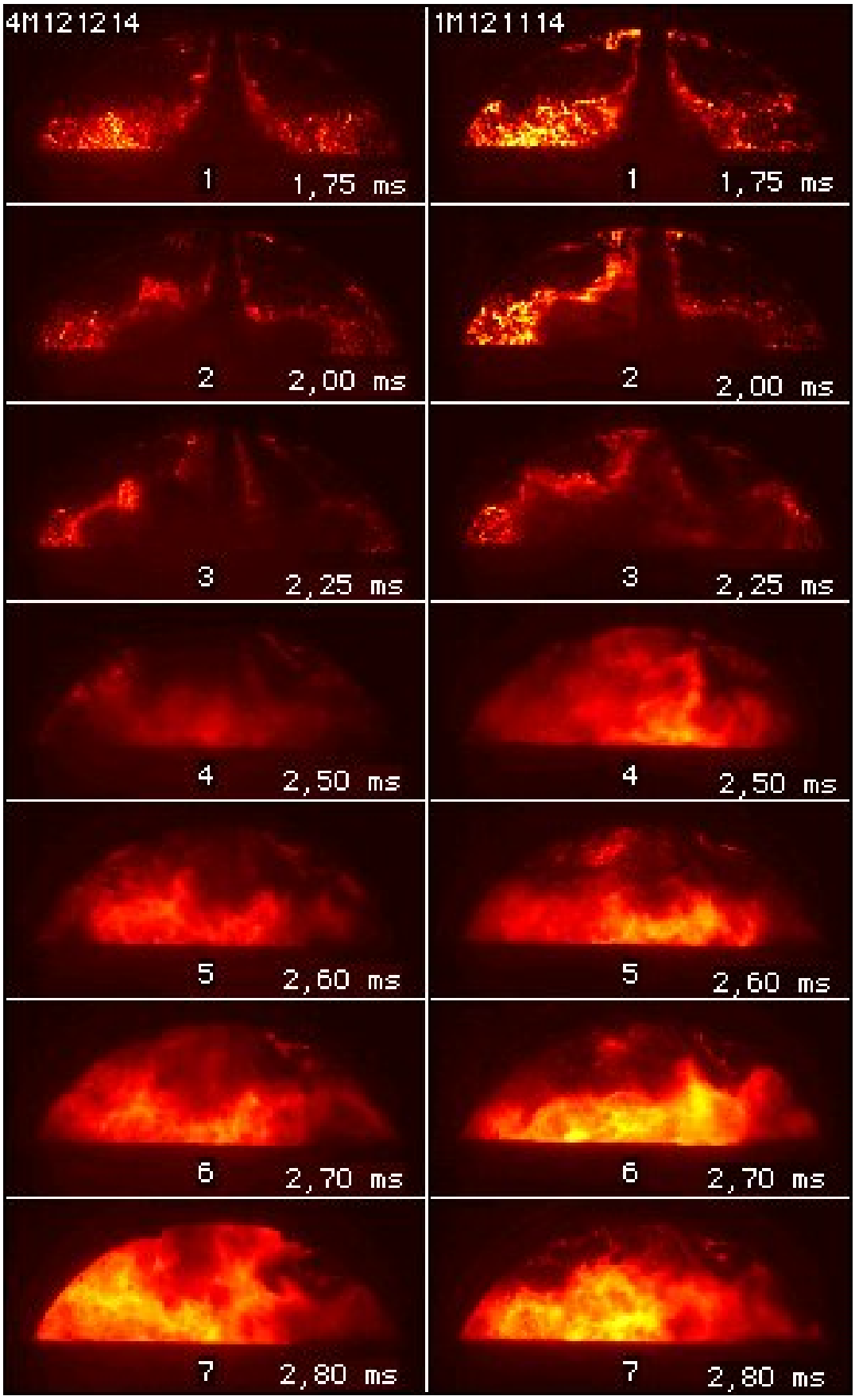

Figure 6.18A Images from injection, ignition and early combustion of pilot ignited VOC Fuel (Propane). Effect of pilot fuel mass (PFM).

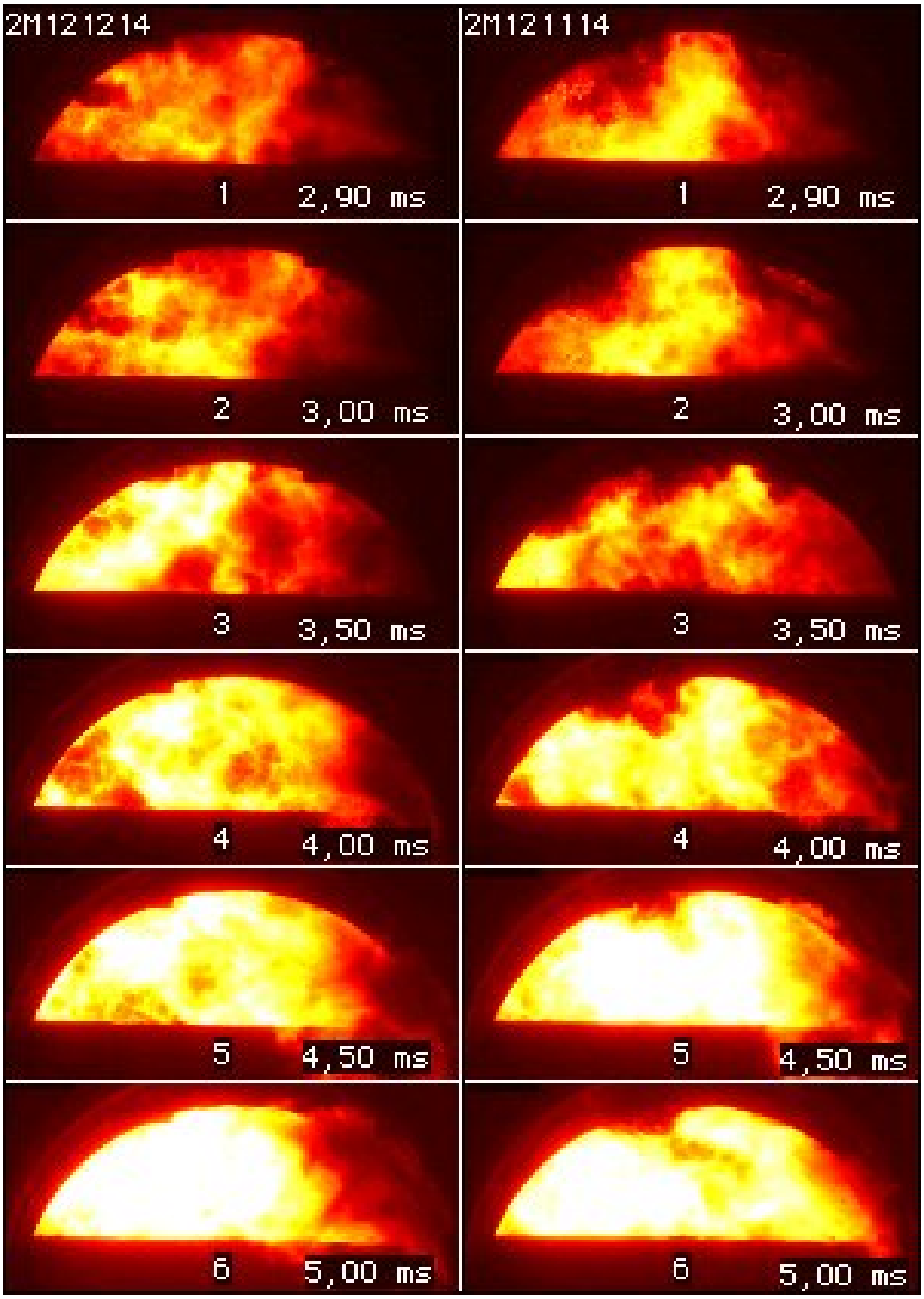

PFM: ***HIGH*** ***LOW***

Figure 6.18B Images from the middle part of combustion of pilot ignited VOC Fuel (Propane). Effect of pilot fuel mass (PFM).

Effect of charge air pressure

To study the effect of varying the charge air pressure on the ignition and early combustion of the VOC Fuel, this parameter has been 2 bar (nominal LOW value, test 111113) and 3 bar (nominal HIGH value, test 112113).

In both test series the charge air temperature was about 70 °C. In test series 1111 the corrected excess air ratio is $\lambda = 5{,}78$. In test series 1121 the corrected excess air ratio is $\lambda = 8{,}67$.

A close-up of the cylinder pressure curves is shown in Figure 6.19. In Figure 6.20 the accumulated heat release for both pilot ignited VOC Fuel and only pilot fuel are shown. By direct comparison of the cylinder pressure curves in these plots no significant effect of the charge air pressure is found.

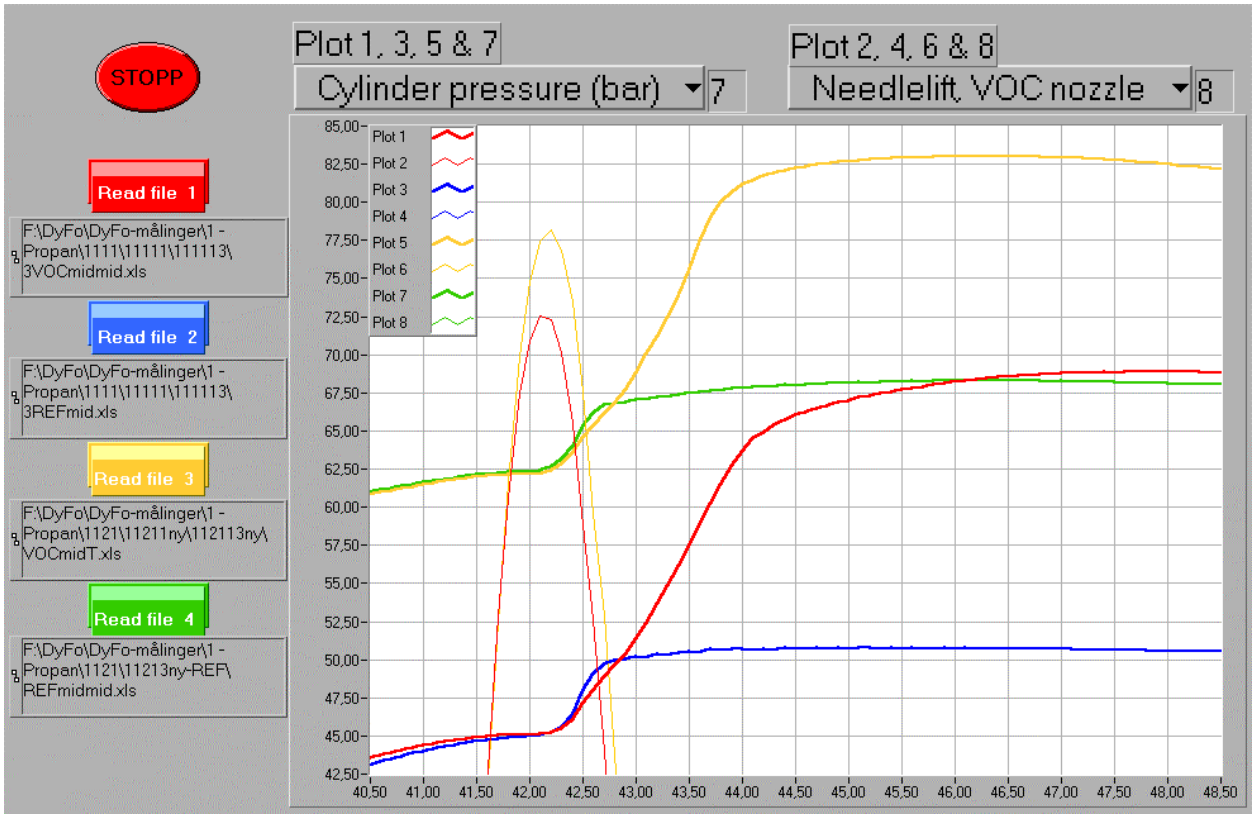

Figure 6.19 Effect of charge air pressure (red & blue curves: Low charge air pressure, yellow & green curves: High charge air pressure). Close-up view of the curves for cylinder pressure and VOC Fuel needle lift from about 1 ms prior to ignition to about 7 ms after. (Pilot ignited VOC Fuel and pilot diesel fuel for comparison).

Accumulated heat release curves from the tests are shown in Figure 6.20. The plot shows the effect of the oscillating nature of the test rig by the wavy curves behind the point where all energy has been released. In addition, the effect of different heat loss to the combustion chamber surface by combustion tests and compression tests (cf. section 3.3.2) is shown by the gradually decreasing level of the curve for pilot ignited VOC Fuel.

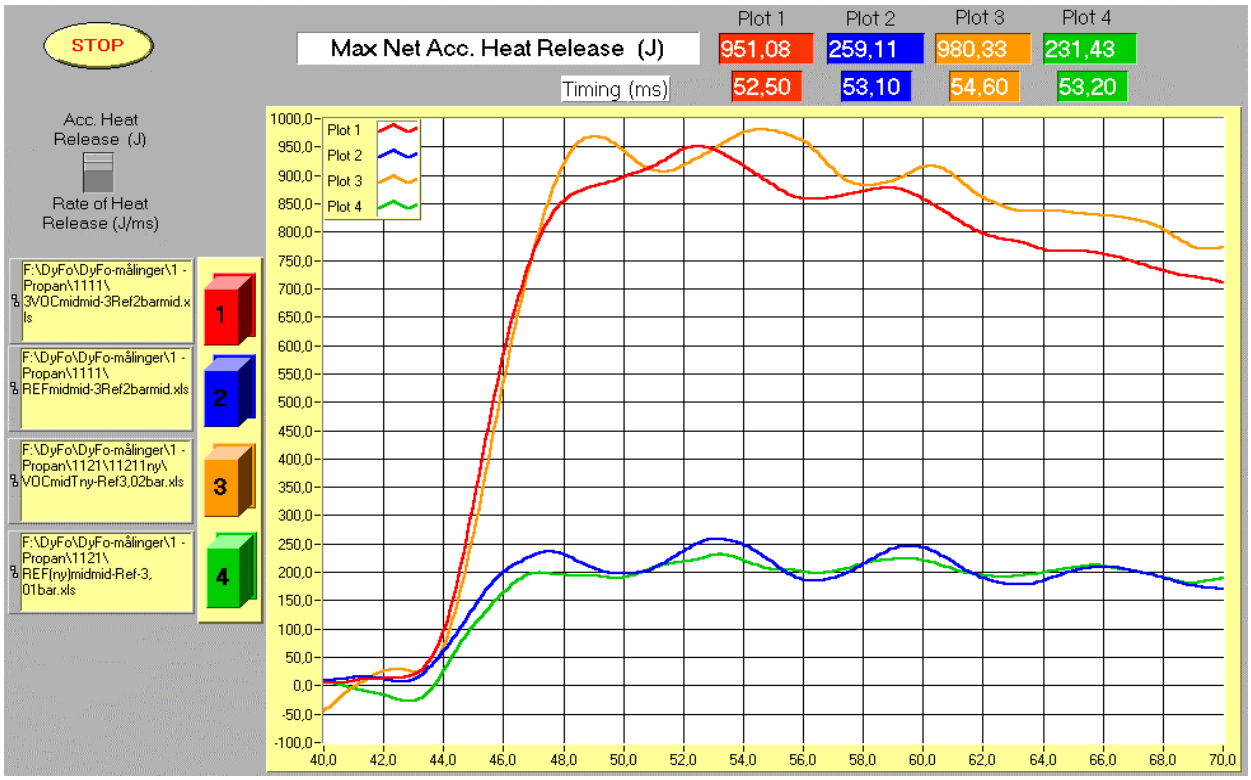

Figure 6.20 *Effect of charge air pressure. Plots of accumulated heat release for tests with pilot ignited VOC Fuel and only pilot diesel fuel. Red & blue curves: charge air pressure 2,0 bar, orange & green curves: charge air pressure 3,0 bar.*

Analysis of the test results, based on both the pressure curves in Figure 6.19 and the accumulated heat release (AROHR) in Figure 6.20, gives the following:

- Heat loss to the walls seems to be little affected by the charge air pressure level.
- Ignition delay of pilot diesel fuel is unaffected of the charge air pressure level.
- VOC Fuel injection reduces the pressure gradient of pilot diesel fuel.

The charge air pressure variation in question does not significantly influence the ignition and combustion of pilot ignited VOC Fuel.

Effect of charge air temperature

To study the effect of varying the charge air temperature on the ignition and early combustion of condensed VOC, this parameter has been set to 30 °C (LOW nominal value) and 70 °C (HIGH nominal value). 6 test series with LOW charge air temperature and 6 test series with HIGH charge air temperature are carried out.

Test series 1121 representing LOW charge air temperature (with corrected overall excess air ratio λ = 8,67) is compared to test series 1221 representing HIGH charge air temperature (excess air ratio λ = 7,55). Each test series consist of 5 sub-series with the 5 different RIT settings, cf. Table 5.6. In both test series the charge air pressure was 3,0 bar. Test 111113 (excess air ratio λ = 5,78) and test 121113ny (excess air ratio λ = 5,03) represents the sixth comparison. In these tests the charge air pressure was 2,0 bars. The tests were performed with propane.

A close-up view of the cylinder pressure curve from one of these comparisons (112113 vs. 122113) is shown in Figure 6.21. This comparison represents the results from all the performed comparisons. Figure 6.22 shows heat release curves for the same two tests.

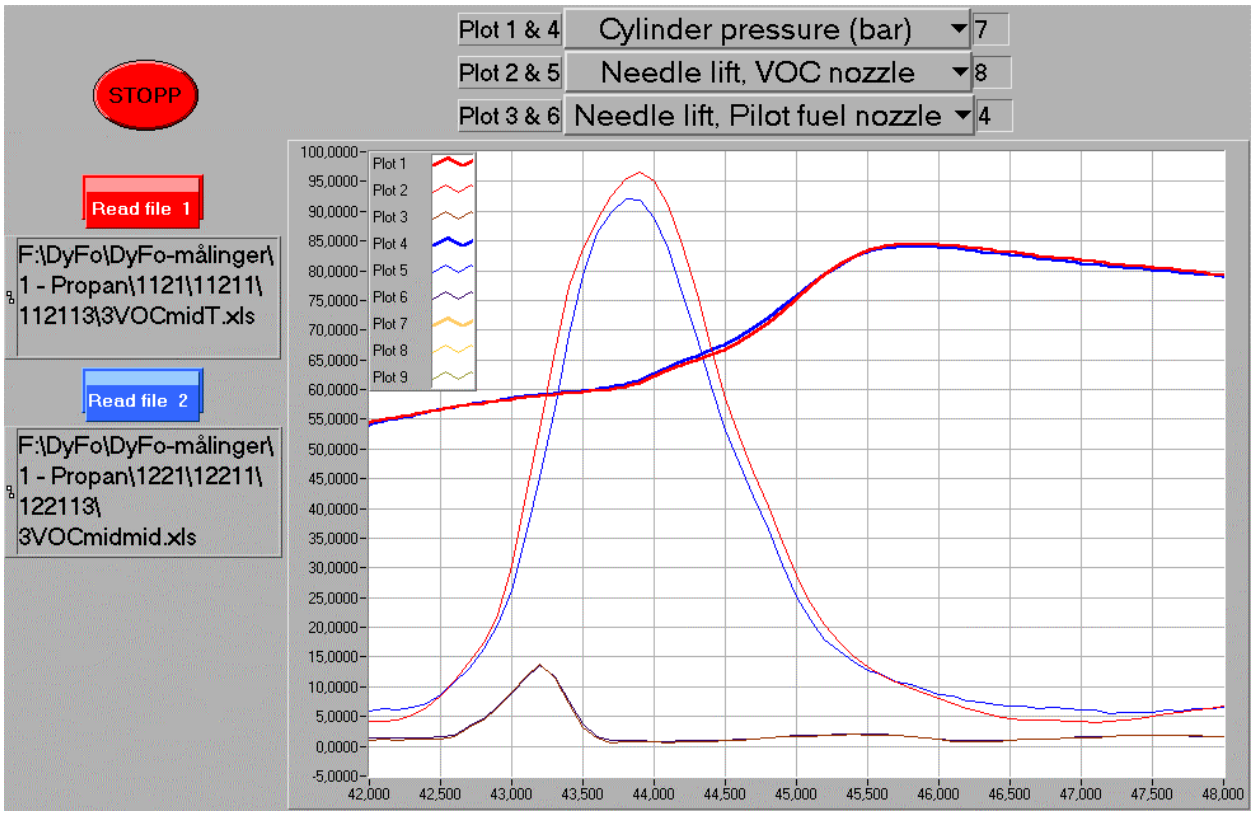

Figure 6.21 *Close-up plot of cylinder pressure and needle lifts for VOC Fuel and pilot diesel fuel for tests performed with different charge air temperatures. Red curves: Low charge air temperature, blue curves: High charge air pressure.*

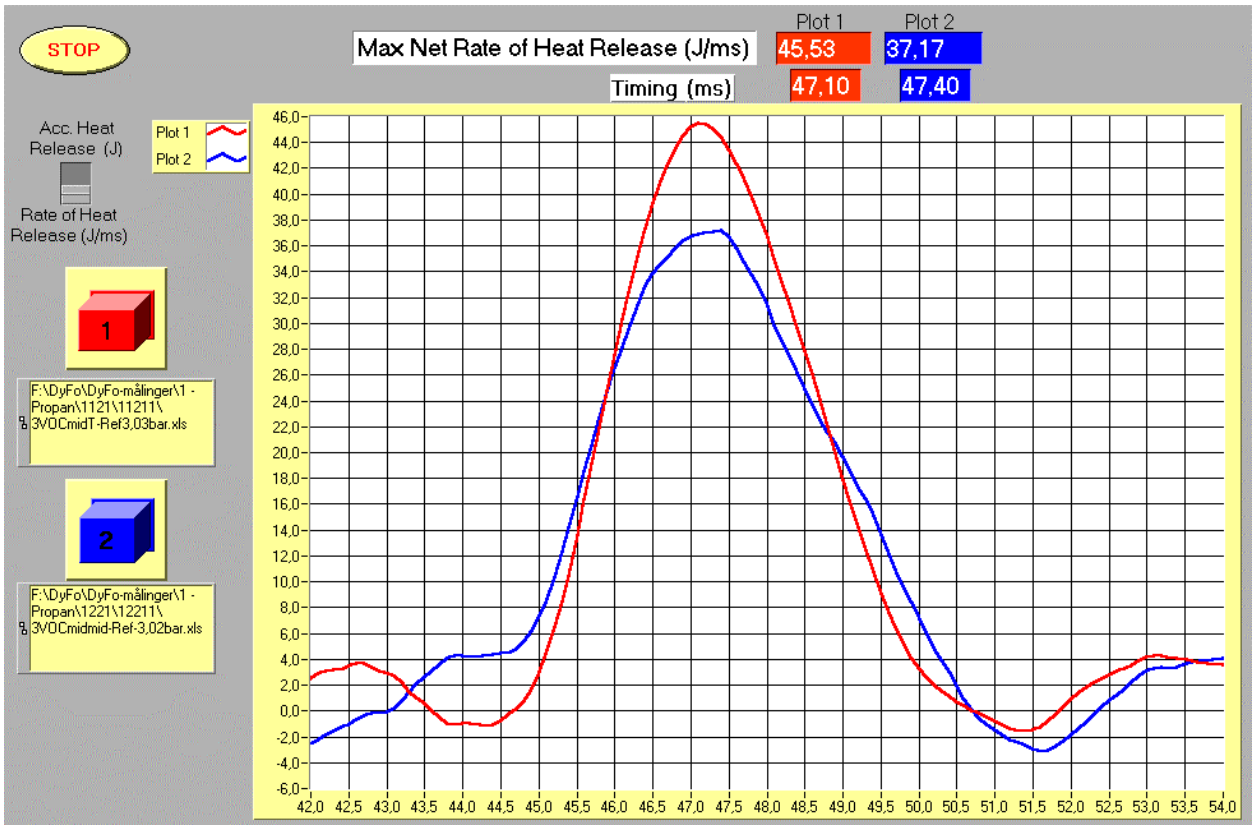

Figure 6.22A *Plot of ROHR for tests performed with different charge air temperatures. Red curve: Low charge air temperature, blue curve: High charge air pressure.*

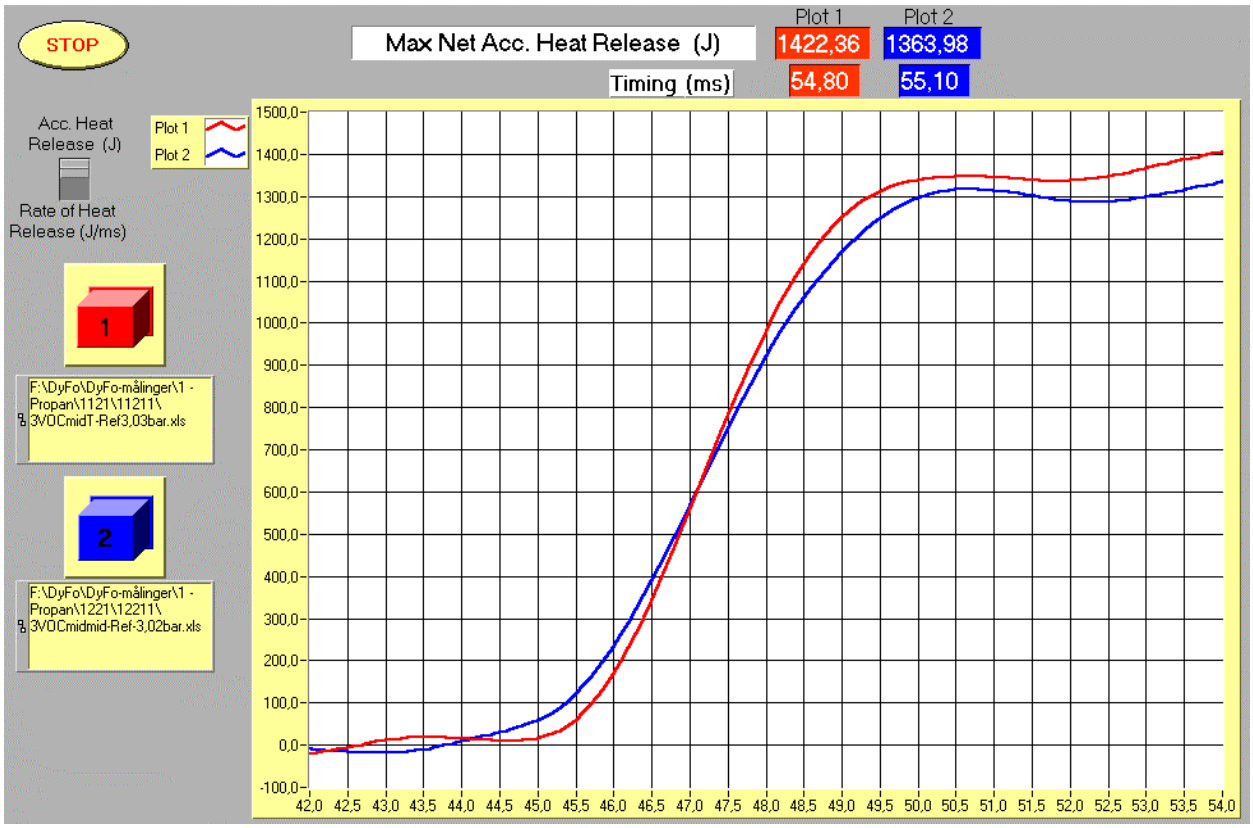

Figure 6.22B Plot accumulated heat release (AROHR) for tests performed with different charge air temperatures. Red curve: Low charge air temperature, blue curve: High charge air pressure.

From these plots no significant effect of the charge air temperature is found to be present. Even though the ROHR curves differ, the difference in accumulated heat release is only 4,3 %. This is well within the measured variation limits of the fuel mass delivery listed in Table 6.3 showing a standard deviation of approximately 7 %.

Effect of fuel type

To study the effect of different components present in the VOC Fuel, 4 different fuel types have been tested – Propane, n-Butane, iso-Butane and a blend of 60% Propane, 10% iso-Butane and 30% n-Butane (VOC mixture). In addition methane is included for comparison since the use of the light VOC fractions – as later discussed in Chapter 8 – most favourably will be by high-pressure injection. Figure 6.23 and 6.24 show some details of the cylinder pressure for these fuels.

By this comparison, the effect of different densities of the VOC components at 400 bars have to be considered. The injected fuel amount is metered by volume and thus the injected mass will vary and correspondingly the heat release.

However, what are considered to be most interesting to study by this comparison are any differences in ignition delay and pressure gradient s in the early combustion phase.

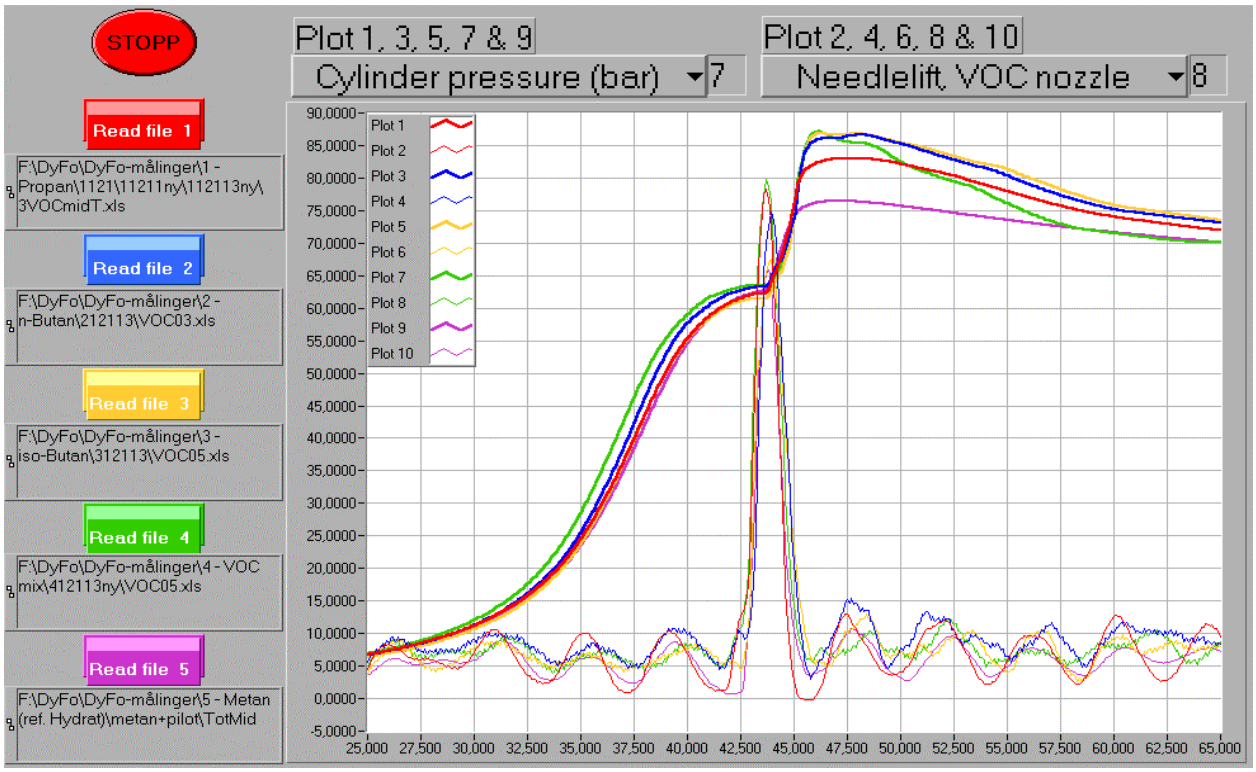

Figure 6.23 *Cylinder pressure and needle lift for different pilot fuel ignited VOC Fuels. Red curve: Propane, blue curve: n-Butane, yellow curve: iso-Butane, green curve: VOC mix and pink curve: Methane.*

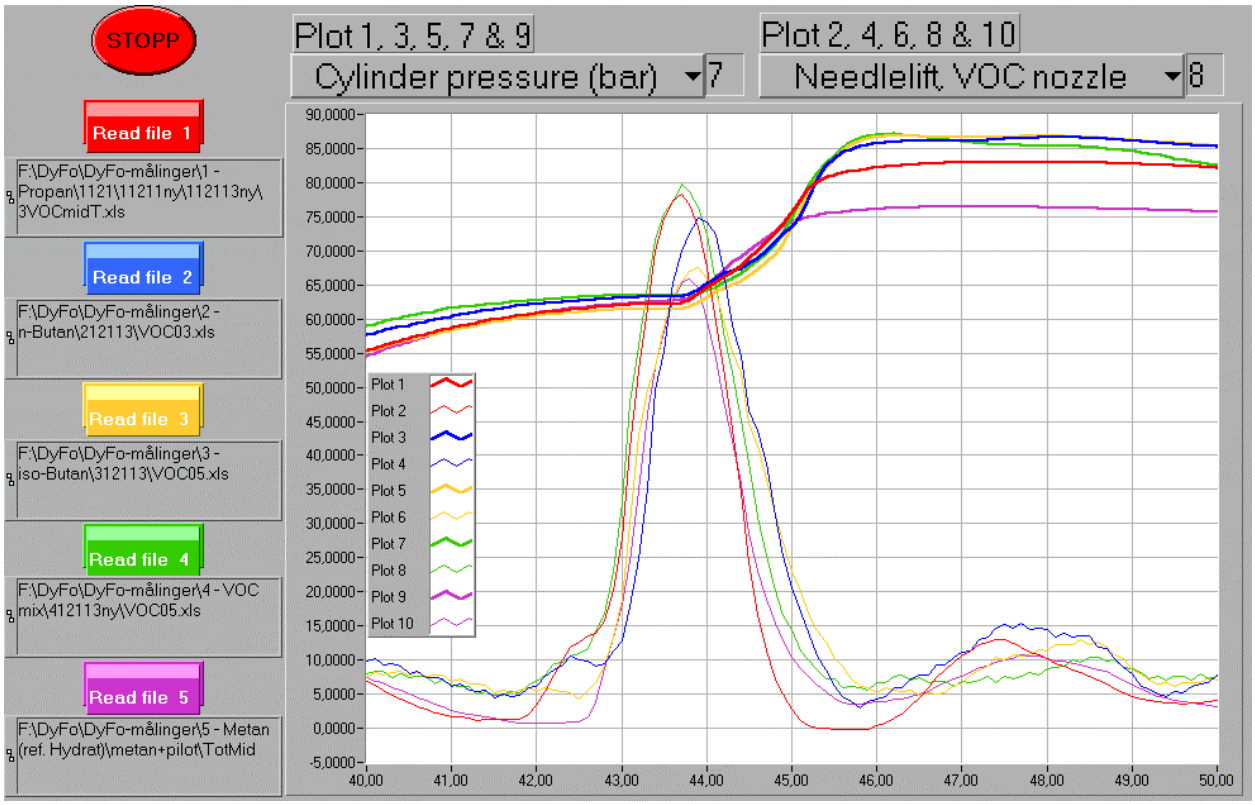

Figure 6.24 *Close-up view of cylinder pressure and needle lift for pilot fuel ignited VOC Fuels. Red curve: Propane, blue curve: n-Butane, yellow curve: iso-Butane, green curve: VOC mix and pink curve: Methane.*

From Figures 6.23 and 6.24 it is seen that no significant differences occur to either ignition delay or to the pressure gradient in the early combustion if different VOC Fuel components are injected and pilot ignited.

7 Homogenous combustion of VOC/air charge.

7.1 Light fraction of VOC for homogenous combustion

The VOC Fuel project initiated by Statoil R&D (cf. section 1.1 and 2.2) is only utilising the condensable part of the VOC emitted. In addition the light fraction of VOC, methane and ethane, constitute a valuable source of energy that should not be wasted (cf. section 1.2).

Different methods to prevent methane and ethane from escaping to the atmosphere have been discussed by the oil industry (cf. section 2.1). In the case of shuttle tankers, as already mentioned in section 2.1, one option is to burn this fraction directly in a diesel engine, without separating it from the inert gas. In this chapter a minor part of the work dealing with this method both theoretically and experimentally is described.

In Chapter 2, Table 2.1 shows typical properties of the raw VOC from the Statfjord oil field. In a typical shuttle tanker the remaining non-condensed gas fraction, the "residual VOC", is calculated to have the composition shown in Table 7.1. As can be seen, a fraction of propane is remaining while the main constituents are methane and ethane. Since the condensation is carried out at approximately 40 bars the residual VOC will be collected at an elevated pressure.

As Table 7.1 shows, there is still a substantial amount of energy available in the uncondensed, light VOC fraction (residual VOC). At the end of loading as the content of hydrocarbons is highest (Alfa = 0.7), the energy of the released light VOC fraction is 27 MW. This is corresponding to 97200 MJ/h or approximately 2314 kg of diesel fuel per hour, which is enough to run an engine larger than 12 MW.

Table 7.1 Typical properties of the residual VOC fraction during loading (Statfjord oil field) (13).

Residual VOC - Statfjord				Alfa = 0,2			Alfa = 0,7		
Constituent	LHV	Density (at 273 K)		Mole fraction	Volume	"Power"	Mole fraction	Volume	"Power"
	MJ/Sm^3	kg/kmole	kg/Sm^3	-	Sm^3/s	MJ/s	-	Sm^3/s	MJ/s
Methane	35,833	16,04	0,716	0,018	0,062	2,24	0,130	0,222	7,96
Ethane	64,438	30,07	1,342	0,036	0,125	8,04	0,167	0,285	18,39
Propane	92,919	44,10	1,969	0,023	0,080	7,41	0,004	0,007	0,64
i-butane	121,667	58,12	2,595	0,001	0,003	0,42	0	0	0
n-butane	123,611	58,12	2,595	0	0	0	0	0	0
i-pentane	125,000	72,15	3,221	0	0	0	0	0	0
n-pentane	130,000	72,15	3,221	0	0	0	0	0	0
Hexane+	140,000	86,18	3,847	0	0	0	0	0	0
N2	0	28,01	1,251	0,784	2,717	0	0,596	1,019	0
CO2	0	44,01	1,965	0,045	0,156	0	0,033	0,056	0
O2	0	32,00	1,429	0,092	0,319	0	0,070	0,120	0
Sum	-	-	-	0,999	3,462	18,10	1,000	1,709	26,99

7.2 Utilisation of "residual VOC" in diesel engines.

The light fraction of the VOC can be utilised as fuel by homogenous combustion. By mixing the "residual VOC" and air in the inlet manifold of a diesel engine, this gas can be used directly. Mixing gaseous fuel in the inlet manifold is a well-proven method. In the case of shuttle tankers, a problem may be the inert gas content which can be as much as 80%. Gas engines with low pressure mixing of gas and air («Dual Fuel Diesel Process», cf. section 2.4) can burn VOC when

it is led into the inlet air ahead of or behind the turbocharger compressor. The limits and conditions for use of low-pressure induced gas are dependent of the gas quality and have to be established.

In this section n a Medium Speed engine available in both diesel and gas version (MAN-B&W 7L32/40) is examined to estimate engine performance (power, air consumption and fuel consumption). Fuelled with diesel, the engine performance (54) is shown in Table 7.2.

Table 7.2 MAN-B&W 7L32/40 engine operating on diesel fuel (2).

MAN-B&W 7L32/40 Diesel operation							
Engine power (Generator-/CPP operation)		Air consumption		Energy consumption			Excess air ratio
				Diesel			
%	kW	kg/kWh	Sm^3/s	kJ/kWh	MJ/s	g/kWh	-
100	3080	7,15	5,010	7771,4	6,65	182,00	2,72
85	2618	7,20	4,289	7643,3	5,56	179,00	2,79
75	2310	7,25	3,810	7643,3	4,90	179,00	2,80
50	1540	7,65	2,680	7984,9	3,42	187,00	2,83

To ensure stable ignition of the gas, injection of 10 % pilot diesel fuel is assumed for the gas version of the engine. With 10% pilot diesel fuel and residual VOC added in the inlet manifold, this engine would get the volume of "fresh air" for combustion significantly reduced, especially at high load. The key question is how this “diet” will limit the engine operation. When calculating the engine performance, the properties of the residual VOC listed in Table 7.1 are used. The volume of this fraction occupies space in the inlet manifold that would otherwise contain “fresh air” for combustion.

The energy demand for the gas engine is higher than for the diesel version (8100 vs. 7771,4 kJ/kWh) (54). With 10 % pilot fuel, this means that 7322,86 kJ/kWh must be added by the gas.

The residual VOC composition may be found in Table 7.1. In Table 7.3 O_2 and a part of the N_2 (= 3,76 times the amount of O_2) coming from the residual VOC is referred to as "Air" used for combustion. The remaining N_2, not included as "Air", and the CO_2 is referred to as "Inert gas".

The volumes of HC, "Air" and "Inert Gas" which sums up to the total volume of the residual VOC, are given by the formulas 7.1 - 7.3. In the list below the formulas, the actual values for calculation are transferred from Table 7.1 and written in parenthesis:

$$V_N(HC) = V_A(HC) * E_N(HC) / E_A(HC) \quad (7.1)$$

$$V_N(\text{“Air”}) = V_N(HC) * x(\text{“Air”}) / x(HC) \quad (7.2)$$

$$V_N(\text{“IG”}) = V_N(HC) * x(\text{“IG”}) / x(HC) \quad (7.3)$$

$V_N(HC)$ - HC volume necessary to operate the engine (shown in column 6 in table 6.3)
$V_A(HC)$ - HC volume available in the residual VOC (α=0,2 / 0,7$\Rightarrow$ 0,270 / 0,514 Sm3/s)
$E_N(HC)$ - Energy in HC necessary to operate the engine (α=0,2 / 0,7$\Rightarrow \leq$ 6,27 MJ/s)
$E_A(HC)$ - Energy available in the residual VOC (α=0,2 / 0,7$\Rightarrow$18.1 / 26,99 MJ/s)
$V_N(\text{“Air”})$ - “Air” volume included in the residual VOC (shown in column 7 in table 6.3)
$x(\text{“Air”})$ - Mole fraction of "Air" in the residual VOC (α=0,2 / 0,7$\Rightarrow$ 0,435 / 0,331)
$x(HC)$ - Mole fraction of HC in the residual VOC (α=0,2 / 0,7$\Rightarrow$ 0,078 / 0,301)
$V_N(\text{“IG”})$ - "Inert Gas" volume included in the residual VOC (shown in col. 8 in table 6.3)
$x(\text{“IG”})$ - Mole fraction of "Inert Gas" in the residual VOC (α=0,2 / 0,7$\Rightarrow$ 0,486 / 0,368)

The results of these calculations give the engine performance shown in Table 7.3. An essential property is the excess air ratio, which should be 2,0 or above for an engine as used in this estimate.

In the gas version, the total energy consumption for the engine will be 8100 kJ/kWh (= 6,93 MJ/s) at full load. The efficiency will decrease from 46,3% to 44,4%, but the power output will remain the same as for the diesel version. The pilot diesel fuel for ignition is assumed to be 10 % of total energy input for the diesel version => 18,2 g/kWh. This energy consumption represents 777,1 kJ/kWh (= 0,66 MJ/s). The residual VOC supplies 7322,9 kJ/kWh (= 6,27 MJ/s) of the total energy demand.

In Table 7.3 the gas version of the engine is fuelled with residual VOC through the inlet air manifold. Since the composition of the residual VOC varies during the loading process, it is necessary to control the operational conditions for the engine at different values of "Alfa" (cf. Figure 2.1). The two limits for "Alfa" (0,2 and 0,7) are used to check if the residual VOC always contains enough energy to run the engine.

Table 7.3 Engine operating on residual VOC with 10% pilot diesel fuel.

MAN-B&W 7L32/40 - ALFA = 0,2 Gas operation (10% pilot diesel fuel)									
Engine power (Gen.-/CPP operation)		Energy consumption			VOC (HC + IG) consumption			New air delivery	New excess air ratio
		Total	Gas	Diesel	HC gas	"Air"	"Inert Gas"		
%	kW	MJ/s	kJ/kWh	g/kWh	Sm^3/s	Sm^3/s	Sm^3/s	Sm^3/s	-
100	3080	6,93	7322,9	18,20	0,093	0,522	0,583	4,334	2,40
85	2618	5,79	7202,2	17,90	0,078	0,436	0,436	3,723	2,46
75	2310	5,11	7220,2	17,90	0,069	0,385	0,430	3,311	2,48
50	1540	3,56	7524,0	18,70	0,048	0,268	0,299	2,333	2,50
MAN-B&W 7L32/40 - ALFA = 0,7 Gas operation (10% pilot diesel fuel)									
Engine power (Gen.-/CPP operation)		Energy consumption			VOC (HC + IG) consumption			New air delivery	New excess air ratio
		Total	Gas	Diesel	HC gas	"Air"	"Inert Gas"		
%	kW	MJ/s	kJ/kWh	g/kWh	Sm^3/s	Sm^3/s	Sm^3/s	Sm^3/s	-
100	3080	6,93	7322,9	18,20	0,132	0,146	0,161	4,717	2,35
85	2618	5,79	7202,2	17,90	0,110	0,122	0,135	4,044	2,41
75	2310	5,11	7220,2	17,90	0,097	0,108	0,119	3,594	2,43
50	1540	3,56	7524,0	18,70	0,068	0,075	0,083	2,530	2,45

This theoretical examination shows that it is enough energy in the residual VOC to run the engine in all periods during loading (Alfa = 0,2 – 0,7). The calculation of excess air ratio is not exact, but still, the excess air ratio will be acceptable at all operating loads. However, it remains to see how well a real engine performs with residual VOC mixed with the charge air. Engine tests are needed to verify this calculation and to see how the engine performs at low load operation.

To get a better understanding of the ignition and combustion properties of the residual VOC, tests were carried out on DyFo.

7.3 Homogenous combustion tests

7.3.1 Calculation of residual VOC composition

Preliminary tests with homogenous combustion of residual VOC ignited by pilot diesel fuel has been conducted at excess air ratios (λ) of 1,0 - 1,4 (30, 55, 56). Diesel engines normally operate at $\lambda \geq 2,0$ and additional tests with an excess air ratio of 2,0 are performed. The mixing procedure for the homogenous gas mixture of hydrocarbons, oxygen and nitrogen was identical in the preliminary and the additional tests. The CO_2 content of the inert gas was exchanged with nitrogen for convenience. The content is small and this exchange is not assumed to have any significant influence on the combustion. Using traditional mass balance equations, the necessary air to burn the gas mixture is calculated:

a* fuel + b*(oxidiser+diluent) Þ c*CO2 + e* H2O + f*(excess oxidiser) + g*(diluent) (7.4)

In this case the fuel constitute of both a gas mixture containing hydrocarbons (fuel), oxygen (oxidiser) and nitrogen (diluent) and diesel fuel. With residual VOC from Statfjord, Table 7.4 shows the components in the residual VOC used for the additional tests in DyFo.

For the combustion tests the amount of pilot diesel fuel ($C_{16}H_{30}$) is set to 10 % of the total energy. The lower heating values for CH_4, C_2H_6 and C_3H_8 are listed in Table 7.4. With a charge pressure of 2,5 bar, a charge temperature of 70 °C and Alfa=0,2 the charge mass will equal a volume of 0,002189 Sm^3 (= 2189 Scm^3) in the DyFo at 1 bar and 273 K. Table 7.4 shows the information necessary to solve the mass balance equation (7.4).

Table 7.4 Charge in DyFo at 2,5 bar, 70 °C and Alfa=0,2

	Mole fraction	Mole fraction of HC	Volumes in DyFo (Sm^3)	LHV (MJ/Sm^3)	Energy content (kJ)
CH_4	0,018	0,231	0,000039	35,833	1,412
C_2H_6	0,036	0,462	0,000079	64,438	5,077
C_3H_8	0,024	0,308	0,000053	92,919	4,881
O_2	0,093		0,000204	0	0
CO_2	0,045		0,000098	0	0
N_2	0,784		0,001716	0	0
Sum	1,000		0,002189		11,370

From Table 7.4 the total energy in the DyFo charge is found to be 12,633 kJ (11,37/0,9=12,633). Then 1,263 kJ => m=29,7 mg diesel (=1,263kJ/42,5MJ/kg) equals the remaining 10% of the total energy content. The number of moles of diesel ($C_{16}H_{30}$) is n= m/M= 29,7 mg/ 222 kg/kmole= 0,0001339 mol. In Table 7.5 the content of the DyFo charge used by the tests is shown.

Table 7.5 Energy and mass content of the charge in DyFo tests.

		Mole fraction (%)	Energy fraction (%)	Energy content (kJ)	Mass content (mg)
Residual VOC	CH_4	1,79976	11,18	1,412	28,24
	C_2H_6	3,59952	40,19	5,077	105,73
	C_3H_8	2,39968	38,63	4,881	103,43
Pilot diesel fuel		0,01339	10,00	1,263	29,70
Oxygen, O_2		9,29875	0,00	0,000	291,52
Nitrogen, N_2		82,88890	0,00	0,000	2269,31
Total		100,00000	100,00	12,633	2827,93

Calculation of stoechiometric factors is performed with no excess oxidiser (i.e. f=0). The following equation suitable for calculations with excess air ($\lambda > 1,0$) then results:

$$(CH_4 + 2C_2H_6 + 1,333C_3H_8 + 0,007439C_{16}H_{30}) + 15,833\lambda(O_2 + 3,76N_2) + 26,611N_2$$
$$\Rightarrow 9,111CO_2 + 13,444H_2O + 15,833(\lambda-1)O_2 + (59,556\lambda+26,611)N_2 \quad (7.5)$$

7.3.2 Test results

Tests are carried out on the DyFo test rig in three series. The first two series were performed prior to the redesign of the test rig (14, 30), but some interesting findings regarding ignition quality was found even in these tests:

- More pilot fuel increases the ignition delay in the DyFo test rig
- Ignition delay decreases when increasing the excess air ratio
- The type of hydrocarbon (methane or ethane) does not affect ignition delay, only the test conditions prior to ignition of the pilot fuel

In the first series the pilot fuel was injected in a charge mix (air/residual VOC/inert gas) with an excess air ratio of 1,0 and 1,4. In the second series the excess air ratio was about 2,0. In addition to the above findings, both series showed some interesting details on the images taken.

In the last test series, from which Figures 7.1 and 7.2 are taken, it is found that the ignition delay is increased by about 100 % (from 0,8 to 1,7 ms). In a real engine this means that even if enough energy is available in the cylinder, the combustion takes place too late. This means that the efficiency will be reduced.

Another important question when charging the combustion chamber with a mixture of air, combustible gas and inert gases is if the ignition energy in the pilot fuel is high enough to start a stable combustion. In addition it is of interest to get an answer to 1) how the combustion starts and proceeds and 2) where it starts. The first question can be answered by studying the cylinder pressure curves from the test (cf. Figure 7.1), the second by studying the video images (cf. Figure 7.2).

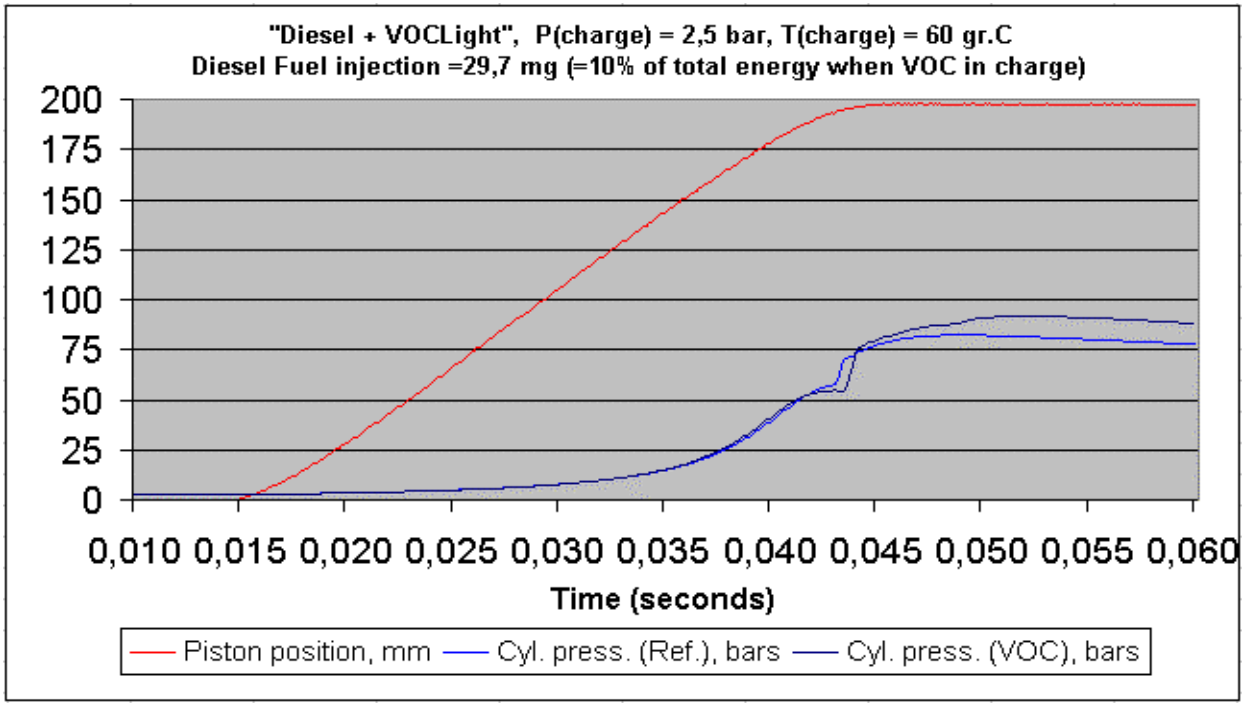

Figure 7.1 Dynamic signals from piston movement and cylinder pressure when burning pilot diesel fuel with and without residual VOC mixed with the charge air at λ=2,0.

Because of the dynamics governing the fuel flow in the injection system, the pilot fuel is not injected until 1,20 ± 0,05 ms after the signal for nozzle opening is given (cf. section 3.1.1). In the left section of Figure 7.2 pilot fuel is injected in a premixed charge consisting of residual VOC and air; in the right section pilot fuel is injected in pure air.

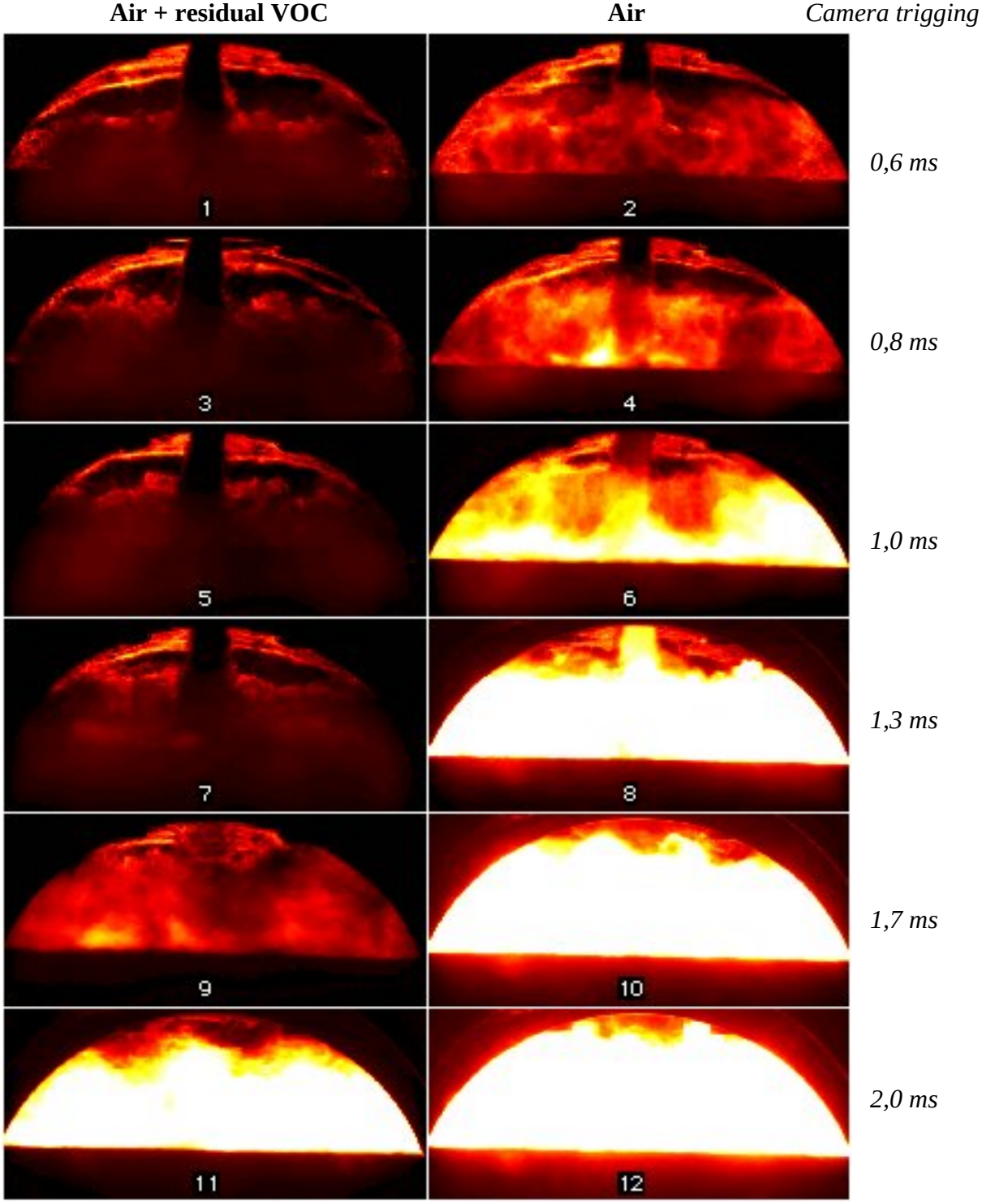

Figure 7.2 *Ignition and combustion of residual VOC by pilot diesel fuel compared to ignition and combustion of pilot diesel fuel in air. Camera trigging is time after start of pilot fuel injection.*

Conclusions.

Homogeneous combustion of residual VOC is shown to be a suitable method for the use of this energy resource. The calculations above show that the energy content is sufficient and that the composition of the gas is of less importance.

The combustion tests in the DyFo test rig shows:

- Ignition delay decreases when increasing the excess air ratio. In a real engine λ decreases and the temperature increases when the engine load increases. Normally the ignition delay then decreases, the main reason being the increased temperature.
- Type of hydrocarbon (methane or ethane) has no effect on ignition delay. This is due to the use of pilot injected diesel fuel contributing to the initial ignition.

These findings support that the use of residual VOC as described above is possible. Some of the contradictory results obtained in the DyFo test rig may not apply to real engines. In the DyFo the following observations were made:

- The ignition delay is greatly increased when mixing the charge air with residual VOC (according to Figure 7.2 its doubled). This will most certainly apply to a real engine.

- More pilot fuel increases the ignition delay in the DyFo test rig. This is in fully agreement with what other researchers have experienced by tests in rapid compression machines and high-pressure, high-temperature combustion vessels (47). In diesel engines, however, more fuel normally means more power (higher engine load) giving a higher temperature level in the cylinder. The observed ignition delay in an engine is normally reduced with higher load.

The test results from the DyFo test rig thus indicate that residual VOC can give ignition problems when charged together with air in a diesel engine due to the extended ignition delay. These findings have later been confirmed by a study carried out for a M.Sc. thesis (33).

The combustion temperature in a rapid compression machine is lower than in a diesel engine. It is therefore likely that the combustion process is better in a real engine than in the DyFo. Complementary engine tests should therefore be performed before the final conclusion can be drawn of whether residual VOC can be used directly in diesel engines or not.

8 Combustion of light VOC trapped in hydrates.

8.1 Introduction

Intentionally, as mentioned in section 1.3, the use of light VOC components captured in hydrates was to be studied intensively in this work. This was in agreement with the original reason for starting the "VOC project". Before the work with this thesis was started, work supported by Statoil FoU was carried out to find suitable ways of producing hydrates for capturing methane and ethane. Storing such hydrates in special designed fuel tanks were thought to be a future way of using these components as engine fuel. Throughout the progress of the study, it showed up that making hydrates was not as easy as first estimated. This is one of several reasons why this part has ended up as a minor, third part of the work reported in this thesis.

8.2 Background

Gas hydrates are compounds where water molecules build a crystal lattice, the “host lattice”, with cavities of one or more kinds. The gas molecules, the “guest molecules”, can occupy these cavities. The crystal lattice is usually not stable in itself, but the encaged “guest molecules” will contribute to stabilize it. The appearance of gas hydrates is like snow or ice. At elevated pressures they can exist at temperatures well above the melting point of ice.

A lot of different gases can form hydrates. In the oil and gas industry hydrates formed of gas components present in natural gas (and crude oil?) is of interest. Although natural gas hydrates were discovered in 1810 (34) the importance was not emphasised until 1934 when it was discovered that gas hydrates were responsible of the plugging of natural gas process equipment and transportation pipelines.

Problems occur when hydrates form and agglomerate in pipelines and make solid plugs. These plugs represent problematic restrictions to the gas and/or crude oil flow. A lot of research has been carried out to find ways of preventing hydrates to form. Since hydrate formation in pipelines is a problem, the stability of the structures has been intensively studied. Methods and substances reducing this stability have been tested to reduce the problems in pipelines. A lot of this research has been carried out in Trondheim at NTNU and Statoil R&D (35-38).

However, the stability of hydrates has given the researchers at NTNU an idea of how to turn the problematic hydrates into a useful product (39-41). A company – Natural Gas Hydrate AS – was formed in June 1999 to develop and commercialise the concept of using natural gas hydrates to transport natural gas from oil/gas fields to shore in tankers. Researchers at Statoil R&D in Trondheim got the idea of storing the light fraction of the emitted VOC from shuttle tankers in hydrates and transport the gas in this way onboard the tankers.

8.3 Structures and properties of hydrates.

The crystal “host lattice” resemble the solid structure of water (known as ice), and dependent of the type of hydrocarbons present together with the water, three different structures can form; cubic structure I (sI, cf. Figure 8.1a), cubic structure II (sII, Figure 8.1b) or hexagonal structure H (sH, Figure 8.1c).

The major difference between hydrates and solid water (ice – structure Ih) is that ice forms as a pure component, while hydrates only forms if the water has one or more “guest” molecules (34).

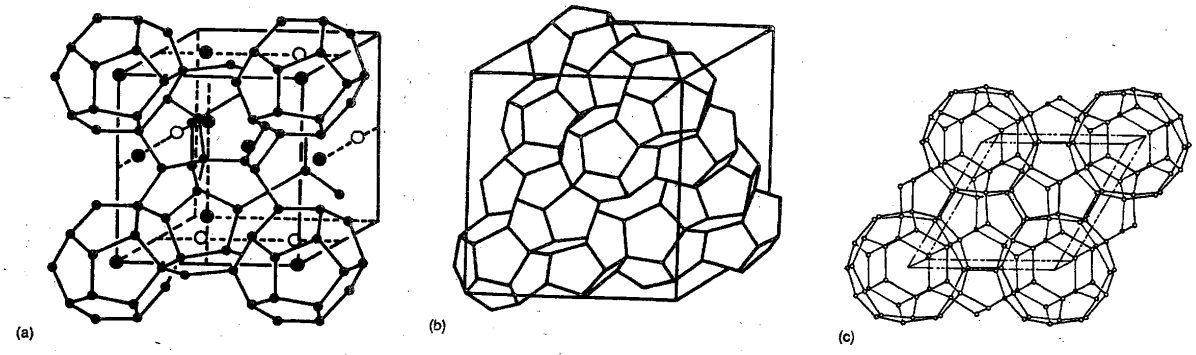

Figure 8.1 Hydrate crystal unit structures - (a) sI, (b) sII, (c) sH (34).

Structure I is formed with single guest molecules with diameter, d, smaller than 6Å (methane, ethane, carbon dioxide and hydrogen sulphide). Molecules with 6Å < d < 7Å (propane, iso-butane) will form structure II. Molecules with 7Å < d < 9Å (iso-pentane, neo-hexane) will form structure H when accompanied by smaller molecules like methane, hydrogen sulphide and nitrogen. Nitrogen and small molecules (d < 4.2 Å) are exceptions and form structure II as single guests.

All three structures contain about 85 % water (mol basis) and many of the mechanical properties of hydrates resemble those of ice (12). The structures are formed by a similar mechanism as the way ice is formed of water. To fully explain how this is done, hydrogen-bonding theory must be applied. As a shortcut to this theory, we accept that each water molecule in the ice is connected to four other by this bonding as shown in Figure 8.2 (left).

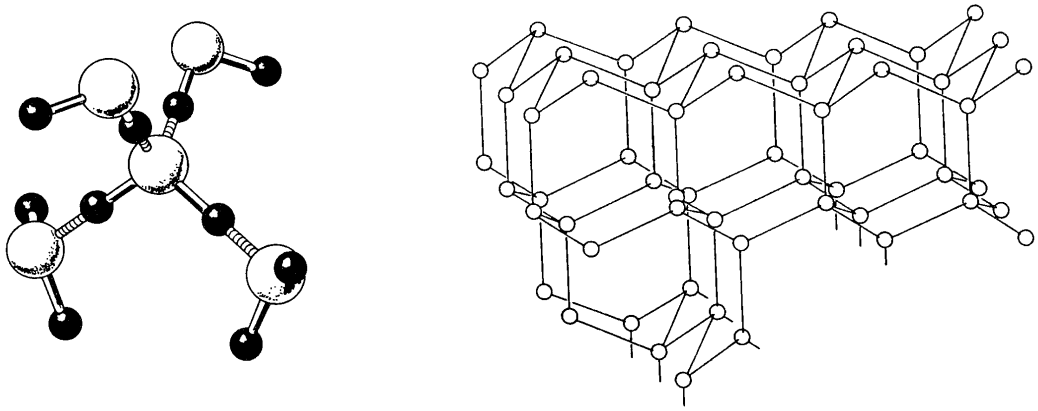

Figure 8.2 Hydrogen bonding (crosshatched) of water molecules (left) and structure Ih of ice (right) (34).

In the Ih-structure of ice, the water molecules then link together as shown in Figure 8.2 (right). They here form hexagons (crystals with six edges), but it is by studies of water found that the most likely structure to spontaneously arise in water is pentagons, followed by hexagons and squares. These polygons then can form different polyhedra as shown in Figure 8.3.

The hydrate structures of natural gases form the same five polyhedra by hydrogen-bonded water molecules, with properties tabulated in Table 8.1.

A nomenclature description (n_i^{mi}) for these polyhedra is suggested, where n_i is the number of edges in face type "i" and mi is the number of faces with n_i edges. The pentagonal dodecahedron (12-sided cavity) shown in Figure 8.3a is labelled 5^{12} because it has twelve pentagonal faces with equal edge lengths and equal angles. The 14-sided cavity (tetrakaidecahedron – Figure 8.3b) is called $5^{12}6^2$ because it has 12 pentagonal and two hexagonal faces. The 16-hedron (hexakaidecahedral cavity – Figure 8.3c) is denoted $5^{12}6^4$ because in addition to 12 pentagonal

faces, it contains four hexagonal faces. The irregular dodecahedron cavity ($4^3 5^6 6^3$ - Figure 8.3d) has three square faces and three hexagonal faces, in addition to six pentagonal faces. The largest cavity ($5^{12}6^8$ – Figure 8.3e) has twelve pentagonal faces, as well as a girdle of six hexagonal faces and a hexagonal face at the cavity crown and foot.

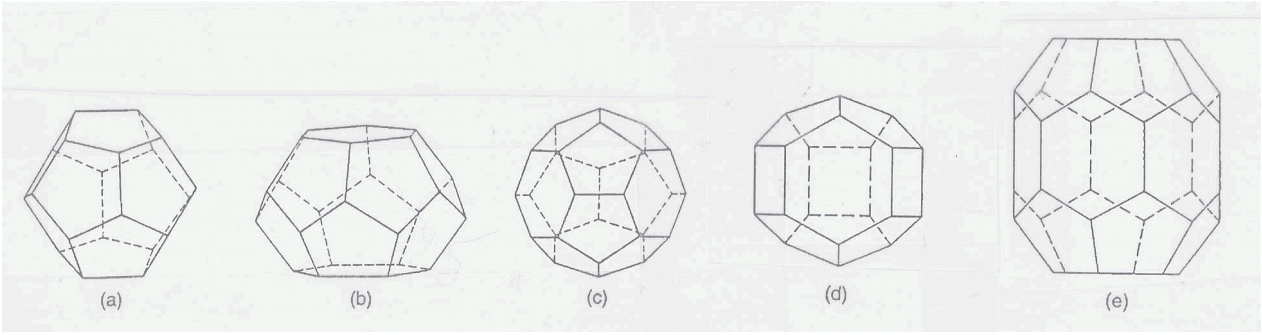

Figure 8.3 The most common polyhedra of water molecules in natural gas hydrates (34).

Table 8.1 Geometry of Cages (34).

Hydrate Crystal Structure	I		II		H		
Cavity	Small	Large	Small	Large	Small	Medium	Large
Description	5^{12}	$5^{12}6^2$	5^{12}	$5^{12}6^4$	5^{12}	$4^3 5^6 6^3$	$5^{12}6^8$
Shown in Figure 7.3, part	a	b	a	c	a	d	e
Number of Cavities/Unit Cell	2	6	16	8	3	2	1
Average Cavity Radius, Å	3.95	4.33	3.91	4.73	3.91[c]	4.06[c]	5.71[c]
Variation in Radius [a] %	3.4	14.4	5.5	1.73	Not Available		
Coordination Number [b]	20	24	20	28	20	20	36

a. Variation in distance of oxygen atoms from centre of cage.
b. Number of oxygen atoms at the periphery of each cavity.
c. Estimates of structure H cavities from geometric models

These polyhedra link to build skeletons of the hydrate structures like Figure 8.4 shows.

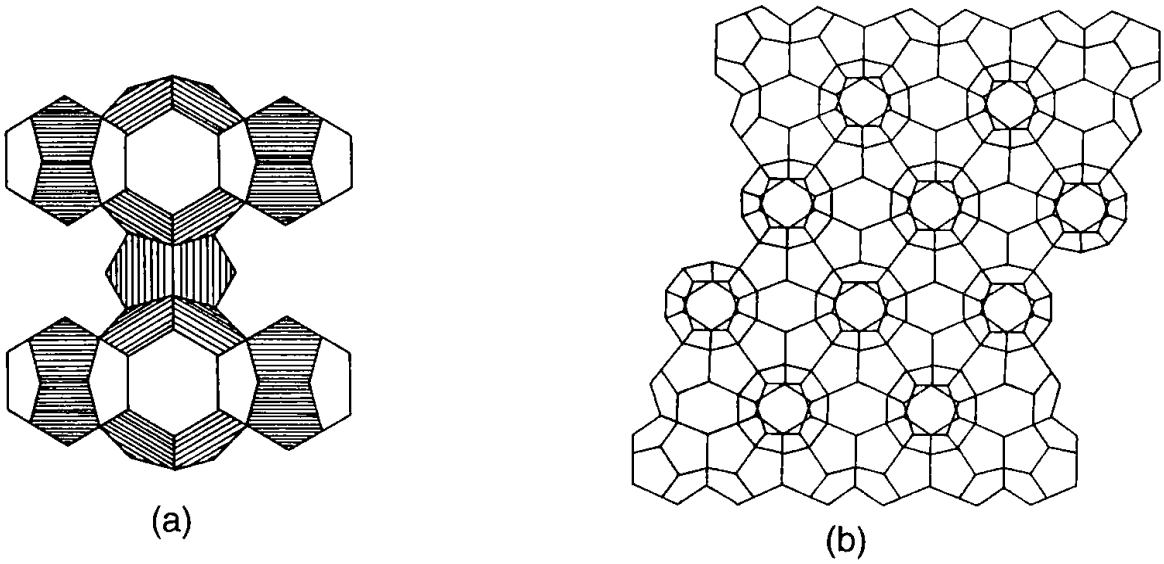

Figure 8.4 Linking of hydrate crystals - (a) Five 5^{12} and two $5^{12}6^2$ polyhedra to form Structure I. (b) 2D-view of face sharing of 5^{12} to form $5^{12}6^4$ polyhedra voids in Structure II (34).

Figure 8.5 shows schematic how the formation and growth of hydrate plugs can form.

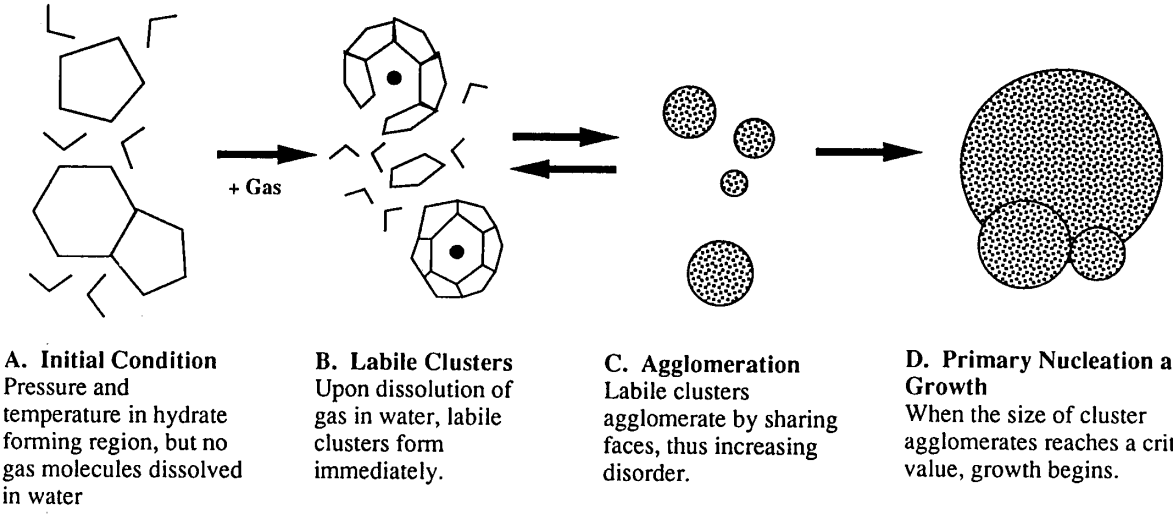

Figure 8.5 Formation and growth of gas hydrates (34).

The pressure and temperature are essential for the formation of hydrates, and of course for the stability of the structure. The different natural gases – the alkanes from C1 – have their own phase diagrams as shown in Figure 8.6.

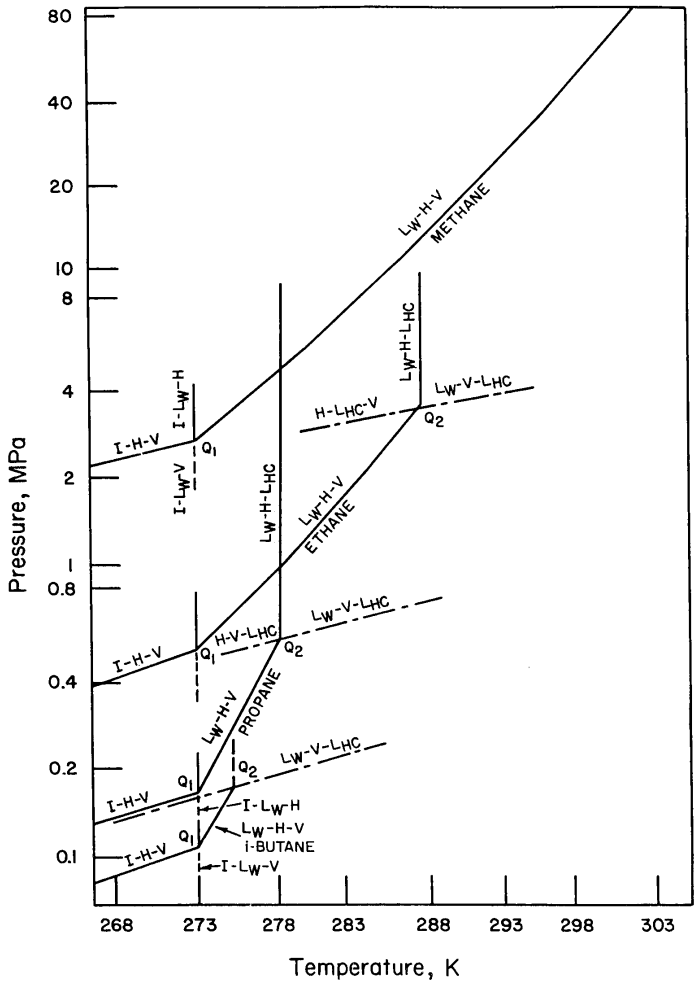

In the Figure the following notation is used:

H for Hydrates,
I for Ice,
V for Vapour
L_W for liquid water and
L_{HC} for liquid hydrocarbon

For each component in the Figure, the hydrate region is to the left of the three phase lines (I-H-V), (L_W-H-V) and (L_W-H-L_{HC}). To the right, fluid phases exist for water and the component vapour.

Figure 8.6 Phase diagrams for some simple natural gas hydrocarbons that form hydrates (34).

In Figure 8.6 the intersection of phase lines (as described) defines both a lower hydrate quadruple point Q_1 (I-L_W-H-V) and an upper quadruple point Q_2 (L_W-H-V-L_{HC}). These points are unique for each gas component (hydrate former) and listed in Table 8.2.

Table 8.2 Natural gas component quadruple points (34).

Component	Quadruple point Q_1		Quadruple point Q_2	
	Temp. (K)	Pressure (MPa)	Temp. (K)	Pressure (MPa)
Methane	272,9	2,563	No Q_2	
Ethane	273,1	0,530	287,8	3,390
Propane	273,1	0,172	278,8	0,556
iso-Butane	273,1	0,113	275,0	0,167
Carbon Dioxide	273,1	1,256	283,0	4,499
Nitrogen	271,9	14,338	No Q_2	

8.4 Possibilities for using hydrates as energy carriers

The concept of capturing the combustible components in the light VOC/inert gas mix in hydrates can be an interesting alternative to the homogenous combustion method. As each volume unit of hydrate can contain as much as 184 volume units of gas at 273 K and 1 atm (34), this method is absolutely of interest. However, a lot of problems connected to the hydrates make it difficult to take advantage of the method directly. The major disadvantage is the density difference between gas and hydrate. The density of methane at STP is 0.68 kg/m^3, while the density of hydrate is more like the density of frozen water – close to 1000 kg/ m^3. Thus the 184 volume units of gas weigh only 125 kilos while the hydrate (water) content weighs 1000 kilos. So much water associated with the fuel will guarantee for some problems! Pure hydrate injected into the combustion chamber in an engine will probably never work for this reason.

The stability temperature is another challenge. As ice-like, hydrates will melt and loose its “guest molecules” at temperatures not very much above 273 K. To raise this level, the pressure must be increased. As snow, hydrate at high pressure tends to form solid plugs (cf. the initial problem leading to the study of gas hydrates) that will block the transporting pipes.

Experiments with transportation of hydrates have been carried out at NTNU and SINTEF (42, 43). Pipe dimensions used were selected from oil production standards, and this means diameters in the range of decimetres to meters. In the fuel systems available for combustion engines today the diameters lay in the millimetre to centimetre range. This means that the friction will be of another magnitude than in the test pipes in the studies mentioned above. Smaller pipe diameter most likely will make the plugging problem even worse.

If the concept of storing light VOC in hydrates is to be implemented onboard a shuttle tanker, a question of where to store the hydrate will arise. However, this question and how the system for making the hydrate is made are not a part of this study.

When utilising the energy of light VOC stored in hydrates, different methods can be considered:

Method I: Melt the hydrate at a controlled rate and:

a. use the freed gas at low pressure in the diesel engines (according to method 3 in section 2.4 - the «Dual Fuel Diesel Process»)
b. use the freed gas at high pressure in the diesel engines (according to method 4 in section 2.4 - the «Gas Diesel Process»)

c. use the freed gas in the incinerators and other equipment with continuous combustion.

Method II: Make slurry of the hydrate with oil at low temperature and high pressure and use the slurry as fuel in the diesel engines.

Method I will not introduce any new problems into the combustion part. Method Ib is identical with the way the main part of the experiments has been performed (Diffusion combustion of VOC Fuel reported in Chapter 6) and method Ia is used in the homogenous combustion tests (Homogenous combustion of VOC/air charge reported in Chapter 7). To take advantage of method II, investigations must be carried out on how the slurry will perform when it is pumped at high pressure as well as how the combustion will be.

8.5 Simple test results

Combustion of light VOC (methane and ethane) according to Method Ia is referred to previously. Therefore only additional combustion tests of methane according to method Ib have been carried out in the DyFo and are referred to here. In Figure 8.7 (cylinder pressure and needle lift curves) and Figure 8.8 (Schlieren images) a comparison of methane and propane as the injected VOC Fuel (compressed to 400 bars at a temperature of ~20 °C) is shown with only pilot fuel as a reference.

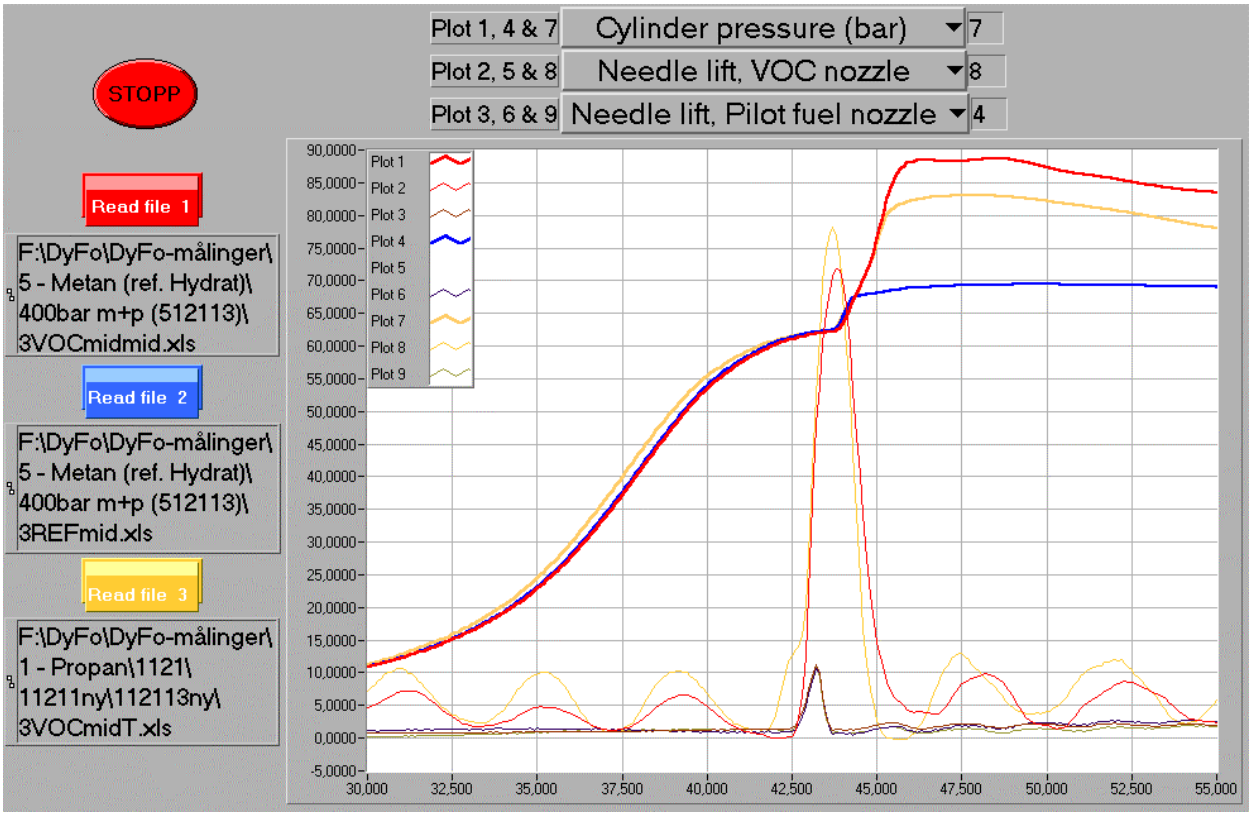

Figure 8.7 Cylinder pressure and injection nozzle needle lift (pilot fuel and VOC Fuel) when injecting methane and propane at 400 bars at room temperature (~20 °C).

There is no significant difference between the two gases injected as VOC Fuel. In Figure 8.7 it is seen that both the ignition delay and the pressure gradient in the first millisecond after ignition

are rather similar. The difference in maximum pressure is due to different injected amount of fuel (the metering system is not more accurate than giving a STD of 7%). The ignition delay similarity is confirmed in Figure 8.8 showing the moment of ignition to occur 2,2 - 2,3 milliseconds after the "start of injection" control signal, meaning that the ignition delay is about 1,0 ms (cf. Figures 3.5 & 3.6).

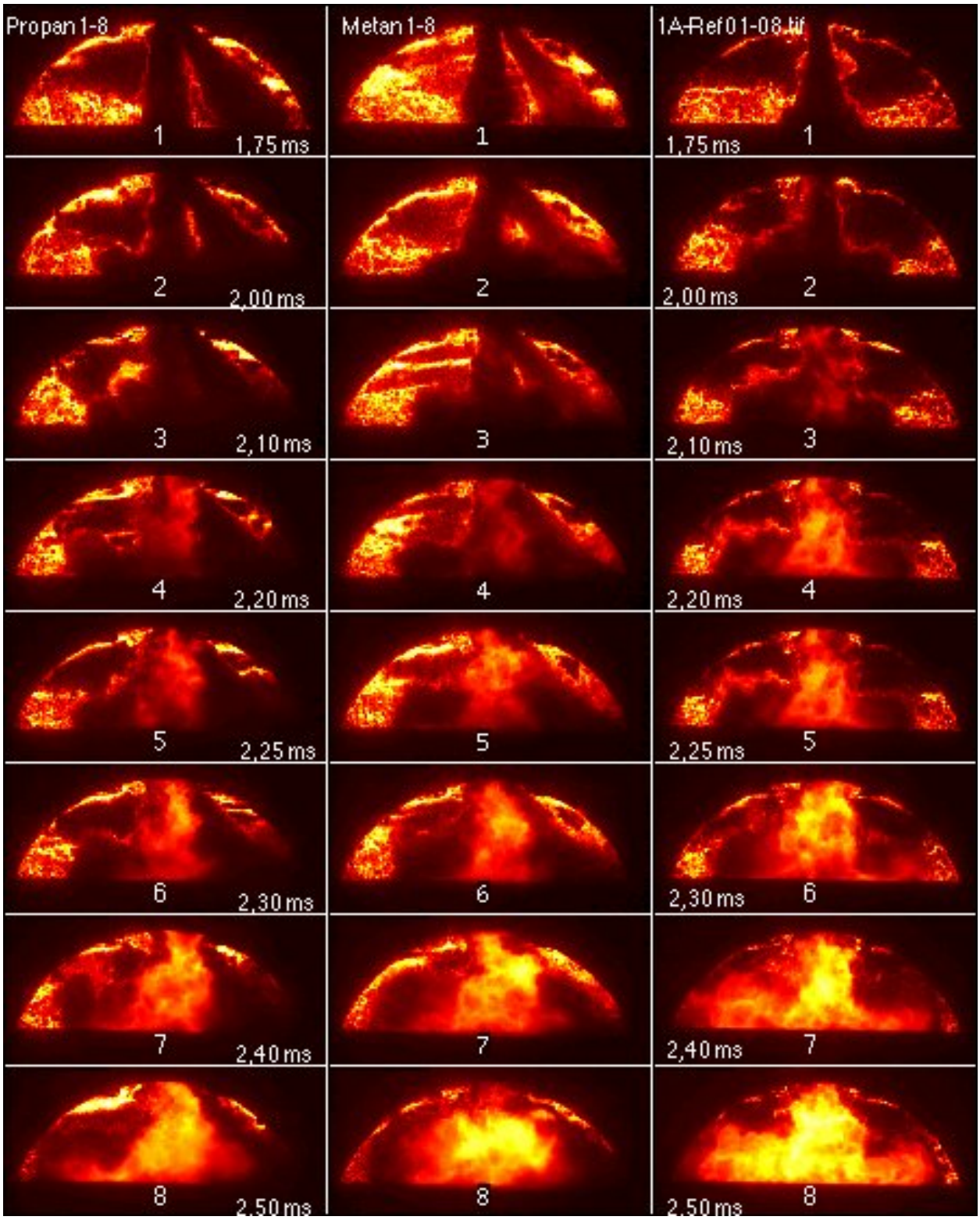

Propane **Methane** **Pilot diesel fuel**

Figure 8.8 *Images of injection and ignition of VOC Fuel + pilot fuel and only pilot fuel. In column 1 the VOC Fuel is propane, in column 2 it is methane.*

8.6 Use and combustion of fuel oil/hydrate slurry

For good combustion of a slurry-like fuel with water present, an upper limit to the water content will arise. The water will lower the combustion temperature, but too much water will give too low temperature for a complete combustion with low exhaust emissions.

However, water in emulsion with fuel oil is actually used in diesel engines today to reduce the NO_x emission. Tests have been successfully carried out with medium speed engines run on an emulsion of 27 - 31 % water in Orinoco Belt bitumen, trade marked as Orimulsion (50). The water/fuel ratio is often limited to about 30 % (on a mass basis), but this is not an absolute limit and emulsions with 50 % water/fuel ratio have been in successful use by others (44).

30 wt% water in the fuel oil/hydrate slurry means less than 3,75 wt% gas. If 50 % water can be used, about 5 % gas will be captured in the slurry (with realistic gas filling of the hydrate cages). In the first moment this seems to be far too little to pay for the extra equipment needed to handle the fuel/hydrate slurry. However, if additional benefits - such as reduced exhaust emissions - is obtained, the investment can turn out to be interesting.

The energy consumption on a shuttle tanker like “Navion Viking” is great, and the light VOC fraction is 20 – 25 % of the total VOC emitted during loading at the Statfjord oil field. In other oil fields this fraction can be more than 60 %. To see how the available Light VOC gas amount at the Statfjord oil field can contribute to the energy delivery for the diesel engines, a calculated example for “Navion Viking” is shown in Table 8.3 below. With 5 % gas in the fuel oil/hydrate emulsion, this engine load will give a total gas consumption of about 284 Sm^3/h. The total available Light VOC gas amount when the loading is finished is around 30000 Sm^3. With the above mentioned engine loads, the gas will last for some 106 hours (= 4 days and 10 hours).

Table 8.3 Energy consumption example for “Navion Viking”.

	Main engines	Auxiliary engines
Installed power (kW)	2 x 12000	4 x 3080
Power in normal operation (kW)	19000	7200
Efficiency at 80% load	0,50	0,46
Energy consumption (MJ/s)	38,0	15,652
5 % residual VOC in slurry (MJ/s)	1,9	0,782
Total gas consumption (Sm^3/h)	284	
Possible total gas operation time (h)	106	

9 Conclusions and future work.

Conclusions

The main purpose of this investigation has been to study the combustion of higher alkanes emitted from crude oil handling when loading shuttle tankers in the North Sea. The primary objective was to verify whether or not the concept of pilot fuel ignition of higher alkanes condensed and injected as liquid "VOC Fuel" can make it possible to utilise these hydrocarbons as fuel in Diesel engines.

As a main conclusion it can be stated that the use of VOC Fuel with pilot ignition by diesel oil is a feasible way of utilising the energy resources otherwise lost by venting the VOC to the atmosphere when loading crude oil into shuttle tankers.

The different components of the "VOC Fuel" have different ignition properties. In separate tests, the ignition and combustion of pure VOC Fuel components (Propane, iso-Butane and n-Butane) and a blend of components (60% Propane, 10% iso-Butane and 30% n-Butane) have been tested. The ignition delay is reduced as the length of the fuel molecule increases. For components other than Propane, the stability of ignition is high, i.e. there is little variation in registered ignition delay from test to test. At moderate to high loads it is not likely that VOC Fuel with no or little Propane will give problems even if the pilot fuel injection should fail.

When it comes to pilot ignition of different VOC components, no significant differences have been discovered in the ignition delay or other important aspects of the combustion process. The test conditions in the DyFo test rig represent low engine load. When no problems have been exposed at these conditions, where the compression temperature is low to moderate, it should be problem free to use the concept of pilot ignition of VOC Fuel at moderate and high engine loads. The results from the tests in the DyFo test rig should even imply that variable VOC Fuel composition not will give any problems regarding ignition delay and ignition stability. The engine power will, however, vary as a function of the energy content in the various VOC Fuel compositions.

The study of the different parameters has not unveiled any surprises regarding the ignition or early combustion of the different VOC Fuels tested according to the concept of pilot ignition in the DyFo.

These conclusions are mainly based on the analysis of the dynamic signals from the pressure sensor giving us the cylinder pressure curves. Where found appropriate, Schlieren images have been included in the discussion. However, the use of Schlieren images have been found to be more complicated when dealing with compression ignition and combustion according to the Diesel process than when studying spark ignition and combustion according to the Otto process.

Future work

The study presented in this thesis is the first study carried out on the DyFo test rig with diffusion combustion in focus. During the test period new knowledge of the test rig operation have been obtained, and other interesting aspects (than those planned to study) of diffusion combustion of both diesel fuel and VOC Fuels - and the visualisation of it - have come to the knowledge of the team of Combustion Engines at the Department of Marine Engineering.

A lot of tedious and time-consuming faults and technical problems have reduced the progress during the test period. The financial status has restricted the possibilities to extend the test work to study any new aspects of the diffusion combustion and the visualisation method.

A better way to obtain good interpretation of the images from the visualisation of the ignition and combustion of both the pilot fuel and the VOC Fuel is a very interesting part of any future work. This part of the work is of a character that most engine engineers know too little about.

The DyFo test rig is well suited for screening tests with different fuels, existing types, pure hydrocarbon components and new, alternative fuels and compositions. During the test work some interesting aspect regarding fuel composition were found occasionally. Further tests to study these findings should be carried out in the future.

Bibliography

(1) John Johnston: "E-094: Technologies for VOC Recovery and Abatement ", Business Communications Company Inc., Connecticut at http://www.buscom.com/waste

(2) "Utilisation of VOC in Shuttle Tankers and Crude oil Tankers". MAN B&W Diesel A/S 1997

(3) "VOC recovery at M/T "Polyviking". Design Basis and Functional Specifications". F&UNED97271/VOC0003 (M/T "Polyviking" is later renamed "Navion Viking").

(4) "Trials commence for VOC recovery system". Article at www.communityedi2000.co.uk/www-hamworthykse/www/voc.html

(5) "Volatile organic compounds in oil tankers to be used for propulsion" Alexander's Gas & Oil Connections. Volume 3, issue #12, 17.04.1998. Article at www.gasandoil.com/goc/reports/rex81660.htm

(6) T. Fukada, M. Ohtsu, M. Hanafusa, P. Sunn Pedersen, O. Grøne and O. Schohr: "Development of the World's First Large-Bore Gas-Injection Engine", 21st CIMAC Conf., Interlaken 1995.

(7) K. K. Sirkar, S. Majumdar, B. Shivashankar: "Recovery of Evaporative Fuel Losses by Vapour Permeation Membranes", Department of Chemical Eng., Chemistry and Environmental Science, New Jersey Institute of Technology, 1997 at http://www.hscr.org/.

(8) K. K. Sirkar, I, Abou-Nemeh, S. Chandra, A. Saraf: "Removal of VOCs from Contaminated Groundwater and Soils by Pervaporation", Department of Chemical Eng., Chemistry and Environmental Science, New Jersey Institute of Technology, 1997 at http://www.hscr.org/.

(9) Ola Ruch, Terje Berg: "Norway's VOC-project for Buoy-loading Crude Oil Carriers. Conceptual Description and Experiences from Two Full-scale Prototype Installations". The 8th ICMES/SNAME New York Metropolitan Section Symposium, New York, May 22- 23 2000.

(10) Peter Sunn Pedersen, Ola Ruch, Knut Brødreskift: "Recovery of Volatile Organic Compounds (VOC) on Shuttle Tankers and Experience by Utilising VOCs as Clean Engine Fuels". 23rd CIMAC conference, Hamburg, May 7 – 10 2001.

(11) Statistics Norway (Statistisk Sentralbyrå) www.ssb.no/luft/f_vocts.shtml

(12) K. Flugsrud, E. Gjerald, G. Haakonsen, S. Holtskog, M. Høie, K. Rypdal, B. Tornsjø and F. Weidemann: "The Norwegian Emission Inventory". SSB/SFT, 2000, ISBN 82-537-4770-5

(13) "Vapour from Crude oil loading used as Propellant and Fuel. Conceptual Process Design – Status by 15.12.96". (In Norwegian). Statoil R&D. NED 96246. Confidential report.

(14) Øyvin Melhus and Terje Almås: "VOC for Power Generation". Internal report to Statoil R&D. The Norwegian University of Science and Technology (NTNU), Department of Marine Engineering, 1998.

(15) T. E. Daubert, R. P. Danner: "Physical and thermodynamic properties of pure chemicals. Data compilation". Dep. of Chemical Engineering, The Pennsylvania State University, 1992

(16) Halvard Paulsen: "A Study of Transient Jet and Spray using a Schlieren Method and Digital Image Processing" Dr.ing. thesis. University of Trondheim, Norwegian Institute of Technology (NTH), Division of Marine Engineering, 1995

(17) John B. Heywood: "Internal Combustion Engine Fundamentals". 1988 ISBN 0-07-100499-8

(18) H. Hiroyashi, T. Kadota and M. Arai: "Supplementary comments: Fuel spray characterization in diesel engines". Hiroshima University. In *Combustion Modelling in Reciprocating Diesel Engines* pp. 369-408 Plenum Press., 1980

(19) Vilmar Æsøy: "Hot surface assisted compression ignition in a direct injected natural gas engine" Dr.ing. thesis. University of Trondheim, Norwegian Institute of Technology (NTH), Division of Marine Engineering, 1996

(20) Irvin Glassman: "Combustion". Department of Mechanical and Aerospace Engineering, Princeton University, 1987 ISBN 0-12-285851-4

(21) Kenneth K. Kuo: "Principles of Combustion". John Wiley & Sons, 1986 ISBN 0-471-62605-8

(22) D. Lee and S. Hochgreb: "Rapid Compression Machines: Heat Transfer and Suppression of Corner Vortex". Dep. of Mech. Eng., MIT. *Combustion and Flame* 114:531-545 (1998)

(23) C. Mohammed: "Suppression of Reaction during Rapid Compression and its Effect on Ignition Delay". School of Chemistry, University of Leeds. *Combustion and Flame* 112:438-444 (1998)

(24) Tor Bjørge, N. I. Lilleheie, S. Byggstøyl and B. Grimsmo: "A Survey of Modelling Principles of Autoignition with Special Emphasis on Diesel Ignition". Marintek-report 222101.00.01.93 (MT22-F93-0031) to ESSO & NTNF, 1993.

(25) John McMurry: "Organic Chemistry" Brooks/Cole Publishing Company, Pacific Grove, California, 1992, ISBN 0-534-16218-5

(26) D. W. Holder and R. J. North: "Schlieren Methods". Notes on Applied Science no. 31, National Physical Laboratory, Teddington, Middlesex, United Kingdom, 1963.

(27) Eastman Kodak Company: "Schlieren Photography", 1960

(28) Thomas Woodlief jr.: "SPSE Handbook of Photographic Science and Engineering" Chapter 20.7, A Wiley-Interscience Publication, John Wiley & Sons, 1967(?)

(29) Tor Øyvind Ask: “Ignition and Flame Growth in Lean Gas-Air Mixtures. An Experimental Study with a Schlieren System”. Dr.ing thesis. University of Trondheim, Norwegian Institute of Technology (NTH), Division of Marine Engineering, 1992.

(30) Marie Bysveen: "Visualisation in Two Directions on a Dynamic Combustion Rig for Studies of Fuel Quality". Dr.ing. thesis. Norwegian University of Science and Technology (NTNU), Division of Marine Engineering, 1999.

(31) "DIS Injection System for STATOIL. Operating Instructions and Injector's Test Results". Ganser-Hydromag AG, Zurich, January 1997

(32) "DIGIVALVE. Digital switching. High performance industrial servo valve designed for microprocessor control". Data sheet no. 861125/E. B&R Engineering B.V. Rotterdam, The Netherlands, 1989.

(33) Bjarte Lund: "Pilottenning av VOC/inertgassblandinger i DyFo" M.Sc. thesis (in Norwegian), Norwegian University of Science and Technology (NTNU), Division of Marine Engineering, 1999.

(34) E. Dendy Sloan Jr., "Clathrate Hydrates of Natural Gases". Colorado School of Mines, Golden, Colorado. ISBN 0-8247-9937-2

(35) Torstein Austvik: "Hydrate formation an behaviour in pipes". Dr.ing. thesis, University of Trondheim, Norwegian Institute of Technology (NTH), 1992.

(36) L. Gjertsen, T. Austvik and O. Urdahl: "Hydrate plugging in underinhibited systems", in Proc. 2nd Intnl. Conf. on Natural Gas Hydrates, p. 155, (Monfort, J.P., ed.) Toulouse 2-6 June 1996.

(37) A. Lund: "The influence from gas-gas interactions on the stability of gas hydrates". Dr.ing. thesis, University of Trondheim, Norwegian Institute of Technology (NTH), 1990.

(38) David Lysne: "An experimental study of hydrate plug dissociation by pressure reduction". Dr.ing. thesis, University of Trondheim, Norwegian Institute of Technology (NTH), 1995.

(39) J. S. Gudmundsson, F. Hveding, A. Børrehaug: "Transport of Natural Gas as frozen Hydrate", in Proc. 5th International Offshore and Polar Engineering Conf., The Hague, The Netherlands June 11 – 16, 1995.

(40) J. S. Gudmundsson, NTNU, Trondheim and A. Børrehaug, Aker Engineering, Oslo: "Natural Gas Hydrates an Alternative to Liquefied Natural Gas", 1996

(41) J. S. Gudmundsson, Vibeke Anderson, O. I. Levik and M. Parlaktuna: "Hydrates Concept for Capturing Associated Gas" SPE 50598 European Petroleum Conf., The Hague, The Netherlands October 20 – 22, 1998.

(42) Vibeke Anderson, NTNU. Personal communication, 1999.

(43) Morten Aarvåg: "Studie av Transportegenskaper til Granulært Hydrat ved Hjelp av Olga". M.Sc. thesis (in Norwegian), University of Trondheim, Norwegian Institute of Technology (NTH), Division of "Kuldeteknikk", 1994.

(44) Magnus Småvik, AS Motorconsult. Personal communications, 2001.

(45) P. M. Einang, S. Koren, R. Kvamsdal, T. Hansen and A. Sarsten: "High-pressure, Digitally Controlled Injection of Gaseous Fuel in a Diesel Engine, with Special Reference to Boil-off from LNG Tankers" 15th CIMAC Conference, Paris, June 1983

(46) P. M. Einang, L. Kolle and H. Valland: " Gas Engines, Environmental and Technical Challenges". SPUNG Seminar, Oslo, October 2 - 3, 1990.

(47) T. Kamimoto and H. Kobayashi: "Combustion Processes in Diesel Engines". Prog. Energy Combust. Sci. 1991 Vol. 17. pp. 163 - 189.

(48) Fredrik Weidemann, Norwegian State Pollution Agency (SFT), Oslo. Personal communications, 2001.

(49) Peter Sunn Pedersen, MAN B&W, Copenhagen, Denmark. Personal commmunications, 2000

(50) G. Besio and M. Nobile: "A Challenging Fuel for Diesel engines: Orimulsion®. From the Concept to the Application". 23rd CIMAC conference, Hamburg, May 7 – 10, 2001.

(51) Ola Ruch, Statoil FoU, Trondheim. Personal communications, 2001.

(52) National Institute of Health (NIH): "NIH Image - Users Manual". Research Services Brand (RSB), National Institute of Mental Health (NIMH), Maryland, 1996.

(53) Gary Johnson: "LabVIEW Graphical Programming" ISBN 007032915X. More literature: http://www.ni.com/devzone/reference/books/labview.htm#lvapt

(54) "Gas and dual-fuel engines from MAN B&W – economic, reliable and ecologically compatible". MAN B&W Diesel A/S (Sales brochure)

(55) Marie Bysveen, T. Almås, T. Hansen and O. Ruch: "development of a hydraulic, dynamic combustion rig for visualisation in two directions by the use of the Schlieren technique". IMechE Combustion engines and hybrid vehicles, London 1998

(56) Marie Bysveen, T. Almås, T. Hansen, S. I. Lien and F. Kvinge: "3 dimensional visualisation og ignition and early flame development of low quality gas blends in a hydraulic, dynamic combustion rig using visualisation in two directions". SAE paper 982591, 1998

Appendix 1 Temperature at the end of compression in the DyFo.

During operation, the charge air in the DyFo undergoes polytropic compression:

$$p_1 V_1^{\,n} = p_2 V_2^{\,n} \qquad \text{(A.1)}$$

The working medium (charge air) is treated as an ideal gas, and therefore:

$$pV = mRT \qquad \text{(A.2)}$$

The compression ratio ε is defined as: $\varepsilon = V_1/V_2$ (A.3)

This gives: $p_2/p_1 = \varepsilon^{\,n} \quad \Rightarrow \quad n = (\ln p_2 - \ln p_1)/\ln \varepsilon$ (A.4)

By substituting V in formula A.1 by using A.2, the end compression temperature can be found. The mass m is unknown, but considered constant in the process ($m = m_2 = m_1$)

$$p_1 V_1^{\,n} = p_2 V_2^{\,n} \Rightarrow p_2 = p_1 \,(m_1 R\, T_1\, p_2 / m_2 R\, T_2\, p_1)^{\,n}$$

$$p_2^{\,1-n} = p_1^{\,1-n} (T_1 / T_2)^{\,n} \quad \Rightarrow \; \underline{T_2} = T_1 \,(p_2/p_1)^{\,n-1/n} = \underline{T_1\, \varepsilon^{\,n-1}}$$

The heat loss in the DyFo is considerable but unknown and therefore the polytropic coefficient *n* is also unknown. The volumes, however, are known and by measurement of pressures during the compression process, the table A1.1 below can be created.

To get an idea of the magnitude of the internal heat loss during compression, the adiabatic conditions after compression can also be calculated. The same formulas are used, only now n is the adiabatic coefficient $\gamma = c_p/c_v$. For simplicity both c_p and c_v are assumed constant in this calculation, c_p = 1,005 kJ/kgK and c_v = 0,7718 kJ/kgK, giving a value γ = 1,3997 kJ/kgK.

Table A1.1 Polytropic and adiabatic compression in the DyFo.

	1	2
Pressure at start of compression, p_1 (bar)	2,00	3,05
Pressure at end of compression, p_2 (bar)	45,5	62,8
Volume at start of compression, V_1 (litre)	1,11792	1,11792
Volume at end of compression, V_2 (litre)	0,100	0,100
Temperature at start of compression, T_1 (K)	348	356
Compression ratio, ε	11,1792	11,1792
Polytropic coefficient, n	1,2943	1,2523
Temperature at end of compression, T_2 (K)	708	655
Adiabatic temp. at end of compression, T_{2a} (K)	913	934

This result means that there is a significant heat loss in the cylinder during compression. It is also shown that the heat loss increases with increasing charge air pressure.

In these calculations the only input measured with uncertainty is the start temperature T_1. This value is measured just outside the charge air heat exchanger (reason – only accessible point) and it is possible to read a different temperature than the real one inside the cylinder.

To illustrate how the temperature level develops in the cylinder, Figure A.1.1 shows an example of the calculated cylinder temperature based on the pressure signal.

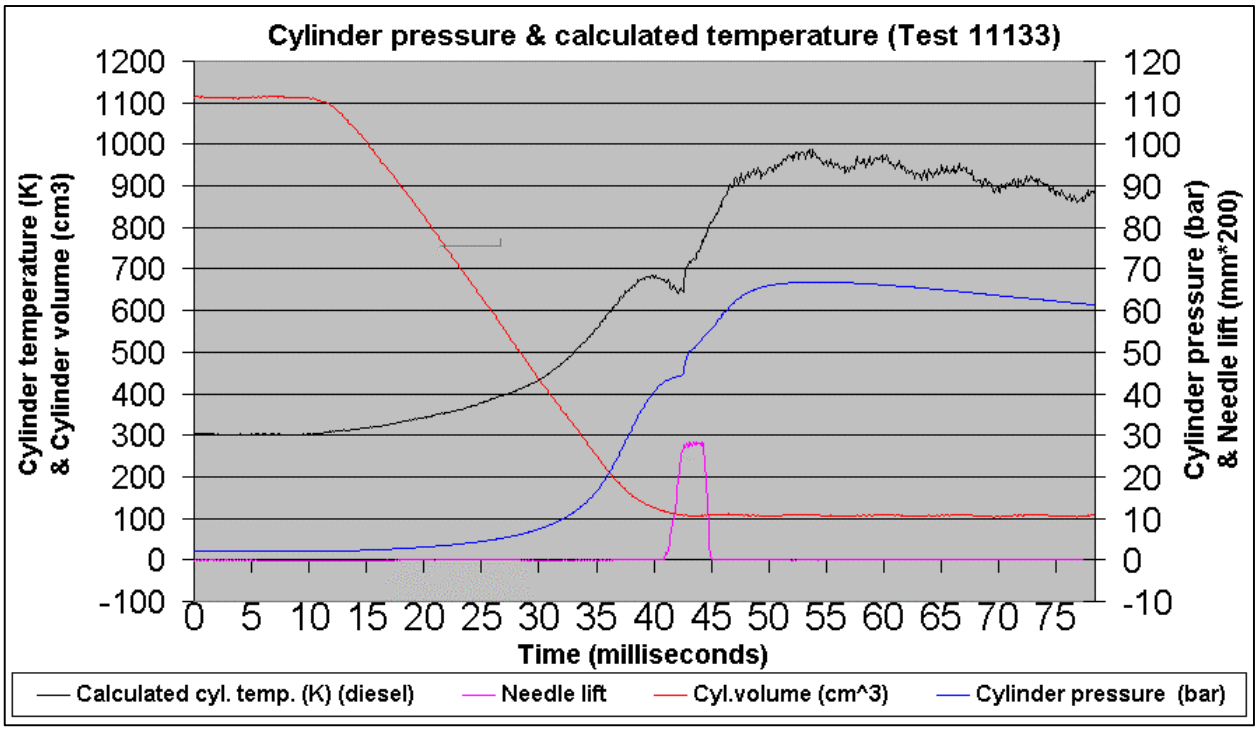

Figure A.1.1 Cylinder pressure and calculated isentropic temperature in the DyFo during test.

As can be seen from the plot, the maximum cylinder temperature occurs ahead of the maximum compression pressure. The calculated temperature is based on no mass loss and registered volumes in addition to the pressure signal from the DyFo during test.

Appendix 2 Main features of the redesigned DyFo.

Originally the DyFo rig was designed for combustion according to the Otto process with spark ignition. For this purpose the compression end temperature is of minor importance. According to normal diesel engine operation, however, the original DyFo construction resulted in a temperature too low leading to an unacceptable long ignition delay (8 – 10 milliseconds). A series of changes were therefore made to increase this temperature and reduce the ignition delay.

First of all the hydraulic oil flow moving the piston was increased by a factor of approximately 16 – from 63 l/s to above 1000 l/s by adding a second, big servo valve to the rig. The mean piston speed increased from approximately 1 m/s to about 7 m/s. Thus the heat loss through the cylinder walls (the cylinder liner, the cylinder head and the piston surface above the piston rings) as well as loss of charge air mass through the piston rings were reduced.

Second the cooling water temperature in the cylinder head and cylinder liner was increased from about 80 °C to about 120 °C (at a pressure slightly above atmospheric). By this action the heat transfer through the cylinder liner and head is further reduced (ΔT through the cylinder wall and head is reduced) during combustion.

The original mechanical design of the DyFo construction for spark ignition combustion is shown in Figure A2.1.

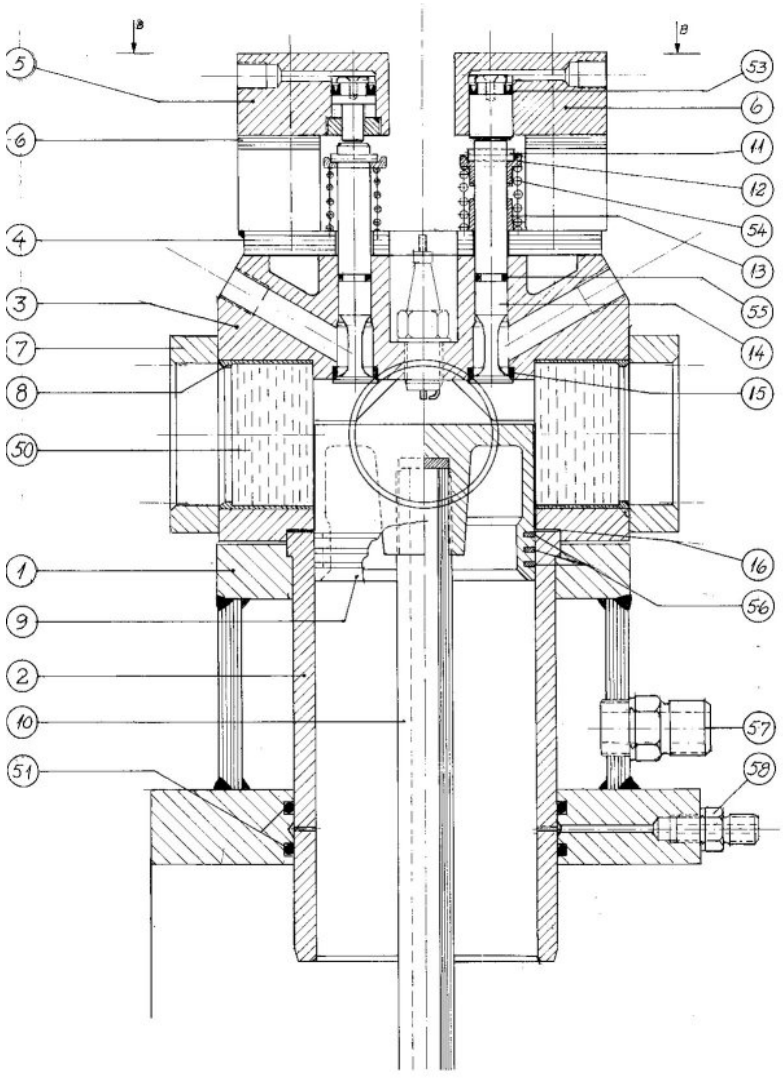

Figure A2.1 Original design of the DyFo construction.

For compression ignition the design has been modified in many details:

Redesign of cylinder cover:
- Combustion chamber design
- Position of inlet and outlet valves
- Position of injectors for pilot diesel and VOC

Redesign of piston:
- Position and number of piston rings

Redesign of cooling water system:
- Pressurized tank to give temperatures above 100 °C.
- Level switch in tank to cut current if water level too low.
- Insulating external cooling water tubes to reduce heat loss.

Redesign of charge air inlet system:
- Installation of water-to-air heat exchanger
- Pressurized water tank to give water temperatures above 100 °C (for giving charge air temperatures up to 100 °C).
- Level switch in water tank to cut current if water level too low.
- Insulation of the system.

Figure A2.2 shows the new cylinder head of the DyFo.

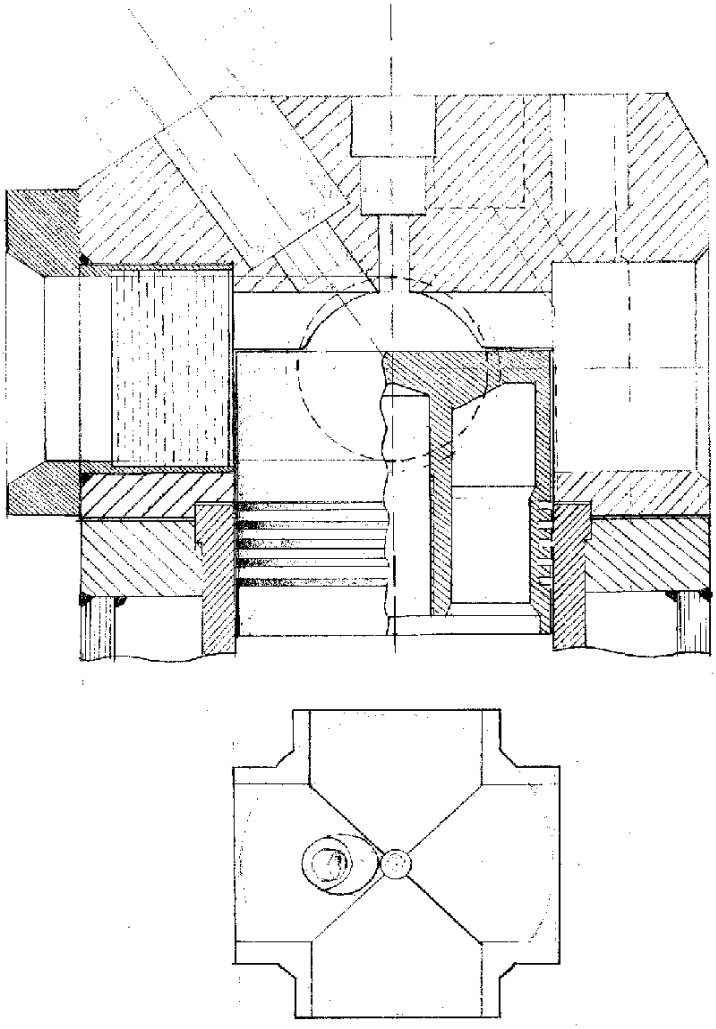

Figure A2.2 New cylinder head of the DyFo.

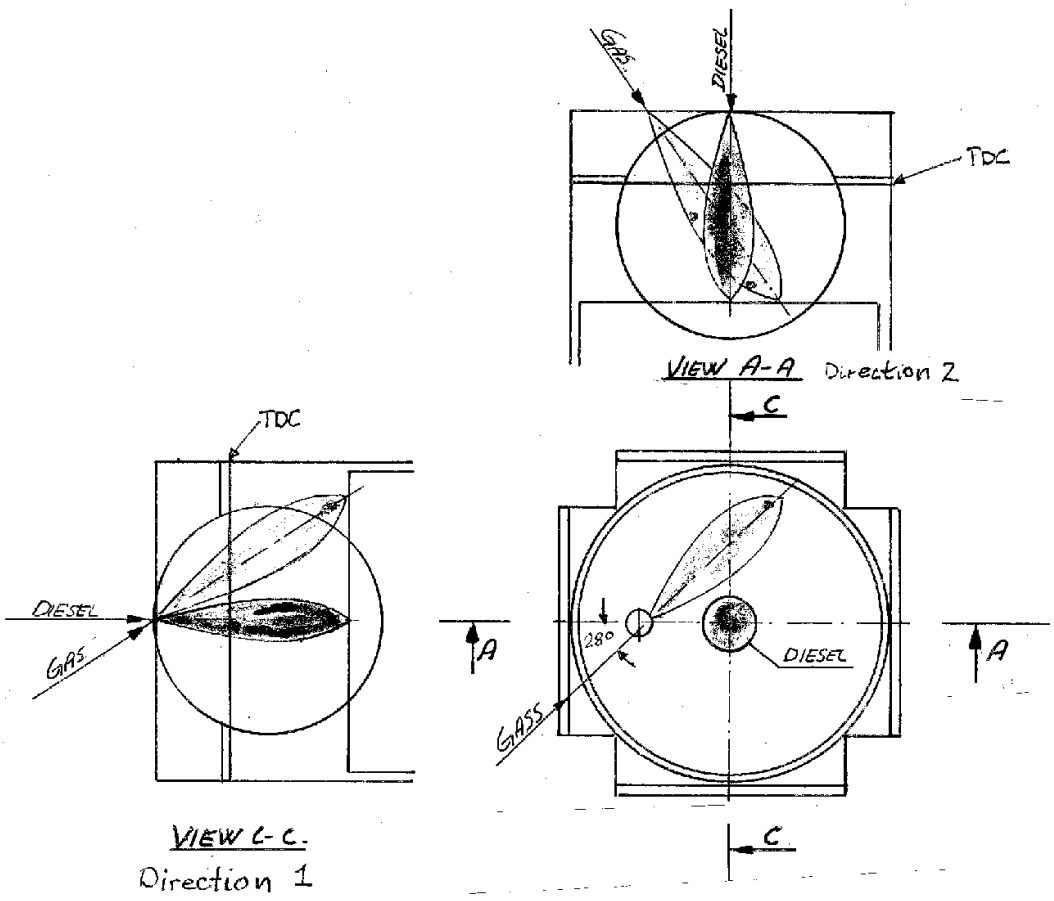

Figure A2.3 Injection scheme in the new cylinder head design of the DyFo.

Instrumentation

Piston position:
- Sensor: Hottinger Baldwin Messtechnik (HBM), WSF LVDT displacement transducer, standard version
- Amplifier: HBM TF-Messverstärker MCA 5101

Cylinder pressure:
- Sensor: Kistler 6053
- Amplifier: Kistler 5011

Needle lift, pilot fuel:
- Sensor: Micro-epsilon Messtechnik, Hall Effect transmitter
- Amplifier: Micro-epsilon Messtechnik, Multi NCDT Series 300; DT 321SM

Needle lift, VOC-HC fuel:
- Sensor: Autronica prototype
- Amplifier: Autronica type 6HA4

Charge air pressure:
- Sensor: Danfoss MBS 33-1621-1AB08, 060G3039
- Amplifier: Metric M1-40

Appendix 3 Test plan for VOC Fuel tests in the DyFo rig.

Table A3.1 shows the different values of the main operating parameters – charge air pressure, charge air temperature, pilot fuel mass and VOC Fuel mass - found by calibration of the fuel nozzles.

Table A3.1 Nominal fuel and charge air conditions in the test series.

Fuel condition (FC)	1	2	3	4
* Nom. Pilot fuel mass (mg)	7,6	7,6	21,7	21,7
* Nom. VOC Fuel mass (mg)	26,2	78,5	26,2	78,5
Charge air condition (CAC)	1	2	3	4
* Pressure (bar)	2,0	2,0	3,0	3,0
* Temperature (° C)	30	75	30	75

The following test scheme was prepared for the «Condensate Diesel Process» tests with propane as the VOC Fuel:

- Charge air temperature LOW vs. HIGH (Test series 1**1**xxx vs. 1**2**xxx)
- Charge air pressure LOW vs. HIGH (Test series 1x**1**xx vs. 1x**2**xx)
- Pilot fuel mass LOW vs. HIGH (Test series 1xx**1**x vs. 1xx**2**x)
- VOC Fuel mass LOW vs. HIGH (Test series 1xxx**1** vs. 1xxx**2**)
- VOC Fuel relative to pilot fuel injection (Test series 1xxxx**1** – 1xxxx**5**)

To make the test work as time efficient as possible to perform (of a total of 80), only one check of each of the 4 first comparisons were made. Table A3.2 shows the test series selected for testing. Corrected values of excess air ratios λ are listed.

Table A3.2 Comparable tests selected from the matrix of test series.

	LOW		HIGH	
	Test series	Corrected λ	Test series	Corrected λ
Charge air temperature	1**1**1113ny	5,78	1**2**1113ny	5,03
	1**1**211*1* 1**1**211*2* 1**1**211*3* 1**1**211*4* 1**1**211*5*	8,67	1**2**211*1* 1**2**211*2* 1**2**211*3* 1**2**211*4* 1**2**211*5*	7,55
Charge air pressure	11**1**113ny	5,78	11**2**113ny	8,67
Pilot fuel amount	121**1**1*1* 121**1**1*2* 121**1**1*3* 121**1**1*4* 121**1**1*5*	5,03	121**2**1*1* 121**2**1*2* 121**2**1*3* 121**2**1*4* 121**2**1*5*	3,61
VOC Fuel amount	1221**1**3ny	7,55	1221**2**3	2,96

The injection timing of VOC Fuel relative to pilot fuel was varied in 5 equal steps (–1,0 ms, -0,5 ms, 0,0 ms, +0,5 ms and +1,0 ms). The actual tests are shown in Table A3.2 (1xxxx***1*** – 1xxxx***5,*** a total of 20 tests from 4 different test series). Even a fifth test series (12212x) was performed, the main aim being to study the effect of the VOC Fuel amount by comparison with test series 12211x. This test series is not listed in the table because an internal fault in the DyFo test rig made this comparison inaccurate. To study the effect of relative injection timing between the pilot fuel and the VOC Fuel, however, may very well be done and in Appendix 5 the result from test series 12212x is shown.

To study the effect of fuel composition, other VOC Fuel types with n-butane and iso-butane were tested according to the evaluation of the results from the tests carried out with propane as the VOC Fuel.

As can be seen from this overview, the air-fuel ratio varies quite much when only one parameter is changed at a time. This fact is impossible to change – if tests with different values of only one specified parameter at a time are to be performed, the variation in air-fuel ratio must be accepted.

In Section 3.1.2 the effect of test conditions on fuel mass delivery was illustrated. By calibration of the fuel injectors both density and pressure differ from what they are during the experiments. Both fuels (pilot diesel and VOC) expand at operational conditions (~ 120 °C, 400 bar) relative to calibration conditions (~ 20 °C, 400 bar). A standard volumetric expansion factor for petroleum ($\gamma = 92*10^{-5}$ K^{-}) is applied for the pilot diesel. For the different VOC Fuels actual densities are found in diagrams of properties (pressure - enthalpy diagrams with lines of constant specific volume =1/ρ). The nominal temperature difference between calibration and test conditions is 100 K. Table A3.3 shows correction factors applied for the different fuel types used.

Table A3.3 Correction factors due to density for the fuel types used in the tests.
**) Calibration with VOC blend*

	Diesel	Propane	iso-Butane	n-Butane	VOC blend
ρ_f (kg/m^3) 20 °C	815	555,6	606,1	614,7	578,3
$\rho_{f,op}$ (kg/m^3) 120 °C	746,3	481,0	536,0	552,1	507,8
$\rho_{f,cal}$ (kg/m^3) 20 °C	815	578,3*)	578,3*)	578,3*)	578,3
Density factor $\sqrt{\rho_{f,op}/\rho_{f,cal}}$	0,957	0,912	0,963	0,977	0,937

In the experiments two different charge air pressures (CAP's), 2 and 3 bars have been used. The cylinder pressure at the time of injection varies when the charge air pressure varies. It also varies for different injection timing settings as shown in Appendix 4, Table A4.1. When applying these factors, the fuel masses shown in Table A3.4 results.

Table A3.4 Corrected fuel conditions in the test series.

Fuel mass level			LOW		HIGH	
			Mean	STD	Mean	STD
* Calibrated pilot fuel mass (mg)			7,60	0,62	21,70	0,12
Actual pilot fuel mass (mg)		2 bar	6,86	0,56	19,58	0,11
		3 bar	6,71	0,55	19,17	0,11
* Calibrated VOC Fuel mass (mg)			26,20	1,83	78,50	4,84
Actual VOC Fuel mass (mg)	2 bar	Propane	22,47	1,58	67,33	4,20
		iso-Butane	23,73	1,67	71,09	4,44
		n-Butane	24,07	1,69	72,12	4,50
		VOC mix	23,09	1,62	69,17	4,32
	3 bar	Propane	21,93	1,54	65,71	4,10
		iso-Butane	23,16	1,63	69,38	4,33
		n-Butane	23,49	1,65	70,39	4,40
		VOC mix	22,53	1,59	67,51	4,22

Variation of parameters for studying the effect on ignition and early combustion has been selected from the matrix shown below.

M:\DyFo\Avhandling\forsøksplan.flo

20. juni 2000

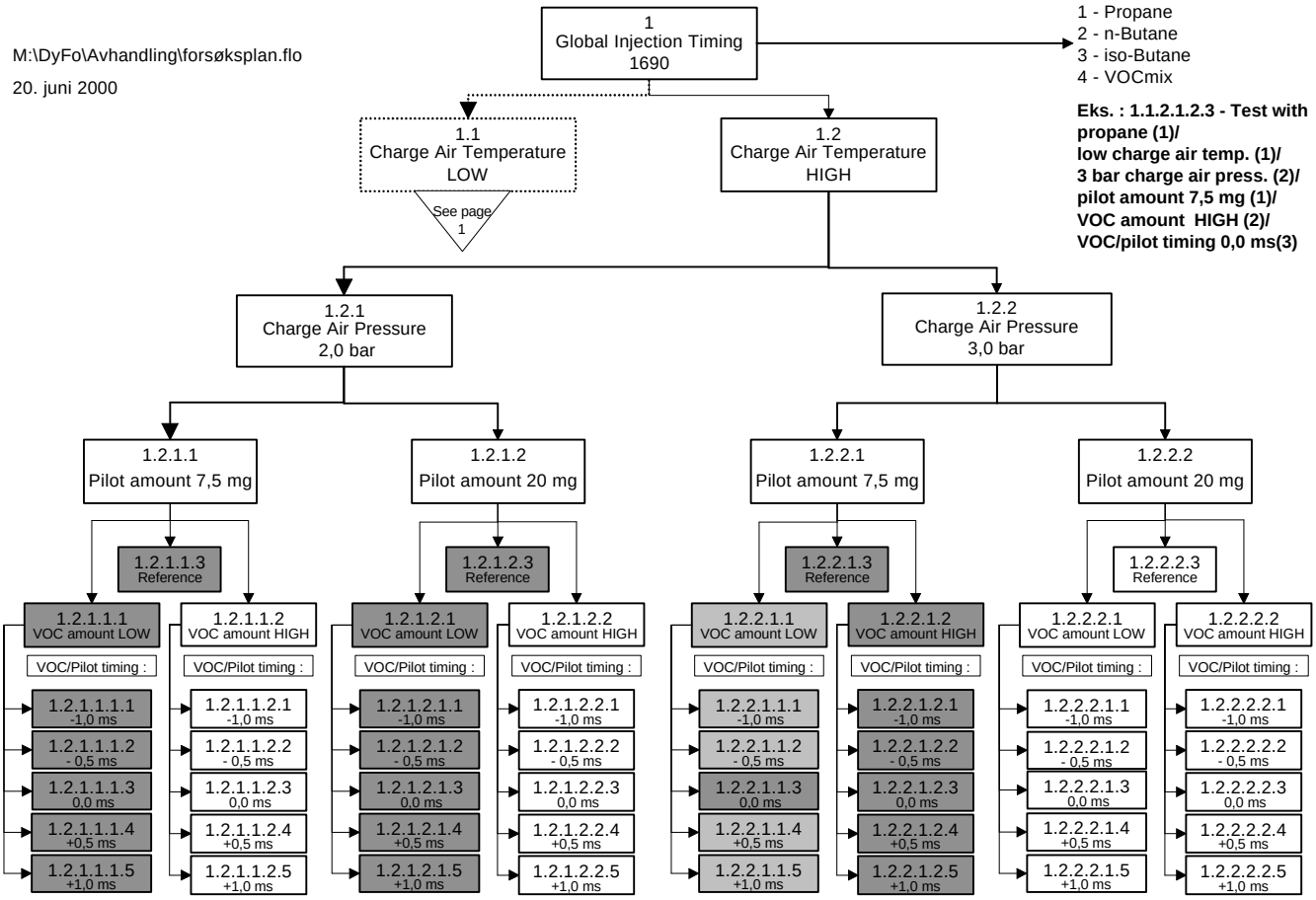

M:\DyFo\Avhandling\forsøksplan.flo

20. juni 2000

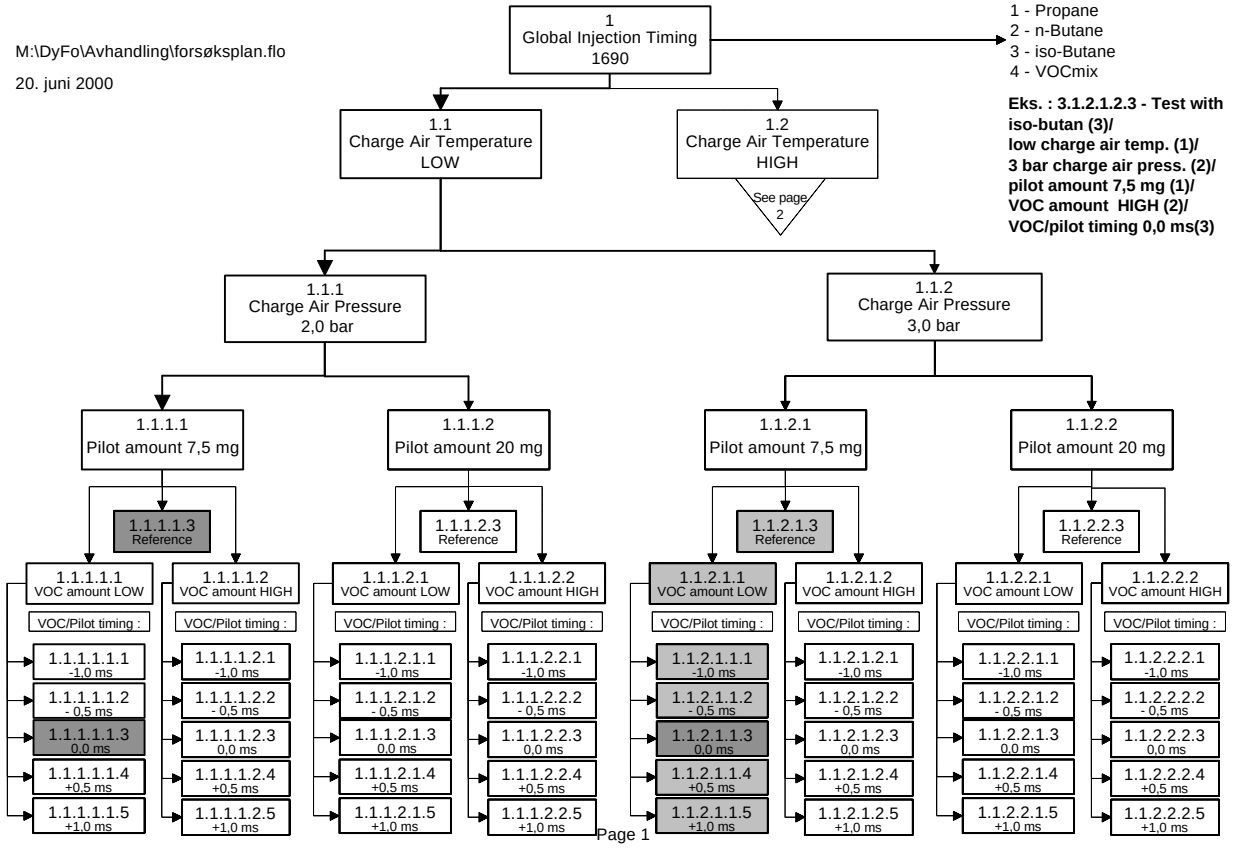

Appendix 4 Cylinder pressure at the instant of VOC injection

In the experiments two different charge air pressures (CAP's), 2 and 3 bars have been used. The cylinder pressure at the time of injection varies when the charge air pressure varies. It also varies for different injection timing settings as shown in Table A4.1.

Table A4.1 Pressure drop across injection nozzles and correction factors due to pressure drop for the fuels used in the tests.

		Diesel	VOC				
VOC/pilot relative injection timing		-	-1,0 ms	- 0,5 ms	0,0 ms	+ 0,5 ms	+ 0,5 ms
Δp, operation (bar)	CAP 2 bar	355	357,5	355	352,5	350	349
	CAP 3 bar	340	343	340	336	332	330
Δp, calibration (bar)		399	399	399	399	399	399
Δp factor $\sqrt{\Delta p_{op}/\Delta p_{cal}}$ (CAP 2 bar)		0,943	0,947	0,943	0,940	0,937	0,935
Δp factor $\sqrt{\Delta p_{op}/\Delta p_{cal}}$ (CAP 3 bar)		0,923	0,927	0,923	0,918	0,912	0,909

The Figures in this Appendix show the cylinder pressure during VOC Fuel injection. They are used to calculate correction factors for the fuel mass delivery in different injection cases carried out in the test series and referred in section 5.1.5.

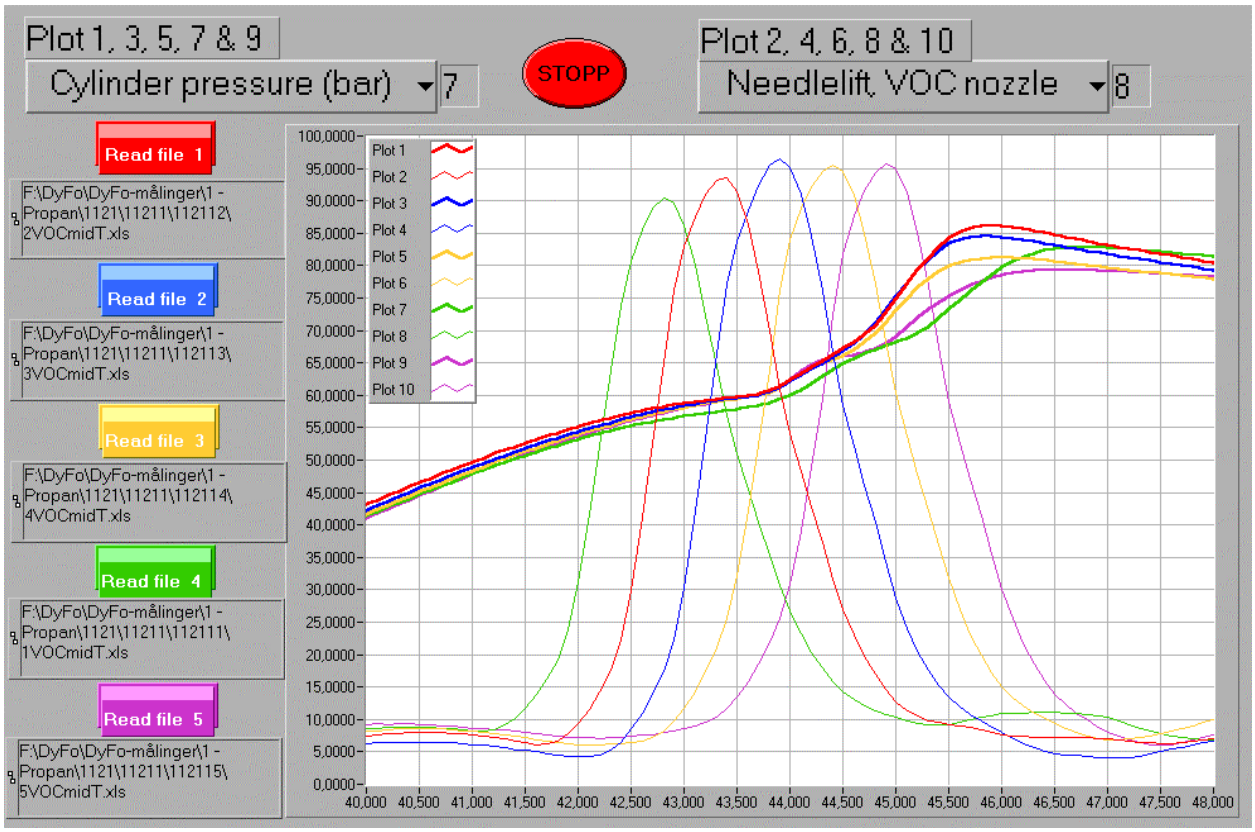

Figure A4.1 Cylinder pressure and VOC Fuel needle lift curves during injection of VOC Fuel in test series 11211.

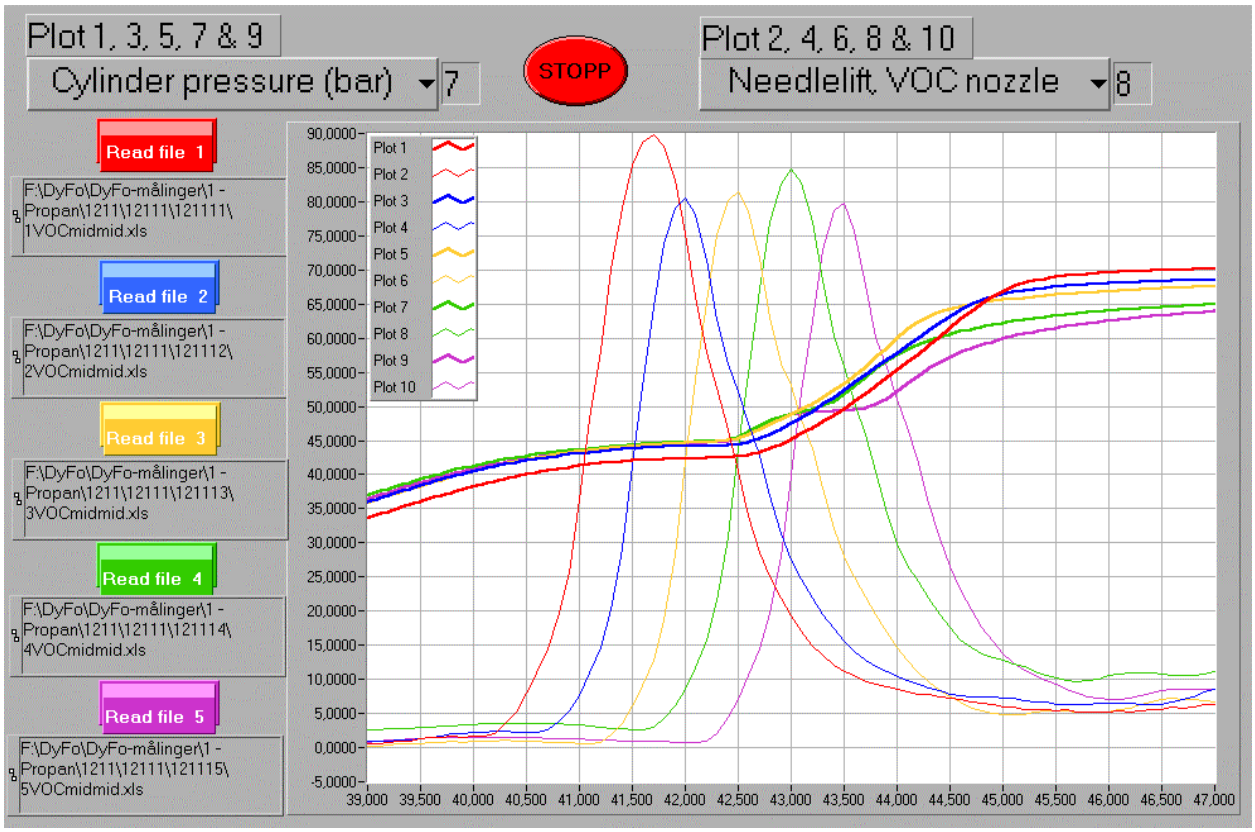

Figure A4.2 Cylinder pressure and VOC Fuel needle lift curves during injection of VOC Fuel in test series 12111.

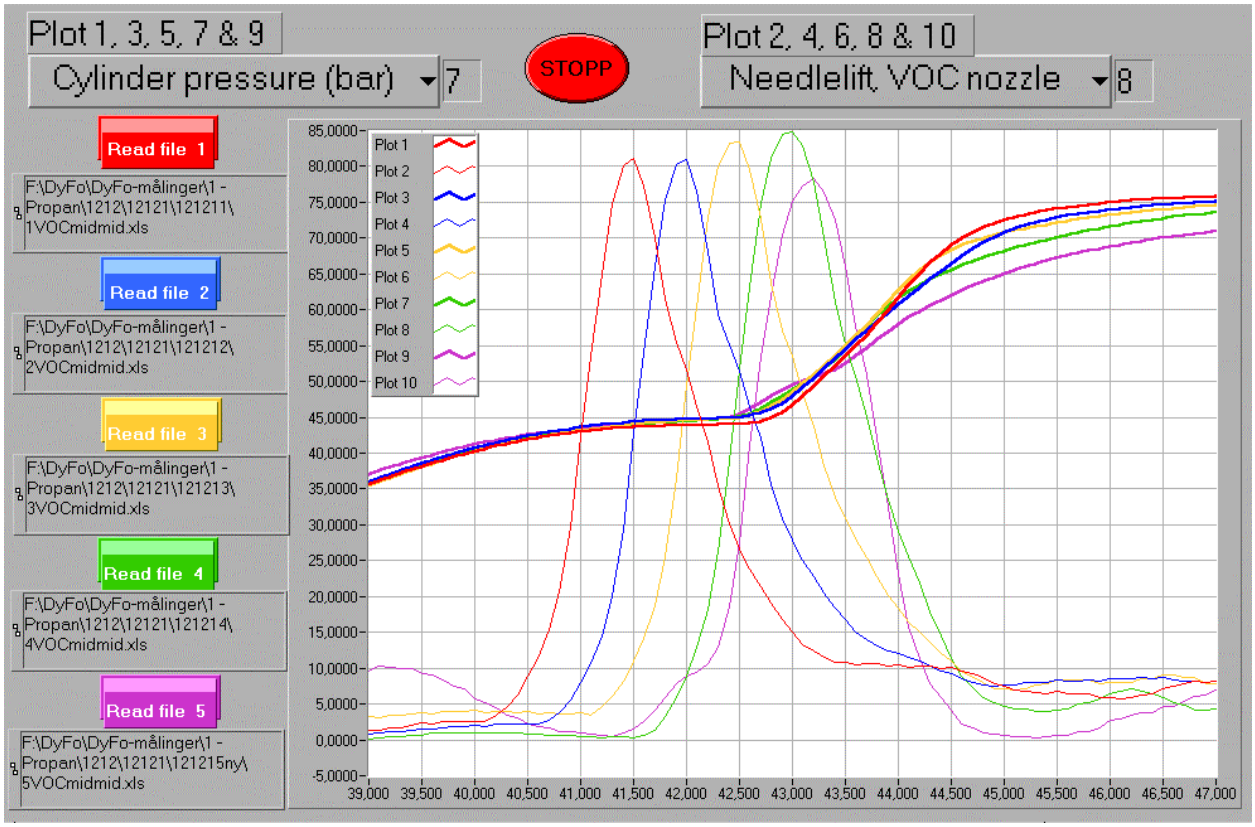

Figure A4.3 Cylinder pressure and VOC Fuel needle lift curves during injection of VOC Fuel in test series 12121.

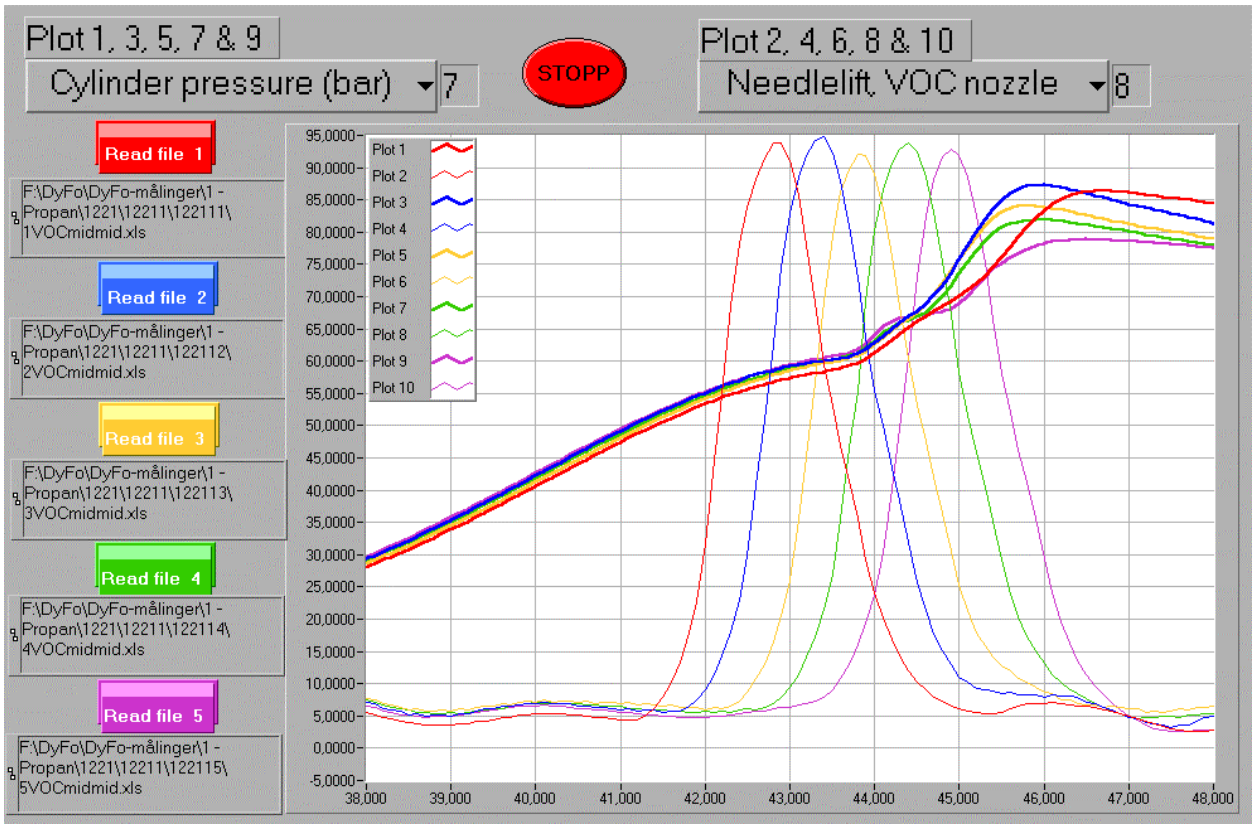

Figure A4.4 Cylinder pressure and VOC Fuel needle lift curves during injection of VOC Fuel in test series 12211.

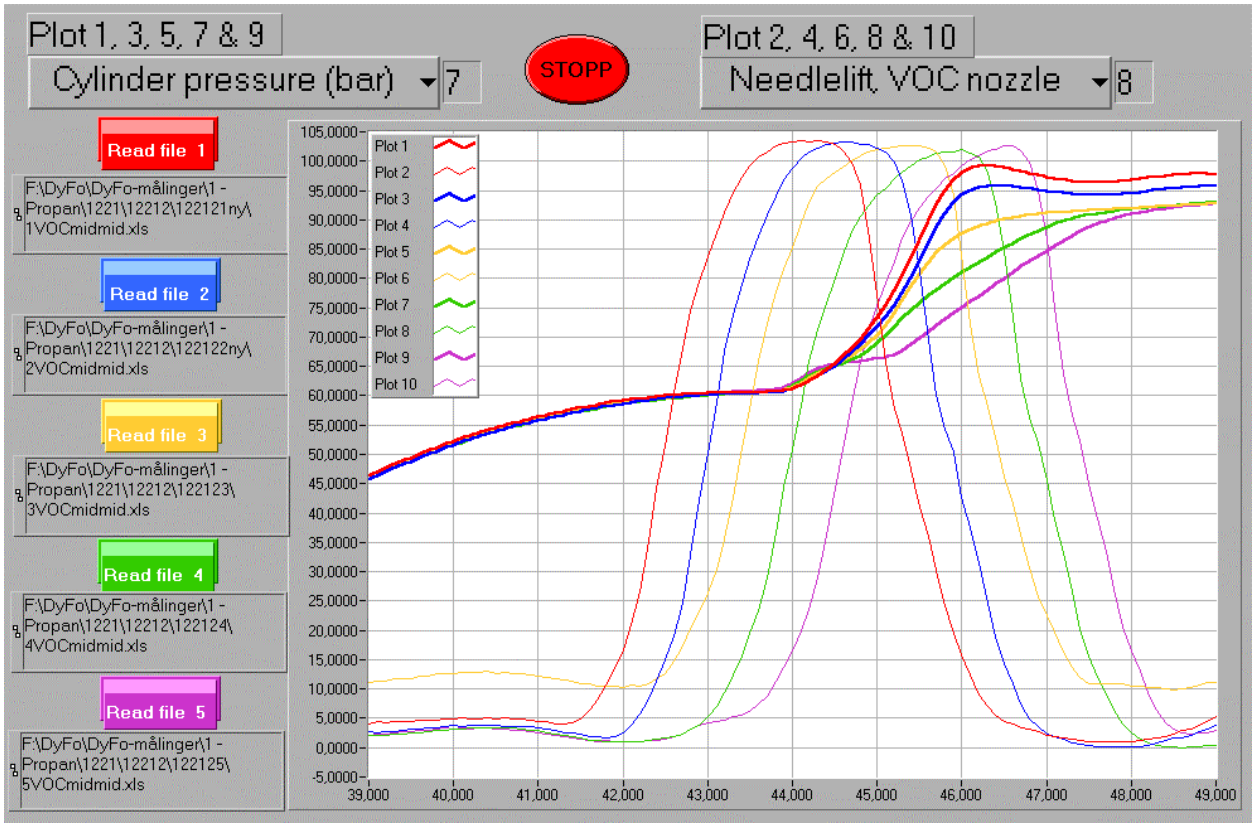

Figure A4.5 Cylinder pressure and VOC Fuel needle lift curves during injection of VOC Fuel in test series 12212.

Figure A4.6 show the cylinder pressure curves for the different test series for one of the relative injection timings (RIT=0,0 ms). It is here clearly seen that two of the test series, 11211 and

12211, were performed with a different piston movement than the others, as referred in section 5.2.5 and 6.4.1.

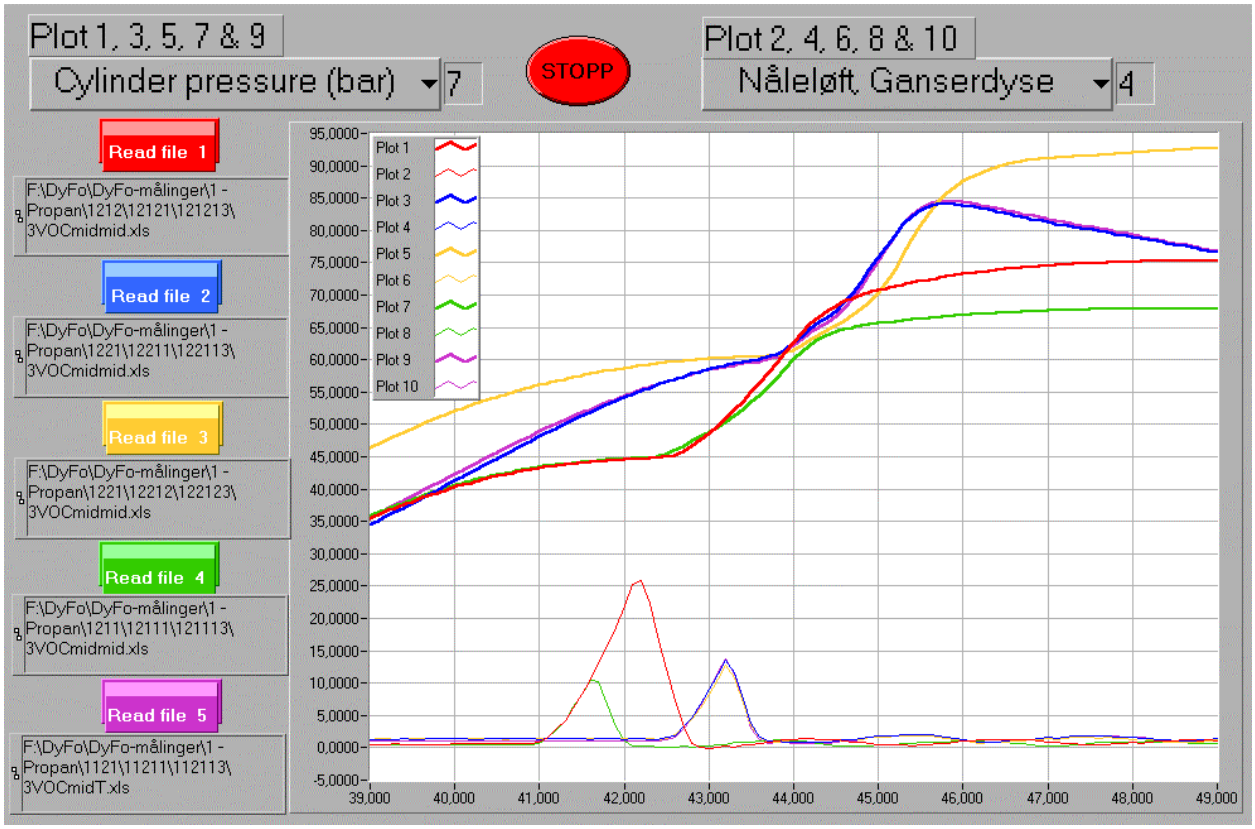

Figure A4.6 Cylinder pressure curves and pilot fuel needle lift curves during injection of VOC Fuel in the different test series.

Appendix 5 Effect of different relative injection timing (RIT).

As an example on how the relative timing of VOC Fuel and pilot fuel injection affect the combustion process, cylinder pressure curves, rate of heat release curves and images from the tests series 12121 (charge air pressure 2,0 bars) is shown in Figure A5.1 – A5.7. Additional cylinder pressure curves and rate of heat release curves from test series 12212 (charge air pressure 3,0 bars) are shown in Figure A5.8 – A5.11. The number in front of "VOCmidmid.xls" (1 – 5) indicates the RIT as explained in section 6.1.5

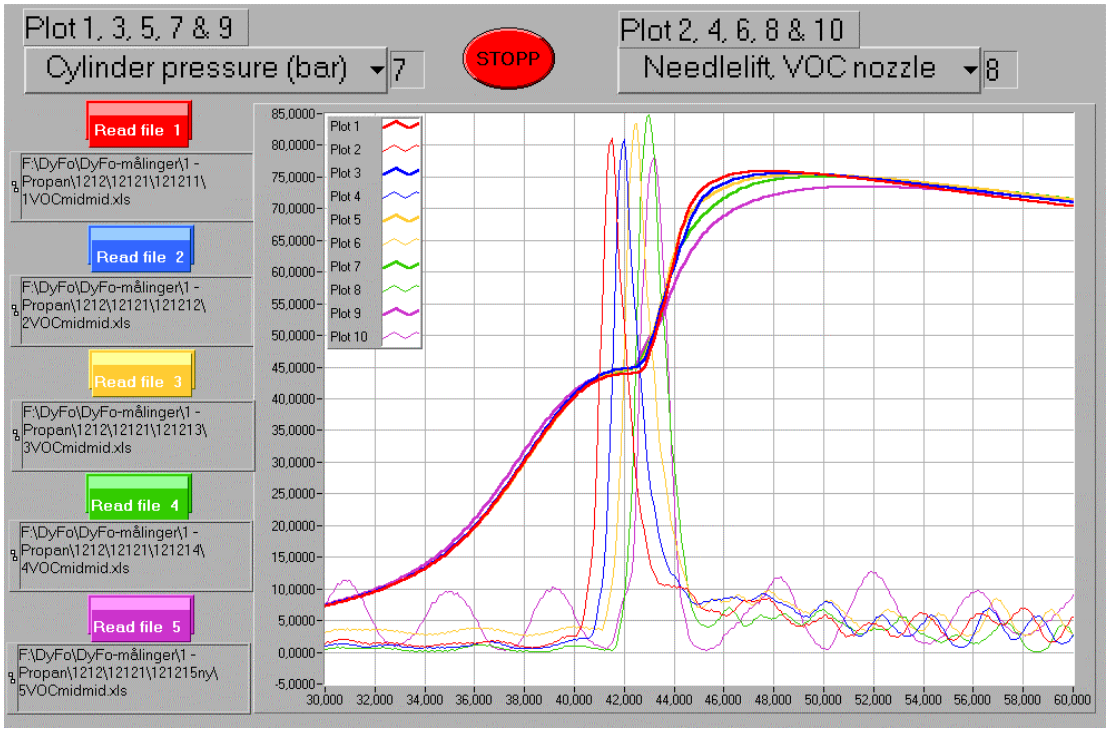

Figure A5.1 Cylinder pressure curves and VOC Fuel injector needle lift when varying the relative injection timing of VOC Fuel and pilot fuel in test series 12121 (charge air pressure 2,0 bars).

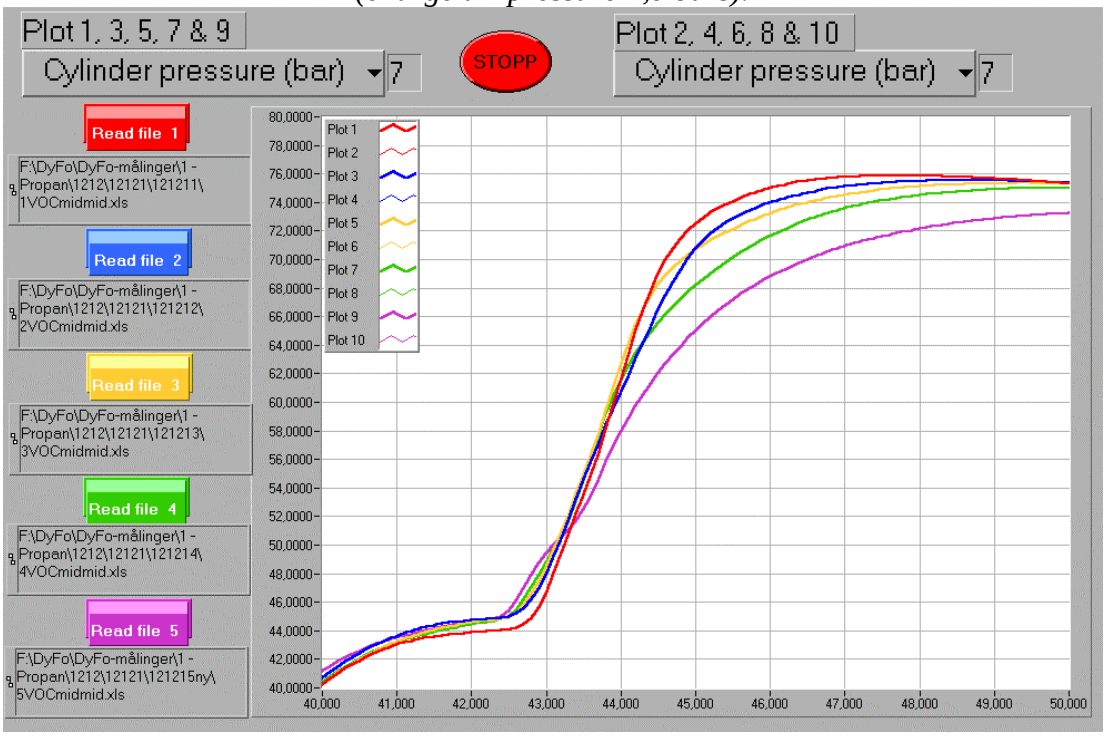

Figure A5.2 Close-up view of cylinder pressure curves shown in Figure A5.1.

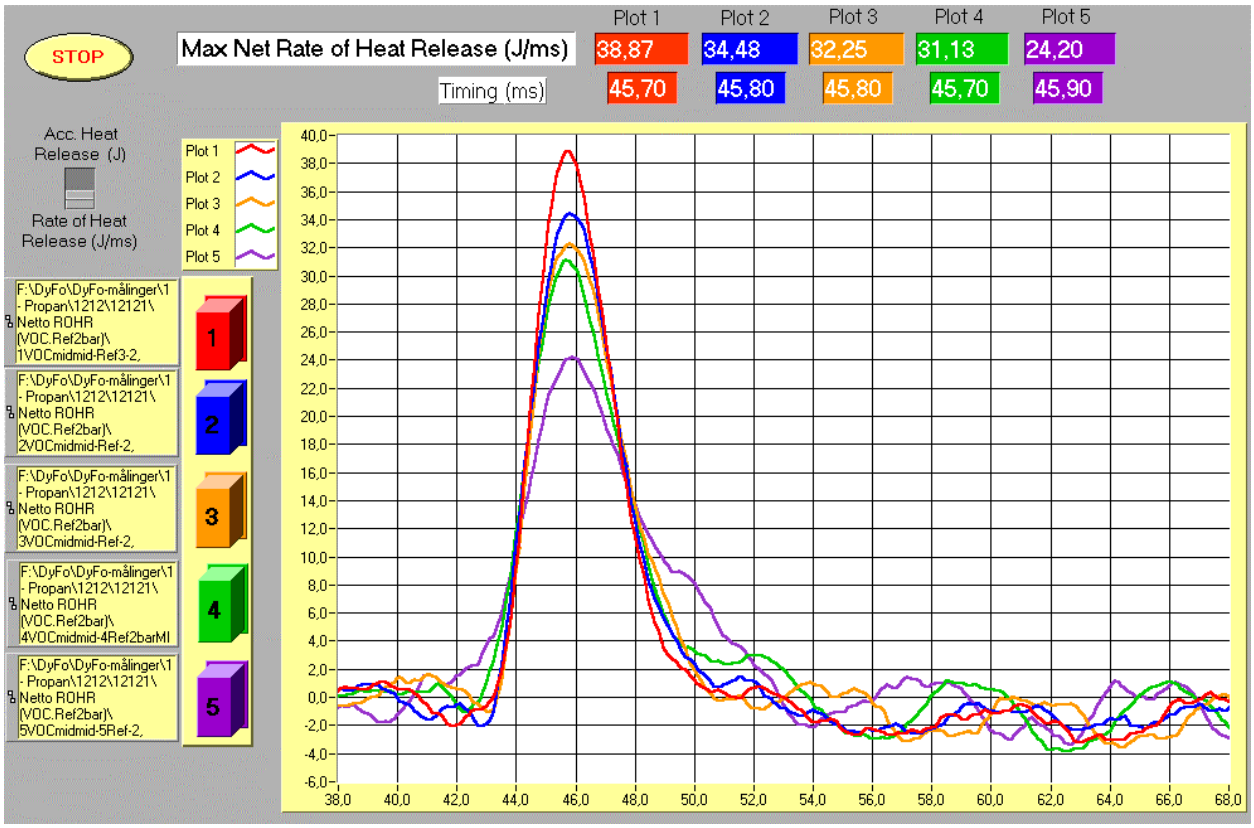

Figure A5.3 Rate of heat release curves when varying the relative injection timing of VOC Fuel and pilot fuel in test series 12121 (charge air pressure 2,0 bars).

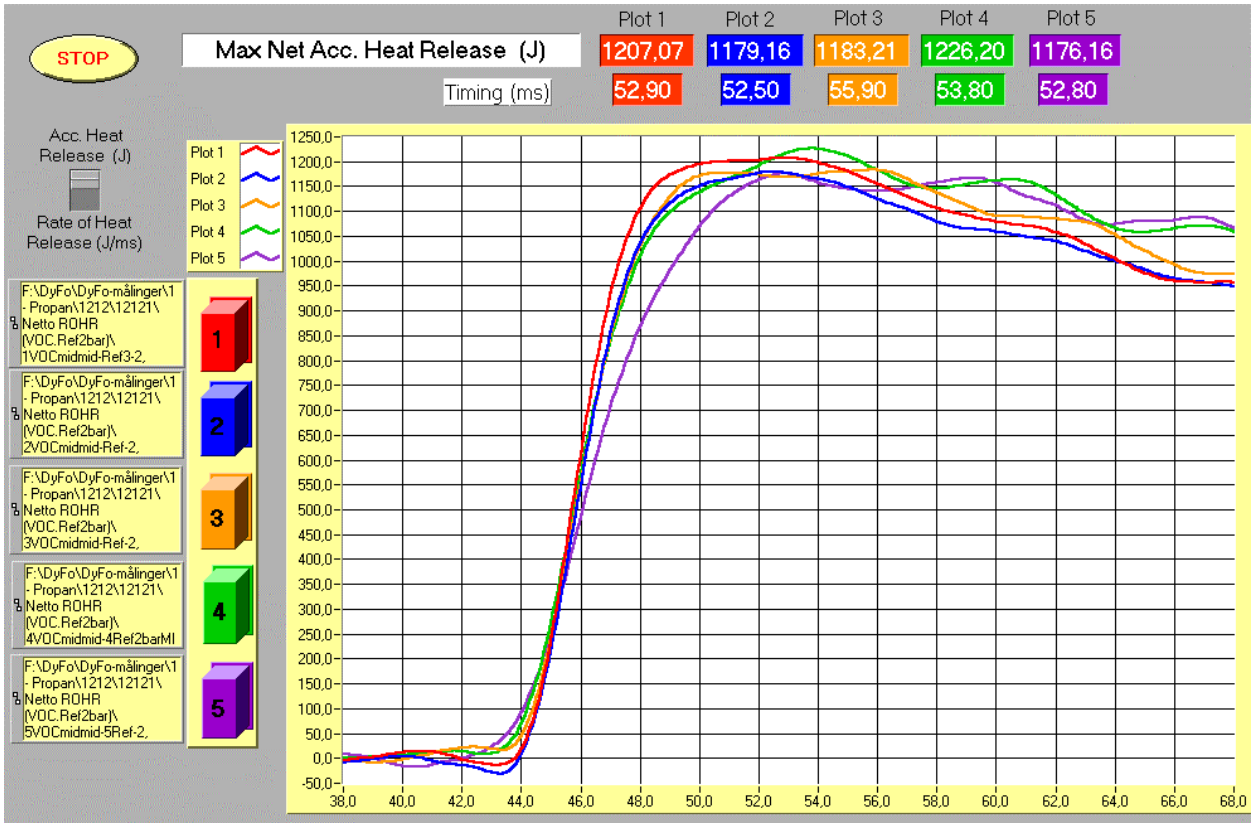

Figure A5.4 Accumulated heat release curves when varying the relative injection timing of VOC Fuel and pilot fuel in test series 12121 (charge air pressure 2,0 bars).

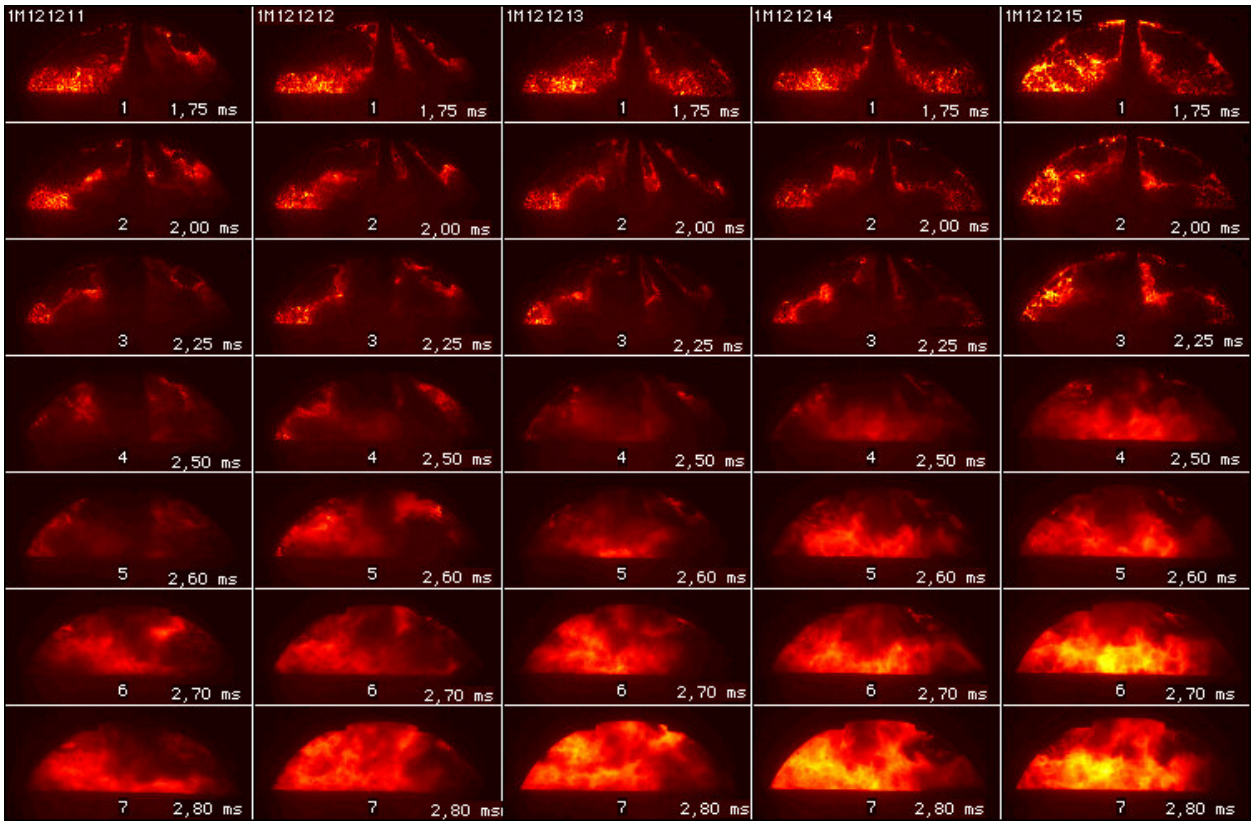

RIT: -1,00 ms -0,50 ms 0,00 ms +0,50 ms +1,00 ms

Figure A5.5 Images of injection and ignition of pilot fuel and VOC Fuel with varying the relative injection timing (RIT) of the two fuels in test series 12121.

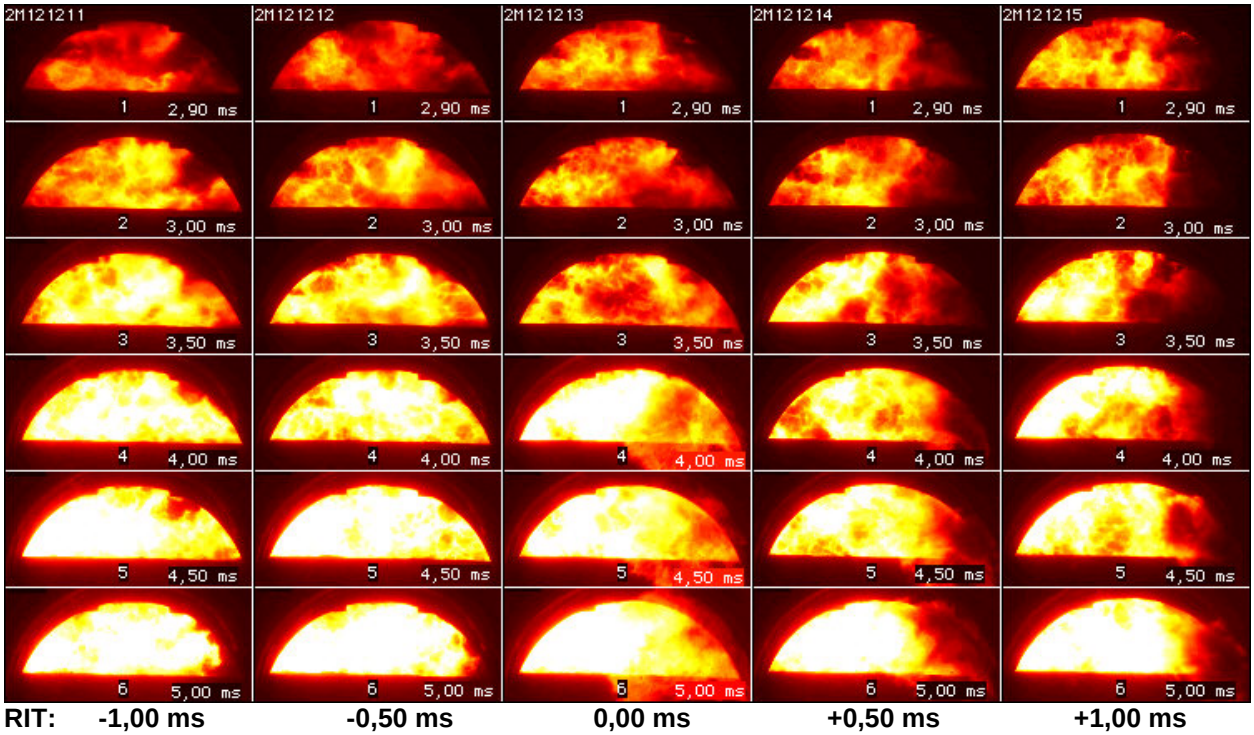

RIT: -1,00 ms -0,50 ms 0,00 ms +0,50 ms +1,00 ms

Figure A5.6 Images of ignition and early combustion of pilot fuel and VOC Fuel with varying the relative injection timing (RIT) of the two fuels in test series 12121.

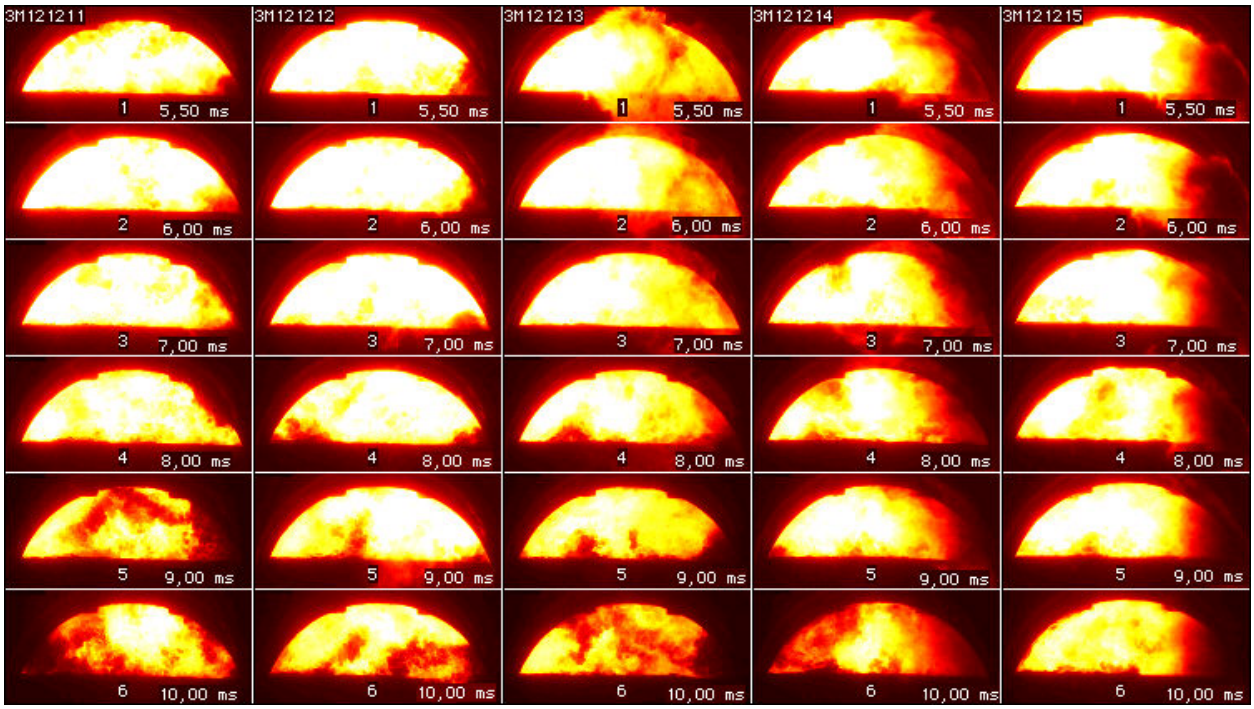

Figure A5.7 Images of late combustion of pilot fuel and VOC Fuel with varying the relative injection timing (RIT) of the two fuels in test series 12121.

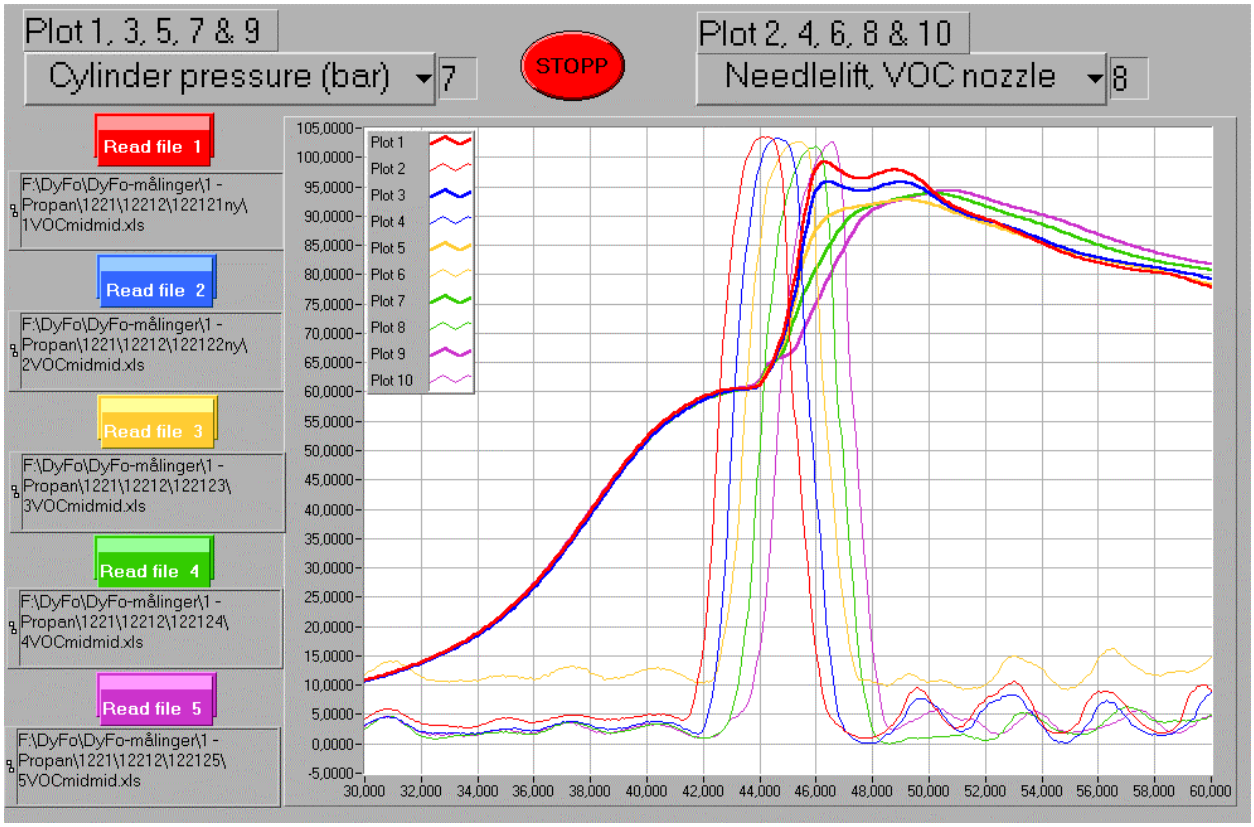

Figure A5.8 Cylinder pressure curves and VOC Fuel injector needle lift when varying the relative injection timing of VOC Fuel and pilot fuel in test series 12212 (charge air pressure 3,0 bars).

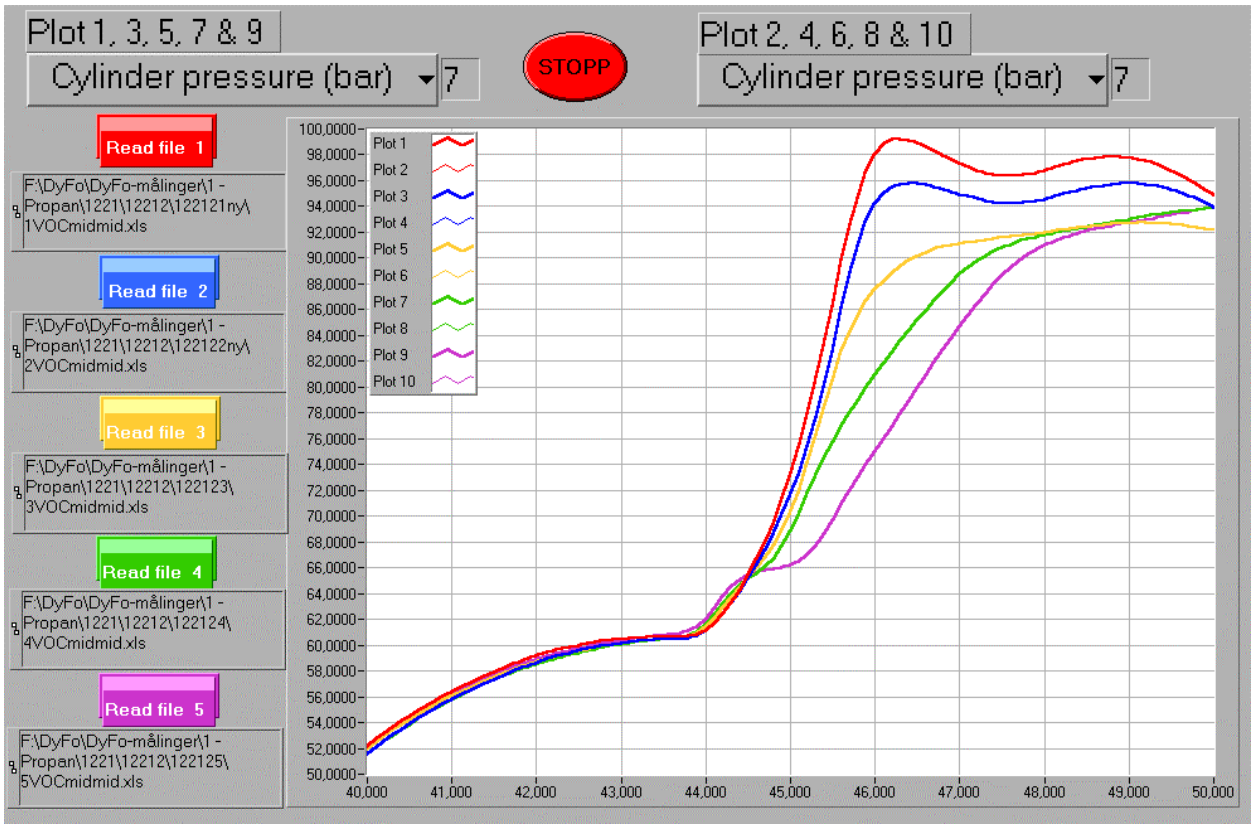

Figure A5.9 Close-up view of cylinder pressure curves shown in Figure A5.8.

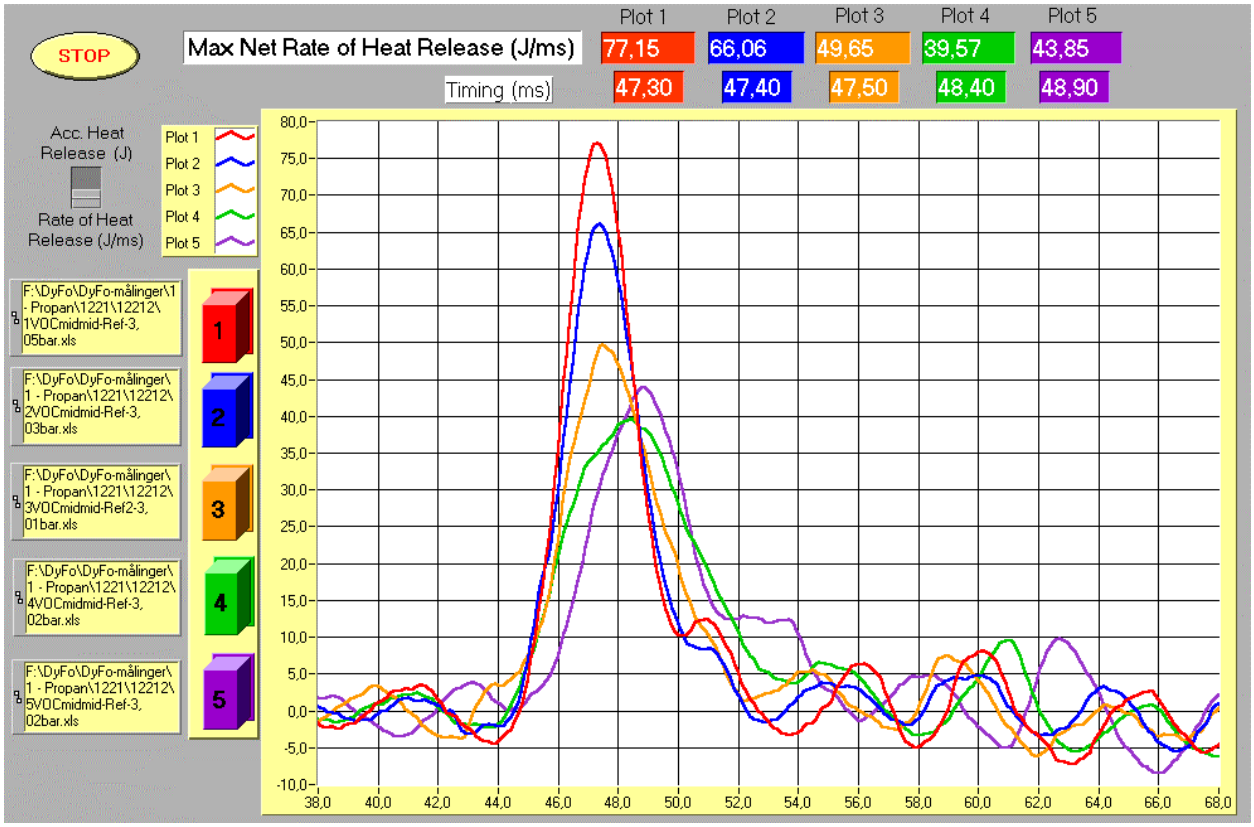

Figure A5.10 Rate of heat release curves when varying the relative injection timing of VOC Fuel and pilot fuel in test series 12212 (charge air pressure 3,0 bars).

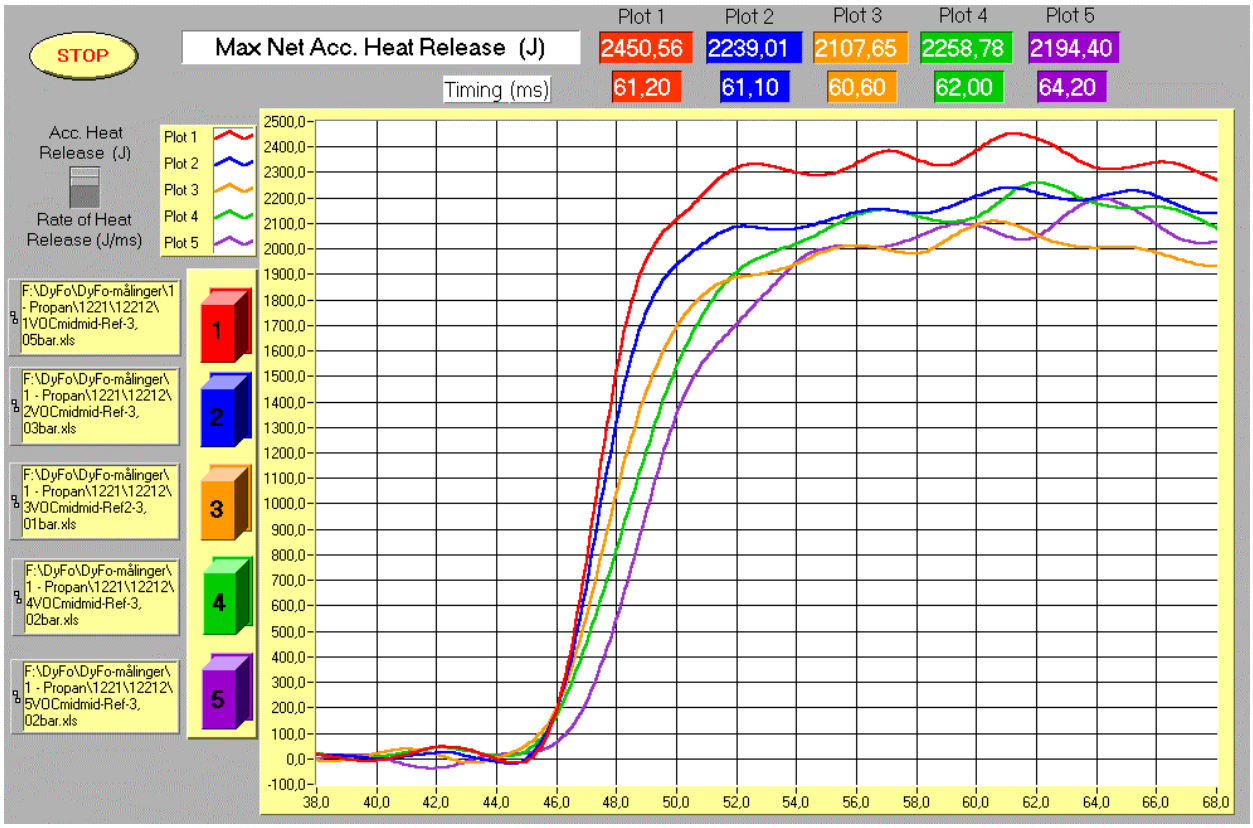

Figure A5.11 Accumulated heat release curves when varying the relative injection timing of VOC Fuel and pilot fuel in test series 12212 (charge air pressure 3,0 bars).

Appendix 6 Effect of different pilot fuel mass (PFM).

For utilising low cetane, gaseous fuel, pilot fuel for ignition has to be used. As little pilot fuel as possible is desirable to reduce the unwanted effects the pilot fuel (diesel oil or HFO) cause when combusted. In this appendix, the effect of different amount of pilot fuel (high and low) is shown by comparison of the results from test series 12121 (PFM=high) and 12111 (PFM=low).

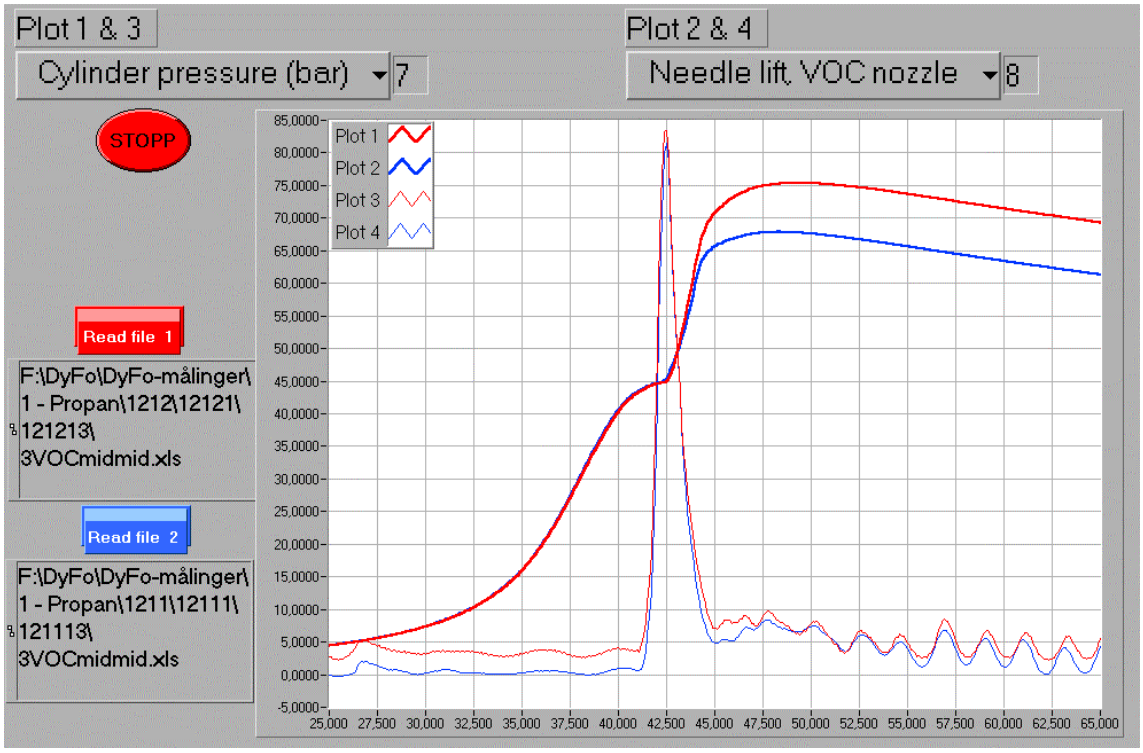

Figure A6.1 Cylinder pressure curves and VOC Fuel injector needle lift curves for test 121213 (PFM=high) and test 121113 (PFM=low).

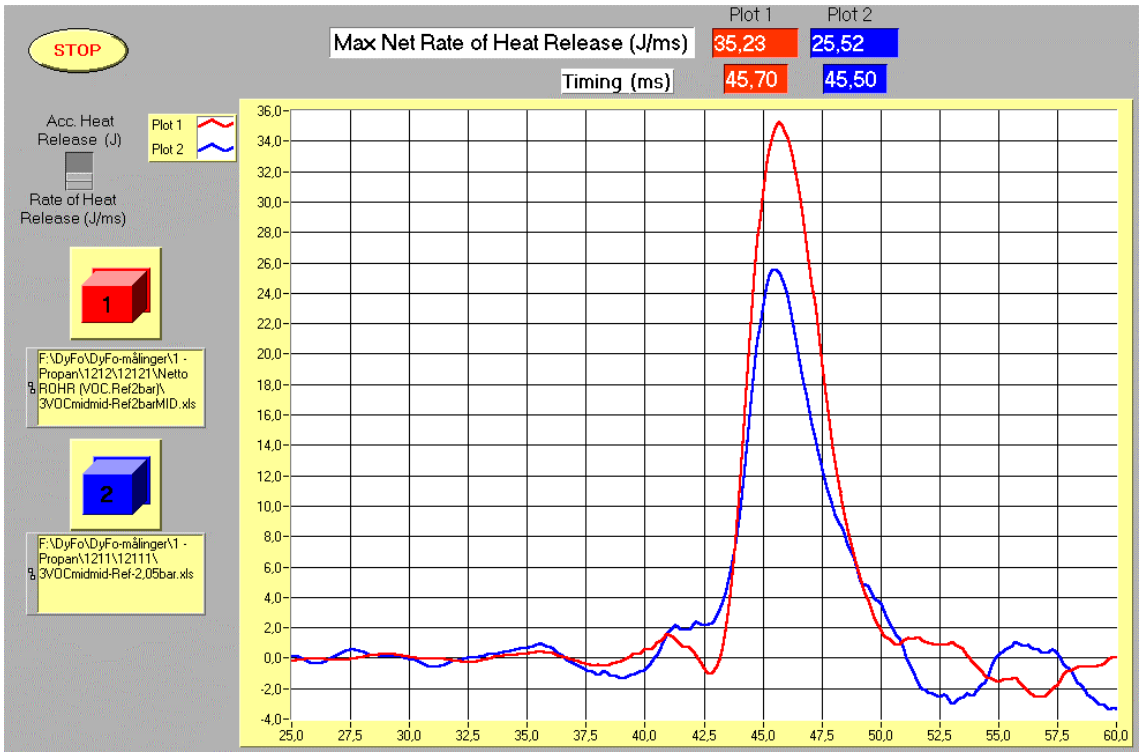

Figure A6.2 Rate of heat release curves for test 121213 (PFM=high) and test 121113 (PFM=low).

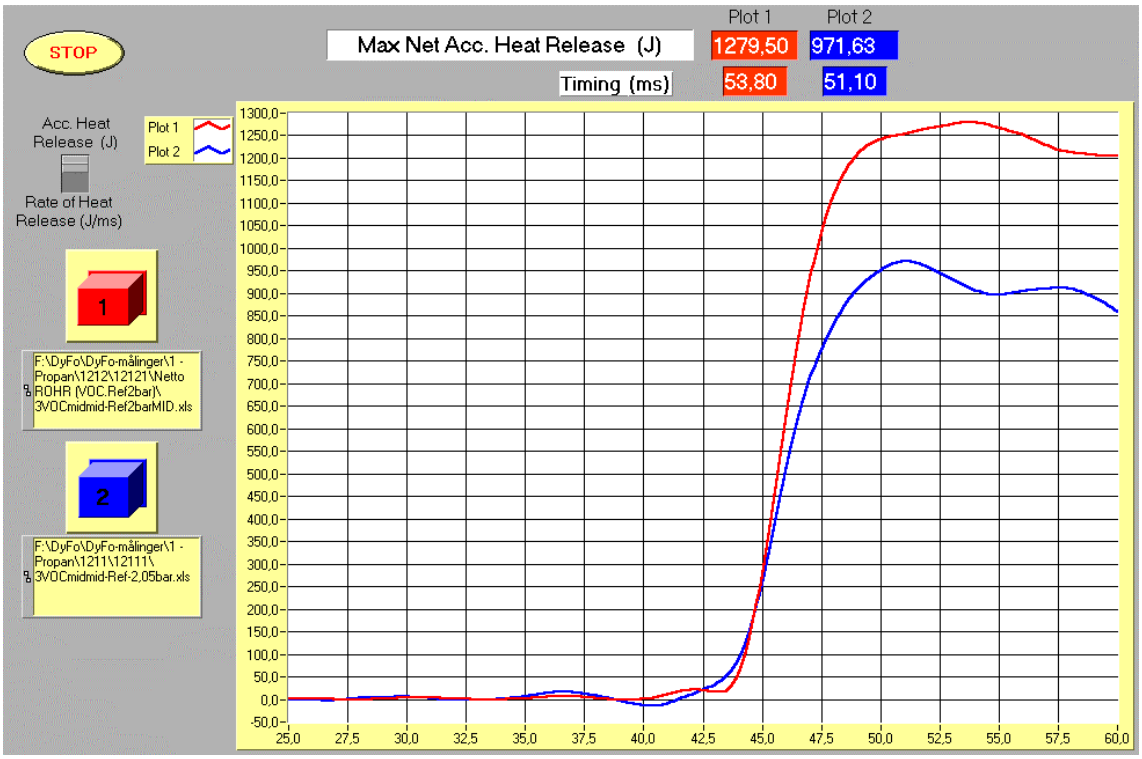

Figure A6.3 *Accumulated heat release curves for test 121213 (PFM=high) and test 121113 (PFM=low).*

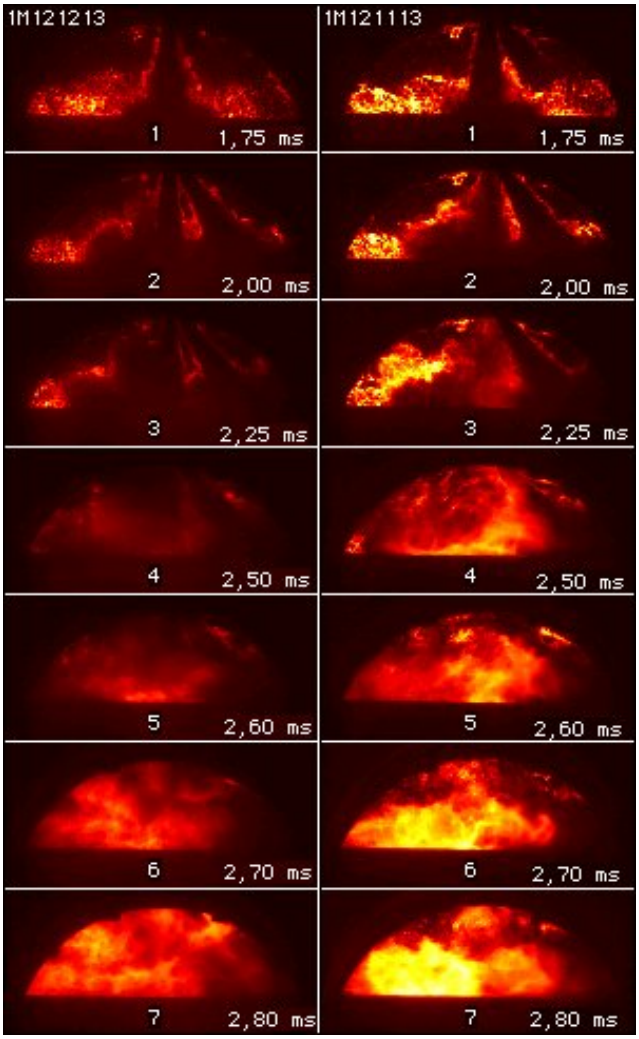

Figure A6.4 *Images of injection and ignition of pilot fuel and VOC Fuel in test 121213 (PFM=high) and test 121113 (PFM=low).*

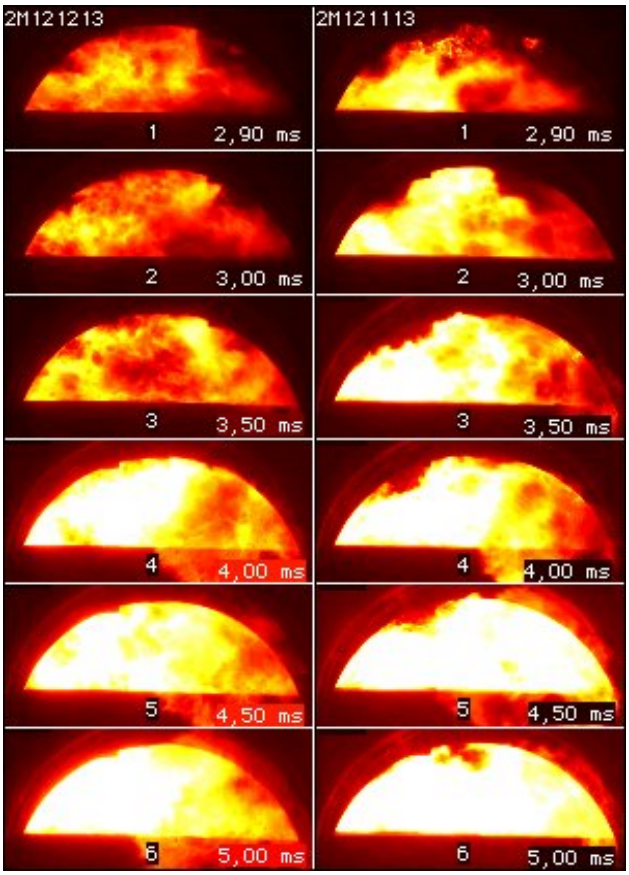

Figure A6.5 Images of ignition and early combustion of pilot fuel and VOC Fuel in test 121213 (PFM=high) and test 121113 (PFM=low).

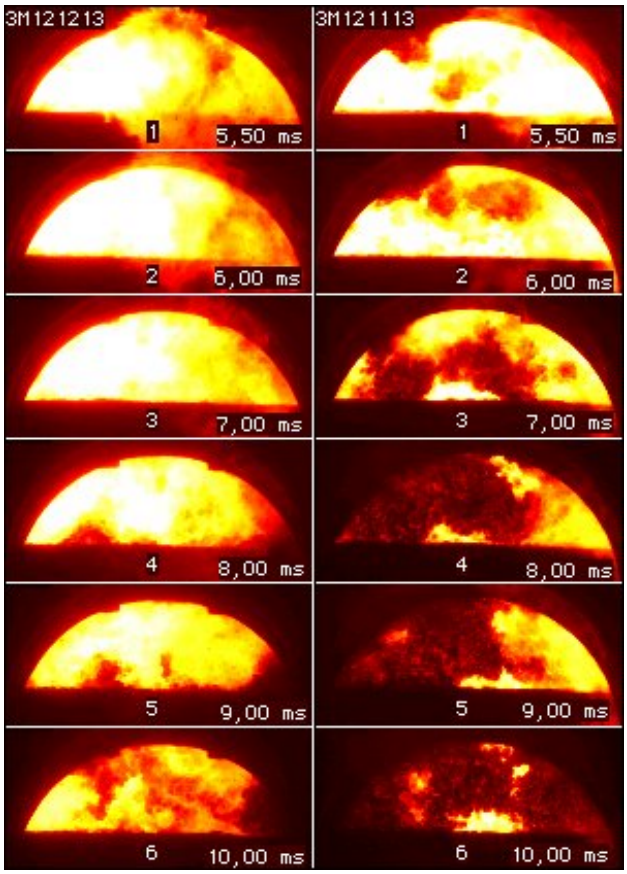

Figure A6.6 Images of late combustion of pilot fuel and VOC Fuel in test 121213 (PFM=high) and test 121113 (PFM=low).

Appendix 7 Effect of different VOC Fuel mass (VFM).

In an engine, the load increases with the fuel mass injected. To study how this fact may affect the ignition and combustion in the DyFo, tests with low (nominal 28,5 mg) and high (nominal 68,7 mg) VOC Fuel mass are performed and compared in the figures below.

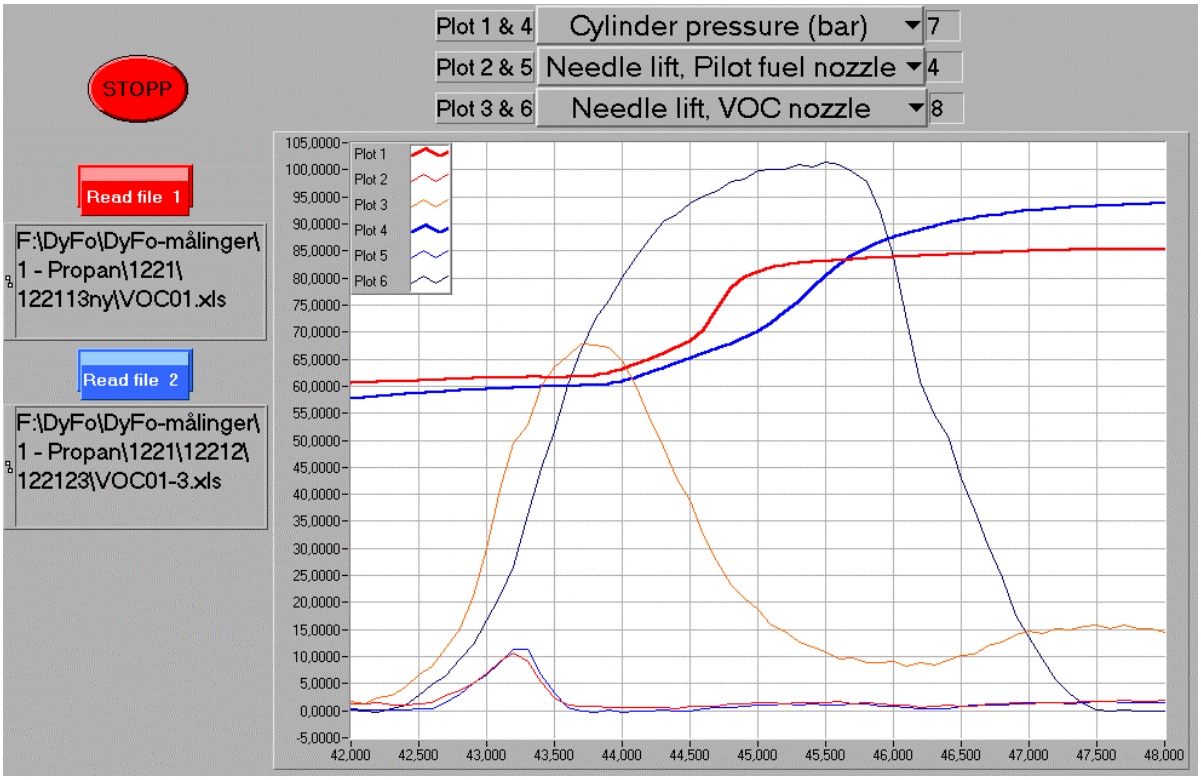

Figure A7.1 Cylinder pressure curves and needle lift curves for single tests in the test series 122113ny (VFM =low) and test series 122123 (VFM=high).

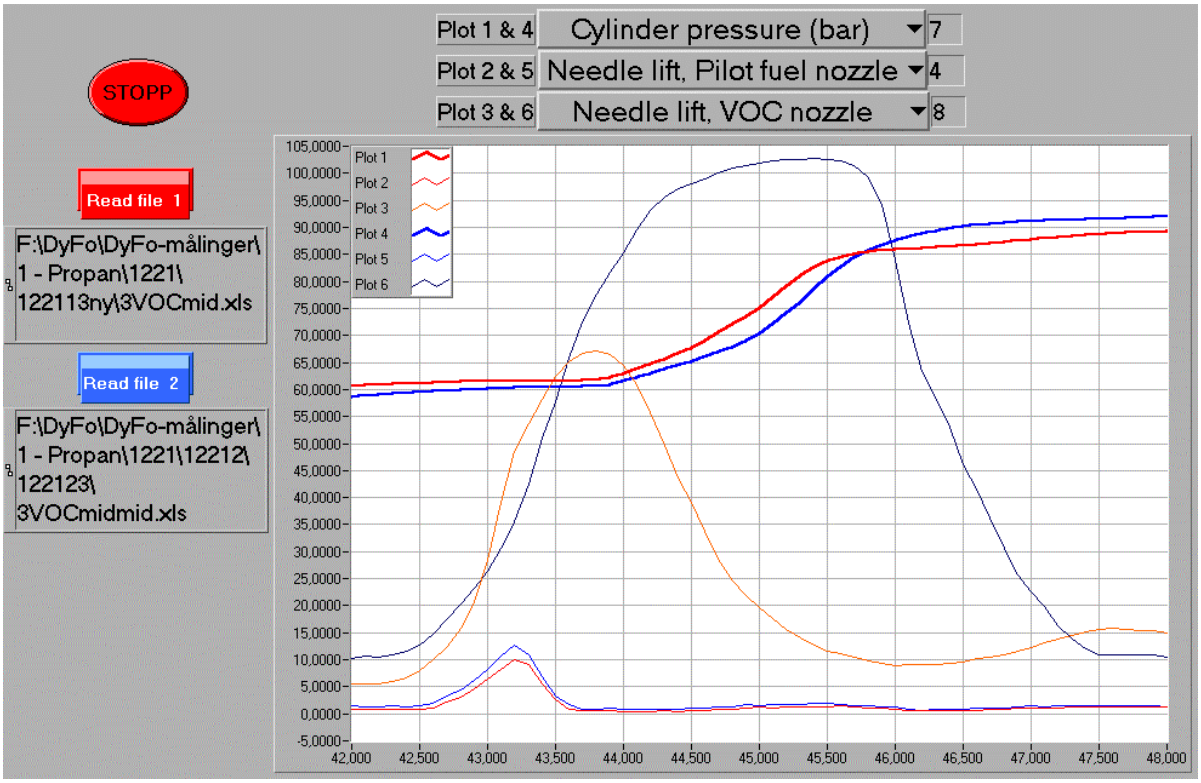

Figure A7.2 Average cylinder pressure curves and needle lift curves for tests in the test series 122113ny (VFM =low) and test series 122123 (VFM=high).

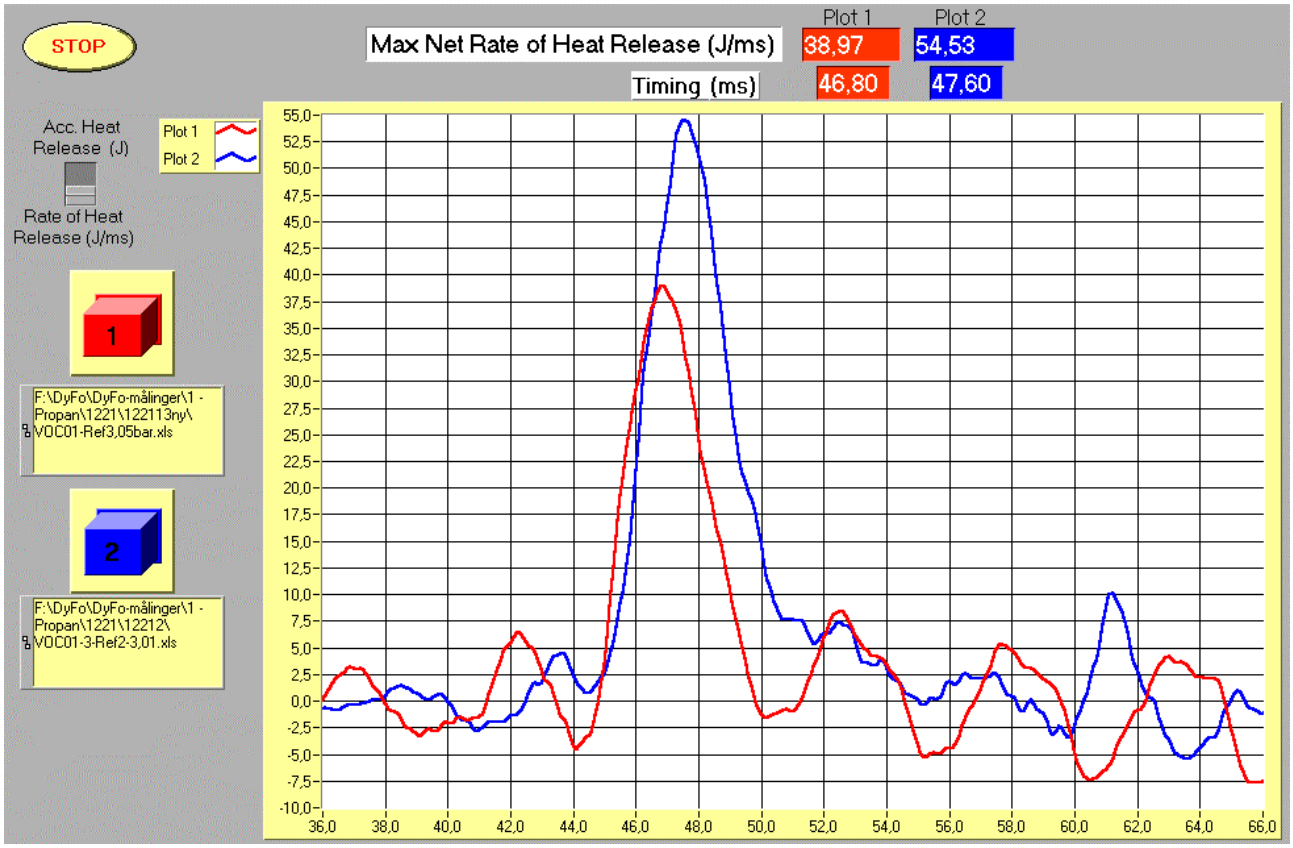

Figure A7.3 Rate of heat release for test 122113ny (VFM low) and test 122123 (VFM high).

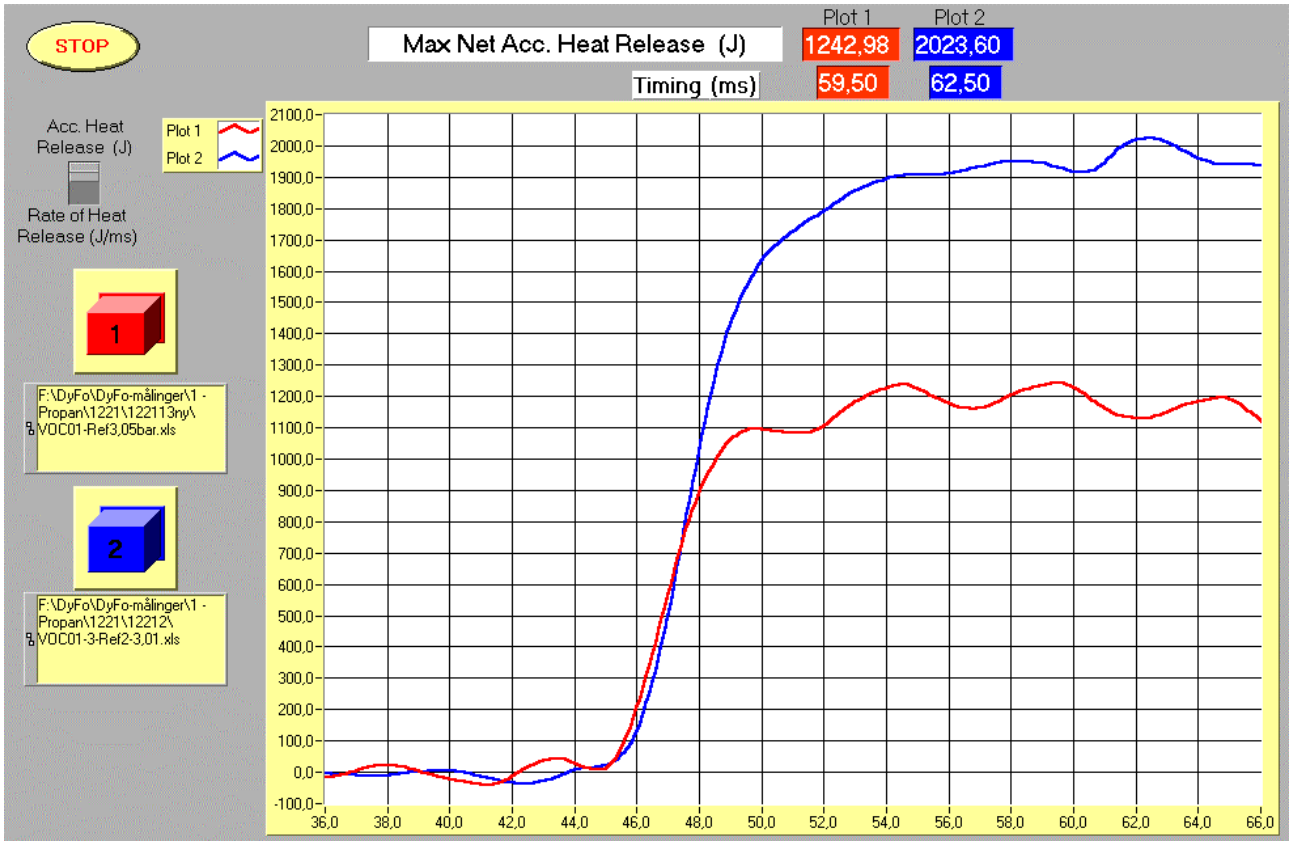

Figure A7.4 Accumulated heat release, test 122113ny (VFM low) and test 122123 (VFM high).

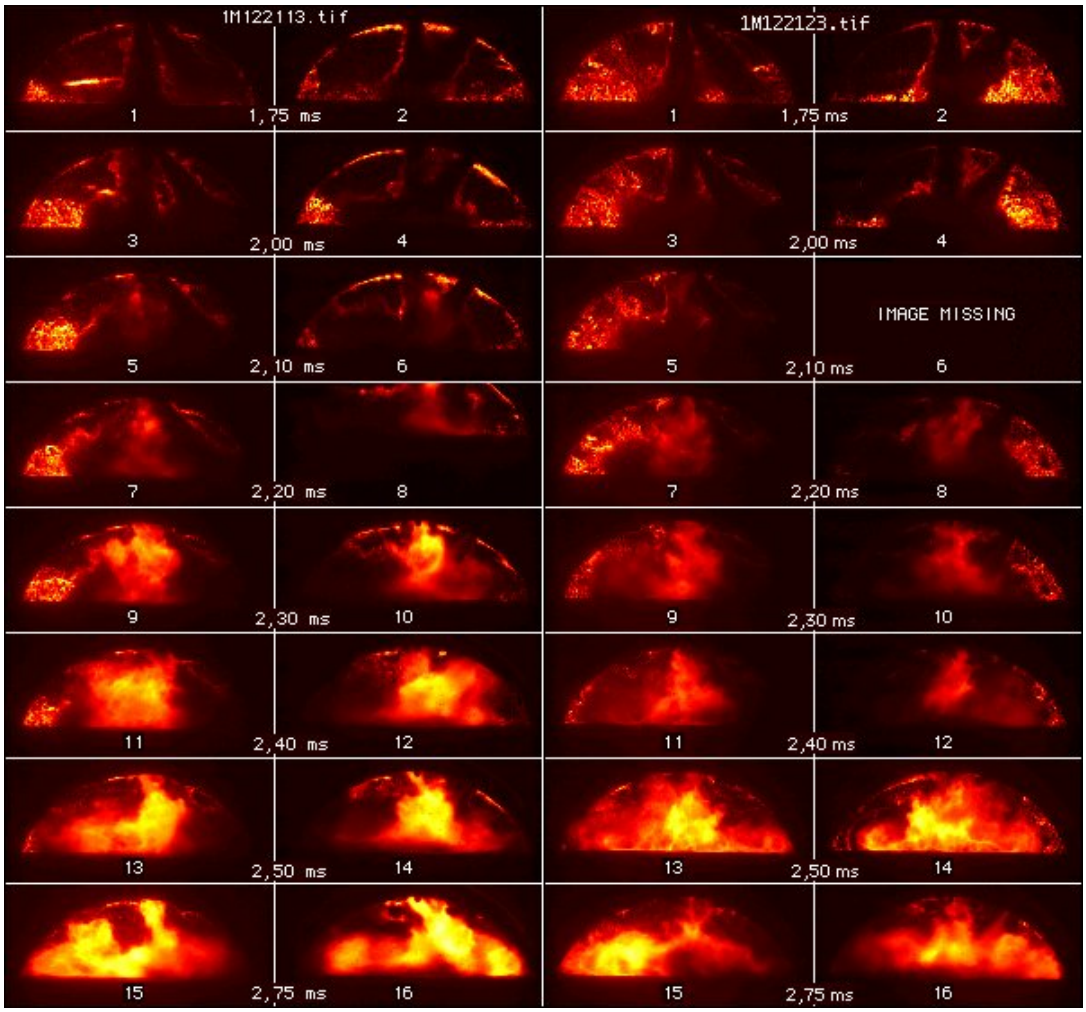

Figure A7.5 Images of injection, ignition and early combustion of pilot fuel and VOC Fuel for test 122113ny (VFM low) and test 122123 (VFM high).

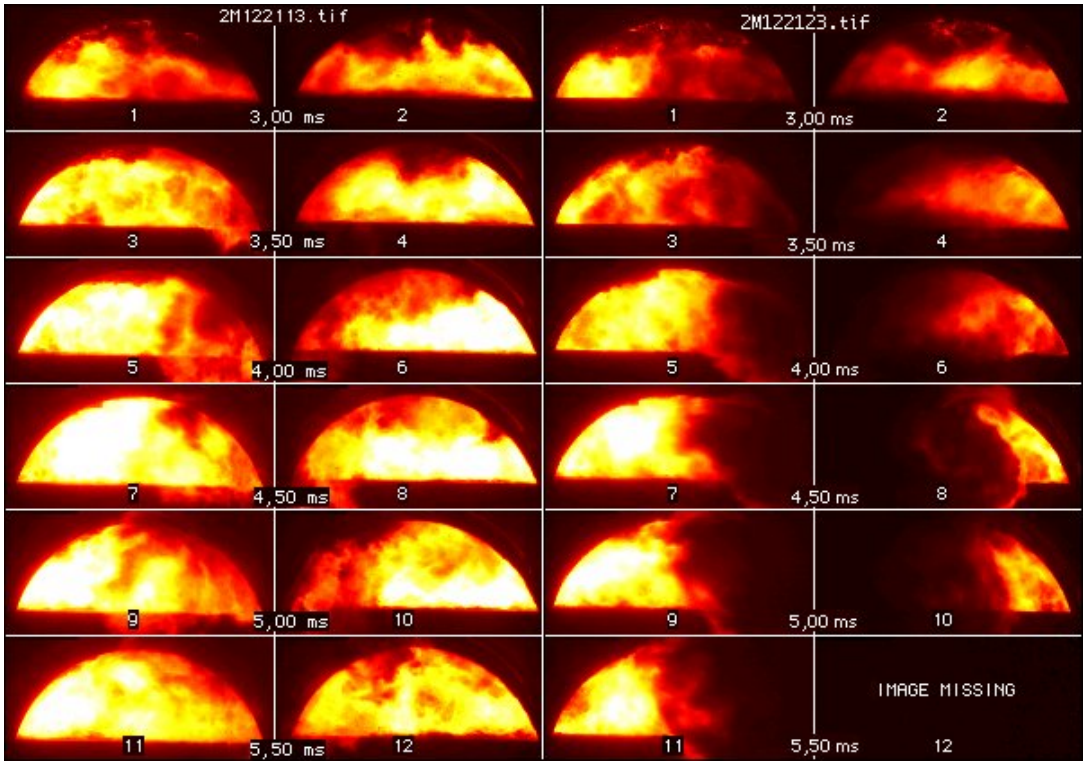

Figure A7.6 Images of the middle part of combustion of pilot fuel and VOC Fuel for test 122113ny (VFM low) and test 122123 (VFM high).

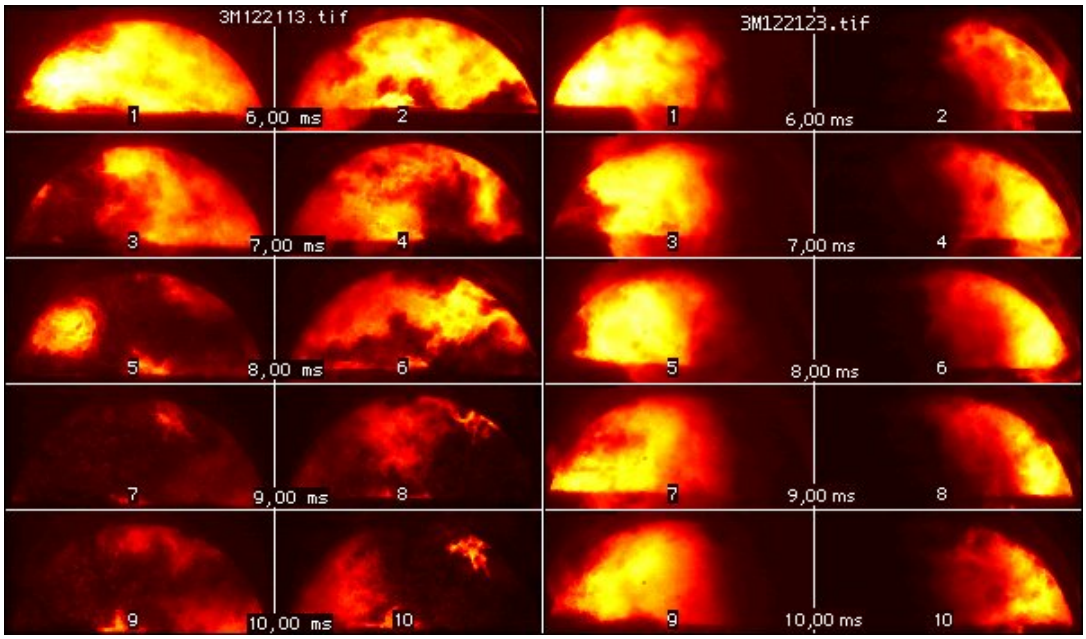

Figure A7.7 Images of late combustion of pilot fuel and VOC Fuel for test 122113ny (VFM low) and test 122123 (VFM high).

Appendix 8 Effect of different charge air pressure (CAP).

In an engine, the charge air pressure normally increases with the engine speed and load. To study how this fact may affect the ignition and combustion of VOC Fuel, tests with charge air pressure 2,0 bar and 3,0 bar are performed and compared in the figures below. Since tests with different charge air pressure are performed with different "global injection timing" (= timing relative to piston position, cf. section 5.1.3), comparison is made by "artificially" correction of this timing to the same position, cf. section 5.3.3 – "*Effect of charge air pressure*".

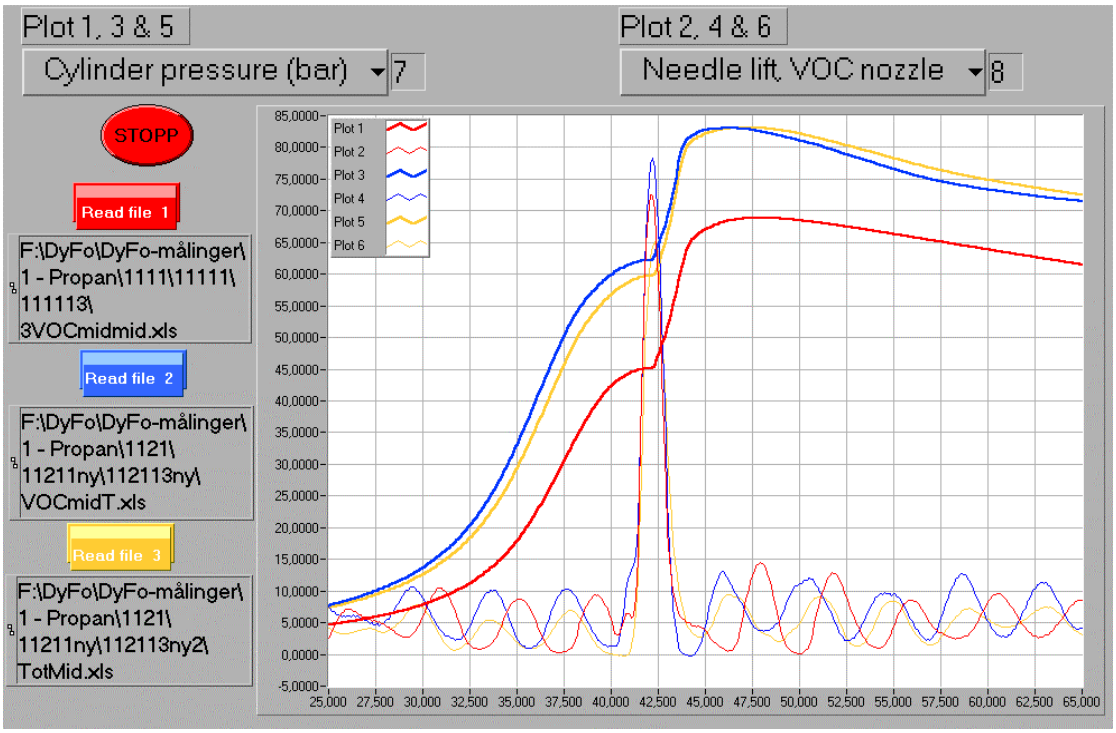

Figure A8.1 Cylinder pressure curves and VOC Fuel injector needle lift curves for test 111113 (CAP =2 bar) and test 112113ny & 112113ny2 (CAP=3 bar).

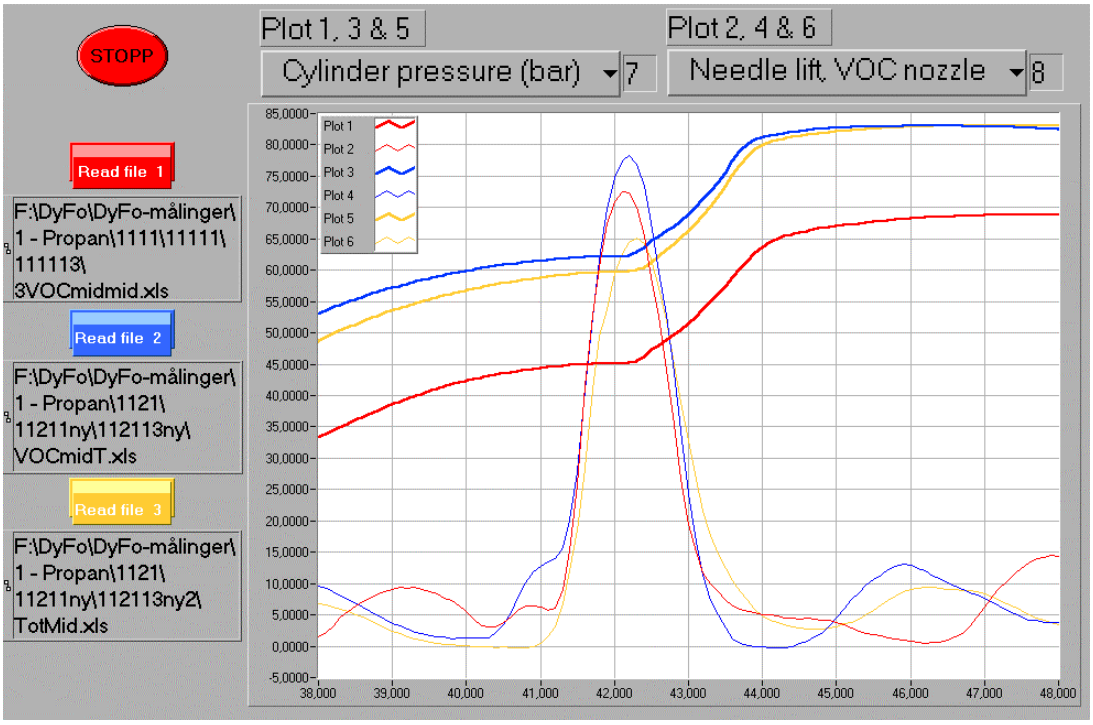

Figure A8.2 Close-up view of Figure A8.1 showing details from 38 to 48 milliseconds.

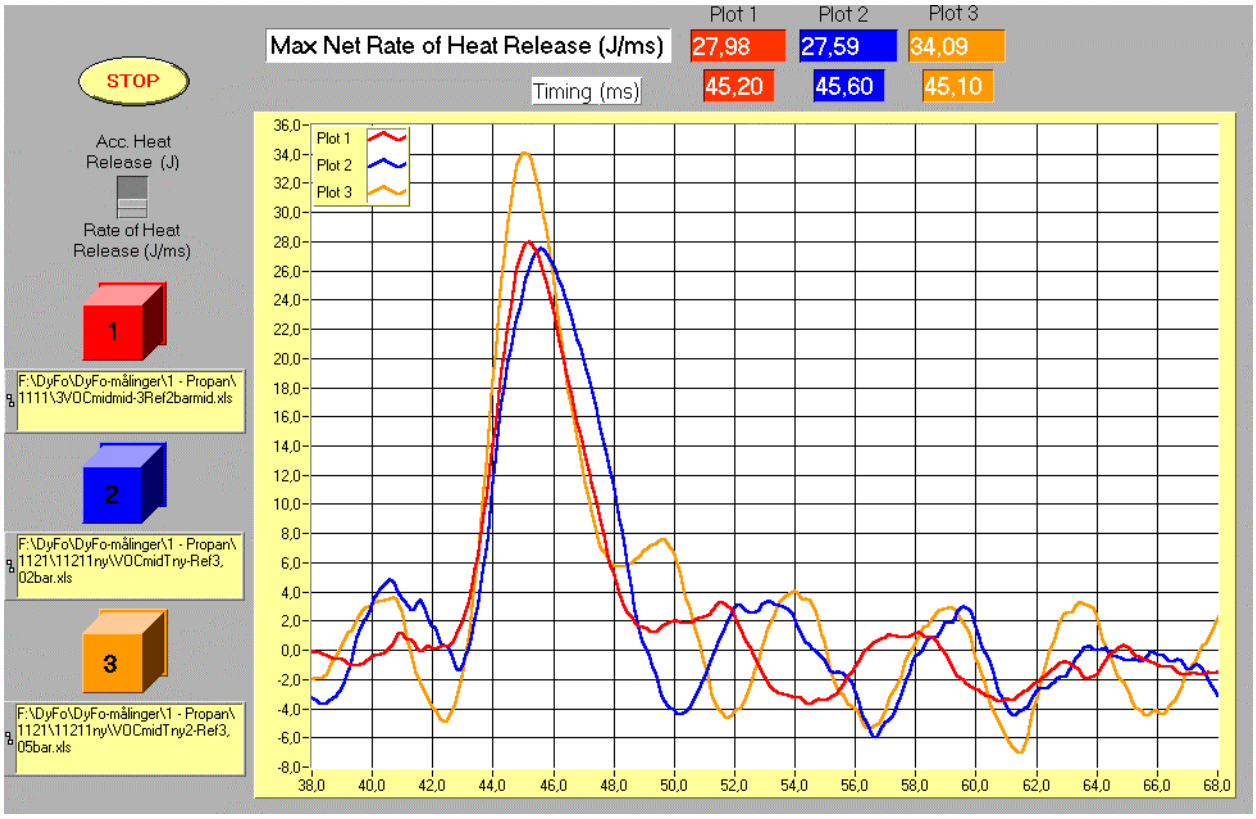

Figure A8.3 Rate of heat release curves for test 111113 (CAP =2 bar) and test 112113ny & 112113ny2 (CAP=3 bar).

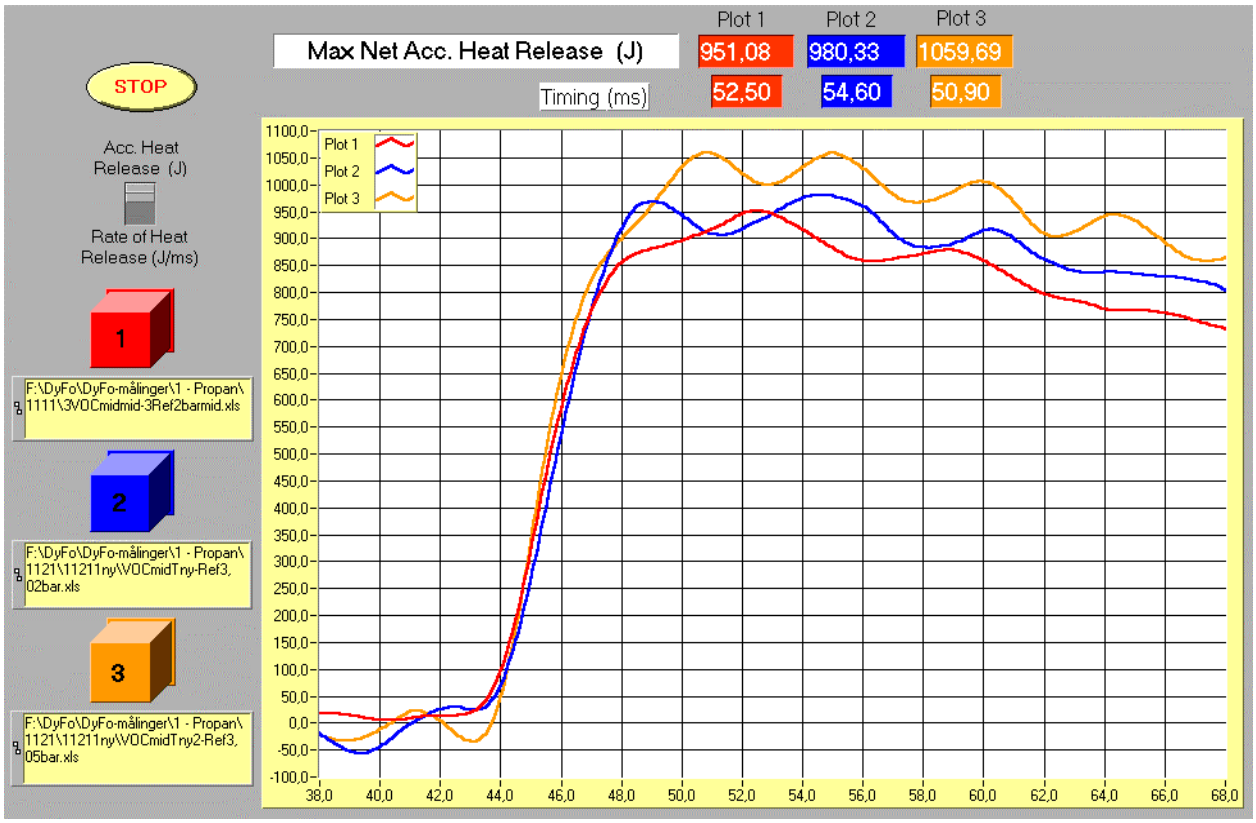

Figure A8.4 Accumulated heat release curves for test 111113 (CAP =2 bar) and test 112113ny & 112113ny2 (CAP=3 bar).

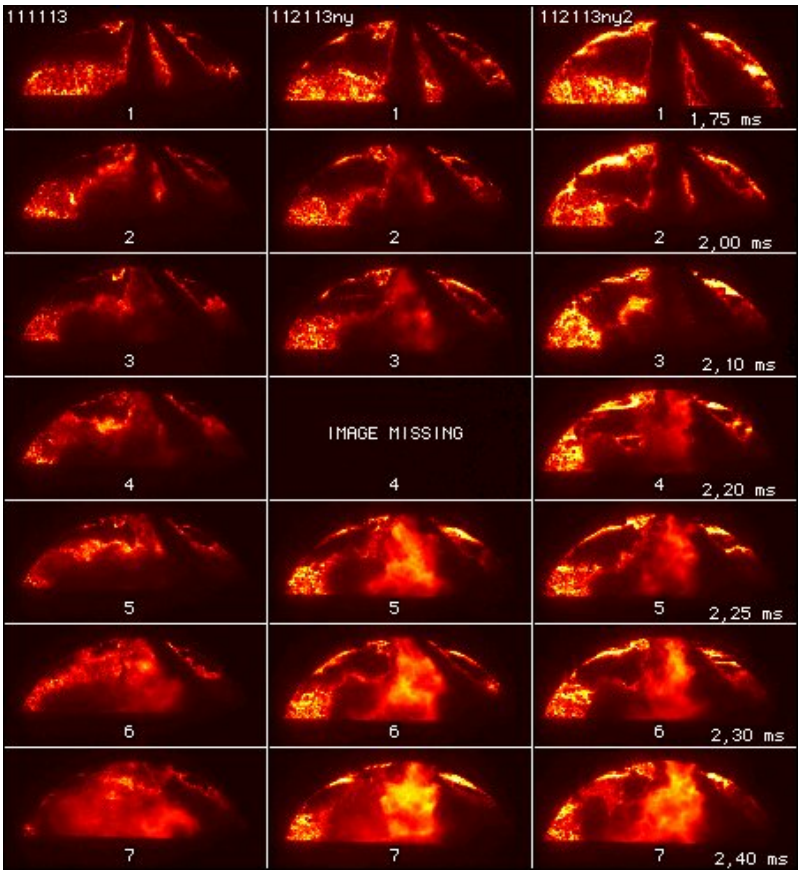

Figure A8.5 Images of injection and ignition of pilot fuel and VOC Fuel for test 111113 (CAP =2 bar) and test 112113ny & 112113ny2 (CAP=3 bar).

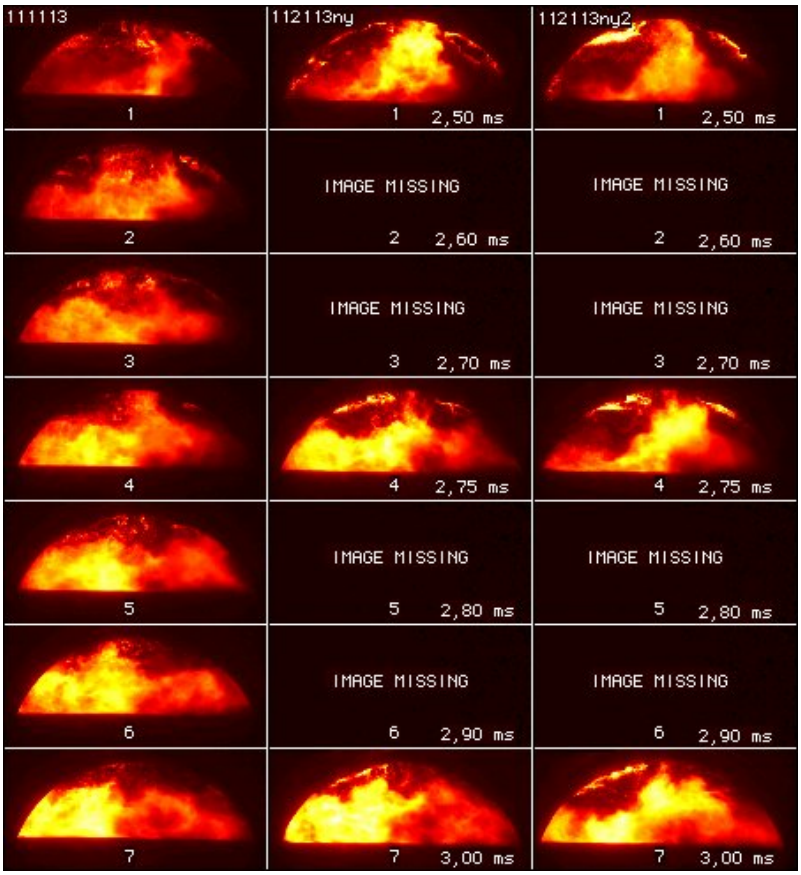

Figure A8.6 Images of ignition and early combustion of pilot fuel and VOC Fuel for test 111113 (CAP =2 bar) and test 112113ny & 112113ny2 (CAP=3 bar).

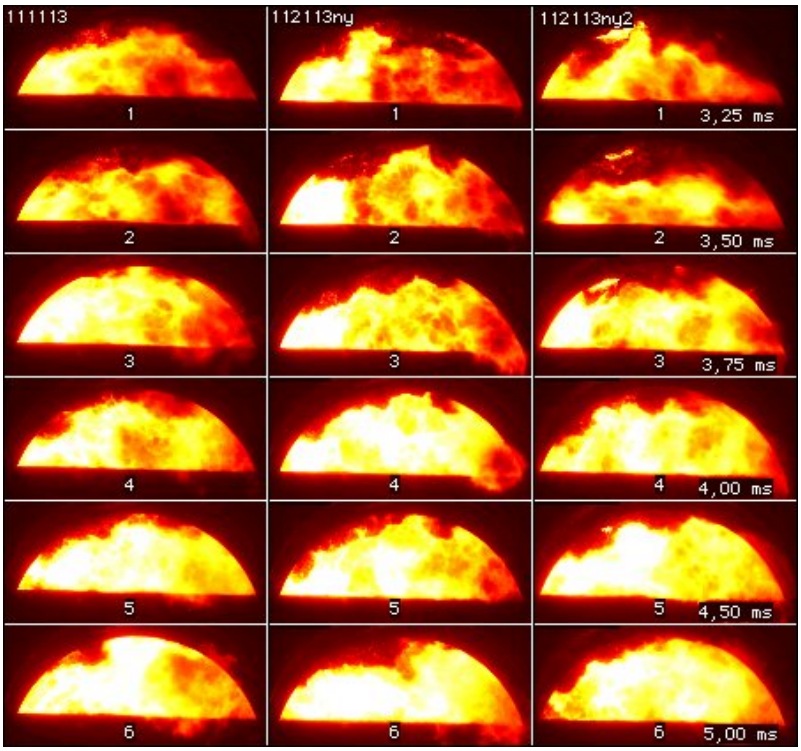

Figure A8.7 Images of middle combustion of pilot fuel and VOC Fuel for test 111113 (CAP =2 bar) and test 112113ny & 112113ny2 (CAP=3 bar).

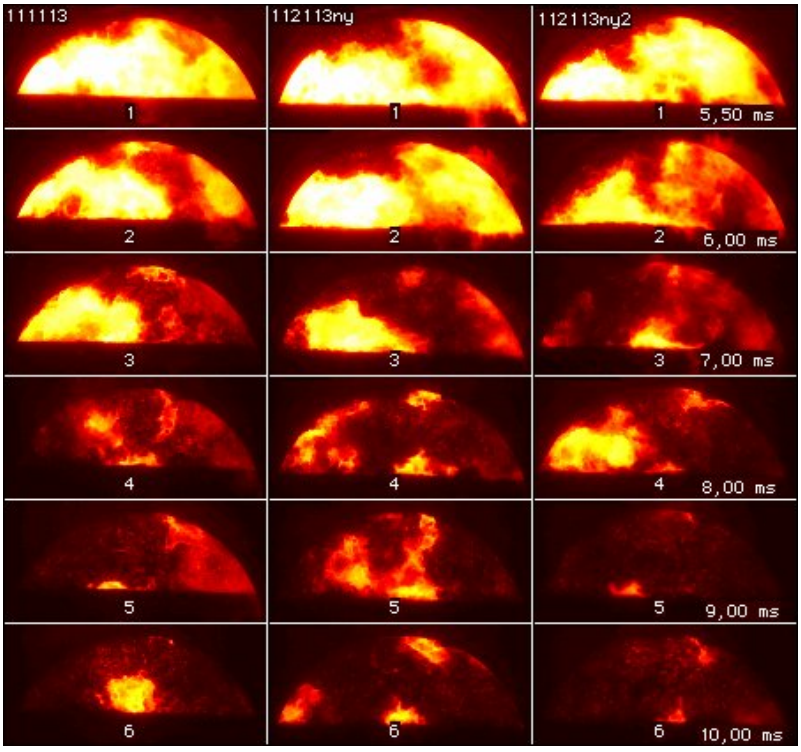

Figure A8.8 Images of late combustion of pilot fuel and VOC Fuel for test 111113 (CAP =2 bar) and test 112113ny & 112113ny2 (CAP=3 bar).

Appendix 9 Effect of different charge air temperatures (CAT).

As short ignition delay is desirable in diesel engines, the charge air temperature is one parameter to vary in order to obtain this. The effect of this parameter on the ignition and combustion of pilot ignited VOC Fuel is studied. Test series 11211 (CAT= 30 °C) and test series 12211 (CAT= 70 °C) (charge air pressure 3 bar) and test series 11111 (CAT= 30 °C) and test series 12111 (CAT= 70 °C) (charge air pressure 2bar) were compared and one test from each series is shown below (112114/122114 and 111113/121113).

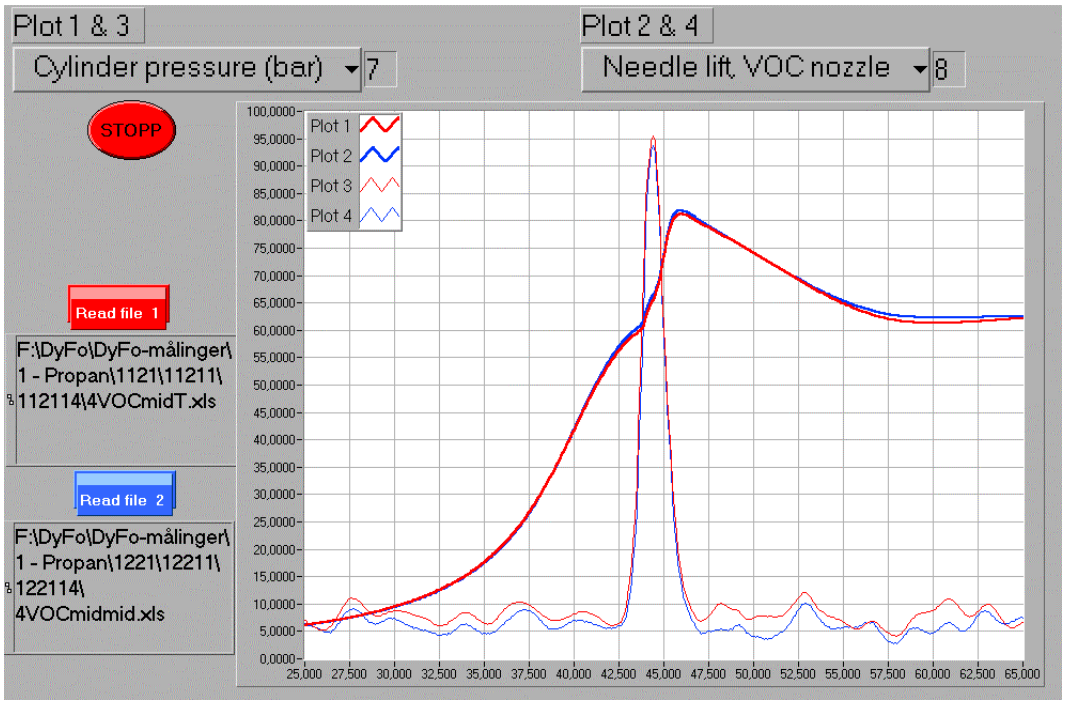

Figure A9.1 Cylinder pressure and VOC Fuel injector needle lift for different charge air temperatures (charge air pressure 3,0 bars). Average of > 20 repetitions.

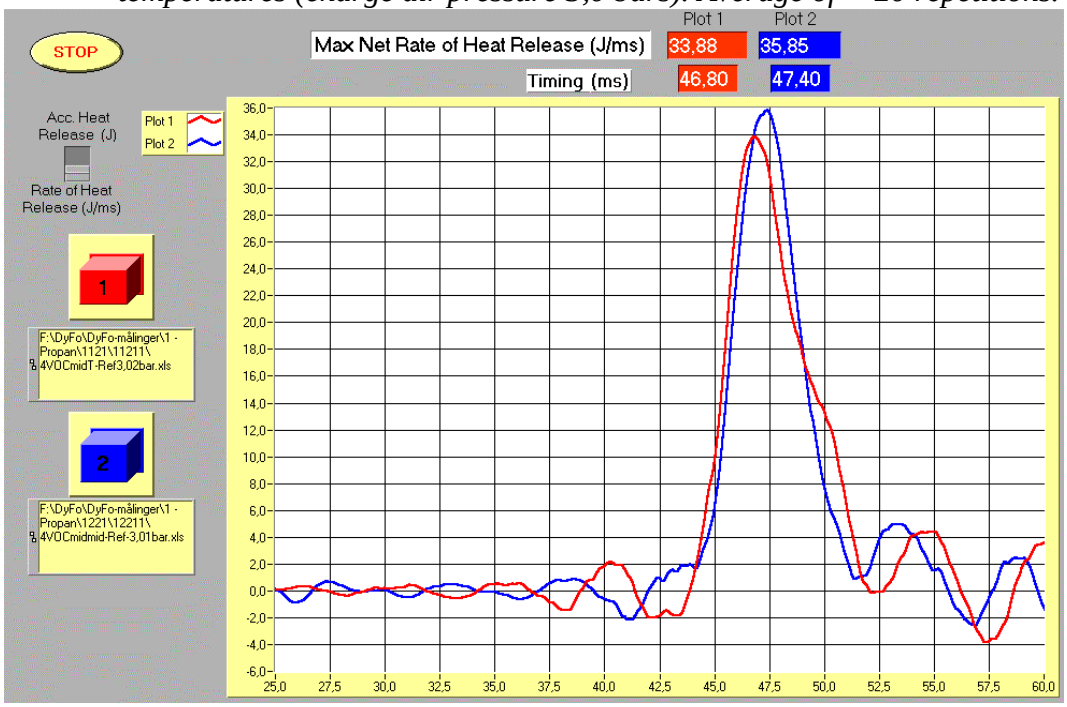

Figure A9.2 Rate of heat release curves when varying the charge air temperature (charge air pressure 3,0 bars). Average of > 20 repetitions.

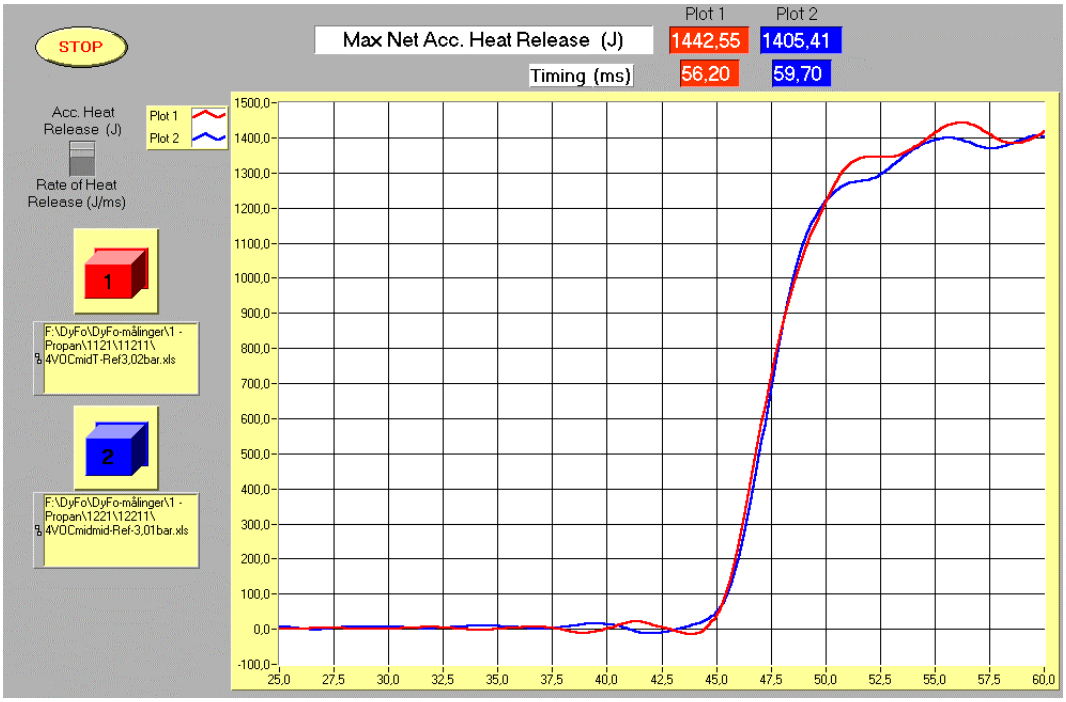

Figure A9.3 Accumulated heat release curves when varying the charge air temperature (charge air pressure 3,0 bars). Average of > 20 repetitions.

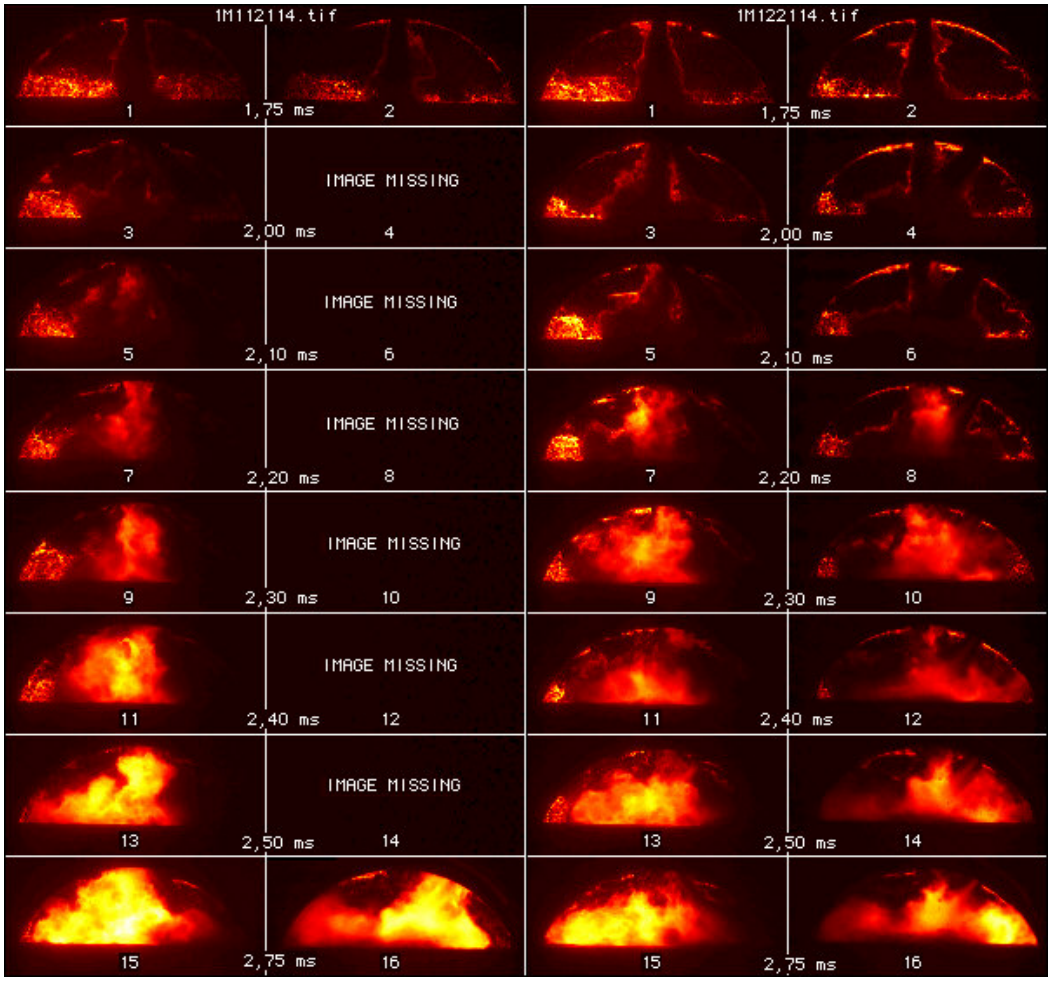

Figure A9.4 Images of injection, ignition and early combustion of pilot fuel and VOC Fuel with different charge air temperature (CAT), CAP=3,0 bars. Images from 2 directions, Right: CAT=low (1M112114), left: CAT=high (1M122114).

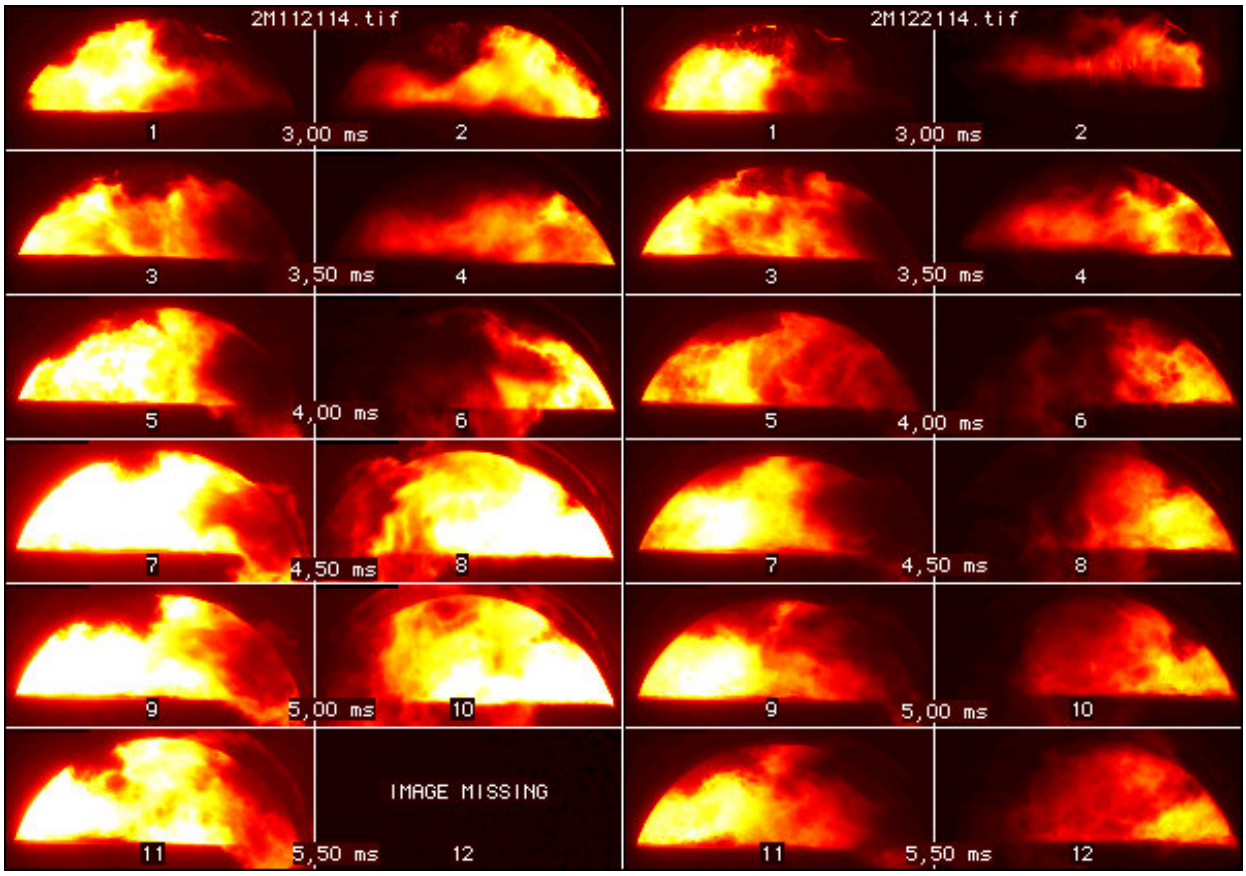

Figure A9.5 *Images of middle combustion of pilot fuel and VOC Fuel with different charge air temperature (CAT), CAP=3,0 bars. Images from 2 directions, Right: CAT=low (1M112114), left: CAT=high (1M122114).*

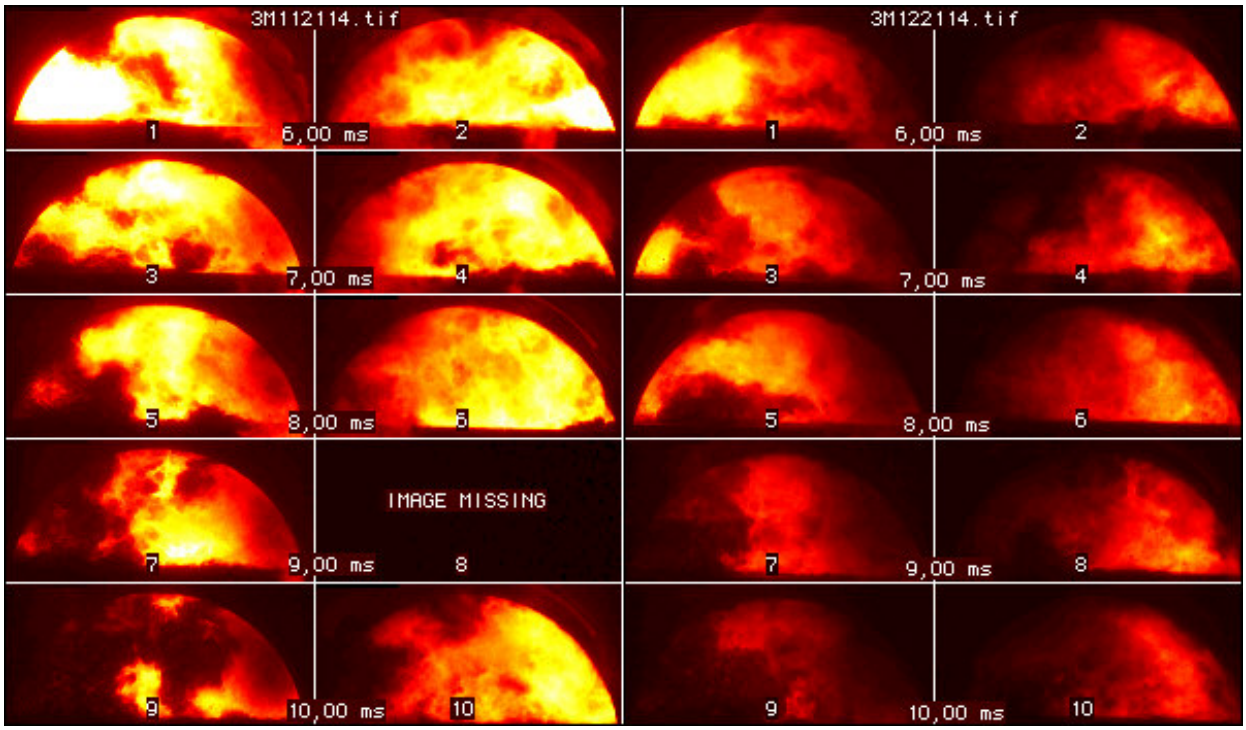

Figure A9.6 *Images of late combustion of pilot fuel and VOC Fuel with different charge air temperature (CAT), CAP=3,0 bars. Images from 2 directions, Right: CAT=low (1M112114), left: CAT=high (1M122114).*

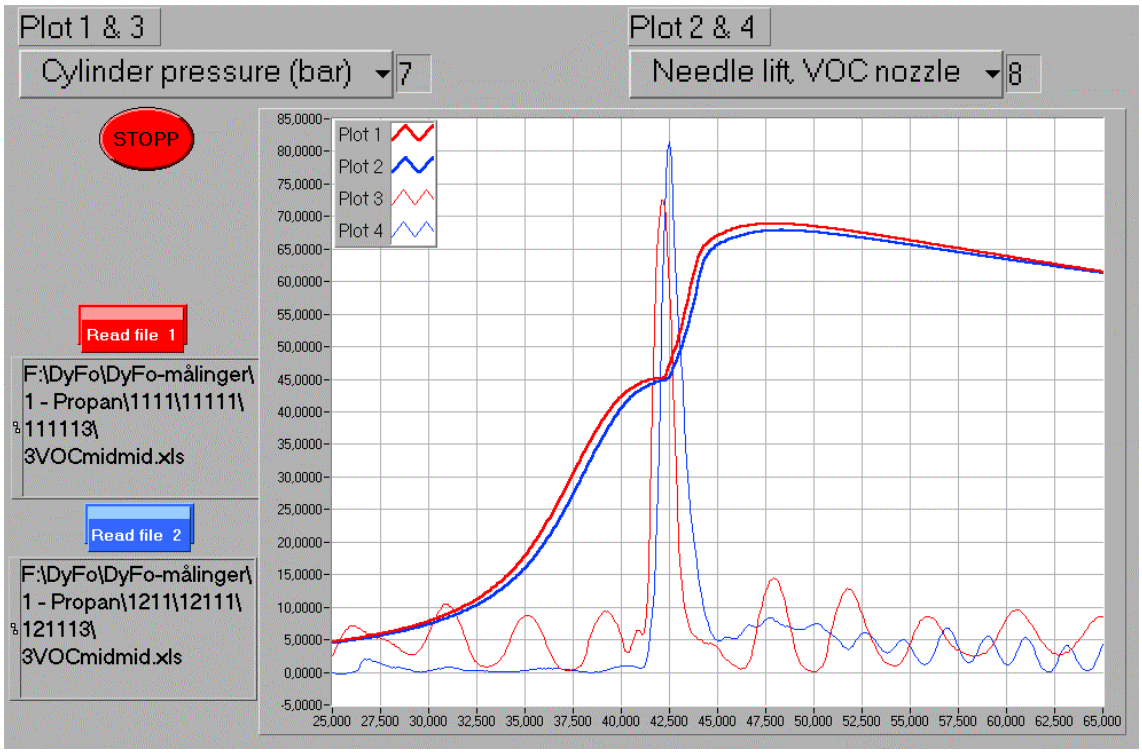

Figure A9.7 Cylinder pressure and VOC Fuel injector needle lift for different charge air temperatures (charge air pressure 2,0 bars). Average of > 20 repetitions.

In Figure A9.7 it can be seen that the cylinder pressure increases earlier in test 111113 than in test 121113. Why this happened is not fully revealed. The needle lift curves for the VOC Fuel injector shows an equal difference. However, the trigging signal for CCD camera in the two test series were equal as shown in Figure A9.8. The same difference is shown in the ignition delay.

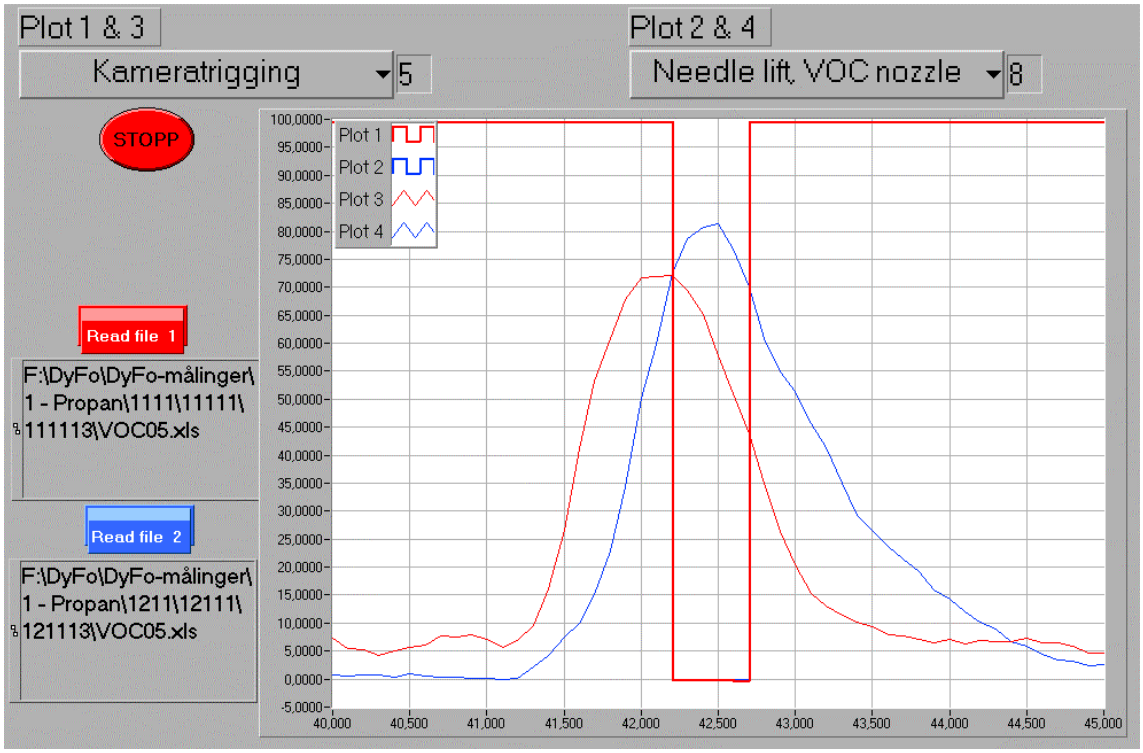

Figure A9.8 Close-up view of the VOC Fuel injector needle lift and the trigging signal for the CCD camera for test 111113 and 121113 (charge air pressure 2,0 bars).

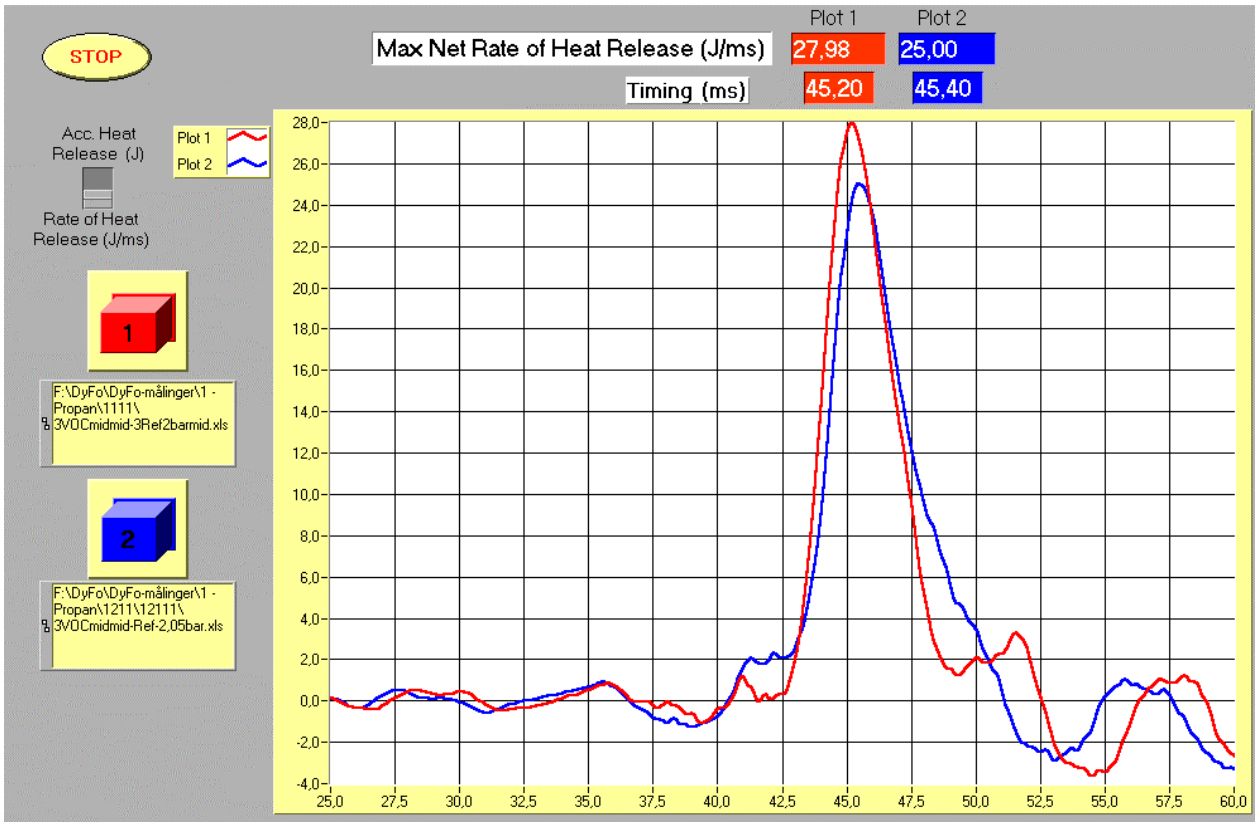

Figure A9.9 Rate of heat release curves when varying the charge air temperature (test 111113 and 121113, charge air pressure 2,0 bars).

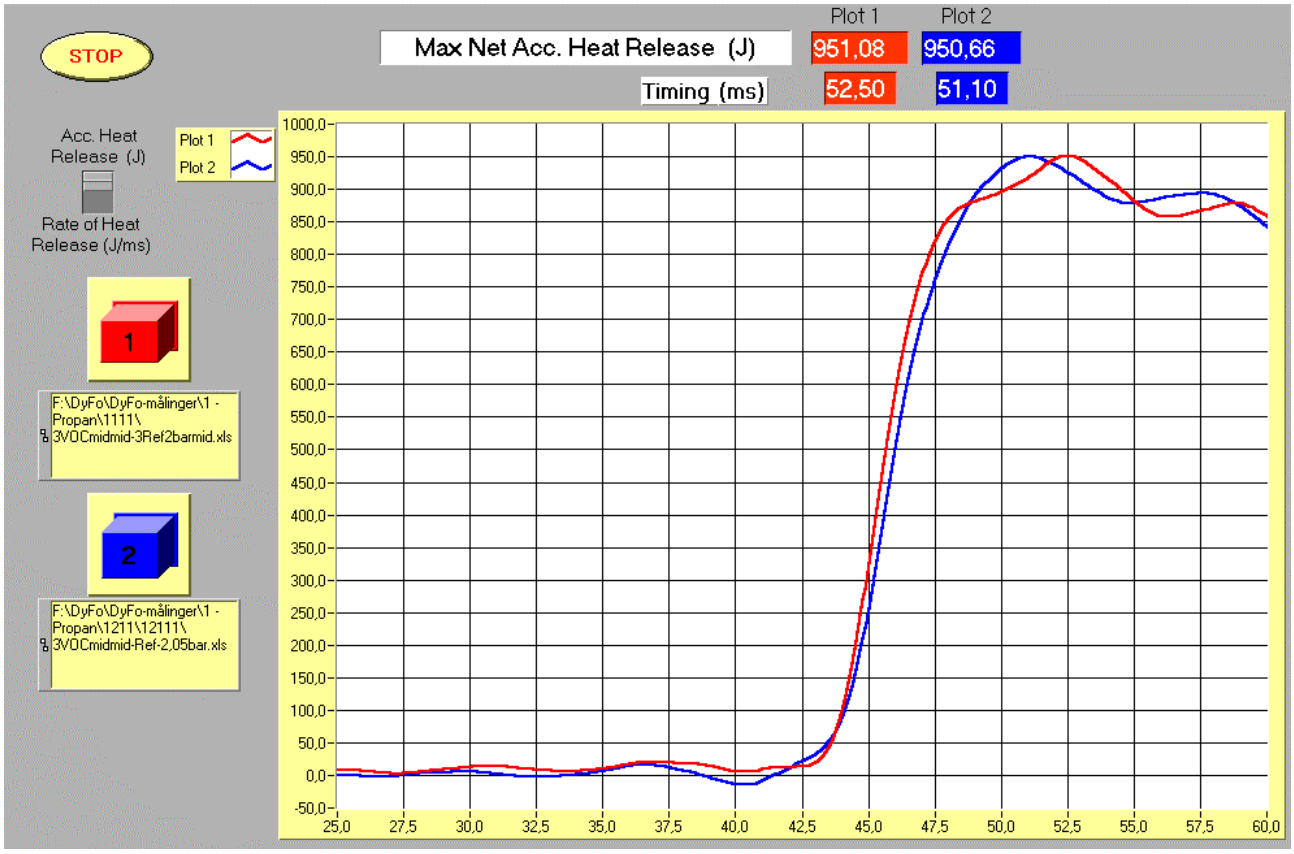

Figure A9.10 Accumulated heat release curves when varying the charge air temperature (test 111113 and 121113, charge air pressure 2,0 bars).

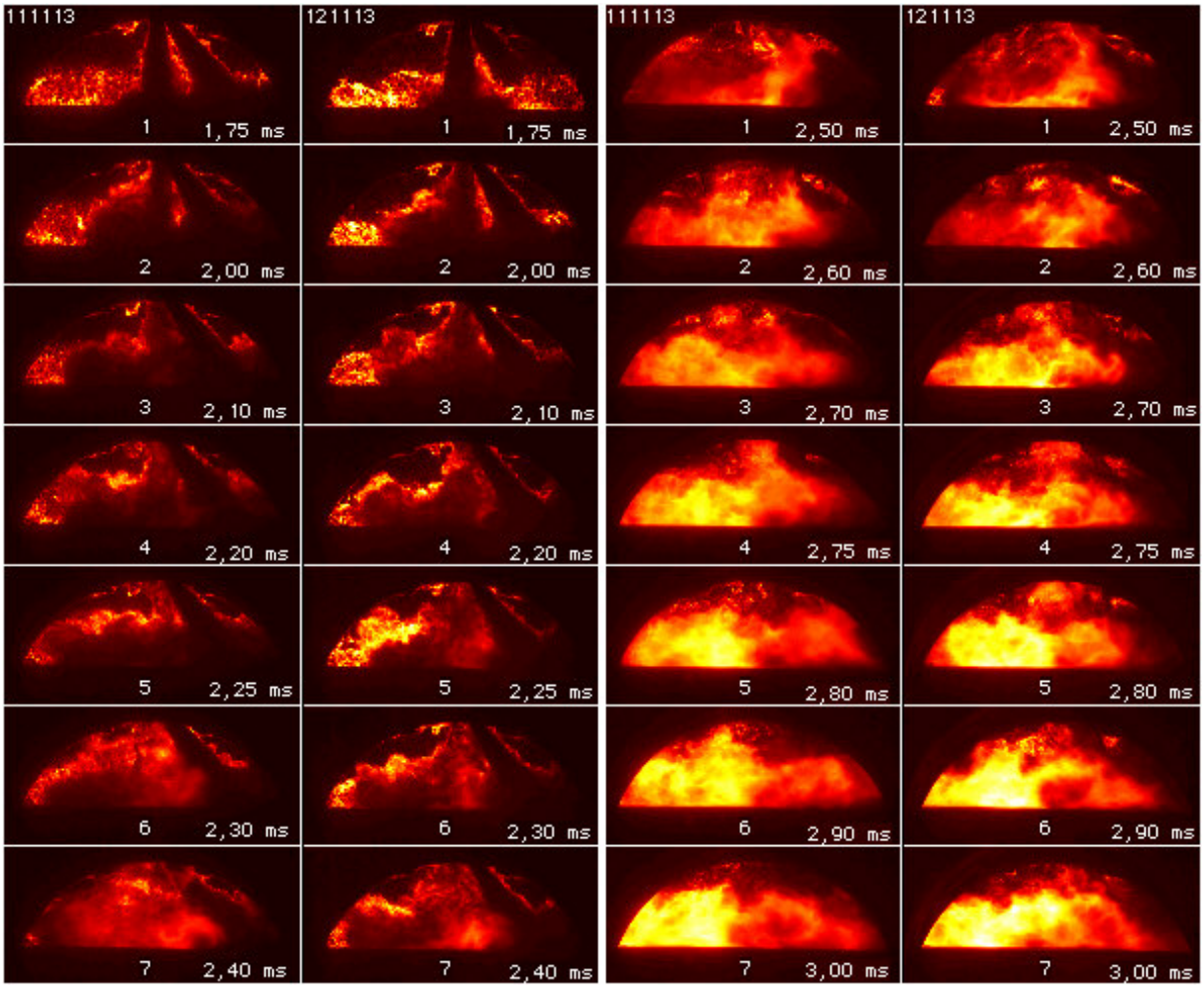

Figure A9.11 Images of injection, ignition and early combustion of pilot fuel and VOC Fuel with different charge air temperature (CAT), charge air pressure 2,0 bars. CAT low to the left (111113) and CAT high to the right (121113).

Appendix 10 Effect of different VOC fuel types

Due to a problem with leaking quarts windows, most of the tests with VOC Fuel components other than propane were made with no Schlieren images taken.

To study images of combustion with different components, results from tests carried out earlier and with other test conditions than in the tests referred to in Section 5.2 "Test results - *Effect of fuel type"* are shown here. The conclusion is, however, the same - combustion of different VOC Fuel components by the «Condensate Diesel Process» with pilot fuel ignition, gives no significant differences.

From Figure A10.1 - 4 it is seen that ignition and combustion differs very little for the three types of VOC Fuel tested. The minor deviations in the timing of needle lifts and pressure rise are due to small inaccuracies in the test equipment. Relative time between injection and ignition for the 3 different fuels is, however, nearly identical, as observed in the close-up view of needle lift and cylinder pressure curves shown in Figure A10.2 below.

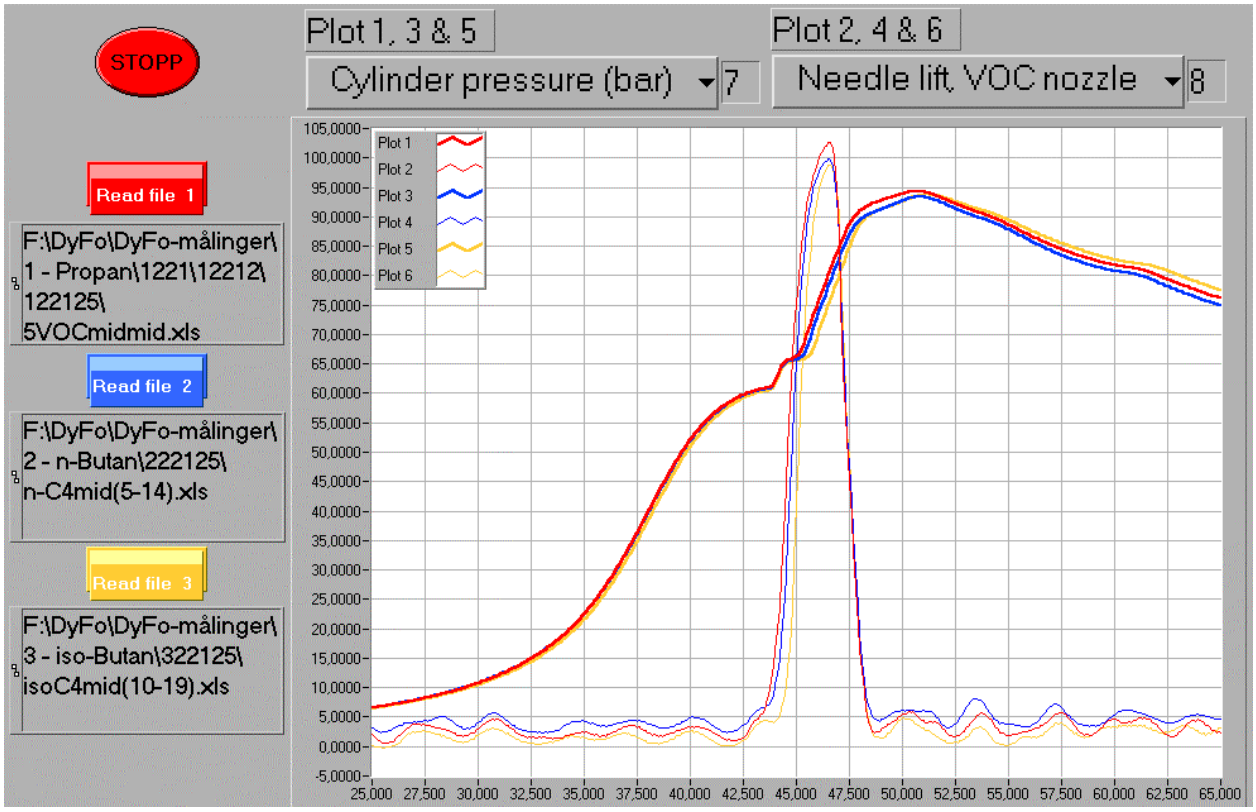

Figure A10.1 Cylinder pressure and VOC nozzle needle lift curves. Red curves: Propane, blue curves: n-Butane, yellow curves: iso-Butane.

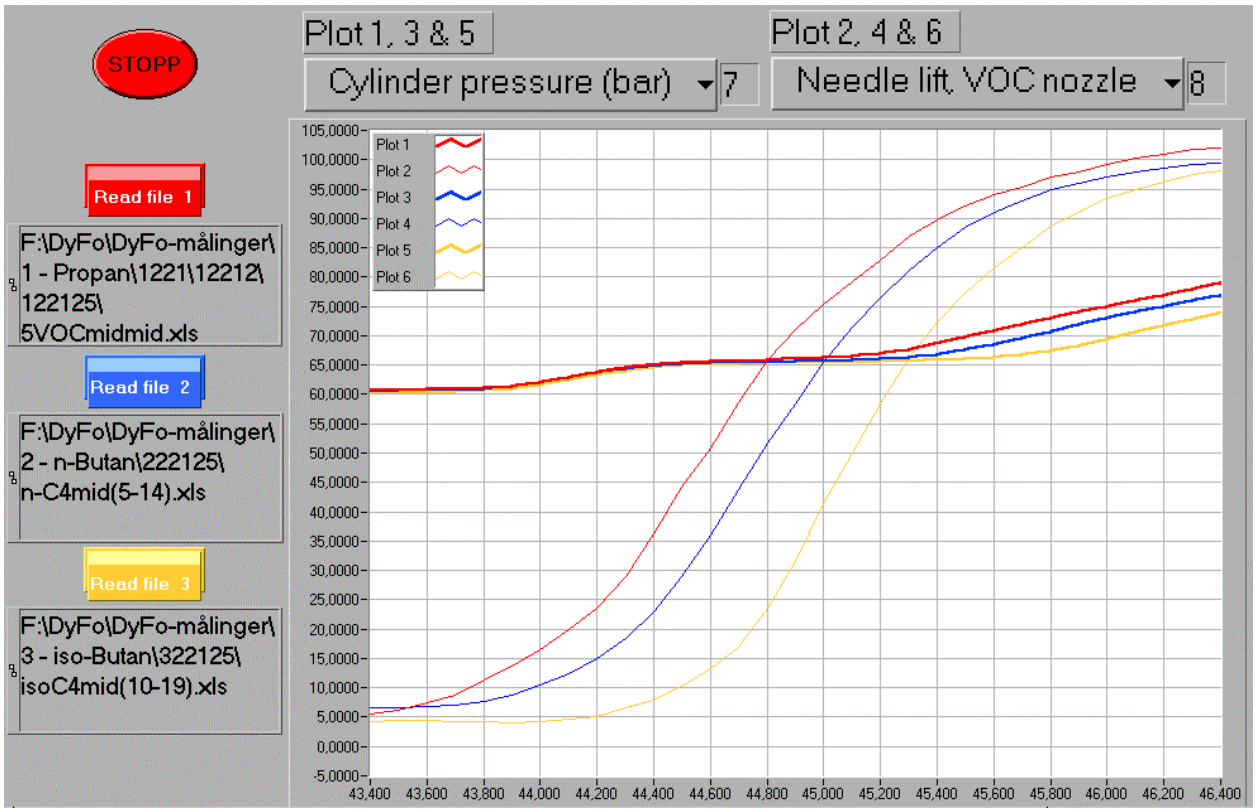

Figure A10.2 Close-up view of cylinder pressure and VOC nozzle needle lift curves. Red curves: Propane, blue curves: n-Butane, yellow curves: iso-Butane.

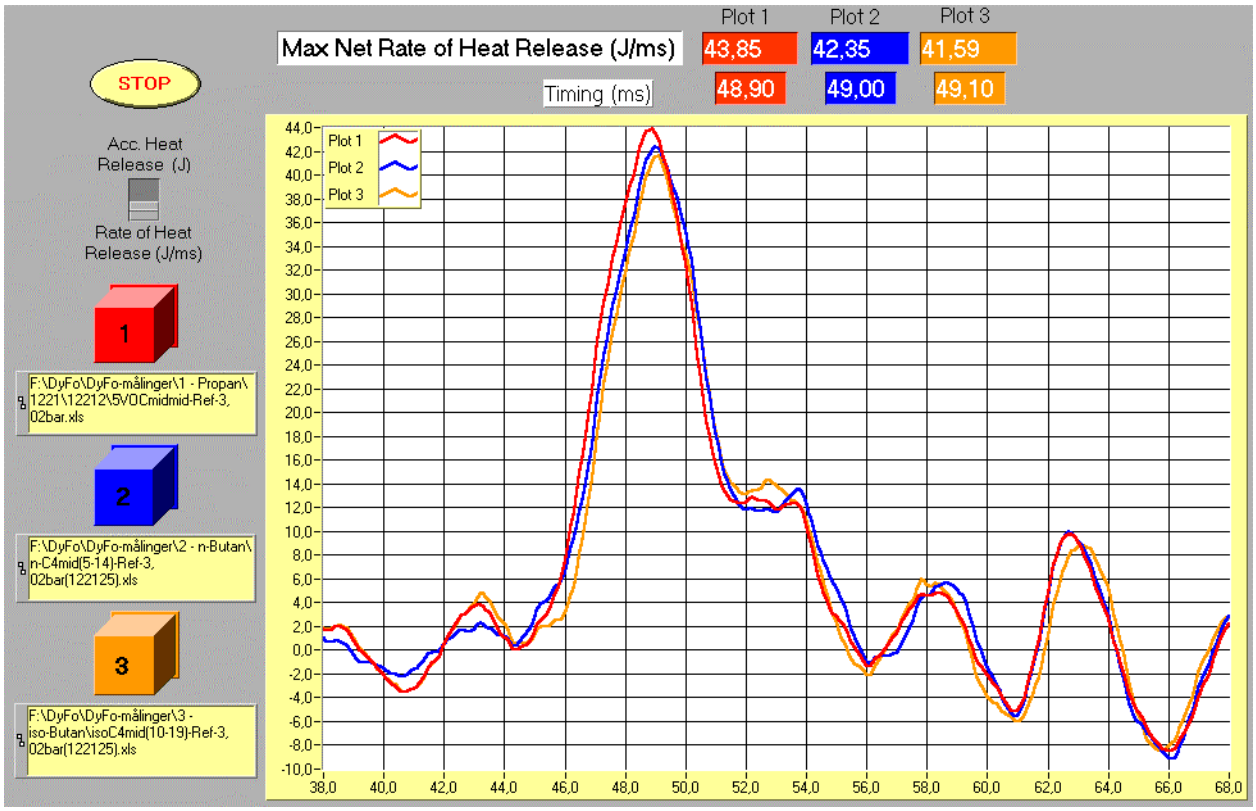

Figure A10.3 Rate of Heat Release curves. Red curve: Propane, blue curve: n-Butane, yellow curve: iso-Butane.

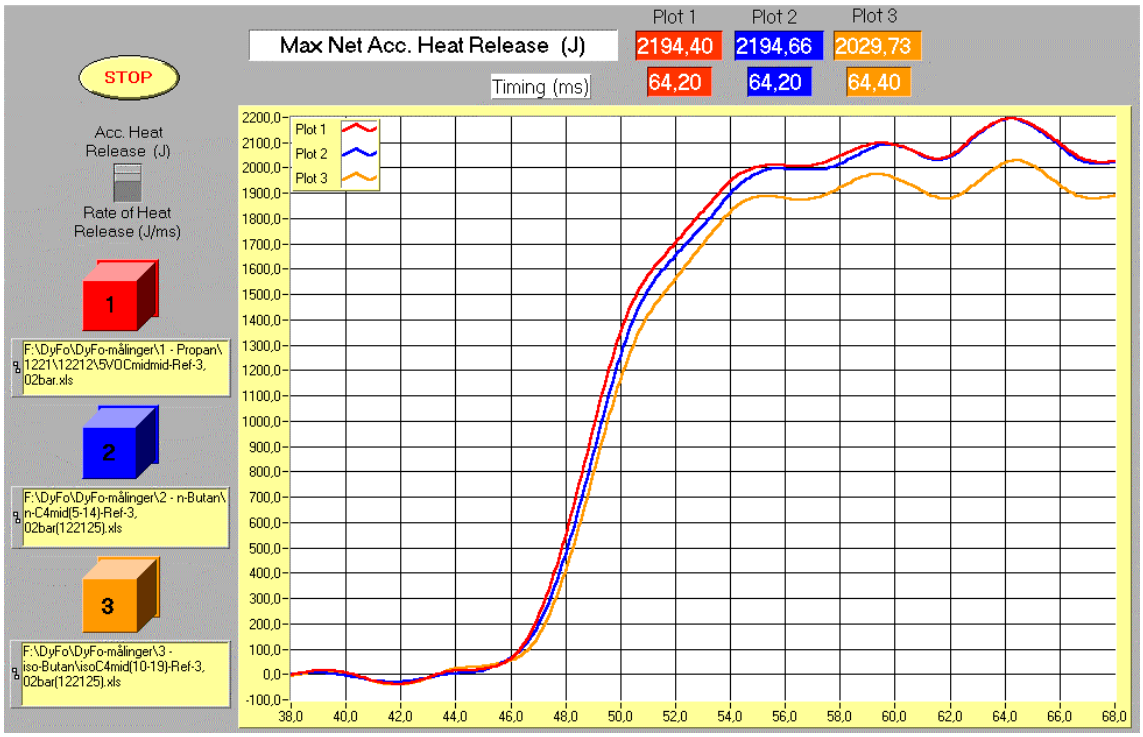

Figure A10.4 Accumulated Heat Release curves. Red curve: Propane, blue curve: n-Butane, yellow curve: iso-Butane.

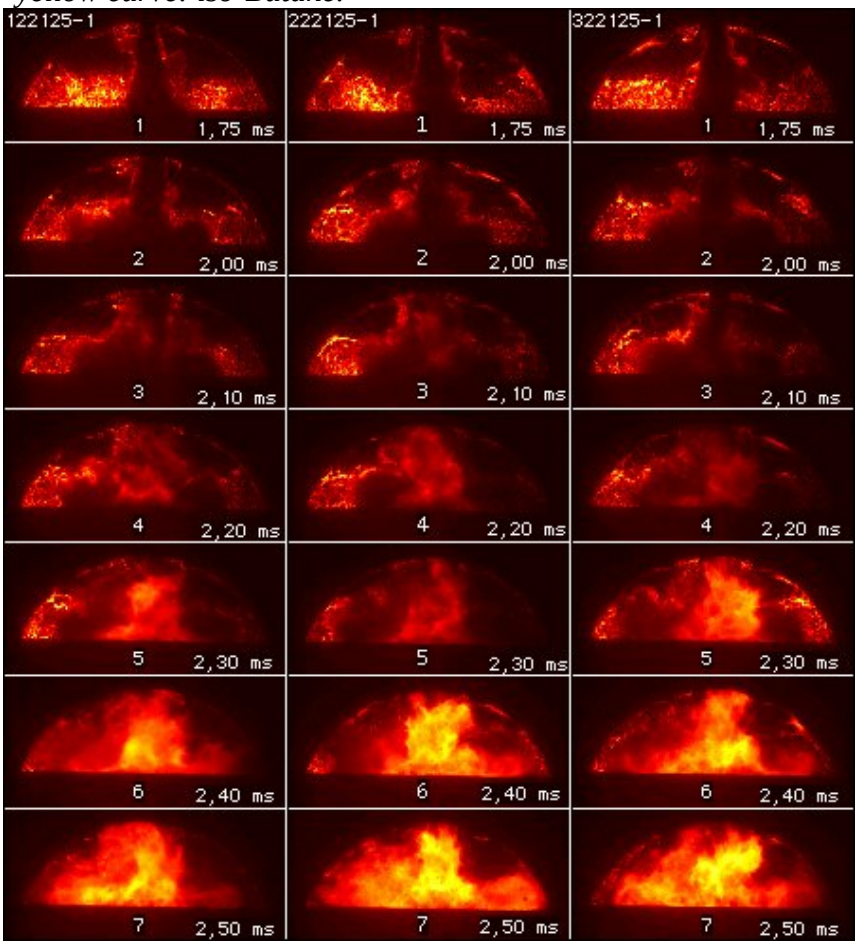

Propane **n-Butane** **iso-Butane**

Figure A10.5 Schlieren images of injection and ignition of different VOC Fuel components.

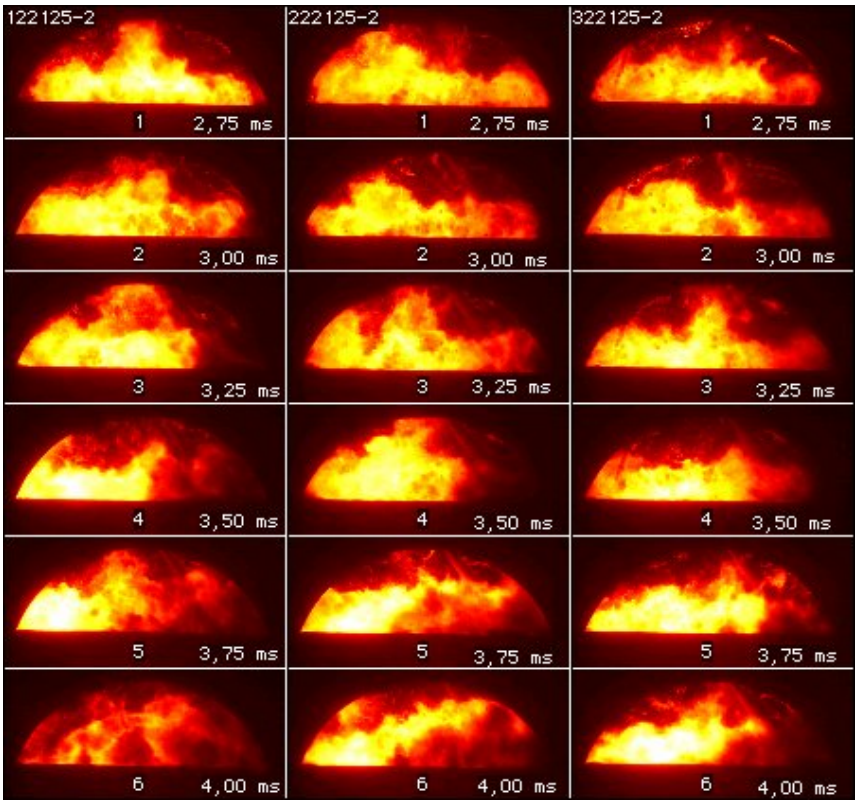

Propane **n-Butane** **iso-Butane**

Figure A10.6 Schlieren images of early combustion of different VOC Fuel components.

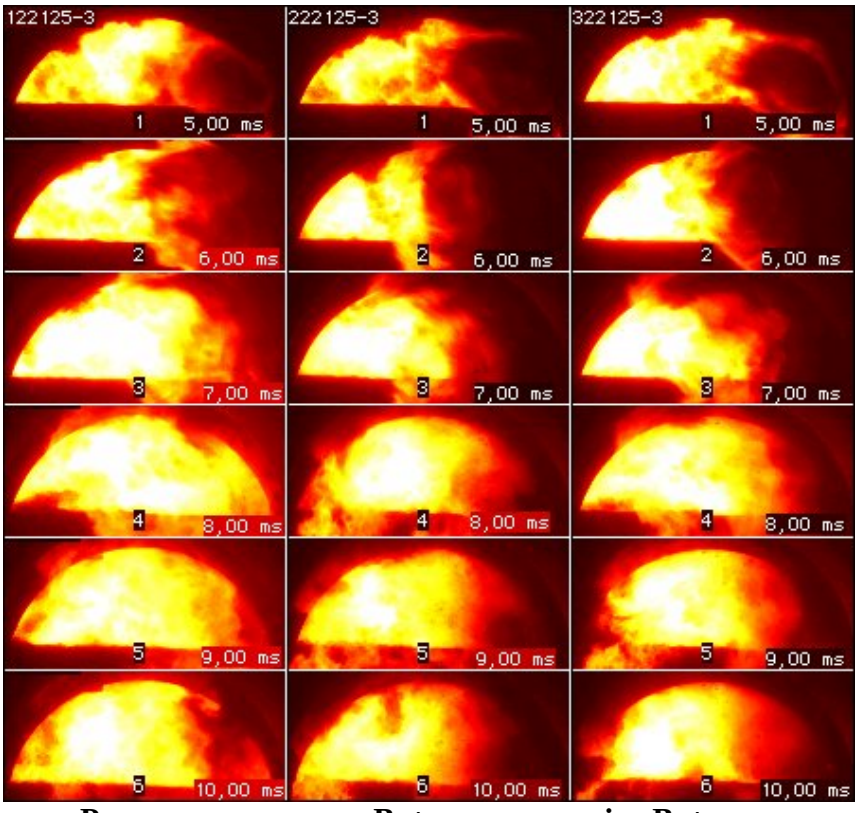

Propane **n-Butane** **iso-Butane**

Figure A10.7 Schlieren images of late combustion of different VOC Fuel components.

Later new tests with the VOC mixture and methane in addition to propane were performed by conditions more identical and different from the conditions by the earlier tests. Results from these later tests are shown in Figure A10.8 below. No schlieren images are recorded by these tests.

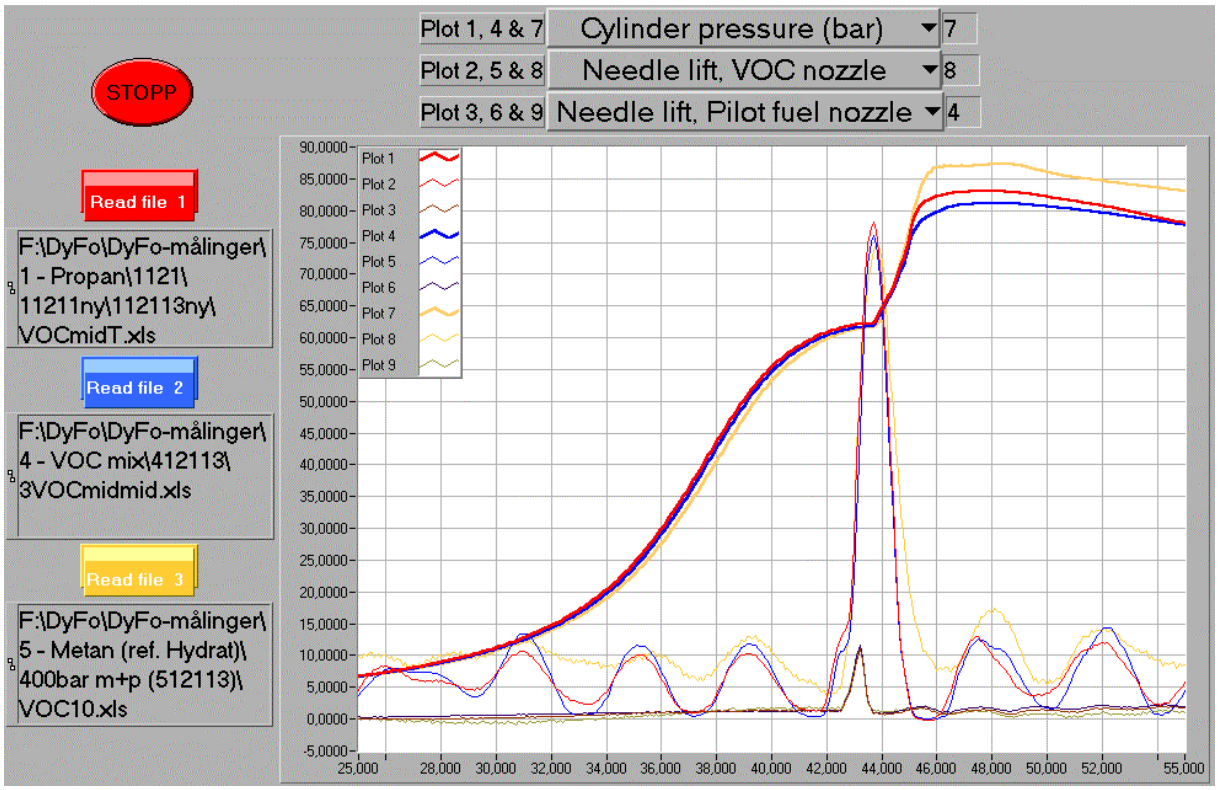

Figure A10.8 Cylinder pressure and VOC nozzle needle lift curves. Red curves: Propane, blue curves: VOC mixture and yellow curves: Methane.

Previous dr.ing.theses

Department of Marine Engineering

Kviteng, Olav	Torsional Vibration Systems with non-linear Elements. 1972. (In Norwegian).
Mathiesen, Tor Chr.	Reliability Engineering in Ship Machinery Plant Design. 1973.
Bøe, Carsten	The Hydrodynamic Lubrication Problem for Engine Sleeve Bearing. 1975.
Rasmussen, Magnus	Evaluation of Structural Properties in Connection with Vibration Analysis for Condition Monitoring of Machinery. 1976. (In Norwegian).
Valland, Harald	Simulation of the Internal Combustion Engine Cycle. 1976. (In Norwegian).
Sandsmark, Nils	Analysis of Stationary and Transient Heat Conduction by the Finite Element Method. 1977. (In Norwegian).
Oldervik, Ole	The Hydrodynamically Lubricated Journal Bearing Subjected to Periodically Varying Load. 1979.
Saugerud, Odd Tore	Fatigue Life Prediction of Thermally Loaded Engine Components. 1981.
Haugslett, Åge	Mathematical Modelling of Hydraulic Systems using Bond-Graphs. 1981. (In Norwegian).
Strand, Kurt	A System Dynamic Approach to One-Dimensional Fluid Flow. 1986.
Småvik, Magnus	Thermal Load and Process Characteristics in a Two-Stroke Diesel Engine with Thermal Barriers. 1987. (In Norwegian)
Haagensen, Sven	Fuel Dependent Cyclic Variability in a Spark Ignition Engine - An Optical Approach. 1991.
Molteberg, Gunnar	The Application of System Identification Techniques to Performance Monitoring of Four Stroke Turbocharged Diesel Engines. 1991.
Chan Siu Hung	Nonlinear Analysis of Rotordynamic Instabilities in High-speed Turbomachinery. 1992.
Ask, Tor Øyvind	Ignition and Flame Growth in Lean Gas-Air Mixtures. An Experimental Study with a Schlieren System. 1992.

Steinebach, Christian	Knowledge Based Systems for Diagnosis of Rotating Machinery. 1993
Nordrik, Rune	Investigation of Spark Ignition and Autoignition in Methane and Air using Computational Fluid Dynamics and Chemical Reaction Kinetics. 1993.
Paulsen, Hallvard	A Study of Transient Jet and Spray using a Schlieren method and Digital Image Processing. 1995.
Æsøy, Vilmar	Hot Surface Assisted Compression Ignition in a Direct Injection Natural Gas Engine. 1996.
Moksnes, Paul Ove	Modelling Two-Phase Thermo-Fluid Systems Using Bond Graphs. 1997.
Torbergsen, Erik	Impeller/Diffusor interaction forces in centrifugal pumps. 1998.
Andersen, Trond M.	Short Term Maintenance Planning. 1999.
Storteig, Eskild	Dynamic characteristics and leakage performance of liquid annular seals in centrifugal pumps. 2000.
Bysveen, Marie	Visualisation in Two Directions on a Dynamic Combustion Rig for Studies of Fuel Quality, 1999.
Samdal, Ole Johan	Modelling of Degradation Mechanisms and Stressor Interaction on Static Mechanical Equipment Residual Lifetime, 2001.